De mechanismen van de robuustheid van vers zelfverdichtend beton

The Mechanisms Governing the Robustness of Fresh Self-Compacting Concrete

Farid Van Der Vurst

Promotoren: prof. dr. ir. G. De Schutter, prof. dr. ir. L. Vandewalle
Proefschrift ingediend tot het behalen van de graden van
Doctor in de ingenieurswetenschappen: bouwkunde (Universiteit Gent)
en Doctor in de ingenieurswetenschappen: bouwkunde (Katholieke Universiteit Leuven)

UNIVERSITEIT
GENT

Vakgroep Bouwkundige Constructies
Voorzitter: prof. dr. ir. L. Taerwe
Faculteit Ingenieurswetenschappen en Architectuur

KU LEUVEN

Departement Burgerlijke Bouwkunde
Voorzitter: prof. dr. ir. J. Monbaliu
Faculteit Ingenieurswetenschappen

Academiejaar 2016 - 2017

ISBN 978-90-8578-983-3
NUR 955, 971
Wettelijk depot: D/2017/10.500/18

Supervisors

Prof. dr. ir. Geert De Schutter
Prof. dr. ir. Lucie Vandewalle

Research Institutes

Magnel Laboratory for Concrete Research
Department of Structural Engineering
Faculty of Engineering and Architecture
Ghent University, Belgium

Building Materials and Building Technology Section
Department of Civil Engineering
Faculty of Engineering Science
University of Leuven, Belgium

Examination Committee

Prof. dr. ir. Geert De Schutter
Prof. dr. ir. Lucie Vandewalle
Prof. dr. ir. Luc Taerwe (chair)
Prof. dr. ir. Joos Vandewalle (co-chair)
Prof. dr. ir. Dimitri Feys
Prof. dr. ir. John Vantomme
Prof. dr. ir. Hans De Backer
Prof. dr. ir. Özlem Cizer
Dr. ir. Karel Lesage
Prof. dr. ir. Mario Smet

Research Funding

This research project was funded by the Research Foundation Flanders (Fonds Wetenschappelijk Onderzoek, FWO).

Acknowledgements

The last four years of my life, I worked with great pleasure on my PhD project. I enjoyed every sip of it and before describing its scientific aspects, I would like to show my gratitude to the people who gave me this opportunity and helped me during this project. Without your support, I would not have made it.

First of all, I would like to thank Geert De Schutter. You were an excellent supervisor. I was given the necessary freedom to investigate major and secondary items in depth, but you also corrected me when necessary. I got plenty of clever suggestions and the right advice in situations where I was doubting. You always supported me and gave me the necessary self-confidence to make this project successful.

I would also like to thank Dimitri Feys, who supervised me during the project extension in Rolla, MO. You supported me, included me in your team, and lifted the research to a higher level. You are incredibly omniscient in the field of rheology and passed your enthusiasm and thirst for knowledge to me. You were always willing to share your knowledge and expertise when I had a question. It was a pleasure to work under your supervision.

Lucie Vandewalle and John Vantomme, you were great supervisors as well. We only had meetings every few months, but each time you had helpful comments and suggestions waiting for me. I also received plenty of feedback and help from Steffen Grunewald, Benny Malengier, Bram Desmet, Karel Lesage, Jeroen Dils, Paul Van der Meeren, Alain Phyfferoen, Steven Feldman, Christian Behrens, Christian Oetzel, and Frederik Schleife. I would also like thank Nicolas Roussel, Harald Justnes, Serina Ng, Emili Taengua, Mohammed Sonebi, Olafur Wallevik, and many other scientists for the interesting discussions, insights, and spirits that you have shared with me during scientific conferences.

However, this project did not only rely on the contribution of promoters and scientific experts. While performing my experiments, I was always backed by the wonderful Magnel laboratory. The building, the equipment, the great team of technicians, my other colleagues, … you were just fantastic. It was an honor to be part of the team. In particular, I would like to thank Tom, Natan, Dieter, and Nicolas for their help during the experiments and the many suggestions they have given to me. Your understanding and experience were also a major contribution to this PhD dissertation. I would also like to thank the CIES laboratory in Rolla: Abbie, Jason, John, and Delbert, you were all great.

Pieter Desnerck, you have earned your own paragraph in this acknowledgement chapter. First of all, I would like to thank you as a good and supportive coach, supervising me and Jonathan Peirs during our master dissertation. Secondly, I would like to thank you for suggesting me to Geert De Schutter as a potential PhD candidate on this FWO project. Without you I would not have started the PhD. We became colleagues and you guided me through the laboratory. Thank you for introducing me to the Magnel laboratory during my first months. Later on, you started working at the CIES laboratory in Rolla. When I came over for the project extension, you helped me with almost everything: selecting the hotel for the first night, you picked me up from the airport, helped me with the machinery in the laboratory, showed me the nice bars in town, … At the end, I even took over your apartment when you moved to the U.K. Thanks for everything, it is great to have a good and warm hearted friend like you. I will never forget our weekend trips and the barbeques we had together with Jason and his kids.

Besides the harsh and serious scientific work in the Magnel laboratory, I was also always able to make time for some fun with colleagues. I wish I had the possibility to devote a separate section to all of my beloved colleagues, but unfortunately the chapter of acknowledgements would have become larger than the actual dissertation. As a compromise, I will only write a limited summary over here and show my gratitude more extensively and in more detail face to face during the reception after my public defense. Moreover, some stuff should better not been written down…

My colleagues at the Magnel laboratory are fantastic. We make jokes in between the work, experience interesting conferences together, and after work, we sometimes went partying together. From the day I met Tommy, I noticed we share the same type of humor. Jason and his sons accepted me as a part of their family. Eshan laughed and cursed together with me during our experiments in Rolla. Even when pregnant with her lovely daughter, Azi was in the laboratory and present for a friendly chat. And the list goes on… In particular I would like to thank all of my

international colleagues who showed me the world and opened my eyes in our delightful discussions on just about everything. Lijie Wang, thanks for all the good times we had together. I will never forget the delicious food you prepare and the kind hospitality of you and your family, who hosted us during our trip in China. Cornelia, Raul and Corina, thank you, for showing me the beautiful nature of Romania, a marvelous country which I will visit over and over again. Thank you Florent, for introducing me into wine tasting in France on our way back from Switzerland. Thank you, Pieterjan, Bjorn, Nati, Hugo, Kunpeng, Wenhao, Yury, João, Ali, Ionel, Jeroen Ruben, Didier, Mathias, Tim, Kenny, Brenda, Peter, Xiang, Yang, Evin, Tan, and many other colleagues for all the good times we shared together. You are always welcome to come over for a dinner and drink as we have done so many times. Han, thank you so much sharing your happiness and everlasting smile during the relaxing walks we had together after lunch. You are now in Heaven, but will always keep shining in my heart.

I would like to thank my comrades of the union. It was a great feeling to not only build on a better knowledge and understanding of self-compacting concrete, but also helping to improve the working conditions within the university. Together we achieved something many people thought was impossible: ending the sequence of short term contracts for many workers at our university, causing stress and insecurity. Keep on the good work.

Last four years I have put plenty of time and efforts into the PhD project, but obviously I never forgot my friends and family. Thank you buddies! I could always rely on you for helping each other, doing foolish stuff together, and for support when I needed it most. Thanks for all the good and bad moments we have shared together.

The last one on this long list is not of the least importance. I would like to thank the society for giving me all of this. You have paid my salary, given me the education, paid for my healthcare, and surrounded me with good people. I hope the research I finished contributes to the understanding of concrete and will help to build an even better society. I hope I have met the high expectations and deserved the trust you have given in me.

“As we express our gratitude, we must never forget that the highest appreciation is not to utter words, but to live by them.” John F. Kennedy

Table of Contents

Abstract (English)

This thesis deals with the robustness of fresh self-compacting concrete (SCC). As no external compaction is necessary, many problems caused by a poor compaction are evaded and a denser reinforcement or more complex formworks can be applied when using SCC. Although reduced construction times, less labour costs, and an improved pumpability encourage the usage of SCC, an inferior robustness – the capacity to tolerate small variations in the mix proportions, material properties and procedures – limits the general use or SCC. A more severe quality control of all constituent materials and a more experienced staff is needed.

SCC has a more complex mix design compared to vibrated concrete. Balancing in between a sufficient flowability allowing air bubbles to escape and a loss of cohesion due to segregation or bleeding, the impact of small changes on the fresh properties is much larger. This thesis aims to investigate the physics governing the robustness, and especially the role of the microstructure and particle clustering on the robustness. Due to the large number of influencing factors, not every aspect governing the robustness could be studied. By focusing on the fundamental mechanisms involved during the analysis of the experimental results, the results can be generalized to other situations or parameters. To study the particle clustering in cement paste more directly, the potential use of new experimental techniques such as ultrasound attenuation and Small Angle Light Scattering (SALS) was evaluated.

A concise overview of the fundamental mechanisms and interactions governing the microstructure of fresh SCC is given in the literature review (Chapter 3). The chemical reactions during the first hours of hydration, the forces and interactions in between particles, the working mechanisms of admixtures, and the impact of shear stresses are explained in more detail in order to obtain a better understanding of the microstructure.

Based on the experimental results, methods to improve the robustness of fresh SCC were developed. Dependent on the mechanism providing stability in SCC, another strategy should be used. As different applications have different workability

demands, SCC with proper rheological properties customized to the application should be used.

When the yield stress is providing stability, the sensitivity of this yield stress to small changes is determining the robustness of the mixture. Because such mixtures generally have a low plastic viscosity, changes in this plastic viscosity due to small variations have no major impact. Based on the experimental program and a qualitative analyses using the yield stress model (YODEL), possible solutions to enhance the yield stress robustness of SCC have been proposed. A higher maximum packing density results in a more robust yield stress and can be achieved with a higher superplasticizer dosage, which can be reached with a lower paste volume. An alternative solution is the combination of a lower paste yield stress and a slightly higher plastic viscosity, for example by adding a VMA combined with a higher superplasticizer dosage.

In mixtures with a low or zero yield stress and the paste plastic viscosity providing stability, the sensitivity of the paste plastic viscosity is determining the robustness of the global mixture. A small decrease in the amount of water can result in an unworkable, sticky mixture; a small excess in water can result in bleeding. The best approach to improve the robustness of such a mixture is to enhance the robustness of the paste plastic viscosity. Based on a set of experiments and considering the Krieger-Doherty model, specific measures have been proposed. A first method is to lower the paste packing density, for example by raising the water-to-powder ratio. Also lowering the paste plastic viscosity helps to enhance the robustness against small variations in the mix composition. Mixtures prone to an excessive stickiness can be improved by reducing the thixotropic buildup, for example by increasing the water-to-powder ratio, a cement replacement by fly ash, or reducing the content of silica fume.

In case the risk of bleeding is limiting the applicability of SCC, a different approach is needed. Bleeding is a result of an imbalance in the intermolecular forces. When steric repulsion forces dominate over attractive Van Der Waals forces for small colloidal particles, the colloidal network is broken and syneresis will manifest itself as a layer of water floating on top of SCC. To eliminate the origin of bleeding, two methods exist: reducing the steric repulsive forces by a reduction of the superplasticizer dosage (higher water-to-powder ratio, higher paste volume), or increasing the attractive Van Der Waals forces inside the fresh concrete, for example by a replacement of cement by silica fume.

An attempt was made to investigate particle clustering and the structural buildup more fundamentally using innovative experimental techniques. Due to the very

broad particle size distribution and the non-transparent opaque nature of cement paste, monitoring the flocculation and deflocculation of the individual cement particles is not evident. Two techniques have been selected for a more thorough examination of their applicability: ultrasound attenuation and Small Angle Light Scattering (SALS).

When ultrasound amplitude losses are measured over a range of ultrasound frequencies, attenuation spectra can be used to characterize an opaque dense solution. As no evolution in the attenuation spectra was observed on samples of cement paste at rest, the flocculation at rest cannot be evaluated using the ultrasound attenuation technique. Different water-to-powder ratios caused variations in the measured attenuation spectra. However, in an apparatus in which the particle size distributions were calculated based on a theory taking into account the viscous attenuation losses and the scattering attenuation losses, no realistic particle size distribution could be generated. Using another apparatus, in which the particle size distribution was calculated based on a calibration with a powder with known properties, realistic particle size distributions were obtained. As paste mixtures varying in water-to-powder ratio all generated similar particle size distributions, no effects of differences of the water-to-powder ratio on the particle clustering could be observed using ultrasound attenuation.

When Small Angle Light Scattering (SALS) was used on diluted samples of a solution of cement in water, the influence of adding a superplasticizer on the scattering patterns could be observed. Because the SALS images were independent on the shear rate applied on the samples, the flocculation / deflocculation mechanisms in cement paste subjected to shear cannot be studied more in depth using this technique. A calculation of the particle size distribution based on the SALS images was not successful. Although this technique is useful in polymer science, its application on cement paste is less promising.

Abstract (Dutch)

In deze thesis wordt de robuustheid van vers zelfverdichtend beton onderzocht. Omdat geen externe verdichting van het verse beton nodig is, worden vele problemen ten gevolge van een slechte verdichting vermeden bij het gebruik van zelfverdichtend beton. Door de uitgespaarde arbeidskosten, een snellere constructieduur, de betere verpompbaarheid en de mogelijkheid om toepassingen met een dichter wapeningsnet of complexere bekistingen te produceren wordt zelfverdichtend beton steeds meer toegepast. Echter, de inferieure robuustheid – de capaciteit om kleine variaties in de mengverhoudingen, de materiaaleigenschappen en procedures te weerstaan – belemmert het algemeen gebruik van zelfverdichtend beton. Een doorgedreven kwaliteitscontrole van alle bestandsdelen, voldoende toezicht en ervaren arbeidskrachten zijn noodzakelijk.

De samenstelling van zelfverdichtend beton is complexer dan deze van traditioneel verdicht beton: het beton is een evenwichtsoefening tussen een voldoende vloeibaarheid waardoor de lucht uit zichzelf kan ontsnappen en voldoende cohesie om problemen zoals segregatie en bleeding te vermijden. Omwille van dit delicate evenwicht zijn de gevolgen van kleine variaties op de verse eigenschappen veel groter. Deze thesis onderzoekt welke fysische eigenschappen de robuustheid beheersen en focust in het bijzonder op de rol van de verse microstructuur en het clusteren van deeltjes. Gezien het grote aantal mogelijke invloedsfactoren kon niet elk aspect van de robuustheid in detail bestudeerd worden. Tijdens de analyse van de experimentele resultaten werd gefocusd op de fundamentele mechanismen zodat de resultaten veralgemeend kunnen worden naar andere situaties of parameters. Nieuwe experimentele technieken zoals ultrasound attenuation en Small Angle Light Scattering (SALS) werden onderzocht op hun capaciteit om het clusteren van deeltjes in de cement pasta te onderzoeken.

Hoofdstuk 3 is de literatuurstudie van deze thesis. In dit hoofdstuk wordt een overzicht gegeven van de fundamentele mechanismen en interacties die de microstructuur van vers zelfverdichtend beton beheersen. De chemische reacties tijdens de eerste uren van hydratatie, de krachten en interacties tussen de deeltjes, de werkingsmechanismen van admixtures en de impact van schuifspanningen

werden in meer detail uitgewerkt om een beter begrip te bekomen van de microstructuur van vers zelfverdichtend beton.

Op basis van een experimenteel programma werden methodes uitgewerkt om de robuustheid van vers zelfverdichtend beton te verbeteren. Afhankelijk van het mechanisme dat de stabiliteit in het zelfverdichtend beton garandeert, moet een andere strategie toegepast worden. Omdat bij verschillende toepassingen andere verse eigenschappen nodig zijn, moet een zelfverdichtend beton met de gepaste reologische eigenschappen voor een bepaalde toepassing gebruikt worden.

Als de vloeispanning instaat voor de stabiliteit, is het de gevoeligheid van deze vloeispanning die de robuustheid van de betonsamenstelling bepaalt. Omdat dergelijke mengelingen een lage plastische viscositeit bezitten, hebben veranderingen in deze lage plastische viscositeit een beperkte invloed. Op basis van de experimentele resultaten en een kwalitatieve analyse op basis van het YODEL model zijn procedures uitgewerkt om de robuustheid van de vloeispanning en dus het globale mengsel te verbeteren. Een betere maximum pakkingsdichtheid helpt en kan bekomen worden met een hogere dosis superplastificeerder, bijvoorbeeld door het pasta volume te verlagen. Een alternatieve oplossing is de combinatie van een lagere vloeispanning en een iets hogere plastische viscositeit van de pasta, bijvoorbeeld door een VMA in de samenstelling op te nemen in combinatie met een hogere dosis superplastificeerder.

Bij mengelingen met een lage vloeispanning waarin de plastische viscositeit de stabiliteit garandeert is het de gevoeligheid van deze plastische viscositeit die de robuustheid van de betonsamenstelling bepaald. Een klein tekort aan water kan resulteren in een onverwerkbaar kleverig beton, een klein overschot aan water kan leiden tot bleeding. De beste methode om de robuustheid te verbeteren is door de robuustheid van de plastische viscositeit van de pasta te verbeteren. Op basis van een reeks experimenten en de principes van het Krieger-Doherty model zijn concrete maatregelen voorgesteld: een verlaging van de pakkingsdichtheid van de pasta, bijvoorbeeld door de water-tot-poeder verhouding te verhogen. Ook een verlaging van de plastische viscositeit van de pasta helpt om de robuustheid te verhogen. In mengelingen die gevoelig zijn aan een hoge kleverigheid is het aangewezen om de thixotropie te verminderen, bijvoorbeeld door het water-tot-poeder verhouding te verhogen, een vervanging van cement door vliegas, of het verminderen van de hoeveelheid silica fume.

Als bleeding de belangrijkste hinderpaal is bij kleine variaties, is een andere aanpak nodig. Bleeding is een gevolg van een onevenwicht in de intermoleculaire krachten. Als sterische repulsiekrachten domineren over de Van Der Waals krachten voor

kleine colloïdale deeltjes, wordt het colloïdale netwerk verbroken wat leidt tot syneresis: de vorming van een laagje water bovenop het betonoppervlak. Om de oorzaak van bleeding weg te nemen bestaan twee mogelijke oplossingen: de sterische repulsiekrachten verminderen door de dosis superplastificeerder te verlagen (hogere water-tot-poeder verhouding, een hoger pasta volume), of de Van Der Waalskrachten in het verse beton te verhogen, bijvoorbeeld door de vervanging van een deel van het cement door silica fume.

Een poging was ondernomen om de structuuropbouw en clustering van deeltjes in de cement pasta meer fundamenteel te onderzoeken met vernieuwende experimentele technieken. Door de heel brede spanne aan deeltjesgroottes en de ondoorzichtige structuur van cementpasta is het niet evident om de flocculatie van individuele cement deeltjes te bestuderen. Twee technieken werden nader onderzocht: ultrasound attenuation en Small Angle Light Scattering (SALS).

Een attenuation spectrum is een grafiek van de gemeten van de amplitude verliezen in functie van een reeks ultrasound frequenties. De ultrasound golven kunnen doordringen in voor licht ontransparante oplossingen. Omdat geen evolutie van de attenuation spectra was waargenomen bij cement pastas in rust, kan de techniek niet gebruikt worden om de flocculatie in rust te bestuderen. Metingen op cement pastas met verschillende water-tot-poeder verhoudingen zorgden wel voor verschillende attenuation spectra. In een apparaat waarin de deeltjesgrootte verdeling bepaald wordt gebaseerd op een theorie van visceuze attenuation verliezen en scattering attenuation verliezen, werden geen realistische verdelingen berekend. In een ander apparaat waarin de deeltjesgrootte verdeling wordt berekend met behulp van een kalibratie met een poeder met gekende eigenschappen werden wel realistische maar ongeveer identieke deeltjesgrootte verdelingen bekomen. Het effect van particle clustering kon dus niet worden waargenomen in de berekende deeltjesgrootte verdelingen.

De invloed van superplastificeerder kon waargenomen worden op de beelden gegenereerd door Small Angle Light Scattering (SALS) op sterk verdunde oplossingen van cement paste in water. Omdat de SALS beelden onafhankelijk zijn van de opgelegde afschuifsnelheid op de monsters konden de flocculatie en deflocculatie mechanismen in cement pasta niet grondig bestudeerd worden met de SALS techniek. Een berekening van de deeltjesgrootte verdeling gebaseerd op de SALS beelden was niet succesvol. Hoewel de SALS techniek zijn nut bewezen heeft in de polymeerwetenschappen, is de toepassing in cement minder veelbelovend.

Chapter 1: General Introduction

1. Self-Compacting Concrete (SCC)

Self-compacting concrete, also referred to as self-consolidated concrete or SCC is a concrete type which is able to flow under its own weight and completely fill the formwork, even in the presence of a dense reinforcement, without the need of any vibration and maintaining its homogeneity under a wide range of shear stresses [1, 2].

The origin of SCC is located in Japan. During the postwar reconstruction of Japan in the 1960's, numerous building and infrastructure projects made use of vibrated concrete. Many structures had a dense reinforcement because of the high risk of earthquakes, especially in the joint of columns and beams. Two decades later, many durability problems were discovered to be a result of a poor compactation of the fresh concrete, resulting in high reparation costs. To avoid similar problems in the future, H. Okamura and coworkers proposed to use concrete with a high flowability and without the need for an external compactation, leading to the development of self- compacting concrete [3, 4].

The use of SCC has many advantages [2, 5]:

- Less errors due to a poor external compactation, resulting in less repair costs.
- Less vibrations and energy consumption.
- Improved working conditions and less noise.
- Reduced construction times and labour costs.
- The possibility of a denser reinforcement network and a more complex formwork.
- Improved pumping ability.
- Potential for further automation.

However, the usage of SCC also has drawbacks, such as:

- Higher material costs.
- Higher formwork pressures.
- SCC is more prone to plastic shrinkage cracking.
- A lower robustness: SCC is more sensitive to small changes in the mix proportions, material properties, or the mixing procedure. Because of this lower robustness, experienced staff and a more severe quality control of all constituent materials is needed.

After 25 years of use and development, SCC has gained its status in the concrete industry. Especially in the precast industry and in applications with a dense reinforcement, a complex formwork, or containing large volumes of concrete, SCC is already generally used. In order to extend the use of SCC even further, innovative research is now focusing on predicting the rheology, a better understanding of the microstructure and hence the durability, and reducing the environmental impact of SCC.

An accurate prediction of the rheology of SCC is needed to simulate the flow in applications with a complex formwork or a dense reinforcement and to further automatize the casting process. In this context, it is not only needed to develop accurate rheological models and simulation tools, but also to reduce the sensitivity of the SCC rheology to slight perturbations.

2. Mix design of SCC

Compared to conventional vibrated concrete, SCC contains a higher powder content, a high dosage of superplasticizers, and sometimes viscosity modifying admixtures (VMA's). This approach enables to combine a sufficient stability to avoid segregation with a sufficient fluidity, allowing air-bubbles to escape and ensuring a complete filling of the formwork.

Dependent on the application, other workability and strength requirements need to be met. The EFNARC guidelines [1, 6] (Figure 1 [6]) or other guidelines (Figure 2 [7]) can be useful to determine the appropriate slump flow and V-funnel time classes for several applications. However, often practical experience is the most important guideline when setting the needed workability properties for a specific application.

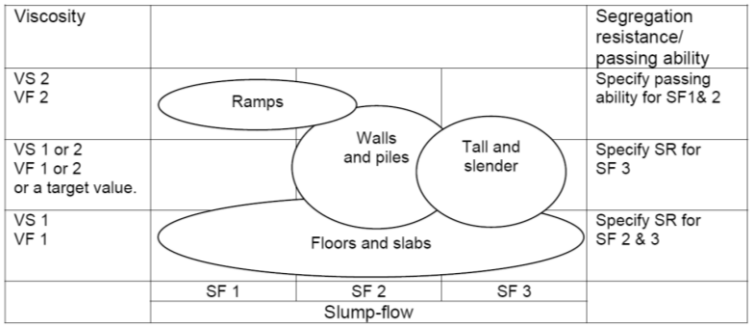

Figure 1: Workability needs for various applications according to the EFNARC guidelines [6]

		Flow Properties								
		Slump flow			U-box			T_{50}		
		<22"	22"-26"	>26"	Rank 3	Rank 2	Rank 1	<2 sec	2-4 sec	>4 sec
Reinforcement level	Low									
	Medium	■			■			■		
	High	■			■	■		■		
Element shape intricacy	Low									
	Medium	■								■
	High	■	■							■
Element depth	Low									
	Medium									
	High							■		
Importance of surface finish	Low									
	Medium	■								
	High	■								
Element length	Low									
	Medium	■								
	High	■	■					■		
Coarse aggregate content	Low									
	Medium						■			
	High					■	■			
Wall thickness	Low	■	■							■
	Medium	■								
	High									

Figure 2: Workability needs for various applications according to Constantiner and Daczko [7]

Once the workability and strength requirements are known, the SCC mix composition can be drafted. Many design methods exist in literature. Shi et al. [8] established the following classification:

- Empirical design methods: Based on empirical data, an initial mix composition is proposed, which should be optimized using trial batches. The great advantage of these methods is its simplicity. A disadvantage is the intensive laboratory testing, needed to be repeated when changing one of the compounds. Examples are the general method of Okamura and co-workers [9] and the UCL method of Domone [10].
- Compressive strength methods: In these methods, the required compressive strength determines the content of cement, additions, water, and aggregate. This straightforward procedure reduces the number of trial batches. Only small adjustments to the proportions of components are needed to reach an optimal mix proportion. An example is the method proposed by Kheder and Al Jadiri [11].
- Close aggregate packing models: After the aggregate packing is optimized using a packing model, the required amount of paste is calculated needed to fill the voids in between the aggregates. As a result, in general less binder is needed. Different packing models coexist: Hwang and Tsai [12] used the densified mixture design algorithm (DMDA), Su et al. [13] the packing factor model (PF), and Sedran and de Larrard [14] the LCPL compressible packing model.
- Statistical factorial models: After intensive laboratory testing, statistical relationships are established to correlate input mix design parameters with output concrete properties. For mixtures within the constraints of the statistical factorial models, an optimized mix composition for a specific application can be generated. Intensive laboratory testing is needed in order to establish the statistical models and needs to be updated in case one of the material properties changes. An example of the application of this approach is described by Khayat et al. [15].
- Rheology of paste models: In order to reduce the amount of laboratory work, the paste rheology is optimized as a function of the average aggregate diameter and aggregate spacing. An example of such a model is the rheology of paste model of Saak et al [16].

The addition of fibers to the mix design of SCC has many advantages, but also complicates the mix design methods. Many authors have established models to obtain a proper mix composition for fiber reinforced SCC [17-20].

3. Robustness of SCC

As described in the previous section, the mix design of SCC is more complex compared to traditional vibrated concrete. SCC mixtures are balancing in between a too high fluidity – resulting in segregation of the coarse aggregates or bleeding – and a lack of fluidity – blocking the release of air bubbles in the fresh concrete and thus eliminating the self-compacting nature of the concrete.

In addition, SCC generally contains more components, has a higher dosage of superplasticizer, and is governed by more complex interactions between the powders and admixtures (superplasticizers, VMA's, retarders, …) in the mix composition compared to vibrated concrete. A lack of compatibility between different admixtures might also induce problems. Unlike the rheology of vibrated concrete which is mainly dominated by friction in between the aggregate particles, the rheology of SCC is governed by hydrodynamic interactions [21]. No adjustment of the intensity and duration of the vibration of the fresh concrete is possible.

Changes in the rheology can be caused by different types of variations:

- Changes in the mix proportions.
- Changes in the chemical of physical properties of the components.
- Changes in the mixing procedure.
- Changes in the temperature.

In the literature survey, the origins and mechanisms of these variations will be discussed in more detail. Often the robustness is only examined using empirical tests. Only few authors have conducted in depth research on the robustness of fresh SCC: Lowke investigated the robustness against segregation of the coarse aggregates, Kubens [22] has performed thorough research on the effect of changes in the material properties, the impact of variations in the temperature has been investigated by Schmidt [23], and Lesage [24] has examined the influence of combining different concrete admixtures on the robustness of SCC. In this thesis, an attempt is made to explore the underlying mechanisms of the robustness against variations in the water content.

4. Particle clustering inside SCC

When studying the sensitivity of the rheology to small variations, it is useful to understand the underlying mechanisms of the rheology. Because the macroscopically observed rheological behavior of SCC is determined by the interaction between the particle size distribution, particle clustering and the impact of admixtures and shear forces inside the mixture, an important part in this thesis is dealing with the mechanisms of flocculation and deflocculation inside SCC.

Next to a detailed literature survey, different possible measuring techniques have been investigated:

- Oscillatory reology: Applying a small amplitude oscillatory shear, the storage G' and loss modulus G" evolution in time can be monitored as a measure of the respectively elastic and viscous response of the fluid [25]. In this thesis, the storage modulus evolution in time is used to quantify the structural buildup of cement paste.
- Small Angle Light Scattering (SALS): This technique, used in polymer science and biology, investigates the scattered image generated by a polarized laser beam on a dilute suspension of particles [26]. In this thesis, an attempt was done to use this technique to study the flocculation and deflocculation of cement particles in a dilute water suspension.
- Ultrasound Acoustic Spectorscropy (UAS): By measuring the ultrasound amplitude losses for different frequencies, the attenuation spectra of a system can be determined. For colloid dispersions, emulsions, and dilute systems without particle-particle interactions, changes in the particle concentration and particle size distribution can be studied when the predominant loss mechanisms are known [27-29]. In this thesis, the application of acoustic spectroscopy on cement pastes has been investigated.

5. Research objectives

The main goal of this research project was, as the title suggests, to study the mechanisms involved in making SCC more robust and thereby facilitating the production of SCC. In many onsite applications, the use of SCC is limited by its inferior robustness, obstructing the use of this more durable, energy efficient, user-friendly concrete. Due to the large number of influencing factors, not every aspect governing the robustness of SCC could be investigated in depth in only one project. All important choices regarding the direction of the research were made with the following research objectives in mind:

- A fundamental understanding of the mechanisms governing the robustness of fresh SCC. Up to now, SCC is known to be less robust than vibrated concrete, but it is not understood yet why. It is also unclear why some SCC mixtures are more or less robust than other mixtures. This thesis aims to investigate the physics governing the robustness, and especially the role of the microstructure and particle clustering on the robustness.
- In literature, several approaches are used to evaluate the robustness of SCC. Some authors describe the robustness as the probability of failure,

others as the variations induced by certain changes. In this thesis, the best approach to define the robustness during experiments on concrete level, mortar level and on paste level will be evaluated.

- The development of certain practical measures enhancing the robustness of fresh SCC. Obviously, the conversion of fundamental research into useful applications for the concrete industry should never should never be overlooked. By implementing the theoretical knowledge of the mechanisms governing the robustness of SCC into practical guidelines, concrete producers can optimize SCC mix compositions in terms of the robustness.
- A fourth goal of this project is the evaluation of the potential use of new techniques to study the particle clustering and structural buildup inside fresh cement paste.

Chapter 2: Literature Review

1. Introduction

In order to understand the mechanisms governing the robustness of fresh concrete, it is necessary to study the microscopic origin of macroscopic changes occurring due to small variations in the mix composition. In such a context, a sound knowledge of the fundamental mechanisms and interactions governing the microstructure of fresh SCC is indispensable. An entire chapter of this thesis is devoted to a literature study summarizing the current state-of-the-art concerning the robustness of fresh SCC. Besides the robustness of fresh concrete, also the microstructure of fresh SCC, flocculation and deflocculation mechanisms, the working mechanisms of superplasticizers and VMA's, and the impact of the mixing procedure and shear forces are explored.

2. Robustness of fresh concrete

Until now, the fundamental mechanisms governing the robustness are still not clear. A lot of practical experience exists about which mixing parameters of the mix design affect robustness and what aspects of the mixing and casting process produce large variations.

2.1. Concept of robustness

The robustness of fresh concrete is defined as the capability of a mixture to tolerate small changes and variations inevitable with the production of concrete on any significant scale [2]. Examples of variations which can occur are weighting errors, other variations in the mix proportions, modifications in properties of the constituents, deviations of the mixing and casting procedures, and variations of the environment temperature. The robustness of self-compacting concrete depends on the mix composition, the mixing history and the application of the mix.

In order to compare the robustness of several concrete mixtures, a more quantitative approach is needed. Several approaches have been used in literature:

- Nunes et al [30] expressed the robustness as the probability that a mix fulfills the acceptance criteria for a certain application.

- Billberg and Westerholm [31] use the coefficient of variation (C.V.) of several workability parameters as the robustness value. Changes are induced by varying mix composition parameters[1].
- Billberg [32] and Kwan and Ng [33] defined the robustness value as the interval in which mix composition parameters can vary while still a satisfying mix is produced
- Billberg [31, 32] also proposed to express the robustness as the measured variation of a workability parameter due to a change of a certain mix composition parameter[2]. Most often, the workability / rheology area in workability box / rheogram is used as robustness value (Figure 3 [32]). The rheology area does not include the effect of variations on the stability of fresh SCC.

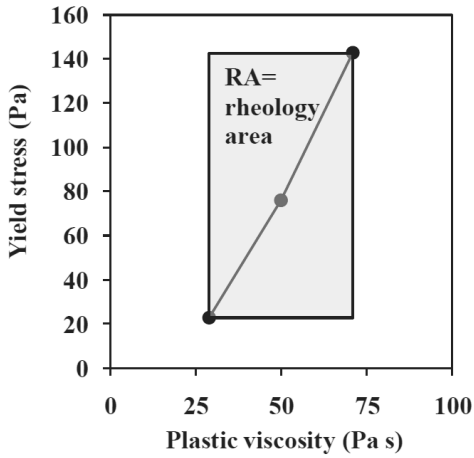

Figure 3: The rheology area as a measure of the robustness [32]

Compared to vibrated concrete, SCC is more sensitive to changes. Due to a more complex mix design, a lower yield stress, more stringent requirements, and the lack of possible adjustments to the intensity and duration of vibration [34-38], a decent quality control and skilled staff is mandatory for the production of SCC.

2.2. Origin of variations

Changes in the material properties, for example due to a new batch of one of the ingredients, can result in variations in the rheology. Although changes in the particle shape, void content and grading curve of aggregates affect the fluidity [39-

[1] According to this definition, the robustness of a mix composition increases as the C.V. of the workability parameter is smaller.
[2] According to this definition, the robustness of a mix composition increases as the C.V. of the workability parameter is smaller.

42], a proper quality control can avoid major problems [42]. Small quantities of clay present in the sand can have a large impact on the fluidity of SCC [43, 44]. The impact of fluctuations in the cement properties of constituent batches has been investigated in detail [22, 45-50]. The inclusion of superplasticizers enhance the sensitivity towards variations in the cement properties [45, 46, 48]. Mainly variations in the C_3A content, cement fineness, sulfate content, and Na_2O equivalent induce large changes in the fluidity of the produced concrete [46, 47, 51, 52] as these parameters are determining the adsorption equilibrium and ratio of adsorbed superplasticizer to cement surface area [53-56]. Differences in the chemical purity, physical properties, and molecular sizes of superplasticizers and VMA's in between different deliveries probably also have a major impact on the fresh properties of SCC, but less information about this subject is available in literature.

Another source of variations in the rheology are measuring inaccuracies [57, 58]. Rigueira et al. [59, 60] have examined which measuring inaccuracies cause the biggest fluctuations in the workability of SCC. Because the amount of admixture and cement are most often measured very precisely and the usual variations in the amount in sand and gravel only have a little influence, mainly variations in the amount of water cause problems with the workability [31, 32, 59-62]. Table 1 summarizes the allowed tolerances according to the standards ACI 117-90 [63], ASTM C94 [64], EN 117-90 [65] and the common errors in concrete factories based on an investigation of Rigueira et al. [59, 60]. A good mix design can withstand a variation of 5 to 10 l/m³ in water content without falling outside the specified classes of performance [6, 66].

Component	Limits ACI 117-90 [63] and ASTM C94 [64]	Limits EN 206-1 [65]	Limits comprising 90% of the cases studied in [59]	Usual range of errors in the cases studied in [60]
Cementitious materials	1%	3%	0.8%	0.79
Sand	2%	3%	1.5%	1.62
Gravel	2%	3%	3.5%	2.75
Water	3%	3%		
Admixture	3%	5%	0.8%	0.61

Table 1: Allowed measuring inaccuracies according to ACI 117-90, ASTM C94, and EN 117-90

Even small changes in temperature can induce severe problems in the workability of SCC. A raise in the temperature accelerates the hydration speed (reduces workability), slows down the sulfates dissolution (reduces workability), accelerates the PCE adsorption (improves workability), and increases the water absorption rate

of aggregates [34, 53, 54, 67-71], which can result in a higher or lower fluidity of the obtained SCC [68, 70, 72-76]. An accelerated growth of ettringite provides more adsorption sites for superplasticizers, which can improve the workability of SCC. Low temperatures cause a delay in the adsorption of superplasticizer and therefore enhance the workability retention [34, 77].

The charge density of the PCE molecules and water-to-powder ratio of the SCC mixture have a major impact on the robustness against temperature changes [34, 35]. SCC mixtures with PCE molecules with longer side chains or higher water-to-powder ratios are more sensitive to cold temperatures [23, 34, 35, 78]. SCC with a high charge density PCE or a low water-to-powder content is more sensitive at high temperatures [23, 34, 78]. It is unclear whether the inclusion of a VMA in the mix design can help to improve the robustness against changes in the temperature. According to Yurug et al. [79] welan gum can help to improve the robustness against changes in the temperature. Schmidt et al. [23, 78] state that diutan gum does not help to improve the robustness against changes in the temperature.

Alterations or deviations from the mixing procedure or casting methods also have an impact on the workability and workability retention. As described in Section 8 of this chapter, a different mixer or changes in the mixing time, speed or addition sequence will affect the mixing energy and therefore result in differences in the particles clustering and hydration kinetics. Differences in cement composition, superplasticizer type or environment temperature can lead to other influences from changes in the mixing procedure on the workability [80-83]. According to Asghari et al. [84], the robustness against changes in the mixing procedure depends on the mixing composition. SCC mixtures with a higher water-to-cement ratio are more sensitive to changes in the mixing procedure compared to changes in the water content and mixtures with a lower water-to-cement content were more sensitive to changes in the water content compared to changes in the mixing procedure.

2.3. Mix design parameters affecting the robustness

Most research concerning the robustness of SCC focusses on the sensitivity against changes in the water content. The focus on variations in the water content is normal, as measurement errors in this component cause most problems in practice [59, 60]. Below, a literature review is given on the mix design parameters affecting the robustness. Chapter 3 of this thesis will explain why certain parameters are important. Based on the literature review and additional experiments, a more fundamental theory concerning the robustness of fresh SCC will be developed.

2.3.1. Water content

When studying the impact of the water content of SCC mix designs, a distinction should be made between the filling water and the excess water in the mixture [85]: the filling water fills the voids in between the solid particles and the excess water forms a film on the surface of the solid particles. Mixtures with a higher water content or in which the solid particles have a larger maximum packing density, have a larger amount of excess water lubricating the mixture.

According to the Krieger-Doherty model describing the viscosity as a function of the packing density for suspensions of rigid spheres [86], mixtures with a higher water content should be more robust against small changes in the water content. As the amount of free water increases, the packing density decreases, which corresponds with lower inclinations of the Krieger-Doherty curve (Figure 4), indicating a lower sensitivity to changes in the amount of free water.

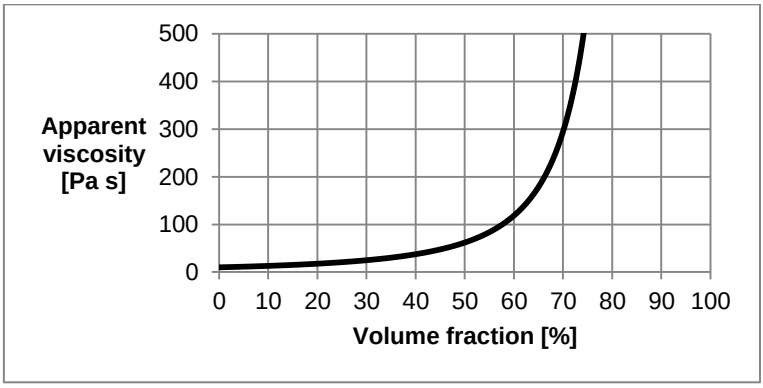

Figure 4: The Krieger-Doherty model of suspensions of rigid spheres [86][3]

The predicted higher robustness with a higher amount of free water is confirmed by experiments [87-89] showing an increase of the robustness when higher water-to-cement ratios and less water demanding powders are used. Also Eco-SCC, with an extremely high water-to-powder ratio and low paste volume has an exceptionally high robustness against small changes in the water content [90].

Kwan and Ng [33] investigated the robustness against variations in the superplasticizer content. The robustness decreases as the water-to-cement ratios increases.

[3] The numbers in the chart are merely indicative

2.3.2. Powder content and composition

Many authors report that an increase of the paste volume enhances the robustness against water variations [39, 91-94]. A higher paste volume separating the aggregates, allows the paste to be more viscous (in order to keep a similar concrete flowability), and therefore lowering the needed superplasticizer content [91-93]. Such a paste appears to be less sensitive to changes in the water content. A more viscous paste also enhances the robustness of the segregation resistance, as can be illustrated using the static segregation rate equation (Equation 1 and Table 2) [91, 95]. A higher paste volume also reduces the negative impact of bad aggregates grading curve or the use of crushed aggregates on the robustness [39, 94].

$$u_a = u_s \cdot \left(1 - \frac{\phi}{\phi_m}\right)^{5.18} = \frac{\left(\frac{(\rho_S - \rho_L)\cdot g \cdot d}{18} \cdot \tau_0\right) \cdot d}{\eta_{pl}} \cdot \left(1 - \frac{\phi}{\phi_m}\right)^{5.18} \quad \text{(Eq. 1)}$$

Symbol	Explanation
u_a	Segregation rate of the entire set of aggregates
u_s	Segregation rate of a single representative particle
ϕ	Volume fraction of aggregates
ϕ_m	Packing density of aggregates
ρ_s	Density of aggregates
ρ_L	Density of paste
g	Gravitational acceleration
d	Diameter of the representative aggregate
τ_0	Paste yield stress
η_{pl}	Paste plastic viscosity

Table 2: The symbols used in the static segregation rate equation (Eq. 1)

Besides the water-to-powder ratio, also the composition of the powder has an impact on the robustness of SCC mixtures. Low alkali cement, which contains less sulfates and C_3A content and producing less heat of hydration, is less robust than high alkali cement [96]. When a part of the cement is replaced by powder additions, a higher resistance against changes in the water content [6, 97] and superplasticizer dosage [66] is observed. Some authors suspect a possible link between the thixotropy and robustness [36, 98], but more research on this field is needed.

2.3.3. Superplasticizer type and dosage

The optimum dosage superplasticizer to obtain a maximum robustness differs from the optimum dosage to obtain a maximum slump flow without segregation [33, 66]. Lowering the superplasticizer dosage with an increase of the water-to-powder ratio or increasing paste volume helps to reduce the sensitivity against changes in the water content [87-89, 91-93].

Certain superplasticizer types result in a more robust SCC compared to others [37, 89, 96, 99-102]. Lignosulfonate [102], polynaphthalene sulfonate (PNS) [37, 99] and polyphosphonic (PPh) [101] based superplasticizers are reported be more robust against changes in the water content compared to polycarboxylate ether (PCE) based superplasticizers which are reported to be more robust against variations in the superplasticizer dosage compared to polysulfonate based superplasticizers [96]. A combination of multiple types of superplasticizers might be able to enhance the robustness [103]. However, care should be given to avoid unexpected interactions between different types of superplasticizers.

2.3.4. Viscosity Modifying Admixtures (VMA's, defined in Section 5.3.)

In literature, the robustness enhancing method most often mentioned is the addition of VMA's in a mix composition. VMA's are reported to enhance the robustness against variations in the water content, superplasticizer dosage, aggregate grading curve, and cement characteristics [31, 38, 79, 88, 93, 104-116]. The higher the water-to-powder ratio, the greater the robustness can be increased using VMA's, although the required dosage of VMA also increases [107]. In order to maintain the same fluidity, the superplasticizer dosage needs to be adjusted when using a VMA.

Nevertheless, as the definition of a VMA covers a wide range of products, not all VMA's will have a similar effect on the robustness [31, 37, 88, 105, 106, 117, 118]. Some VMA's are even reported to reduce the robustness of SCC [31, 88].

Explanations for these differences will be discussed in the next chapter, discussing the experimental results gathered in this project. Shindoh and Matsouka [115] suggested that the robustness enhancing effect of VMA's is caused by the improved segregation resistance. When using a VMA, higher dosages of superplasticizer can be added without static segregation of the coarse aggregates, meaning a broader range of superplasticizer dosages still leads to acceptable SCC mixtures. A more detailed explanation about the positive or negative impact of VMA's on the robustness will be discussed in the Chapter 3 of this thesis.

2.3.5. Aggregates grading curve

A proper aggregate grading curve is needed to obtain an acceptable segregation stability [2, 119]. The grading curve can be optimized to obtain a higher robustness [33, 91, 93-95] by increasing the ratio of fine-to-coarse aggregates [33, 91], decreasing the maximum size of the coarse aggregates [91, 93], and the use of rounded aggregates instead of crushed aggregates [94]. All measures lead to a decrease of the packing density of the aggregates and thus increased the paste

content available to lubricate the aggregates [120]. As the ratio of fine to coarse aggregates decreases, less superplasticizer is needed.

3. Hydration of fresh cement paste

During the first hours after mixing, different complex hydration reactions are occurring in fresh concrete, leading to an evolution of the rheology of fresh self-compacting concrete in time. In this section, a short summary of the main hydration reactions and their impact on the microstructure during the first two hours of hydration is described. Because the influence of admixtures will be discussed after describing their chemical en physical properties, only cases without admixtures are considered in this section. The presence of mineral fillers in SCC will also affect the hydration kinetics, depending on the morphology of the filler [121]. As this is not within the focus of the current research, it is not discussed in detail.

3.1. Early hydration chemistry

Cement powder consists mainly of two mineral phases and gypsum:

- The silicate phase, consisting of alite, an impure form of tricalcium silicate SiO_2 . 3 CaO (hereafter abbreviated as C_3S), and belite, an impure form of dicalcium silicate SiO_2 . 2 CaO (hereafter abbreviated as C_2S).
- An interstitial phase composed of two more or less crystalized phases: tricalcium aluminate Al_2O_3 . 3 CaO (hereafter abbreviated as C_3A) and tetracalcium aluminoferrite 4CaO . Al_2O_3 . Fe_2O_3 (hereafter abbreviated as C_4AF).
- Dependent on the type of grinding, part of the gypsum is dehydrated into calcium hemihydrate or completely dehydrated into anhydrite [52].

Immediately after contact of cement and water, the hydration reaction starts (Equation 2 and 3). The phases resulting from this dissolution – precipitation process can be predicted using a combination of thermodynamics and kinetics [122]. The hydration rate depends on thermodynamics, the chemical composition, the fineness, and the amount of reactive phases.

$$C_2S \,/\, C_3S + water = CSH + portlandite \qquad \text{(Eq. 2)}$$

$$C_3A \,/\, C_4AF + CaSO_4 + H_2O = ettringite + monosulphoaluminate \qquad \text{(Eq. 3)}$$

The hydration process of cementitious materials is divided into five stages as illustrated in Figure 5 [52]. The first liberation of heat and the dormant period will be discussed in more detail because of their impact on the workability and rheology of concrete.

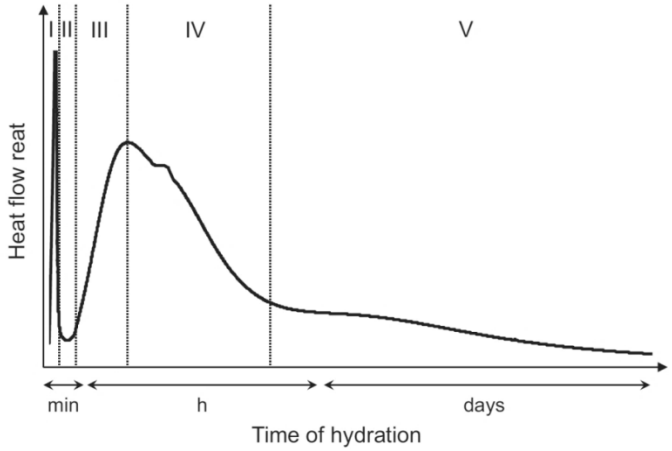

Figure 5: Five stages of the hydration process [52]

A fast dissolution of the anhydrous phases and the initial hydration of C_3A provokes a large exothermic peak. This first liberation of heat is considered as Stage I of the hydration reaction, also referred to as the initial dissolution period. During this stage, ettringite precipitates due to high reactivity of aluminates and availability of calcium sulfate.

After the first liberation of heat, a longer period of low chemical activity follows, manifested as a period of low heat release in Figure 1. During this period, referred to as the dormant period or induction period, the processes of Stage I continue: ettringite and C-S-H nuclei are formed and grow slowly [52, 71, 123]. The origin of the slowdown of dissolution rate is still a point of discussion [52, 122, 124]:

- **<u>Metastable barrier hypothesis.</u>**
  According to this hypothesis, a thin protective membrane of calcium silicate hydrates on the cement grains is assumed to block further dissolution and thereby slowing down the reaction. The barrier restricts the access to water and limits the diffusion of detached ions away from the surface of the clinker phases [125].
  However, the morphology of ettringite (needles) and C-S-H (precipitates as isolated clumps) differs fundamentally from C_3A and is unlikely to form a dense impermeable barrier layer blocking dissolution of an otherwise smooth or pitted surface [122, 124]. Moreover, no direct proof for this protective membrane hypothesis has been observed yet [52, 122, 126, 127]. Nuclear resonance reaction analysis (NRRA) results for hydrating triclinic C_3S has shown a thin continuous hydrated layer [128], but the necessary passivizing influence of this layer to effectively block the diffusion is unclear.

- **Slow dissolution step hypothesis.**

  Another theory assumes the slowdown of the reaction rate at the end of Stage I is a result of dissolution control of C_3A and C_3S [52, 126, 127, 129]. Dissolution is the detachment of molecular units from the surface of the cement grains in contact with water. The rate of dissolution depends on the undersaturation with respect to the dissolving phase. According to the dissolution step hypothesis, the high rate of dissolution is dominated by the formation of etch pits at dislocations of the clinker surface during Stage I. When the level of undersaturation decreases, the rate of dissolution is slowed down because the driving force is insufficient to activate etch pits openings. As a result, dissolution happens by the slower step retreat mechanism [124, 127, 129] during Stage II, explaining the rapid decrease in reaction rate when the undersaturation decreases.

  The formation of etch pits in Stage I has been confirmed by imaging techniques [127, 130, 131] and makes the presence of a barrier layer unlikely [127]. Studies of dissolution rates of C_3S in stirred suspensions also confirmed the slow dissolution step hypothesis [132]. Measurements of the activation energy of C_3S indicate the rate controlling step remains the same during early hydration [133]. The dissolution process of C_3A is slowed down by the adsorption of sulfates on active sites of C_3A [122].

At the end of the dormant period, two things happen almost simultaneously and mark the beginning of Stage III, the acceleration period: a rapid growth of CSH and precipitation of calcium hydroxide (Portlandite). According to the protective membrane hypothesis, the end of the dormant period is caused by a rupture of the protective membrane layer [71, 134] but cannot explain the precise and repeatable timing of the end of the dormant period [124]. The slow dissolution step hypothesis explains the onset of the acceleration period by a continuous increase of the concentration of ions during the dormant period up to the level of supersaturation, triggering the precipitation of Portlandite [52]. The formation of Portlandite increases the degree of undersaturation and therefore accelerates the dissolution of C_3S, inducing an acceleration of the CSH precipitation [52]. Nucleation and growth of CSH control the rate of hydration during the acceleration period [129]. The increase of the dissolution rate of C_3S results in a strong increase of the heat flow rate as illustrated in Figure 5 [52].

3.2. Morphology of early hydration products

The anisotropic growth of the hydration products depends on the rate of hydration and of the content of ions and admixtures in the pore water, resulting in different morphologies of ettringite and CSH. Hydrated lime $Ca(OH)_2$ is created in the crystalline form of Portlandite. The formed crystals are shown in Figures 6 to 9, originally from Aïtcin and Flatt [52].

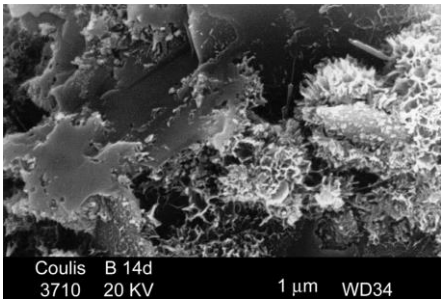

Figure 6: Calcium silicate hydrate (CSH) [52]

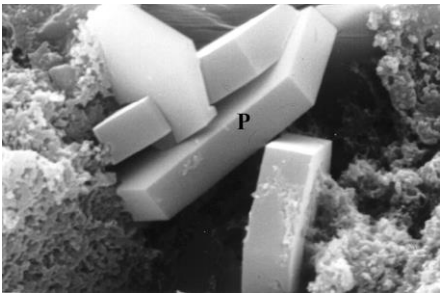

Figure 7: Portlandite crystals (CH) [52]

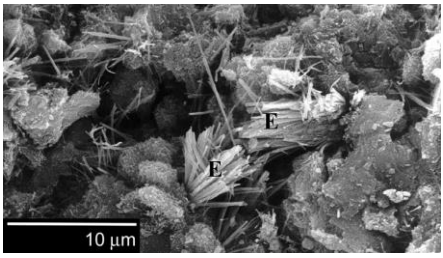

Figure 8: Ettringite crystals [52]

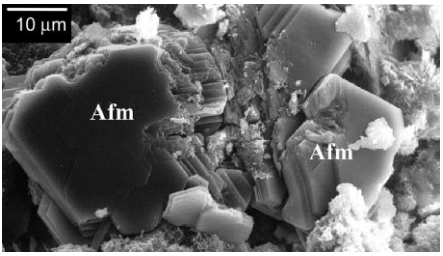

Figure 9: Hydrated tetracalciumaluminate crystals (Afm) [52]

CSH has two macroscopic morphologies: a fibrous and directional morphology on the surface of cement grains growing towards the pore space, and a more compact and homogeneous morphology formed in volumes of the cement grains originally filled by the anhydrous phase. The CSH precipitates formed on the cement grains during the dormant period are small sheets with dimensions 60x30x5 nm [135-137]. Several minutes after mixing, the CSH particles start building up a network inside of the fresh concrete [138, 139]. Because the network has a very low critical strain (10^{-4}), the cohesion is most probably a result of short range forces such as ion-ion correlations between the strong negative charge density of CSH particles in the presence of many counter ions [136]. At the end of the dormant period, CSH needles start to grow out from the disorganized CSH precipitates on the cement grains [140] as illustrated in the SEM pictures shown in Figure 10 [129, 141].

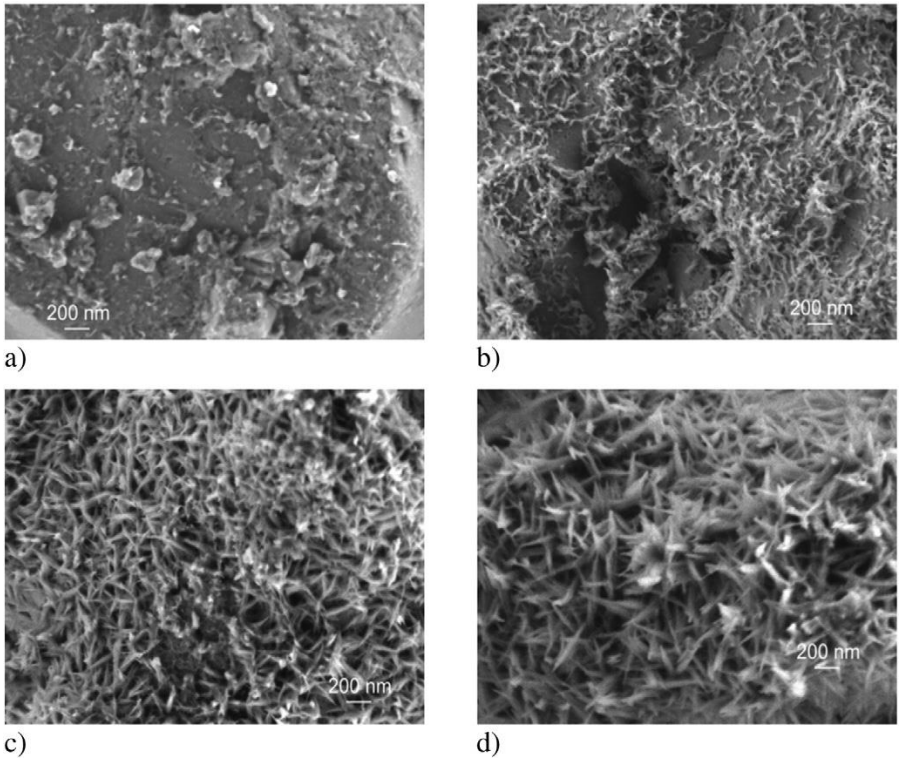

Figure 10: SEM observations of the growth of CSH at a) 1h30m, b) 3h, c) 6h, and d) 9h [129, 141]

C_3A is the most reactive clinker material and strongly influences the initial rheology. Dependent on the degree of supersaturation, ettringite presents different morphologies: from short hexagonal prisms to long needles [52]. Also the presence of Na^+ ions inside C_3A affects the reactivity of the C_3A and the crystal structure of the formed ettringite: Na^+ ions induce an orthorhombic crystal structure of ettringite, without Na^+ ions a cubic crystal structure occurs. As a result, less Na^+ ions result in more cubic C_3A and hence a more reactive C_3A [52].

The reaction rate of C_3A is also controlled by the adsorption of sulfates on C_3A, which slows down the dissolution process of C_3A [122]. When no more sulfate ions are available in the solution, a second sharp exothermal peak due to fast C_3A dissolution and faster precipitation of ettringite happens. The reactive ettringite and C_3A forms monosulphoaluminate. The morphology and composition of the formed aluminate phases and length of the dormant period is determined by the amount and origin of the sulfates in the cement [71].

Using high pressure freezing, Focused Ion Beam Nanotomography (FIB-nt), and a Scanning Electron Microscope (SEM), the evolution of the hydrating microstructure

of fresh cement pastes has been studied [142-145]. The high pressure (2 kbar) prevents phase transformations and the formation of artifacts inside of the fresh cement pastes during freezing, preserving the original particle arrangements. The impact of early hydration on the microstructure of unhydrated cement [143] is illustrated in Figure 11 [142]. The unhydrated cement contains almost no particles smaller than 500 nm. After 6 minutes, numerous submicron hexagonal prismatic crystal shaped ettringite particles are well dispersed in the interstitial phase [142, 143]. The increase of the amount of sub-micron particles is a result of the nucleation and precipitation of small crystal seeds and the fragmentation of particles containing fractures into distinct subgrains due to dissolution [143]. The early precipitations triple the specific surface of the cement paste during the first 6 minutes [142, 143].

Once the first liberation of heat (Stage I) is over, no large changes happen to the microstructure until the end of the dormant period [142, 144]. At the end of the dormant period, small interstitial grains will create bridges in between the larger particles and create a long range particle network [146].

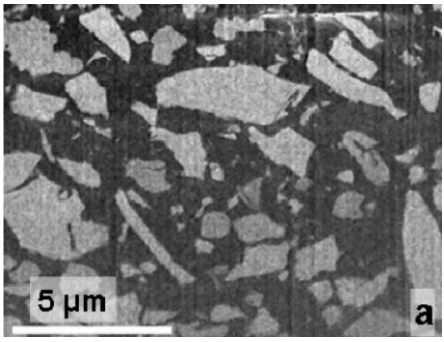

a) Unhydrated cement

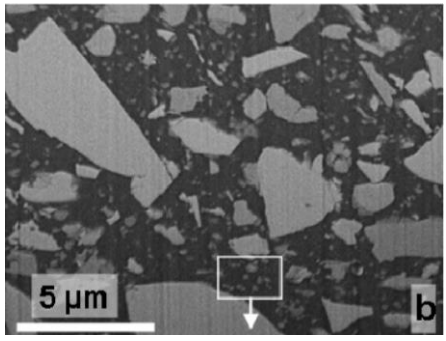

b) Cement paste at 6 min

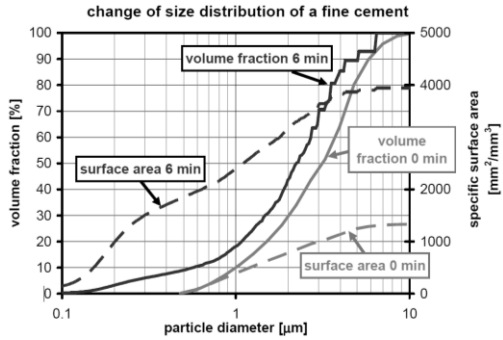

c) Particle size distribution before and after 6 min of hydration

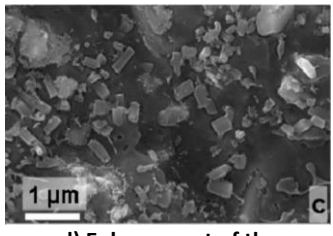

d) Enlargement of the interstitial domain

Figure 11: Impact of hydration on the particle size distribution [142]

4. Forces acting on particles inside fresh SCC

The complex interactions in between particles inside fresh concrete, ranging from fine fibrous early C-S-H phases of 20-40 nm up to coarse gravel particles of several centimeters, are governed by several interaction forces: Brownian motion, colloidal interactions, contact forces, hydrodynamic forces, and gravity of the earth [25, 52, 147, 148]. Dependent on the particle size, volume fraction, and external forces, one or two of these forces will dominate the others [149, 150].

Table 3 provides an overview of a rough estimate of the order of magnitudes of the various interaction forces on particles of a different size. The energy of most forces depends strongly on the surface properties and presence of admixtures for the smaller particles, and the shear rate for the larger particles.

Type of interaction	**Energy for particles of a given size [Nm]**						
	10 nm	100 nm	1 µm	10 µm	100 µm	1 mm	10 mm
Brownian motion	10^{-19}	10^{-19}	10^{-19}	10^{-19} *	10^{-19} *	10^{-19} *	10^{-19} *
Colloidal forces:							
Van Der Waals	10^{-16}	10^{-15}	10^{-14}	10^{-13}	10^{-12} *	10^{-11} *	10^{-10} *
Electrostatic	$0 - 10^{-18}$	$0 - 10^{-17}$	$0 - 10^{-16}$	$0 - 10^{-15}$	$0 - 10^{-14}$ *	$0 - 10^{-13}$ *	$0 - 10^{-12}$ *
Steric repulsion	10^{-21}	10^{-20}	10^{-19}	10^{-18}	10^{-18} *	10^{-17} *	10^{-16} *
Contact forces	10^{-36} *	10^{-31} *	10^{-26} *	10^{-21}	10^{-16}	10^{-11}	10^{-6}
Hydrodynamic forces							
Viscous drag forces	10^{-20} *	10^{-17} *	10^{-14} *	10^{-11}	10^{-8}	10^{-5}	10^{-2}
Inertia forces	10^{-20} *	10^{-17} *	10^{-14} *	10^{-11}	10^{-8}	10^{-5}	10^{-2}
Gravity	10^{-21} *	10^{-18} *	10^{-15} *	10^{-12}	10^{-9}	10^{-6}	10^{-3}

*) The interaction energy is negligible compared to other forces for this particle size

Table 3: Order of magnitude of the various interaction forces

4.1. Brownian motion

Brownian motion is the thermal movement in random directions (translational and rotational) of particles in a suspension. The energy associated with Brownian motion $E = \frac{1}{2}\, k_B\, T$ (with k_b representing the Boltzmann constant and T the temperature) is rather small compared to other particle interactions and only of importance for the microsized particles in the cementitious system.

4.2. Colloidal interactions

Three types of colloidal interactions are important in cement: Van Der Waals forces, electrostatic forces and steric repulsion forces.

4.2.1. Van Der Waals forces

Van Der Waals forces are weak short-range electrostatic attractive or repulsive forces between uncharged molecules arising from the interaction of permanent or transient electric dipole moments. The magnitude of Van Der Waals forces depends on the packing density, particle size and geometry, species adsorbed onto the

particle surface, and the nature of the liquid medium [151]. According to their origin, three types of Van Der Waals forces are distinguished: Keesom forces (two permanent dipoles), Debye forces (a permanent dipole and an induced dipole), and London-dispersion forces (two instantaneously induced dipoles).

The potential energy associated with Van Der Waals interactions is given in Equation 4, in which A is the Hamaker constant, R_1 and R_2 are the particle diameters, and r is the interparticle distance. During the calculation of the order of magnitude for all particles in Table 3, a Hamaker constant of 1.7 . 10^{-21} J [55] and an interparticle distance of 0.1 µm was assumed.

$$E = -A\frac{R_1 R_2}{6\,(R_1+R_2)\,r} \qquad \text{(Eq. 4)}$$

4.2.2. Electrostatic forces

Electrostatic forces are attractive or repulsive forces between particles with a respectively opposite or similar charge. The dissociation of surface groups and the adsorption of ions or ionic polymers in water provide a charge on the surface of the cement grains. This surface charge rearranges the ions present in the pore water into a specific ion distribution described by the double layer model of Goüy-Chapman: a Stern layer consisting of counter ions immobilized by the charged surface, and a diffuse layer of mobile ions, most of them with the same charge as the surface [52]. This ion arrangement results in an exponential decreasing electric potential as given in Equation 5 in which Ψ_0 is the surface potential and κ^{-1} is the Debye length, the thickness of the diffuse layer. The associated potential energy is given in Equation 6 in which k_e is the Coulomb constant, q and Q are the point charges, and r is the interparticle distance.

$$\Psi_{ES} = \Psi_0 \cdot \exp(-\kappa x) \qquad \text{(Eq. 5)}$$

$$E = k_e\frac{q\,Q}{r} \qquad \text{(Eq. 6)}$$

The high repulsive potential over the Debye length (typically a few nm) is a result from the overlap electric double layers, inducing a strong osmotic pressure. For suspensions with a high ionic strength, such as cement suspensions, the Debye length decreases and electrostatic repulsion is only felt at a very short distance, where the attractive Van Der Waals forces are predominant [52].

4.2.3. Steric hindrance

Steric hindrance is a force of entropic origin which prevents the flocculation of cement particles by adsorbing polymer molecules with long side chains. Particles are prevented to come too close together, as an overlap in electron clouds would result in a strong increase of the potential energy as the adsorbed polymers would have to distort from their preferred conformation. The steric repulsion depends on the thickness of the adsorbed layer (a few nm) and increases sharply once a particle enters the geometrical barrier created by the adsorbed polymer [152]. The steric repulsion potential can be determined using Equation 7 [153] or Equation 8 [154], using the symbols listed in Table 4.

$$E = \frac{4\pi \cdot k_b \cdot T \cdot {C_V}^2}{3\vartheta^2 \cdot {f_2}^2} \cdot (\psi_1 - \kappa) \cdot (\delta - d)^2 \cdot \left(3R + 2\delta + \frac{d}{2}\right) \quad \text{(Eq. 7)}$$

$$E = \frac{k_b \cdot T \cdot \Gamma \cdot \delta}{\sqrt{1/\Gamma}} \cdot \left(\left(\frac{2 \cdot \delta}{d}\right)^{2.25} - \left(\frac{d}{2 \cdot \delta}\right)^{0.75}\right) \quad \text{(Eq. 8)}$$

Symbol	Definition	Value used for Table 1
E	Steric repulsion potential	
k_b	Boltzmann constant	$1.381 \cdot 10^{-23}$ m² kg s^{-2} K^{-1}
T	Temperature	293.15 K
C_V	Concentration of the adsorbed polymer	
ϑ	Molecular volume of the solvent molecules	
f_2	Density of the adsorbate	
ψ_1	Entropy	
κ	Enthalpy	
δ	Adsorbed layer thickness	3 nm
d	Distance between two adsorbate particles	0.1 µm
R	Radius of the adsorbate	
Γ	number of adsorbate molecules per unit area of the surface	0.5 nm^{-2}

Table 4: Abbreviations used in Equation 7 and 8

4.3. Hydrodynamic forces

During shear flow, viscous drag forces result in energy dissipation. The order of magnitude of the hydrodynamic forces depends on the concentration of rigid particles, the particle size distribution, the shape of the rigid particles, the viscosity of the medium, and the density difference [151]. The drag force exerted by the paste on an aggregate with a certain size can be calculated using Equation 9, the associated kinetic energy using Equation 10, with symbols summarized in Table 5 [155, 156].

$$F_A = a\ b\ c\ \left(9\ \eta_{pl}\ \Delta V\ \left(\frac{\phi_1}{{r_1}^2} + \frac{\phi_2}{{r_2}^2} + \frac{\phi_3}{{r_3}^2}\right) + \pi^2\ \tau_0\ \frac{21}{4}\ \left(\frac{\phi_1}{{r_1}^2} + \frac{\phi_2}{{r_2}^2} + \frac{\phi_3}{{r_3}^2}\right)\right) \quad \text{(Eq. 9)}$$

$$E = \frac{1}{2}\, m\, v^2 \qquad \text{(Eq. 10)}$$

Symbol	Definition
a, b, c	Dimensions of the concrete sample (height, with, and length)
τ_0	Paste yield stress
η_{pl}	Paste plastic viscosity
ΔV	Difference in velocity between aggregate and paste
$\phi_1,\ \phi_1,\ \phi_1$	Volume fractions of different aggregates
r_1, r_2, r_3	Radii of the aggregates
E	Kinetic energy
m	Mass
v	Velocity

Table 5: Abbreviations used in Equation 9 and 10

For most particles, the inertia forces are negligible compared to other forces acting on the particle. Only for particles with a Reynolds number Re_p above 0.1 (Equation 11 [157]), the inertia is important. The symbols used in Equation 11 are summarized in Table 6. The inertial energy summarized in Table 3 corresponds with a flow speed of 5 m/s.

$$Re_p = \frac{\rho_s \cdot \dot{\gamma} \cdot D^2}{4\, \eta_s} \qquad \text{(Eq. 11)}$$

Symbol	Unit	Definition
Re_p	-	Is the particle Reynolds number
ρ_s	kg/m³	Is the density of the suspending medium
$\dot{\gamma}$	1/s	is the shear rate
D	m	Is the particle diameter
η_s	Pa s	Is the apparent viscosity of the suspending medium

Table 6: Abbreviations used in Equation 11

4.4. Contact forces

In dense particle suspensions such as SCC, direct contact interactions between the larger particles are happening. Contact forces can be continuously applied or delivered in a short impulse. Examples of contact forces are hard sphere collisions, friction, normal forces, and tension.

4.5. Bouyancy

Gravity forces can result in segregation of the coarse aggregates.

5. Admixtures

5.1. Introduction

When a polymer is added to a cement suspension, several mechanisms might occur [25]:

- Neutral interaction: The polymer does not interact with the particles and therefore does not affect the flocculation of the particles. The polymer might thicken the liquid phase.
- The flocculation of the particles can decrease when parts of the polymers adsorb onto the particle surface and other parts protrude into the liquid phase.
- Bridging flocculation: High molecular weight macro polymers anchor particles by attractive Van Der Waals forces. Most often bridging flocculation leads to relative strong agglomerates which can resist high shear stresses.
- Depletion flocculation: because large polymers are excluded from the small gaps in between particles, an osmotic pressure pulls all water out of these small gaps and brings particles closer together. The agglomerate strength is generally relatively small.

In this section, the influence of superplasticizers and Viscosity Modifying Admixtures (VMA's) on the hydration and particle forces in a fresh SCC is discussed. Although many other superplasticizer types can be used to make SCC, this section only deals with polycarboxylate (PCE) superplasticizers, the most commonly used superplasticizer type in SCC. Also discussing lignosulphonates, polynaphthalene sulphonates (PNS), polymelamine sulphonates (PMS), or other types of superplasticizers would result in a too expanded discussion.

5.2. Polycarboxylate (PCE) superplasticizers

5.2.1. Working mechanism

Polycarboxylate ethers, polycarboxylate esters, polycarboxylates or also called PCE molecules are superplasticizers consisting of a main chain (referred to as the backbone) bearing carboxylic groups to which non-ionic side chains made of polyethers are attached (Figure 12 [52]). The carboxylic groups give a negative charge to the backbone, required for adsorption onto the positively charged cement particles. A great diversity of chemically different PCE products are available on the market: MPEG-type PCE's, APEG-type PCE's, VPEG-type PCE's, HPEG-type PCE's, IPEG-type PCE's, XPEG-type PCE's, and PAAM-type PCE's [158].

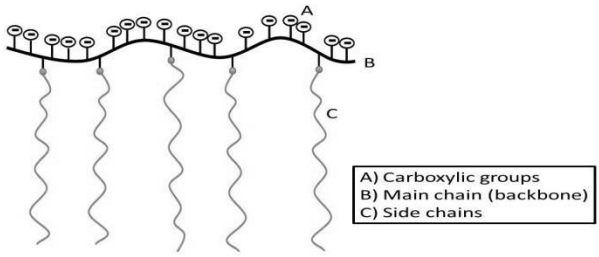

Figure 12: The molecular structure of PCE superplasticizers [52]

Two effects contribute to the working mechanism of PCE molecules: negatively charged carboxylate groups adsorb onto positively charged surface areas of hydrating cement while the non-adsorbing polyethylene glycol side chains intrude in the interstitial pore space and provide the steric hindrance onto the surface of the cement particles [52, 71, 159]. As a result, the effectiveness of PCE superplasticizers is determined by the amount of adsorbed molecules and the conformation in their adsorbed state [160]. Both effects depend on the properties of the cement grains and the molecular architecture of the PCE molecules [23, 53, 55, 56, 142, 161-166].

The adsorbed amount of PCE molecules onto the cement surface depends on the dosage of superplasticizer, the available surface of cement, competitive adsorption, the anionic charge of the backbone, and the flexibility and stiffness of the backbone [53-56, 160]. The adsorption happens preferentially onto the interstitial phases of the cement grains, ettringite and monosulphate [167, 168]. A part of the PCE molecules can be lost due to the formation of organo-aluminate phases during hydration or by adsorption onto clay minerals [44]. The competitive adsorption with sulfates, hydroxyls, retarders or other molecules is governed by their relative affinity for cement surface and their relative concentrations [53, 160].

The thermodynamic condition for adsorption is given in Equation 12 [169], in which ΔG_r is the Gibbs free energy [J], needed to be negative to allow adsorption spontaneously, ΔH_r the reaction enthalpy [J], T the temperature [K], and ΔS_r the reaction entropy [J/K]. Langmuir isotherms can be used to describe the adsorption of PCE superplasticizer [169].

$$\Delta G_r = \Delta H_r - T \cdot \Delta S_r < 0 \qquad \text{(Eq. 12)}$$

The spontaneous adsorption of superplasticizers is a result of four energy contributions [169]:

- **Attractive energy $\Delta H_r < 0$**
  The attractive energy between the carboxyl groups (COOH) and the cement surface decreases with higher anionic charge densities [169] and decreases when more counter ions such as chlorides or sulfates are present in the pore solution [53, 55, 56, 170]. The release of enthalpy due to this lower energy state is the driving force of the adsorption of PCE molecules with short side chains.
- **Entropic gain from the release of counter ions $\Delta S_r > 0$**
  The release of counter ions from the cement surface into the pore solution results in an entropic gain [169]. This contribution decreases with higher anionic charge densities of the PCE molecules and increases with increasing concentration of Ca^{2+} ions in the pore solution [169]. For PCE molecules with long side chains, the entropic gain from the release of counter ions determines the adsorption equilibrium.
- **Electrostatic repulsion by PCE adsorbed on the cement surface $\Delta H_r > 0$**
  Adsorbed PCE molecules on the cement surface induce an increase of the electrostatic repulsion towards PCE molecules still in solution [169], resulting in an increase of the enthalpy in the system.
- **Entropic loss due to a reduced mobility after adsorption $\Delta S_r < 0$**
  PCE molecules loose part of their mobility by being absorbed onto the cement surface, resulting in an entropic loss.

Because PCE molecules only have a low electrostatic charge and the pore solution has a high ionic strength, the electrostatic contribution can be ignored compared to the dispersing effect of steric repulsion [56]. The steric repulsion force depends on the amount and thickness of the layer of adsorbed PCE molecules [171], which on itself depends on the side chains length of the PCE polymers [172, 173].

5.2.2. Impact on rheology and workability retention

PCE superplastizers are the perfect example of how small changes on nanoscale can have an immense impact on the macroscopic rheological behavior of concrete: the increase in repulsive forces results in a lower yield stress of the cement paste [174, 175] (Section 6.1). The influence on the plastic viscosity and shear thickening is less clear [174-180].

In order to explain why different types of PCE superplasticizers have another influence on the plastic viscosity and thus stickiness of SCC [176, 177, 179], a better understanding of the mechanisms governing the energy dissipation in flowing concrete is needed. Krieger and Dougherty [181] suggested in 1959 energy

dissipation during flow concentrates in strongly sheared fluid layers between neighboring particles in mixtures with a high solid volume fraction. Superplasticizers can therefore affect the plastic viscosity in two ways: modify the thickness of the fluid layers which are sheared, and modify the viscosity of the sheared fluid layers. More recently, several mechanisms have been suggested by various authors:

- **Larger fluid layers in which shear concentrates [177]:**
  According to Hot et al. [177], more free water is available in the mixture when superplasticizer disperses the cement particles. As a result the thickness of the fluid layers of interstitial fluid in which shear concentrates increases, reducing the viscous dissipation of energy during flow. This mechanism does not explain the different impact of various PCE superplasticizers.
- **PCE molecules increase the viscosity of the pore water [177].**
  Hot et al. [177] observed that highly adsorbent PCE types result in a lower plastic viscosity compared to weakly adsorbent PCE types for the same dispersion state and proposed the following hypothesis: for a similar dispersion state, more weakly adsorbing PCE molecules would be present in the pore water, increasing the viscosity of the pore water, and thereby increasing the plastic viscosity of the cement paste.
- **PCE molecules as lubricant in the pore solution [182-184]**
  The lubricating effect of non-adsorbing polymers present between densely packed cement particles has been suggested as a possible mechanism to explain the reduction of stickiness observed when non-adsorbing non-ionic polymers such as di-ethylene glycol and polyether amine were used in SCC with low water-to-cement ratios [182, 183]. Perhaps similar mechanisms reduce the viscosity when PCE molecules are present in the mixing water.
- **Polymers with a higher grafting ratio increase the local viscosity in the shear zones [177].**
  PCE superplasticizers with a higher grafting ratio will induce a higher density of side chains in the gap between grains, leading to higher local viscosities in this gap and thus a higher plastic viscosity of the cement paste.
- **Changing the anionic charge of the pore solution [185]**
  To explain why phosphate polymers reduce the plastic viscosity of concrete with a low water-to-cement ratio, Stecher and Plank [185] have suggested that phosphate groups with a high affinity towards calcium ions might reduce the anionic charge of the pore water solution.
- **Superplasticizers affect the surface tension of water [142].**
  Different types of superplasticizers will affect the surface tension of the pore water and therefore influence the air bubble size distribution. A more hydrophobic superplasticizer will result in a lower surface tension and reduce

the air bubble size. At high shear forces (in a sticky SCC), the small air bubbles become deformable and their size affects the macroscopic observed plastic viscosity.

- **The hydrophilic – lipophilic balance (HLB) value [158, 186, 187]**
  When the hydrophilic-lipophilic balance (HLB) value of a PCE molecule is above 18.5, the PCE molecules are very hydrophilic resulting in a much lower plastic viscosity of the produced SCC [158, 186, 187]. The actual mechanism causing a reduction in the plastic viscosity is still unknown. Both the influence of PCE on the surface tension of the interstitial water [188] and weak hydrophobic Van Der Waals interactions in between the polymers absorbed on the cement surface [186] have been suggested as possible mechanisms.

The workability evolution in time depends on the superplasticizer type and dosage. Both the increase of the surface area, the amount of PCE polymers in solution and the decrease of the sulfate content of the pore water in time determine the evolution of the main parameter determining the workability evolution: the ratio of adsorbed PCE molecules to the surface area of the solid phase [53, 54, 162]. The evolution of the surface area of the solid phase depends on the particle size distribution of the powders and the hydration reactivity of the cement during the first hours. Polymers with a lower amount of charges on the backbone (lower initial adsorption) and short side chains provide an extended workability in time [162, 164]. Because a high dosage of superplasticizer is added to SCC, significant amounts of PCE do not adsorb immediately after mixing but upon the formation of ettringite. As a result, the formation of ettringite – which reduces the workability of systems without superplasticizer – can enhance the flowability of SCC [34].

5.2.3. Superplasticizer and early cement hydration

PCE superplasticizers retard the hydration of the silicate and aluminate phases of cement [159, 161, 189-198]. The induction period is prolonged more with increasing charge density, also resulting in more adsorbed PCE molecules. After an extended dormant period, ettringite and portlandite precipitate almost simultaneously in presence of PCE superplasticizer – which does not happen when no superplasticizer is added [190, 191]. Due to the dispersive action of superplasticizer, the acceleration phase has a faster hydration rate [196].

Up to now, the mechanism by which superplasticizer prolongs the dormant period is not clear. The following hypotheses have been proposed in literature [159]:

- **Complexation of calcium ions in the pore solution:**
  As a result of the formation of chelates of PCE molecules and calcium ions, the concentration of calcium ions in the pore solution decreases [190-192, 196, 198], which slows down the buildup of supersaturation needed for hydrates nucleation. Many authors doubt the existence of the calcium-PCE chelates [161, 189, 193].

- **Absorbed PCE molecules slow down dissolution of the anhydrous phases [189-191, 196]:**
  Some authors claim the adsorbed PCE also induces changes in the ionic composition of the aqueous phase, affecting as well phase diffusion, nucleation and growth of the hydration reaction [161, 190-193]. Others claim the PCE has no influence on the pore solution [189]. This hypothesis explains why PCE which adsorbs best (higher charge density) slows down the most [199], but does not explain why both the hydration of C_3A and C_3S is retarded to the same extend, as C_3A sites with a higher opposite charge have a preferred adsorption of PCE [191].

- **Changes in the nucleation, growth, and shape of the hydrate phases [161, 193, 196, 200]:**
  Adsorbed PCE alters the morphology and therefore growth kinetics of nuclei [142, 194, 195]. Because the rate determining mechanism during the dormant period is the dissolution of anhydrous phases and not the growth of hydrates, this hypothesis cannot explain the observed extension of the dormant period.

The shape and size of the early hydration products is affected by the presence of superplasticizer (Figure 13 [144]). When a mixture contains no superplasticizer (Figure 14b [142]), most of the smaller hydration products (< 500 nm) are attached to the surface of the unhydrated clinker grains (2-5 µm) and create irregularly shaped hydration rims around the clinker particles [142, 144]. Ettringite particles form agglomerates (1-3 µm), bridging the larger clinker particles and creating an interconnected particle network. Few submicron particles remain in the interstitial pore space [142-144].

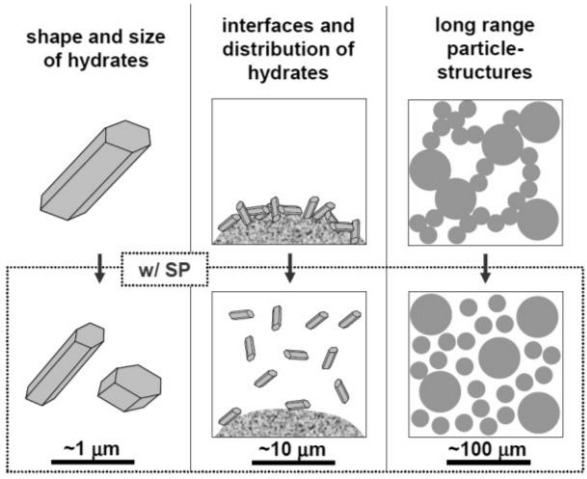

Figure 13: Impact of PCE superplasticizers on the hydration of cement [144]

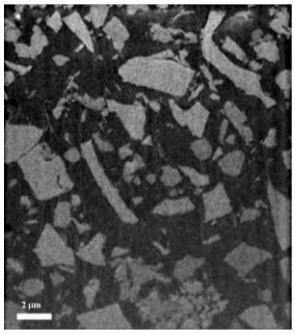

a) Unhydrated cement in a frozen glycol matrix

b) Cement paste not containing superplasticizer at 24 minutes

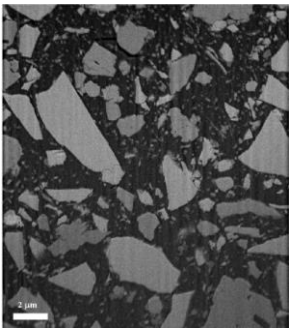

c) Cement paste with superplasticizer at 6 minutes

Figure 14: Influence of superplasticizer on the cryo-FIB images [142]

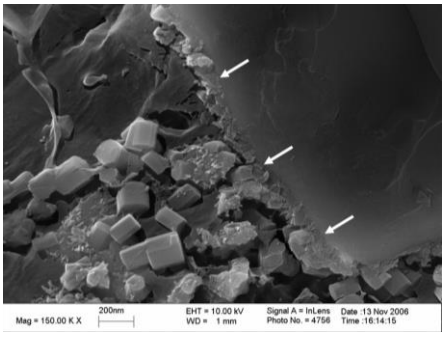

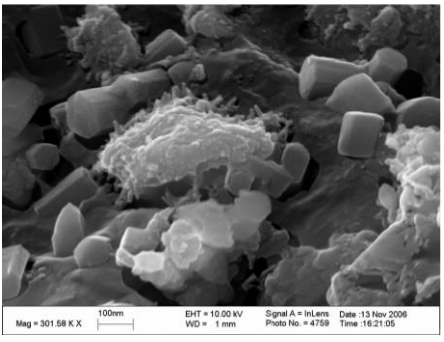

Figure 15: Enlargements of cryo-FIB images of superplasticized cement [142]

The appearance of a superplasticizer slows down the ettringite precipitation [145] and disperses the hydration products in the interstitial pore space, preventing the precipitation of ettringite crystals onto the clinker surface (Figures 14 and 15 [142]). Because the small hexagonal and short-prismatic ettringite particles in the pore space (100-500 nm) do not create agglomerates, no flocculation of the larger clinker particles is happening [142, 144]. A second type of hydration products are fine fibrous early C-S-H phases, agglomerated and partially intergrown with ettringite crystals, forming a rim (0-20 nm) of small fibrous crystals embedded in a gel-like mass on the clinker particles [142]. The inclusion of a superplasticizer increases the precipitation of ettringite and reduces the size of the ettringite crystals, resulting in a 6 times higher specific surface area of the ettringite particles [145].

5.2.4. Incompatibilities

Incompatibilities between cement and PCE superplasticizers can lead to early stiffening or slump loss. An unexpected insufficient dispersion – related to an insufficient PCE adsorption – is caused by either PCE consumption by organo-mineral phases [161, 170, 193, 201-206], competitive adsorption with sulfates [53, 54, 206-208], or adsorption of PCE on clays [44].

The amount of sulfates determines how much superplasticizer will be adsorbed or intercalated by aluminate hydrates. Below a certain threshold, the formation of organo-mineral phases will easily consume a large part of the PCE molecules, making them unavailable for cement dispersion. When sufficient sulfates are available, part of the PCE intercalates. However, most PCE molecules adsorb onto the cement grains and disperse properly. An excess of sulfates dominates in competitive adsorption with PCE and therefore blocks the adsorption of PCE, preventing a proper dispersion.

Part of the superplasticizer is consumed by intercalation, the formation of new organo-mineral phases which fix part of the superplasticizer [201, 202, 204, 205]. Less intercalation is occurring with PCE molecules with larger side chain lengths and a higher side chain density as more steric hindrance is occurring [161, 190, 193, 203, 204]. An excessive steric size of PCE molecules can prevent intercalation [205]. Delayed addition of the superplasticizer during the mixing procedure can reduce the amount of lost superplastizer [198, 206, 209, 210].

Certain PCE types suffer from a lack of robustness. Small changes in the C_3A or alkali sulfate content of cement should not result in excessive changes of the fluidity [53, 142, 203, 208]. PCE molecules with longer backbones or side chains are more resistant to changes in the sulfate content [53]. The sensitivity of PCE to

competitive adsorption with sulfates depends on the architecture of the PCE molecules: polymers with small side chains and larger grafting degree are less sensitive PCE molecules [207, 211].

The last problem discussed is a lack of fluidity retention. When only little unabsorbed superplasticizer is present in the pore solution after mixing, the workability of the mixture will decrease rapidly [53]. As the specific surface area of the mixture continuously increases during hydration, more and more superplasticizer should be adsorbed to maintain the same fluidity. The competitive adsorption of PCE with sulfates helps to keep more superplasticiser in the pore solution.

5.3. Viscosity Modifying Admixtures (VMA's)

Viscosity Modifying Admixtures (VMA's), also referred to as Viscosity Enhancing Admixtures (VEA's), can be added to enhance the cohesion of concrete, shotcrete, underwater concrete, and cement grouts. In SCC, VMA's are mainly used to provide stability against segregation or to improve the robustness of SCC [212]. In this section, the classification of different types and working mechanisms of VMA's are clarified together with their interaction with superplasticizers or the cement hydration reaction.

5.3.1. Classification

A wide range of materials can enhance the cohesion of concrete and therefore be considered as a VMA [213]. Because the working mechanisms of the different types of VMA's are still a matter of debate, a classification based on the molecular structure has been used in this chapter, similar to the ones proposed by [52, 214, 215]. Other authors have proposed classifications based on the assumed working mechanisms [216-218].

A. Natural polymers
    i. Starch
    ii. High molecular weight microbial polysaccharides
B. Semi-synthetic polymers
    i. Cellulose ether derivatives
    ii. Modified starch
    iii. Guar gum derivatives
C. Synthetic polymers
    i. Polyethylene oxide
    ii. Polyacrylamides
    iii. Polyacrylate
    iv. Polyvinyl alcohol
D. Inorganic powders
    i. High specific surface area inorganic powders
    ii. Swelling clays

5.3.2. Working mechanism

Different mechanisms may contribute to the increase of the plastic viscosity of SCC:

5.3.2.1. Fixing part of the mixing water [115, 216, 219-222]

According to this hypothesis, hydrophilic parts of the polymers could adsorb and immobilize part of the mixing water by hydrogen bonds. As a results, less free water is available and VMA molecules inside the mixture swell, leading to an increase of the interstitial solution viscosity and consequently also the macroscopic viscosity. This mechanism is sometimes referred to as part of the viscosity increasing action of welan gum and diutan gum.

5.3.2.2. Association and intertwining between polymers [25, 160, 216, 220, 223-225]

At low shear rates, polymer chains might interact with each other and build a three dimensional network of associated polymers, blocking motion of the interstitial water and thus increasing the macroscopic observed viscosity of the mixture. Also polymer entanglement at higher concentrations can enhance the viscosity. Under shear, the three dimensional network is broken and polymers align with flow, resulting in a decrease of the apparent shear rate. No polymer adsorption onto the clinker surface is necessary for this mechanism.

Association and intertwining between polymers is most commonly mentioned as the working mechanism for welan gum and diutan gum [2, 23, 105, 106, 216, 223, 226]. Some authors suggest cellulose ether derivatives [216-218, 225, 227-231], modified starch [218, 225, 232] and certain types of synthetic polymers [217, 218, 225] obtain their viscosity enhancing effects due to this mechanism.

5.3.2.3. Bridging flocculation [2, 25, 160, 216, 220-222, 225, 233-235]

The bridging flocculation mechanism occurs when hydrophilic high molecular weight macropolymers adsorb onto the cement surface and physically hold two or more cement particles together by attractive Van Der Waals forces, increasing the flocculation of cement particles in the concrete. Bridging flocculation leads to relative strong agglomerates and therefore a significant increase of the macroscopic observed yield stress [25]. Competitive adsorption between adsorbing VMA molecules and the superplasticizer might also lower the superplasticizer efficiency [2, 233, 236-238].

Cellulose ether derivatives [2, 216, 233, 236-240] and synthetic polymers [2, 225] are often mentioned as examples of polymers causing bridging flocculation. Some authors also assume high molecular weight microbial polysaccharides [217, 218,

225, 234, 235, 241] and clays [217, 218, 225, 232, 234, 235] adsorb and favor flocculation

5.3.2.4. Depletion forces [23, 25, 160, 222, 242, 243]

Non-adsorbed polymers with a large size are depleted from a *'volume exclusion shell'* around larger cement particles, inducing a concentration difference in polymers and therefore osmotic pressures. According to the depletion forces hypothesis, this osmotic pressure is responsible for an increase in the flocculation of cement particles.

Some authors suggest depletion forces are the working mechanism for cellulose ether derivatives [243] or high molecular weight microbial polysaccharides [222]. However, because the dosage of VMA is always much too low to generate depletion forces [23], it is unlikely depletion forces are the real viscosity enhancing mechanism inside SCC. The steric hindrance forces from PCE superplasticizer molecules are also much stronger than the osmotic pressure generated from depletion forces [52].

5.3.2.5. Summary

It is still a matter of debate which mechanisms induce the viscosity enhancing effects of VMA's. Most probably, different types of VMA's are controlled by other mechanisms. In many cases, the stabilizing effect of VMA is affected by the use of a superplasticizer [244].

It is unclear whether high molecular weight microbial polysaccharides such as welan gum and diutan gum can still adsorb on the cement surface in the presence of PCE superplasticizers: some authors argue they adsorb and provide attractive forces in between the cement particles [217, 218, 241], others claim the superplasticizer will win the competitive adsorption for cement surface and the increase in viscosity is solely due to the increase in the viscosity of the interstitial water [23, 105, 106, 226].

Several working mechanisms are mentioned to explain the viscosity-enhancing effect of cellulose ether derivatives. Most authors advocate bridging flocculation [2, 216, 231, 233, 236-240], others association and intertwining between polymers [217, 218, 227-230]. Recently, it has been suggested that a critical concentration exists below which the viscosity-enhancing effects are mainly due to the increase of the viscosity of the interstitial solution, and above which the associative nature of cellulose ether molecules induces cellulose ether aggregates of a few µm which further increase the viscosity of the interstitial fluid [229, 230].

5.3.3. Impact on hydration

Most polysaccharides used as a VMA induce a retardation of the hydration reaction, manifesting itself as an extension of the induction period [219, 221, 227, 245-252]. The precipitation and growth of hydrates are more affected than the dissolution of anhydrous particles [245, 251]. The impact on the acceleration period depends on the used VMA.

Several possible causes have been explored.

- **Poisoning of the hydrate products:**
  This hypothesis claims the retardation of VMA polysaccharides is caused by similar mechanisms as for the retardation induced by sugars: poisoning of the hydrate products prevents them to grow despite the accelerated initial dissolution of ions, resulting in a homogeneous nucleation of small nucleates instead of the attachment of ions to existing poisoned sites (heterogeneous nucleation) [245, 252-254]. When no more sugar is available to poison the nucleation sites, future sites are no longer poisoned and an accelerated hydration starts due to an excess of ions in the pore solution [255].
- **Incorporation of VMA's into the crystal structure of hydrates:**
  According to this hypothesis, the growth of hydrates is slowed down by the incorporation of admixtures into their crystal structure [256].
- **Formation of a less permeable coating on the cement surface:**
  Adsorbing VMA's are assumed to form a diffusion barrier on the surface of the first hydrates, preventing the transport of ions necessary for hydrate growth [248, 257]. The assumption of a diffusion barrier induced by VMA's is considered as very improbably by Pourchez et al. [250].
- **Complexation of the rate controlling alkalis:**
  Complexation between VMA's and calcium ions is assumed to decrease the level of saturation in the pore solution and therefore to slow down the growth of hydrates [258]. However, the amount of VMA molecules is far too low to have an impact on the high concentration of calcium ions [221] and the complexation of calcium ions by cellulose ethers is negligible [252, 259]. Therefore, this hypothesis is probably not at the origin of the observed retardation of the hydration reaction.
- **Additional nucleation sites:**
  Inorganic powder VMA's, such as microsilica and nanosilica slurries provide additional nucleation and growth surfaces consuming ions and therefore accelerating the cement hydration [117].

6. Particle clustering

The macroscopic rheology is a culmination of several complex interactions: effects from the packing density, the particle size distribution, the particle shape, the surface properties for all constituents, and the presence of admixtures in the concrete mixture. As a result, some understanding of particle packing [260, 261], the physics of granular media [149, 150], hydration chemistry [262], colloidal chemistry, and polymer chemistry is needed in order to understand the rheological behavior of concrete [148]. The dispersion of fines is of major importance and will be explored in more detail in this section.

6.1. Equilibrium of forces

Due to the broad poly-dispersity of SCC, several interactions happen within the particles in suspension (described in Section 4 of this chapter). Dependent on the volume fraction and external forces, one of these forces dominates the flow behavior of a particle with a certain size [149, 150, 263]. Figure 16 [149] summarizes the predominant interactions governing the macroscopic observed yield stress of non-plasticized cement paste [149]:

- Brownian motion forces are always dominated by Van Der Waals forces.
- Above the percolation volume fraction ϕ_{perc}, direct contacts or distance interactions occur between the cement particles. The suspension has a yield stress governed by Van Der Waals forces. The percolation volume fraction ϕ_{perc} is the critical solid fraction below which the suspension has no yield stress. Above this volume fraction (20-40% for cement suspensions), the material has a network of colloidal interactions resisting deformations up to a certain yield stress [149].
- As the solid volume fraction increases, the soft repulsive interactions between cement particles become less capable of resisting the normal forces and direct contact forces between the rigid cement grains.
- At the transit volume fraction of about 0.8 ϕ_{div}, the yield stress becomes dependent on a direct contacts network instead of the Van Der Waals forces. The transit volume fraction of about 0.8 ϕ_{div} is the volume fraction at which direct contacts network forces dominates the Van Der Waals forces.
- Above a divergent volume fraction ϕ_{div}, the yield stress and viscosity rise sharply. A very high shear stress is needed in order to deform the network of rigid grain to grain contacts. The divergent volume fraction ϕ_{div} is the volume fraction at which the yield stress becomes dominated by rigid grain to grain contact forces.

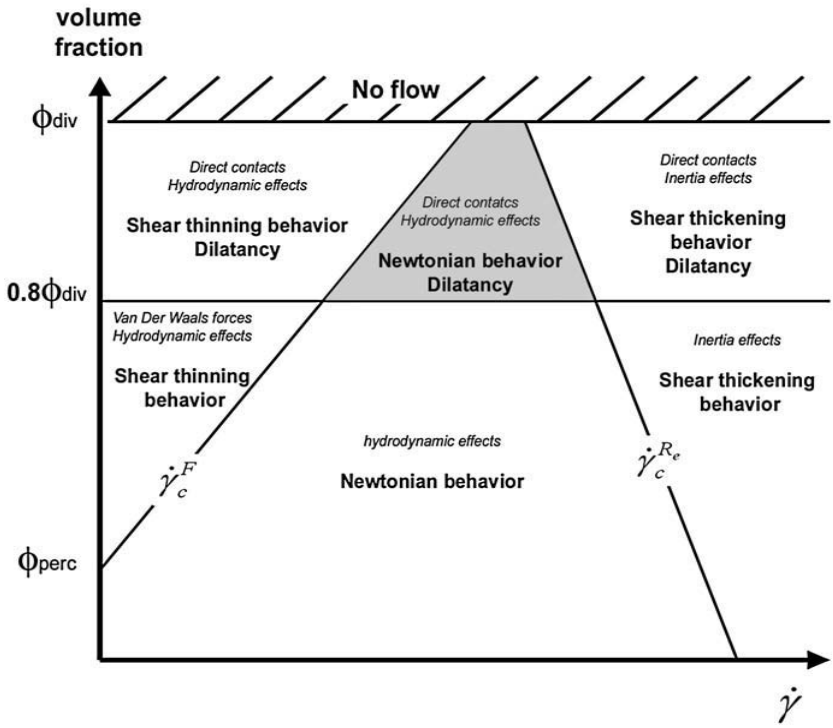

Figure 16: Impact of the shear rate and volume fraction on the rheological behavior of cement paste [149]

In non-plasticized concrete mixtures, Van Der Waals forces dominate and will create a contact network by particles flocculation some seconds after mixing [264]. Especially the fraction of particles with sizes smaller than 1 µm – which is about 10% of the cement weight – are flocculating and form a three-dimensional network in the fresh concrete mixture, macroscopically manifesting itself as the yield stress of the concrete mixture [21, 149, 265-270]. When a PCE superplasticizer is added, steric repulsion forces will oppose the attractive Van Der Waals forces, resulting in a lower yield stress. When too much superplasticizer is added, the repulsive forces can start dominating over the attractive forces for the smallest colloidal particles, destroying the colloidal network and thereby leading to syneresis, more often referred to as bleeding [271].

As the energy dissipation during flow concentrates mostly in strongly sheared fluid layers in between neighboring particles [181], the plastic viscosity of concrete is mainly dependent on the volume fraction of solid particles and how densely they are packed [270], modifying the thickness of the fluid layers which are sheared. Admixtures might have an impact on the viscosity of the sheared fluid layers, as described in Section 5.2.2. of this chapter.

6.2. Structural buildup at rest

Flocculation of colloidal cement particles at rest manifests itself as a macroscopic structural buildup of the fresh concrete and can be monitored using static yield stress measurements or oscillatory rheology. The structural buildup inside fresh concrete consists of two contributions: a reversible part which will rebuild itself after breaking, also referred to as thixotropy, and a non-reversible part which cannot recover after being ruptured, referred to as a loss of workability. The differences in the characteristic time of thixotropy (10 – 100 sec) and loss of workability (> 1000 sec) allow to study the two phenomena separately from each other [147, 149, 272, 273].

As shown in Figure 17 [274], two static yield stresses can be studied: the onset of viscoelasticity ending the linear elastic behavior $\tau_{y(s)}$, and the peak yield stress $\tau_{y(d)}$ [274]. After breaking down the structural network interactions between the particles, the measured shear stress reduces to an equilibrium level and the sample is sheared.

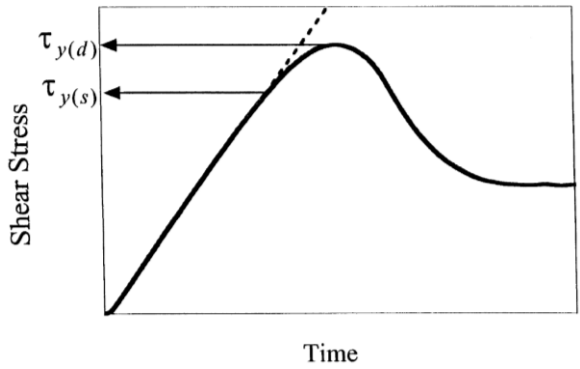

Figure 17: Two approaches to define the static yield stresses

Possible mechanisms resulting in thixotropic behavior of a material have been resumed by Mewis [275]: a balance between attraction and repulsion forces in a colloidal dispersion, chemical bonds which can be ruptured reversibly by mechanical action, hydrogen bonds, the entanglement of molecules, and the buildup of cardhouse-like structures.

Roussel et al. [264] investigated the mechanisms governing the thixotropy of concrete. A small critical strain of a few 10^{-2}% is assumed to be associated with strong short range interparticle forces associated with the growth of early hydrates at the contact points between cement grains [139, 264, 276] and a larger critical strain of several % is associated with the buildup of a network of colloidal interactions (Figures 18 and 19) [264]. Although in strict sense the nucleation and

rupture of early hydrates on contact points is an irreversible process, the CSH links made up by short-range forces (ionic correlation) are weak enough to be broken and can be rebuilded generating a reversible macroscopic behavior [265].

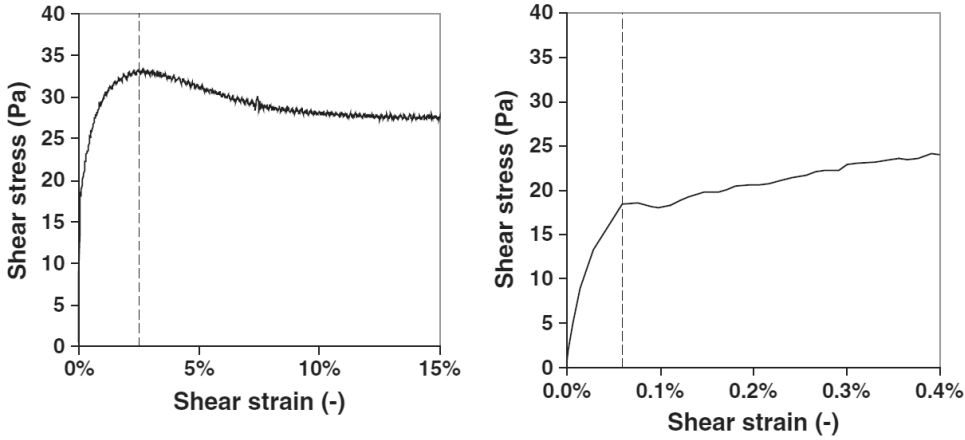

Figure 18: Linear behavior before two critical strains corresponding with different mechanisms of structural buildup [264]

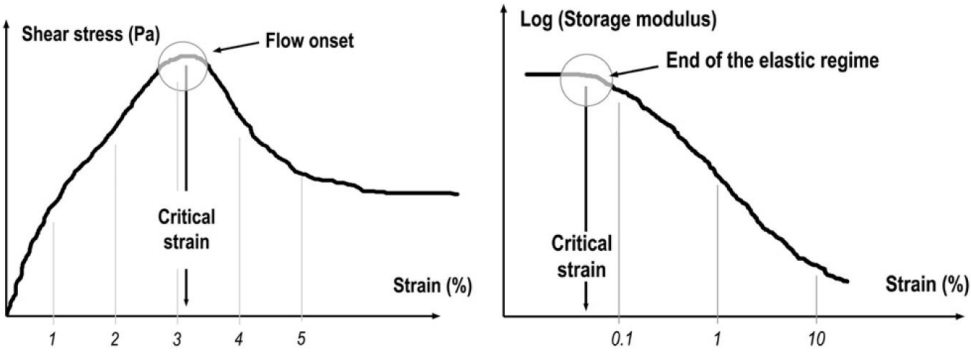

Figure 19: Two critical strains corresponding with different mechanisms of structural buildup [264]

Colloidal forces result in a short term flocculation / deflocculation behavior (characteristic time of several seconds), explaining why nonreactive powders such as a paste of limestone powder and water also possess thixotropic properties [113]. As the colloidal network is not evolving anymore after several seconds, the thixotropic behavior of practical interest (characteristic time of several minutes) is most probably solely due to the formation of C-S-H bridges in between particles at rest [264]. Despite the very low degree of hydration during the dormant period, the effect of nucleation on macroscopic level is not negligible as it preferentially happens at the pseudo contact zones between the cement grains which are the most crucial zones of the interacting particle network [264, 276].

The hypothesis of CSH nucleation being the main mechanism is confirmed by:

- A calculation of the time needed to build a CSH linkages [264].
- Cement with a higher heat generation leads to more structural buildup [277, 278]. The structuration rate is proportional to the heat rate [24, 278].
- Increased temperatures result in increased structural buildup rates [265].
- The addition of accelerators increases the rate of structural buildup [265, 279]. Set retarding agents reduce the rate of structural buildup [278, 279].
- The addition of fine particles such as silica fume with strong nucleation properties results in a higher rate of structural buildup [265, 277, 280]. The addition of limestone powder provides more nucleation sites and thereby also increases the rate of structural buildup [281].
- The substitution of cement by fly ash slows down the hydration rate and results in a reduction of the rate of structural buildup [282].
- A reduction of the water-to-cement ratio leads to a higher amount of neighboring particles and a faster rate of structural buildup [265, 279, 281-284]. The addition of superplasticizer reduces the nucleation rate and the rate of structural buildup [265, 283-287].

A small dosage of clays added to SCC provides a large increase in the structural buildup [277, 280, 284, 288-297]. Several contributions can explain the increased structural buildup induced by clays: (1) electric charges on surfaces create a stable network of clays in the microstructure which breaks down under shear [295]; (2) attractive forces between clay particles and other particles in the cementitious suspension promote flocculation and thus increase viscosity [284, 289, 291, 295]; (3) small clay particles act as a nano filler, filling the gaps in between the cement particles and thereby providing more contact points [294, 295]; and (4) the adsorbion and absorption of water reduces the distances among particles in suspension [294, 295].

6.3. Impact of shear stresses

Shear forces can break down agglomerates by surface erosion (i.e. the rupture of small particles from the surface of the agglomerate) or by large-scale fragmentation (i.e. the rupture of agglomerates into several large particles due to tensile stresses perpendicular to the agglomerate surface) [298]. In the low shear rate range, Van Der Waals forces dominate the macroscopic behavior, at intermediate shear rates, hydrodynamic forces dominate, and at high shear rates, the flow behavior is determined by particle inertia [149].

Experiments using Focused Beam Reflection Measurements (FBRM) have shown the kinetics of flocculation is much slower than the kinetics of deflocculation when

a paste is subjected to shear flow [235]. When aggregation dominates, small flocs (< 1 µm) form intermediate sized flocs (1 – 22 µm) and intermediate sized flocs aggregate until larger flocs. Because larger flocs become weaker and less stable, a limiting floc size of 250 µm was observed. The disaggregation process under shear mainly affects the largest particles (95-250 µm), resulting in an increase of the total amount of particle counts. Larger flocs are ruptured first because of an increased possibility of flaws, a more porous floc structure, and higher velocity gradients at the flocs surface [235, 299].

Coagulation of the cement particles is happening at low shear rates (smaller than 10 s^{-1}), especially in the 80 to 150 µm range. At higher shear rates (above 100 s^{-1}), deflocculation is occurring [299]. As illustrated in Figures 20 and 21 [299], the observed decrease in viscosity is related with an increase in packing density, calculated using the compressible packing model of de Larrard [260] using the measured particle size distribution [299]. The evolution of the rheology of the mixture follows the same trend as the evolution of the packing density under a constant strain rates. The measurements shown in Figures 21 appear to contradict the predicted increase of the viscosity with increasing packing density expected according to the Krieger–Dougherty equation valid for monodisperse spheres [86] as the equilibrium packing density was also lower at a strain rate of 10 s^{-1} (78%) compared to the equilibrium packing at a strain rate of 1 s^{-1} (81%) or 100 s^{-1} (80%). However, the maximum packing density in the Krieger – Dougherty equation might also be affected by the differences in shear rate. Further research on the influence of particle density models and their impact on the rheology of cement pastes is necessary. The higher specific surface corresponding with the strain rate of 100 s^{-1} also has an impact on the observed viscosity.

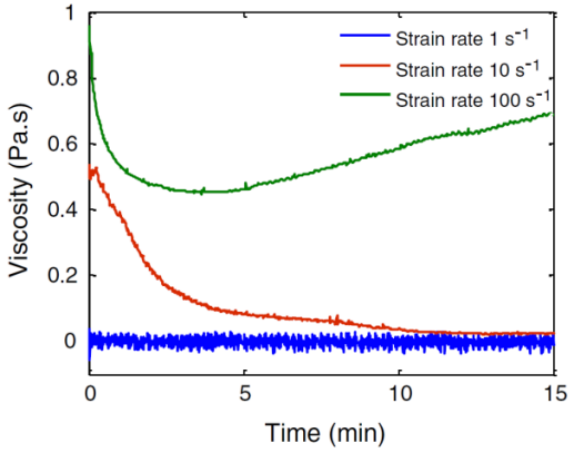

Figure 20: Viscosity evolution under a constant strain rate [299]

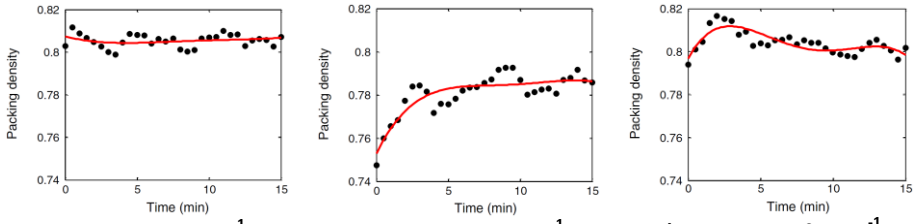

a) Strain rate of 1 s^{-1} **b) Strain rate of 10 s^{-1}** **c) Strain rate of 100 s^{-1}**

Figure 21: Packing density evolution under a constant strain rate [299]

Addition of a superplasticizer leads to a more dispersed state, a cellulose based VMA has no influence, and clays result in a more flocculated structure of the cement paste [235]. The clays are acting as micro fillers with high surface charges connecting the network structure and might also interact with the superplasticizers, leading to stronger, larger, and more stable flocs which are less sensitive to dynamic disturbances.

The population balance model of Thomas [300] and Negro [301] (shown in Equation 13 and 14 [235], abbreviations summarized in Table 7) assumes the flocculation is governed by orthokinetic aggregation, the aggregation by collision of cement particles above 0.1 µm during shear, and the disaggregation of flocs is governed by pressure differences at the surface of the flocs. This model might serve as a basis to establish a relation in between the microstructure and rheology observed during shear flow if the flocculation mechanisms are adapted as aggregation by collision is unlikely for particles smaller than 50 µm. However, because the relation between the interparticle forces and the rheology of concrete is still unclear and the cement chemistry during early hydration is complicated, the model is mainly usefull to describe observed experimental results and not to predict the concrete rheology.

$$\frac{dn}{dt} = -k_1 \cdot n^2 + k_2 \cdot n \qquad \text{(Eq. 13)}$$

$$n = \frac{k_2/k_1}{1-\frac{n_0-k_2/k_1}{n_0}\exp(-k_2 \cdot t)} \qquad \text{(Eq. 14)}$$

Symbol	Unit	Definition
n	[-]	Number of particles
k_1	[-]	Aggregations kinetics constant
k_2	[-]	Disagregation kinetics constant

Table 7: Abbreviations used in Equations 13 and 14

6.4. Thixotropic models

Generally, two main approaches to describe the thixotropic behavior of concrete are used: the microstructural approach, also referred to as the generalized continuum theory, and the structural kinetics approach. In the microstructural approach, a rheological model is expanded with time-dependent parameters such as exponential fading memory functions in the Modified Hattori Izumi model of Wallevik [302, 303]. The structural kinetics approach describes the rheological behavior based on two equations: a kinetic equation and a structural equation describing the structuration of the material.

6.4.1. The particle flow interaction theory of J.E. Wallevik [304]

After previous modifications of the Hattori-Izumi theory [302, 303, 305], Wallevik [304] has proposed a theory explaining the macroscopically observed thixotropic behaviour based on the number of particles and clusters at microscopic level. Both the colloidal flocculation / deflocculation junctions as the breaking and rebuilding of chemically formed linkages are taken into account. A distinction is made between linkages and junctions.

- Linkages are two cement particles adhered together by the formation of a membrame of gelatinous calcium silicate/sulphoaluminate hydrate. The thickness of the membrame determines whether it is a permanent or reversible linkage.
- Junctions are two or more cement particles coagulated due to potential energy interactions (Van Der Waals forces). The coagulation can also be reversible or permanent.

Dependent on whether or not the connections are reversible, the particles are divided in different classes. The benchmark of a particle size of 40 µm is chosen as a border between the smaller particles still affected by colloidal effects and larger particles which have sufficient kinetic energy to overcome the energy barrier against coagulation and cause hard sphere collisions.

J_3^s	The number of reversible linkages of particles smaller than 40 µm per unit volume.
$J_3^{p,c}$	The number of permanent junctions of particles smaller than 40 µm per unit volume.
$J_3^{p,s}$	The number of permanent linkages of particles smaller than 40 µm per unit volume.
J_4^s	The number of reversible linkages of particles larger than 40 µm per unit volume.
J_4^p	The number of permanent linkages of particles larger than 40 µm per unit volume.

The particle flow interaction theory describes as well the thixotropic behavior as the structural breakdown of concrete based on the physical background of the coagulation, dispersion, recoagulation, and breakage of cement particles and their junctions or linkages. In contrast to older versions of this model (the Modified Hattori-Izumi theory [302, 303]), no fading memory integrals for the shear rate history are used in the particle flow interaction theory.

The system of equations used to describe these mechanisms (Equation 15), can predict the time-dependent behavior of concrete using 18 parameters, based on the perikinetic coagulation rate theory of Verwey and Overbeek [306] and the orthokinetic coagulation theory of Smoluchowski [307]. The 18 parameters of the model are calculated in order to obtain the best approximation of measured data. However, because of the large number of parameters, the estimated value of each parameter becomes more sensitive to experimental noise. The large number of parameters also difficults the use of this model in practical applications.

$$\begin{cases} \dfrac{\partial U_3^s}{\partial t} + v \cdot \nabla U_3^s = -I_3^s \, U_3^s \\ \dfrac{\partial U_3}{\partial t} + v \cdot \nabla U_3 = H_3 \left(\left(1 - U_{3(0)}^s\right) - U_3 \right)^2 - I_3 \, U_3^2 \\ \dfrac{\partial U_4^s}{\partial t} + v \cdot \nabla U_4^s = -I_4^s \, U_4^s \\ \rho \left(\dfrac{\partial v}{\partial t} + v \cdot \nabla v \right) = \nabla \cdot \sigma + \rho g \end{cases} \qquad \text{(Eq. 15)}$$

Symbol	Definition
$U_3 = \frac{J_3}{n_3}$	Reversible coagulated state of particles and coagulated particles smaller than 40 µm
$U_3^s = \frac{J_3^s}{n_3}$	Reversible linked state of reversible linkages of particles and coagulated particles smaller than 40 µm
$U_{3(0)}^s$	Reversible linked state of reversible linkages of particles and coagulated particles smaller than 40 µm at time t=0
$U_4^s = \frac{J_4^s}{n_4}$	Reversible linked state of reversible linkages of particles and coagulated particles larger than 40 µm
n_3	Number of primary particles and coagulated particles smaller than 40 µm per unit volume
n_4	Number of primary particles and coagulated particles larger than 40 µm per unit volume
$\dot{\varepsilon}$	Rate-of-deformation tensor of the cement paste
v	Velocity of the cement paste
p	Pressure of the cement paste
ρ	Density of the cement paste
$\sigma = -p \cdot I + 2\eta\dot{\varepsilon}$	Constitutive equation of the cement paste
η	Apparent viscosity of the cement paste
g	Gravitational acceleration
I	Unit dyadic tensor of the cement paste
I_3	Dispersion rate of coagulated particles smaller than 40 µm
I_3^s	Dispersion rate of reversible linkages of particles smaller than 40 µm
I_4^s	Dispersion rate of reversible linkages of particles larger than 40 µm
H_3	Coagulation rate of particles smaller than 40 µm

Table 8: Abbreviations used in the particle flow interaction theory (Eq. 15)

6.4.2. Structural kinetics approach

Two equations are used to describe the rheological behavior: a kinetic equation computing the shear stress as a function of the shear rate and the degree of structure $S(t)$, and a structural equation describing the change in the degree of structuration as a function of the shear rate and current degree of structure (Equation 16). Papo [308], Coussot et al. [309], and Roussel [310] have developed a structural kinetics model for concrete based on the general model for thixotropic fluids of Cheng and Evans [311].

$$\begin{cases} \tau(t) = f\big(\dot{\gamma}(t), S(t)\big) \\ \frac{dS(t)}{dt} = g\big(\dot{\gamma}(t), S(t)\big) \end{cases} \quad \text{(Eq. 16)}$$

The degree of structuration in the structural kinetics approach is defined as the number of links contributing to the thixotropic behavior $n(t)$. Equation 17 describes the evolution of the number of links based on single-order kinetics [275]. In this equation, the parameters c, d, k_1, k_2, α, and β are constants and n_∞ is the limiting number of thixotropic links. Most often, β is close to zero, $c = 0$, and $d = 2$.

$$\frac{dn(t)}{dt} = -k_1 \cdot n^c \cdot \big(\dot{\gamma}(t)\big)^\alpha + k_2 \cdot \big(n_\infty - n(t)\big)^d \cdot \big(\dot{\gamma}(t)\big)^\beta \quad \text{(Eq. 17)}$$

Because not all links have a similar contribution to the thixotropic behavior and the broad particle size distributed concrete cannot be described by only one dominant force governing the flocculation / deflocculation kinetics as all forces depend vastly on the particle size, most authors prefer to use a structural parameter λ not related to the number of links [311]. When such a kinetic equation $\frac{d\lambda(t)}{dt}$ is integrated in time, it becomes a memory function of the shear rate over the complete duration of the experiment [311], converting the structural kinetics approach into a microstructural approach.

An example of a model based on the structural kinetics approach is the thixotropy model of Roussel [310] given in Equation 18 in which T, m and α are the thixotropic parameters and λ is the structural parameter.

$$\begin{cases} \tau = (1 + \lambda) \cdot \tau_0 + k \cdot \dot{\gamma}^n \\ \frac{d\lambda}{dt} = \frac{1}{T \cdot \lambda^m} - \alpha \cdot \lambda \cdot \dot{\gamma} \end{cases} \quad \text{(Eq. 18)}$$

7. Models relating the microstructure and rheology

Although the previous section helps to understand the impact of changes in the mix design and methods on the rheology of SCC, it is evident that an accurate prediction of the rheology based on the mix composition is still unfeasible. The heterogeneous composition of clinker particles, irregular particle shape, very broad particle size distribution, many interparticle interactions, and complex impact of admixtures and shear forces complicate the determination of the dominant force governing the macroscopic observed rheological behavior. As a result, rheological models are highly simplified and ignore many influences. Some are based on an equilibrium of forces such as in the YODEL [148, 266, 267], others based on the packing density or/and aggregate volume fraction [148, 260, 266, 267, 312, 313], and others on the average distance separating aggregate particles from each other [85, 314, 315]. Yammine et al. [21] presented a relation between the average distance between aggregate particles and the aggregates volume fraction, shown in Equation 19 (abbreviations explained in Table 9).

$$b = d\left(\left(\frac{\phi}{\phi_m}\right)^{-\frac{1}{3}} - 1\right) \quad \text{(Eq. 19)}$$

Symbol	Unit	Definition
b	[m]	Average distance between aggregate particles
d	[m]	Average aggregate particles size
ϕ	[-]	Aggregates volume fraction
ϕ_m	[-]	Maximum aggregates volume fraction

Table 9: Abbreviations used in Equation 19

7.1. Difference SCC and vibrated concrete

Other mechanisms govern the rheological behavior of SCC and vibrated concrete [21]. Vibrated concrete mixtures, with aggregates volume fractions above 70%, are dominated by direct contact forces between the aggregate particles resulting in yield stresses of several thousand Pa, while SCC most often has an aggregate volume fraction below 60% [316] and is dominated by hydrodynamic interactions, resulting in a yield stress of several ten Pa. The hydrodynamic interactions result in a SCC yield stress more or less proportional with paste yield stress (Equation 20 [21]). Between the aggregates volume fraction of 60 and 70%, a critical aggregates volume fraction ϕ_c exists, corresponding with a spectacular increase of the yield stress due to the formation of a continuoes network of particles in contact with each other [21].

$$\tau_{0,SCC} \approx \tau_{0,paste} \cdot f\left(\frac{\phi}{\phi_m}\right) \quad \text{(Eq. 20)}$$

7.2. Yield Stress Model (YODEL) of Flatt [148, 266, 267]

Based on the contribution of the particle size distribution, the geometrical maximum packing density, the percolation threshold, interparticle forces, and microstructural features of the constituents on the yield stress of SCC, Flatt [266, 267] developed the yield stress model (YODEL), given in Equation 21 and 22. This model predicts the yield stress of concentrated suspensions based on a theory estimating the number of particles connected to each other able to withstand a certain shear stress. Table 10 summarizes the meaning of all abbreviations in Equation 21 and 22.

The yield stress model allows an accurate prediction of the yield stress of nonreactive particle systems such as mixtures of sub-micron ceramic powder or alumina powder suspensions [266, 267]. The accuracy of the model depends on a good prediction of the maximum packing density [267], which is affected by agglomeration, interparticle forces and geometrical considerations. Results on cement paste are less good due to the chemical and physical processes inside this system [142]. The changing solid volume fraction, mean particle size, and particle size distribution complicate the implementation of the YODEL model.

$$\tau_0 = m_1 \cdot \frac{\phi(\phi-\phi_0)^2}{\phi_{max}\cdot(\phi_{max}-\phi)} \qquad \text{(Eq. 21)}$$

$$m_1 = \frac{1.8}{\pi^4} \cdot G_{max} \cdot a^* \cdot u_{k,k} \cdot \frac{F_{PSD}}{R_{v,50}{}^2} \qquad \text{(Eq. 22)}$$

Symbol	Unit	Definition
τ_0	[Pa]	Yield stress
m_1	[-]	Prefactor accounting for the interparticle forces, particle size, and particle size distribution
ϕ	[-]	Volume fraction
ϕ_0	[-]	Percolation treshhold
ϕ_{max}	[-]	Volume fraction at maximum packing
G_{max}	[-]	Maximum attractive interparticle force, normalized by the radius of curvature at the contact points
a^*	[-]	Average fixed radius of curvature of the contact points
$u_{k,k}$	[-]	Normalization function $u_{k,k} = \frac{16\pi}{2-\sqrt{3}}$
F_{PSD}	[-]	A function accounting for the particle size distribution
$R_{v,50}$	[-]	Mean volume radius

Table 10: Abbreviations used in the YODEL model (Eq. 21 and 22)

7.3. Compressible Packing Model of de Larrard [260, 317]

The Compressible Packing Model of de Larrard [260] predicts the yield stress of concrete out of a dry packing model of all particles in the concrete. Although all granular fractions have an impact, the yield stress (Equation 23) is assumed to be mainly dominated by fine particles generating intergranular friction and the presence and dosage of superplasticizer. The plastic viscosity, however, is mainly dominated by the packing density of the mixture [318], complicating the flow of water in the porosity of the granular system and cannot be predicted by the compressible packing model of de Larrard.

$$\tau_0 = 2.537 + \sum_i (0.736 - 0.216 \cdot \log(d_i)) \cdot \frac{\phi_i}{1-\phi_i^*} + \left(0.224 + 0.910 \cdot \left(1 - \frac{P}{P^*}\right)^3\right) \cdot K'_C \quad \text{(Eq. 23)}$$

Symbol	Unit	Definition
ϕ_i	[-]	Volume fraction
ϕ_i^*	[-]	Maximum packing volume fraction
d_i	[m]	Size of the particles
P	[-]	Superplasticizer dosage
P*	[-]	Saturation dosage of the superplasticizer
K'_c	[-]	Cement partial compaction index

Table 11: Abbreviations used in Equations 23

7.4. The homogenization approach

Applying the Farris approach [319], the complex rheology of concrete, mortar, or sometimes even paste is simplified to a suspension of particles into a homogeneous matrix. Some authors use a multi modal approach, in which an iterative calculation first calculates the rheological behavior of the paste, then the mortar rheology, which is afterwards scaled up to concrete level. Often, the relative yield stress and relative plastic viscosity are used instead of absolute values.

Although the arbitrary division at certain sizes in the continuous particle size distribution neglects the interparticle interactions inside the fresh concrete [320], reasonable results for the plastic viscosity are obtained [148]. The predicted yield stresses differ largely from the measured values.

7.4.1. Krieger – Doherty equation for suspensions

For monodisperse suspensions of rigid spheres, the relation between the packing density and rheology can be described by the Krieger – Doherty equation [86]. Table 12 summarizes the meaning of all abbreviations in Equation 24. Although the model provides some insight on the effect of an increase of the packing density on the rheology, it cannot be used for concrete. The model is not suitable for high

packing densities and concrete has a very broad particle size distribution of non-spherical particles. The maximum packing density of concrete is also sensitive to small changes in the particle size distribution [25, 321].

$$\frac{\eta}{\eta_m} = \left(1 - \frac{\Phi}{\Phi_m}\right)^{-\eta_i \cdot \Phi_m} \quad \text{(Eq. 24)}$$

Symbol	Unit	Definition
η	[Pa s]	Viscosity of the suspension
η_m	[Pa s]	Viscosity of the matrix
Φ	[-]	Packing density
Φ_m	[-]	Maximum packing density allowing flow of the suspension
η_i	[-]	Intrinsic viscosity (2.5 for rigid uncharged spheres)

Table 12: Abbreviations used in the Krieger-Doherty model (Eq. 24)

7.4.2. The Nielsen model [322, 323]

Considering SCC as a composite Bingham fluid with non-flexible particles, Nielsen [322, 323] has established a model predicting the rheology of concrete based on the paste Bingham parameters and the volume fractions and shape functions of the aggregates, given in equations 25 to 27. The method to determine the shape factors $\alpha_{particles}$ and α_{matrix} of the geometry function γ_∞ (Equation 27) is described in [268, 322, 323].

$$\frac{\tau_{0,suspension}}{\tau_{0,matrix}} = \frac{1+\gamma_\infty \cdot \phi}{1} \quad \text{(Eq. 25)}$$

$$\frac{\mu_{suspension}}{\mu_{matrix}} = \frac{1+\gamma_\infty \cdot \phi}{1-\phi} \quad \text{(Eq. 26)}$$

$$\gamma_\infty = \frac{3}{2} \cdot \frac{\alpha_{particles}+\alpha_{matrix}-1}{\alpha_{matrix}} \quad \text{(Eq. 27)}$$

The Nielsen model is capable of predicting the plastic viscosity of SCC [268, 322] (Figure 22 [322]), but fails to predict the yield stress of concrete [148]. Flatt [148] has suggested that the agglomeration of particles at low shear rates might result in deviations of the predicted yield stress. Because the agglomeration is broken down during flow, the prediction of the plastic viscosity is not affected.

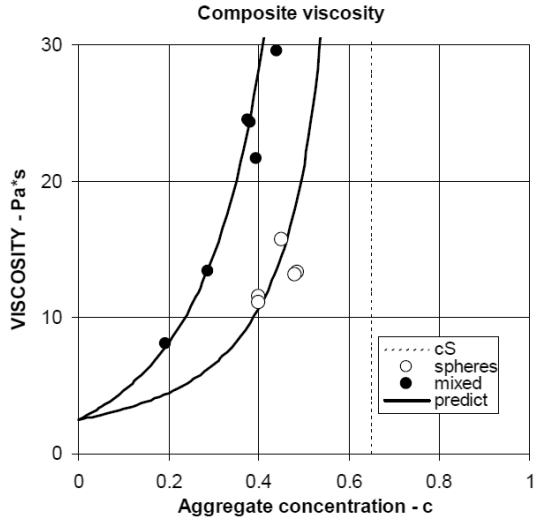

Figure 22: Plastic viscosity of SCC, experimental values and the Nielsen model [322]

7.4.3. The Chan and Powell model [320]

Ferraris and de Larrard [320] determined the relative plastic viscosity of SCC based on the model of Chan and Powell [324] fitted to 78 concrete and mortar batches (Figure 23). Both concrete and mortars follow the curve given in Equation 28 [320]. The packing density parameter ϕ^* in Equation 28 includes the effect of the superplasticizer dosage and the water demand of the paste.

$$\frac{\mu_{concrete}}{\mu_{paste}} = \exp\left(26.75\left(\frac{\phi}{\phi^*} - 0.7448\right)\right) \qquad \text{(Eq. 28)}$$

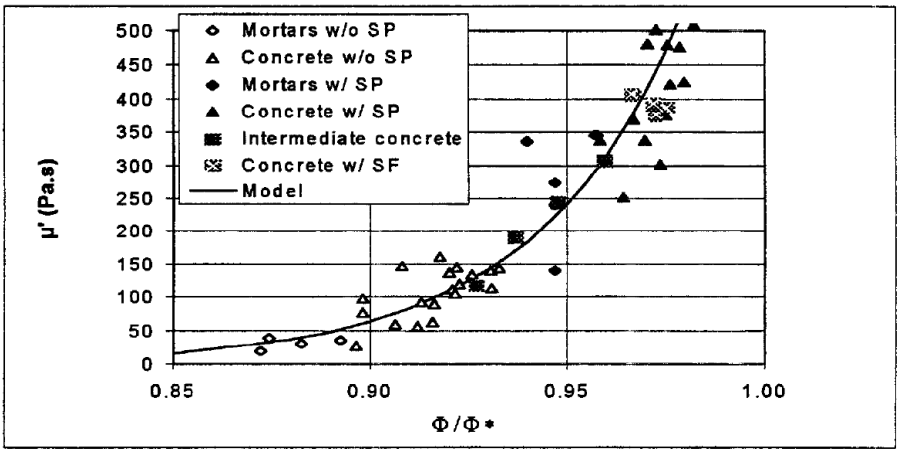

Figure 23: The model of Chan and Powell fitted to 78 concrete batches [320]

7.4.4. Dissipative particle dynamics models [325]

Ferraris and Martys [326] have compared experimental results and relative viscosity models based on dissipative particle dynamics [325] as a function of the volume fraction of coarse aggregates. The dissipative particle dynamics models calculate the viscosity based on the average stresses for a given strain rate and are consistent with the experimental results measured on several rheometers (Figure 24 [326]).

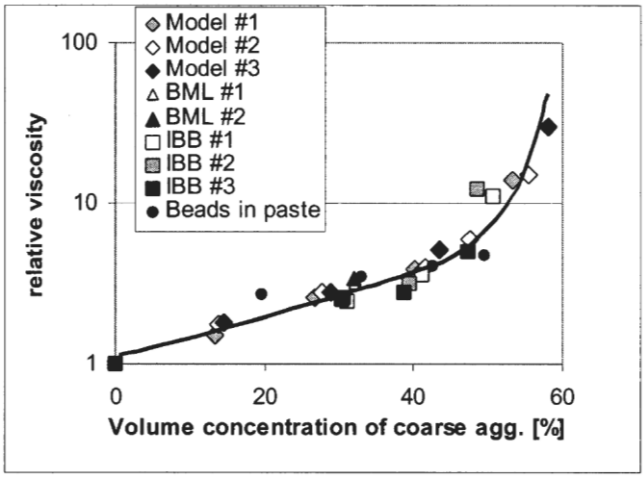

Figure 24: The relative plastic viscosity as a function of the coarse aggregates packing density [326]

7.5. Water Film Thickness (WFT) and Paste Film Thickness (PFT)

The concept of the water film thickness (WFT) and paste film thickness (PFT) is based on the concept of a lubricating layer (respectively water or paste) separating solid particles in a suspension. The film covering the solid particles is larger when more of the lubricating medium is available in the mix proportion and for mix proportions providing a larger maximum packing density. The packing density should be determined in wet conditions [85, 327-329].

For self-compacting concrete, the WFT has a significant impact on the rheology of paste (Figure 25 and 26 [330]), mortars (Figure 27 [314]), and concrete (Figure 28 [85]). All graphs are based on concrete mixtures having a constant superplasticizer dosage (2% of the cement weight in the concrete mixtures [85] and 3% of the cement weight in mortar mixtures [314]). On the mortar mixtures shown in Figure 28 [314], bleeding started rising as soon as the WFT became larger than 0.20 µm [314].

Based on experimental results, design charts have been proposed for mortars and concretes with this superplasticizer dosage [85, 314]. In mortars, the W/C ratio is chosen based on strength requirements and the WFT based on the workability demands [314], defining the needed cement content based on Figure 29 [314]. A similar approach was proposed for concrete mix designs in Figures 30 and 31 [85]. The area covering segregating mixtures is covered in red in Figure 31 [85]. The segregation can probably been overcome by adjusting the superplasticizer dosage.

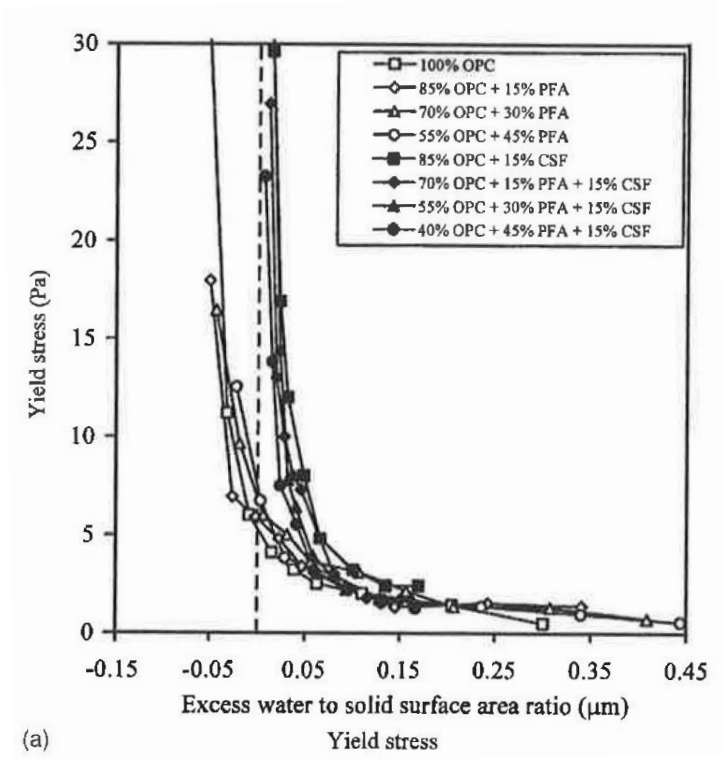

Figure 25: Impact of the water film thickness on the yield stress of paste [330]. Not all pastes in the graphs are self-compacting.

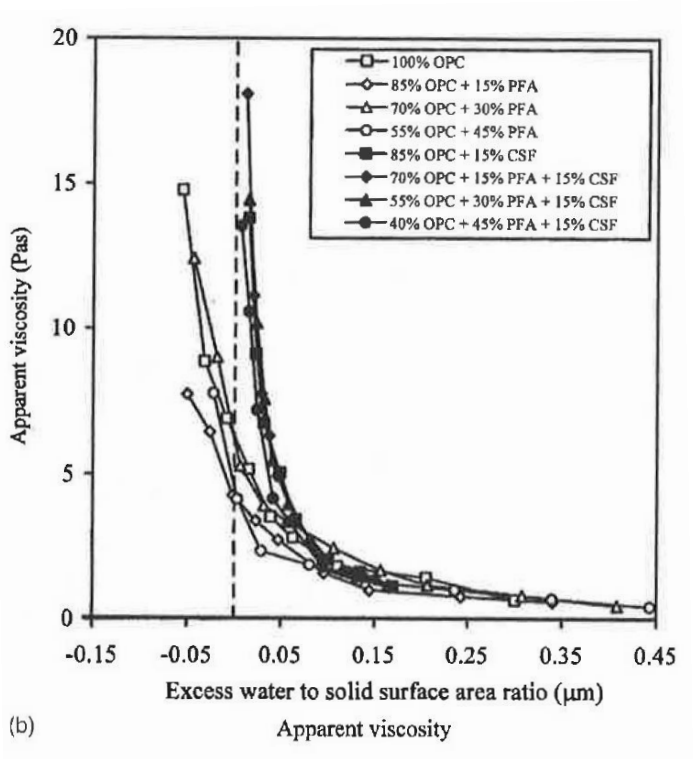

Figure 26: Impact of the water film thickness on the apparent viscosity of paste [330]. Not all pastes in the graphs are self-compacting.

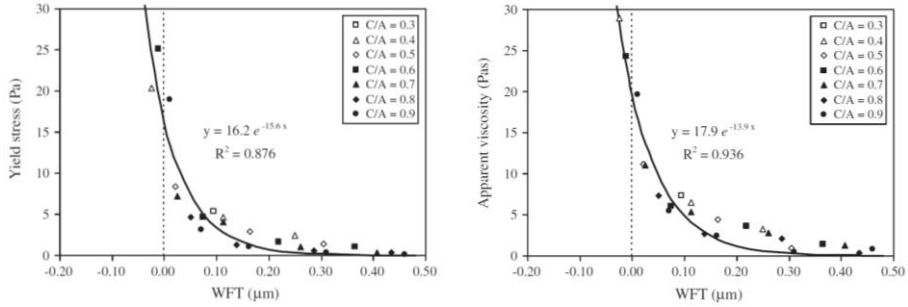

Figure 27: Impact of the water film thickness on the rheology of mortars [314]. Not all mortars in the graphs are self-compacting.

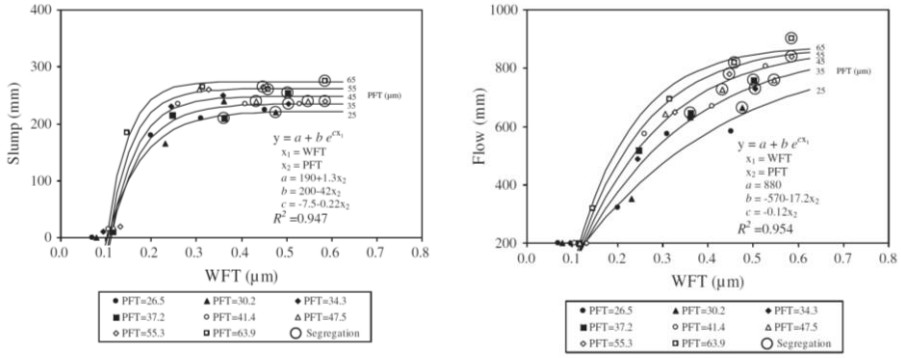

Figure 28: Impact of the water film thickness on the rheology of concrete [85]. Not all concrete mixtures in the graphs are self-compacting.

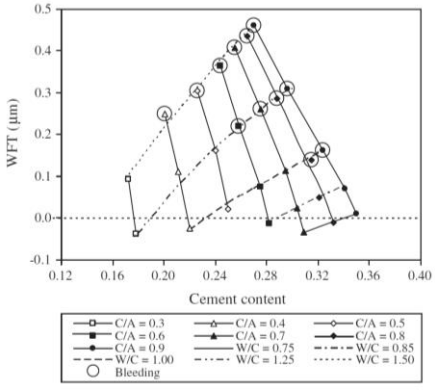

Figure 29: Design charts for mortars [314]

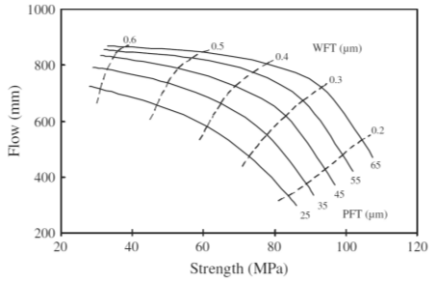

Figure 30: Design chart for self-compacting concrete [85]

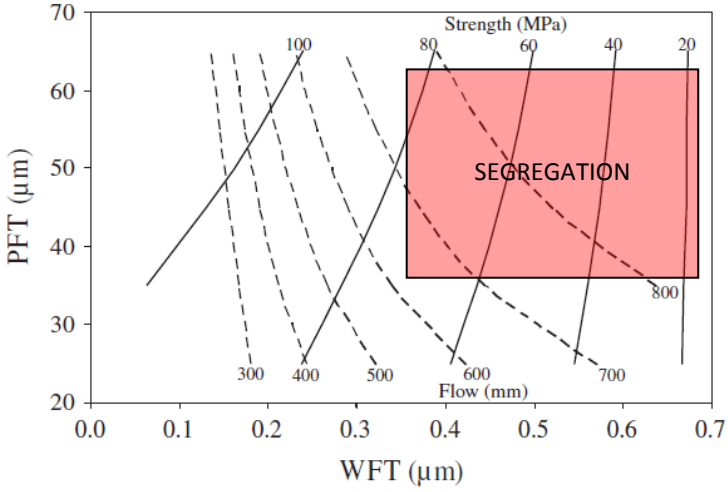

Figure 31: Design chart for self-compacting concrete [85].
The mixtures with segregation are marked in red

An increase of the superplasticizer dosage prevents the flocculation of fines and therefore increases the packing density and WFT [331]. The rheology of mortars depends on both the WFT and superplasticizer dosage (Figure 32) [331].

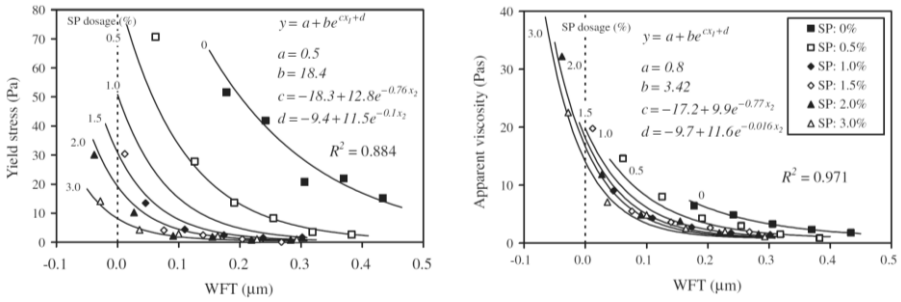

Figure 32: Impact of the superplasticizer dosage on the WFT [331]

8. Impact mixing procedure

As the shear history has an important impact on the microstructure of SCC, parameters such as the mixing time, mixing speed, and mixing sequence also have a large impact on the rheology of concrete. SCC can be produced in all types of mixers [57, 332], but the type of mixer will cause differences: mixers with a larger volume require lower superplasticizer dosages [333], more intensive mixers provide higher plastic viscosities, a higher rate of structural buildup, a more flocculated microstructure and accelerated hydration kinetics [334].

8.1. Mixing process

Based on the power consumption curve of mixers, the mixing process has been subdivided into three stages: the dispersing stage, the stage of optimum dispersion, and the overmixing stage [335-337] (Figure 33 [335]). The added water first creates fluid bonds between the particles, building clusters of powder, sand and water inside the mixture due to capillary and viscous forces and leading to a sharp increase of the power consumption curve. Once all particles are suspended in the liquid, the mixing action crushes the clusters by collision, resulting in a decrease of the power consumption curve in the end of the dispersing stage [335-340]. During the optimum dispersion stage, the power curve decreases asymptotically according to Equation 29 [341], reaching a plateau of optimum dispersion and maximum fluidity [341, 342]. The more coarse aggregates available, the faster the decrease of the power curve [343]. In the last stage of overmixing, the total solid surface area increases due to the further breakdown of clusters [335-337, 340, 342], the abrasion of first hydration products [335, 336, 342, 344], and the abrasion and breakage of aggregates [335, 336, 342, 345].

$$P(t) = P_0 + P_1 * \exp\left(-\frac{t}{t_1}\right) \quad \text{(Eq. 29)}$$

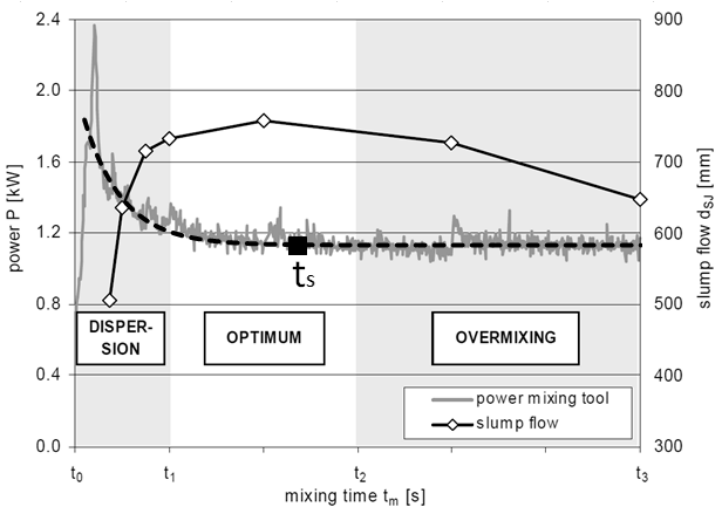

Figure 33: The mixing stages and stabilization time [335]

The stabilization time (the moment of optimum dispersion), is defined as the time at which the power consumption curve reaches its horizontal asymptote (a slope of $-4 \cdot 10^{-4}$ s^{-1}) and can be calculated using Equation 30 [335, 341-343, 346]. SCC has a longer stabilisation time compared to vibrated concrete due to its higher paste volume and lower amount of coarse aggregates which are providing a ball bearing effect during mixing [336, 343, 346].

$$t_s = -t_1 * \ln\left(4 \cdot 10^{-4} * \frac{t_1}{P_1}\right) \quad \text{(Eq. 30)}$$

8.2. Mixing energy

The mixing energy is a combination of the mixing time and the mixing rate. Higher shear rates accelerate the hydration kinetics by providing a more efficient solution exchange and a more extensive formation of etch pits on the particle surface resulting in a higher rate of dissolution, more CSH nuclei, a higher rate of hydrate precipitation, an increased particle dispersion, and an increase of the rate of superplasticizer adsorption [127, 162, 334-336, 342, 344, 346-350]. Dependent on the mixing time, an increased mixing energy can result in an higher flowability due to an increased dispersion [337, 344, 351-353], or a decreased flowability due to over-mixing [162, 334-336, 342, 345, 349, 352, 354] as illustrated in Figure 34 [335, 336, 342].

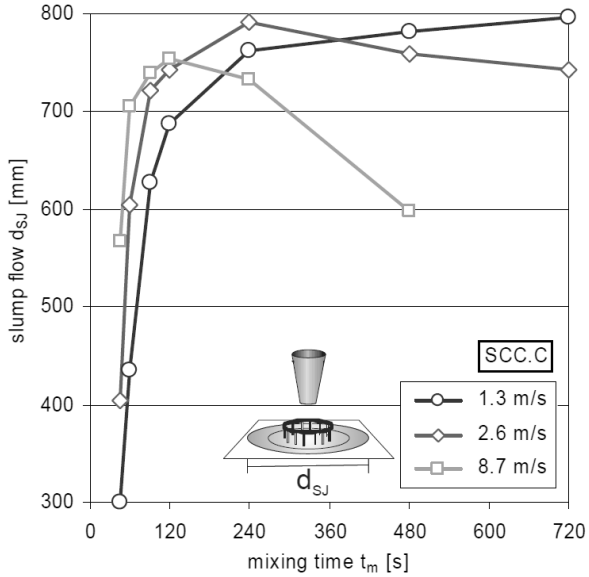

Figure 34: Impact of the mixing speed on the slump flow after mixing [335]

8.3. Addition time of admixtures

A delayed addition of superplasticizer avoids the intercalation of part of the superplasticizer in organic mineral phases during the first liberation of heat during cement hydration (Stage I) [206, 355]. As a result, a more flowable mixture is obtained compared to the direct addition of superplasticizer immediately after first contact of cement and water [198, 206, 209, 210, 355, 356]. Differences between the delayed and direct addition of PCE type superplasticizer are larger when the dose of superplasticizer and the temperature of the mixture decrease [210].

8.4. Differences in mixing paste and concrete

Because the ball milling action of aggregates is absent during the mixing of paste mixtures, even the most vigorously laboratory mixer cannot provide the same energy to the particles in the paste as during the mixing of a concrete mixture. Especially experimental results obtained on paste mixtures made in a Hobart mixer are not representative for paste in concrete mixtures and should therefore be interpreted carefully [352, 357, 358]. A high shear also accelerates the hydration kinetics of cement, causing huge differences in the structural buildup [334].

9. Stability of self-compacting concrete

In the previous sections, mainly the parameters affecting the rheology of concrete have been discussed. However, major changes in the rheology are only one aspect of the robustness. Not only the flowability and passing ability of a self-compacting concrete mixture should be met, also the stability demands are important.

A lack of stability can manifest itself in three possible phenomena, which will be discussed separately as they are governed by different mechanisms.

- Static segregation: Sinking of the larger aggregates at rest when gravitational forces dominate for these particles [91].
- Dynamic segregation: Particle migration during flow due to the domination of shear forces [155].
- Excessive bleeding: When repulsive forces dominate, the paste cohesion vanishes and an upwards water migration occurs. This results in the formation of a water layer at the top surface of the fresh concrete [359].

9.1. Static segregation

Static segregation is the segregation of the coarsest particles in a yield stress fluid at rest. Based on the static segregation rate equation of Shen et al. [91, 156] (given in Equation 31[4], abbreviations explained in Table 13), a minimum paste yield stress needed to counter static segregation can be calculated using Equation 32. Equation 32 has been confirmed by Roussel [360].

$$u_a = u_s \cdot \left(1 - \frac{\phi}{\phi_m}\right)^{5.18} = \frac{\left(\frac{(\rho_S - \rho_L)\cdot g \cdot d}{18} - \tau_0\right)\cdot d}{\eta_{pl}} \cdot \left(1 - \frac{\phi}{\phi_m}\right)^{5.18} \qquad \text{(Eq. 31[4])}$$

$$\tau_0 \geq \frac{(\rho_S - \rho_L)\cdot g \cdot d}{18} \qquad \text{(Eq. 32)}$$

Because of interparticle interactions and modifications in the flow pattern around the particle, the rate of static segregation can be reduced by optimizing the aggregate gradation and increasing the packing density [156, 361]. Based on the mechanical interactions in between the particles, Roussel [360] developed a second

[4] The segregation rate of a single particle in Equation 31 was originally reported as $u_s = \frac{\left(\frac{(\rho_S - \rho_L)\cdot g \cdot d}{18} * \tau_0\right)\cdot d}{\eta_{pl}}$. However, based on the mathematically derivation of this segregation rate, it should be $u_s = \frac{\left(\frac{(\rho_S - \rho_L)\cdot g \cdot d}{18} - \tau_0\right)\cdot d}{\eta_{pl}}$. The larger the paste yield stress, the slower the segregation rate.

criterion taking into account the effect of the solid fraction (Equation 33). When one of both criterions is met, no static segregation happens.

$$\phi \geq \phi_m \left(\frac{9\,\tau_0}{2\,(\rho_s - \rho_f)\,d\,g} + 1 \right)^{-3} \quad \text{(Eq. 33)}$$

Symbol	Definition
u_a	Segregation rate of the entire set of agggregates
u_s	Segregation rate of a single representative particle
ϕ	Volume fraction of aggregates
ϕ_m	Packing density of aggregates
ρ_s	Density of aggregates
ρ_L	Density of paste
g	Gravitational acceleration
d	Diameter of the representative aggregate
τ_0	Paste yield stress
η_{pl}	Paste plastic viscosity

Table 13: Abbreviations used in Equation 31 to 33

When the paste volume increases, less interparticle friction in between the aggregates happens and less superplasticizer is needed to reach a certain slump flow. Because the impact of the paste yield stress is more important than the impact of the aggregate friction, a more robust static segregation resistance is obtained with higher paste volumes [91].

Shen et al. [91] investigated the influence of the aggregate grading: smaller aggregates appeared to have a more pronounced influence than a higher aggregate packing density on the static segregation resistance. Most authors [361-363] recommend the use of a Funk and Dinger curve [364] (Equation 34) with a q value around 0.25 [2, 90, 119, 362, 365] to obtain a proper particle size distribution of the aggregates. Aïssoun et al. [366] reported an increase in aggregate packing density from 0.69 to 0.79 by optimizing the sand-to-aggregate ratio.

$$P(d) = \frac{d^q - {d_{min}}^q}{{d_{max}}^q - {d_{min}}^q} \quad \text{(Eq. 34)}$$

9.2. Dynamic segregation

During the flow of SCC, the paste exerts a drag force on the coarse aggregates [367, 368]. This drag force can be calculated using Equation 35 (abbreviations in Table 14) [155, 156]. In mixtures with a higher paste yield stress and plastic viscosity, higher drag forces are acting on the aggregates particles and therefore more dynamic segregation occurs [155, 369]. A lower yields stress increases the risk of dynamic segregation [369].

$$F_A = a\ b\ c\ \left(9\ \eta_{pl}\ \Delta V\ \left(\frac{\phi_1}{{r_1}^2} + \frac{\phi_2}{{r_2}^2} + \frac{\phi_3}{{r_3}^2}\right) + \ \pi^2\ \tau_0\ \frac{21}{4}\ \left(\frac{\phi_1}{{r_1}^2} + \frac{\phi_2}{{r_2}^2} + \frac{\phi_3}{{r_3}^2}\right)\right) \qquad \text{(Eq. 35)}$$

Symbol	Definition
a, b, c	Dimensions of the concrete sample (height, width, and length)
τ_0	Paste yield stress
η_{pl}	Paste plastic viscosity
ΔV	Difference in velocity between aggregate and paste
$\phi_1,\ \phi_1,\ \phi_1$	Volume fractions of different aggregates
r_1, r_2, r_3	Radii of the aggregates

Table 14: Abbreviations used in Equation 35

9.3. Bleeding

Bleeding is caused by the upward displacement of water through a dense network of interacting cement grains [147]. In stable SCC mixture, colloidal interactions create a percolated network of interacting particles, resulting in a macroscopic yield stress of the material. For the largest coarse aggregates, gravity might dominate the colloidal forces keeping the network together, leading to static or dynamic segregation (see Section 9.1 and 9.2). For small colloidal particles, a too high dosage of superplasticizer can make the repulsion forces dominant over the attractive forces, destroying the colloidal network, macroscopically observed as bleeding [271]. Bleeding occurs only in mixtures with a very low yield stress, most often due to a high superplasticizer dosage.

The mechanism determining the rate of the upward displacement of water is still unclear: a homogeneous consolidation of deformable porous media which can be described by a combination of Darcy's law of water flow and Terzaghi's calculation of the effective stresses out of soil mechanics [370-381], or a heterogeneous water migration process through vertical water extraction channels within the paste [359, 382-384] as has been visually observed in paste mixtures with a water-to-cement weight ratio of 0.6 [382].

The risk of bleeding can be reduced by accelerating the hydratation process [385], the addition of colloidal silica fume [66, 386-388], welan gum [241], sepiolite clays [290], or propylene carbonate (PPC) [389, 390]. When the hydration process is accelerated with admixtures, ettringite formation and CSH-nucleation increases the amount of small colloidal particles in the fresh SCC, consuming part of the superplasticizer and thus countering bleeding [385].

Chapter 3: Robustness of SCC

1. Introduction

This chapter investigates the fundamental mechanisms determining the robustness of fresh SCC. Based on an extensive experimental program, conceptual models are developed to understand why certain measures improve the robustness of specific mix designs and worsen the robustness of other mix designs. Once the possible mechanisms are uncovered, several theoretical rheology models are used to study the practical implications of a few mix design parameters. At the end of this chapter (Section 6), the conceptual model is transformed into some practical guidelines which can be used to enhance the robustness of fresh SCC.

2. Experimental setup

During the experimental test program, various materials and test methods were used. As small variations can have large implications on the workability of fresh SCC, a detailed description of all materials and test methods is given in this section.

2.1. Materials

2.1.1. Aggregates

Figure 35 summarizes the grading curves of sand 1, sand 2, sand 3 gravel 1, gravel 2 and gravel 3. The corresponding densities of these aggregates are respectively 2640 kg/m³, 2575 kg/m³, 2625 kg/m³, 2670 kg/m³, 2660 kg/m³, and 2590 kg/m³.

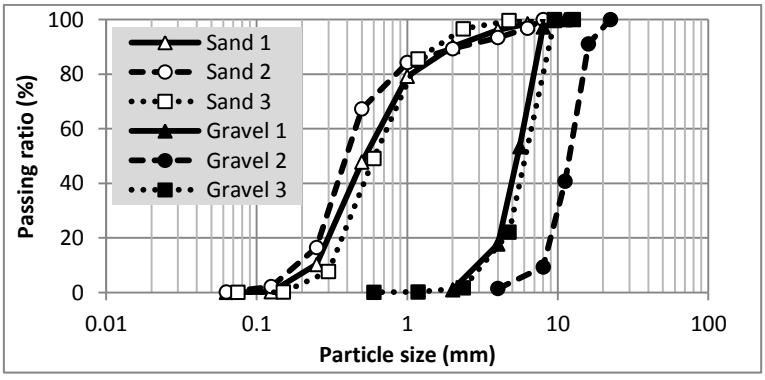

Figure 35: Aggregates grading curve

2.1.2. Cement and Fillers

The chemical composition and grading curve of the cement and mineral additions are summarized in Table 15 and Figure 36. Cement 1, 2, and 3 are successive supplies of Portland cement of type CEM I 52.5 N. Cement 4 (type I/II[5] [391], density 3120 kg/m³), Limestone powder 3 (density 2650 kg/m³), Fly ash 2 (class C, density 2400 kg/m³), and Silica fume 2 (density 2200 kg/m³) were used during an extension of this project in the Missouri University of Science and Technology. The mineral composition and grading curve of these materials were not determined.

	Cement 1 14/261	Cement 2 14/418	Cement 3 15/043	Limestone filler 1	Limestone filler 2	Fly ash 1 (class C)	Silica fume 1
CaO	61.50	63.01	63.0	-	0.00	7.02	0.58
SiO_2	18.66	18.55	18.9	1.04	0.11	52.75	96.24
Al_2O_3	5.86	5.83	5.8	0.15	0.04	22.60	0.34
Fe_2O_3	3.88	4.09	4.2	0.12	0.04	7.69	1.95
MgO	1.09	1.22	1.1	-	0.32	1.89	0.56
K_2O	0.63	0.60	0.60	-	0.00	3.24	1.64
Na_2O	0.50	0.53	0.44	-	0.01	1.05	0.37
$CaCO_3$	-	-	-	97.85	98.8	-	-
SO_3	3.25	2.97	3.5	0.11	0.02	0.94	-
Cl^{2-}	0.082	0.086	0.06	-	<0.008	0.003	-
L.O.I.	1.85	1.24	1.2	-	-	1.84	-
Insoluble residue	0.95	0.94	0.3	-	-	-	-
Density [kg/m³]	3110	3120	3150	2680	2670	2140	-
Blaine index [m²/kg]	467	312	364	700	-	-	-

Table 15: Composition and properties of cement and fillers

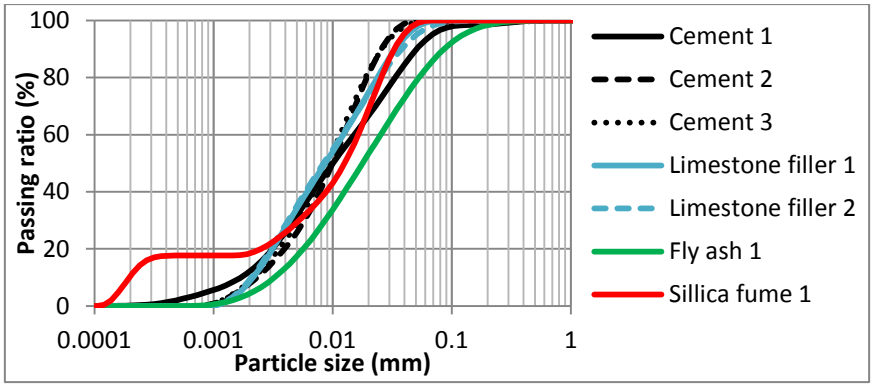

Figure 36: Grading curve of the cement and fillers

[5] Cement type I/II is cement meeting both the requirements for type I (general purpose) and type II (low C_3A content, higher sulfate resistance) of the ASTM standard C150 [1]

2.2. Mix compositions

In all mix compositions, a PCE superplasticizer with a solid concentration of 35% was used. More details about the choice of the various mixtures is given in the sections in which the experimental results are described. The mortars used in Section 3.3.1. were designed using the concrete equivalent mortars approach of Nachbaur et al. [276, 392].

Paste volume / water-to-powder ratio (by volume) [l/m³] / [-]	Sand 1 [kg/m³]	Gravel 1 [kg/m³]	Gravel 2 [kg/m³]	Cement 1 [kg/m³]	Limestone filler 1 [kg/m³]	Water [kg/m³]	SP dosage [l/m³]
400 / 0.75	800	279	459	312	346	171	3.31
400 / 0.90	800	279	459	344	269	189	2.50
400 / 1.05	800	279	459	373	204	205	1.95
375 / 0.75	835	291	478	292	324	161	3.95
375 / 0.90	835	291	478	323	252	178	2.80
375 / 1.05	835	291	478	349	191	192	2.00
350 / 0.75	869	303	498	273	302	150	5.31
350 / 0.90	869	303	498	301	236	166	3.63
350 / 1.05	869	303	498	326	178	179	2.38

Table 16: Mix compositions used in Section 3.1.

Mix nr	Water-to-powder ratio (by volume)	SP dosage	Cement 2	Limestone filler 2	Water	SP dosage
	[-]	[%]	[kg/m³]	[kg/m³]	[kg/m³]	[kg/m³]
1	0.85	0.118	948	632	459	1.12
2	0.90	0.118	923	615	474	1.09
3	0.95	0.118	899	600	487	1.06
4	1.00	0.118	877	585	500	1.03
5	0.85	0.159	948	632	459	1.51
6	0.90	0.159	923	615	474	1.47
7	0.95	0.159	899	600	487	1.43
8	1.00	0.159	877	585	500	1.39
9	0.75	0.200	1002	668	429	2.00
10	0.80	0.200	974	650	444	1.95
11	0.85	0.200	948	632	459	1.90
12	0.90	0.200	923	615	474	1.85
13	0.95	0.200	899	600	487	1.80

Table 17: Mix compositions used in Section 3.2.

Component	No VMA	Diutan gum	Corn starch	Attapulgite clay	Propylene carbonate
Sand 1 [kg/m³]	1140	1140	1140	1140	1140
Cement 3 [kg/m³]	487	487	487	487	487
Limestone filler 1 [kg/m³]	348	348	348	348	348
Water [kg/m³]	243	243	243	243	243
Superplasticizer [l/m³]	4.00	5.08	4.15	4.23	4.00
VMA [kg/m³]	-	0.12	2.43	0.75	1.22

Table 18: Mix proportions of the reference mixtures used in Section 3.3.

	Mix A – High yield stress SCC	Mix B – High plastic viscosity SCC
Gravel 2 [kg/m³]	470	470
Gravel 1 [kg/m³]	266	265
Sand 2 [kg/m³]	835	834
Cement 2 [kg/m³]	390	350
Limestone filler 2 [kg/m³]	160	250
Water [kg/m³]	195	175
PCE superplasticizer [l/m³]	1.86	4.00

Table 19: Reference mixtures used in Section 3.4

	Reference - bleeding	Silica fume replacement	Fly ash replacement
Gravel 1 [kg/m³]	576	576	576
Sand 2 [kg/m³]	1036	1036	1036
Cement 2 [kg/m³]	300	258	250
Limestone filler 2 [kg/m³]	283	283	283
Silica fume [kg/m³]		30	-
Fly ash [kg/m³]		-	39
Water [kg/m³]	154	154	154
PCE superplasticizer [l/m³]	12.29	13.43	9.29

Table 20: Mix C – Bleeding (Section 3.4.)

	Reference stickiness	Silica fume replacement	Fly ash replacement	Limestone filler replacement
Gravel 1 [kg/m³]	576	576	576	576
Sand 2 [kg/m³]	1036	1036	1036	1036
Cement 3 [kg/m³]	350	308	250	250
Limestone filler 2 [kg/m³]	241	241	241	325
Silica fume [kg/m³]	-	30	-	-
Fly ash [kg/m³]	-	-	77	-
Water [kg/m³]	154	154	154	154
PCE superplasticizer [l/m³]	14.29	14.57	8.57	11.43

Table 21: Mix D – High stickiness (Section 3.4.)

Component	Amount	
Sand 3	1064	kg/m³
Gravel 2	510	kg/m³
Cement 4 (not described above)	300	kg/m³
Limestone filler 3 (not described above)	300	kg/m³
Water	165	kg/m³
PCE superplasticizer	4.15	l/m³

Table 22: Mix composition used in Section 3.5.

2.3. Rheometer settings

As the measured rheogram depends on the rheological procedure and rheometer used during testing [393-396], it is important to describe exactly which test parameters have been applied during the experiments. For each rheometer, a short description of the apparatus is also included.

2.3.1. Anton Paar rheometer

2.3.1.1. Rotational rheometry

The Modified Bingham parameters [397] of paste and mortar were determined using an Anton Paar MCR 201 coaxial cylinder rheometer with a wide gap concentric cylinder configuration (Figure 37). The inner cylinder has a radius of 20 mm, a height of 60 mm and has a sanded surface; the outer cylinder has a radius of 35 mm and is provided with ribs to prevent wall slip (Figure 38). The rotational velocity profile, illustrated in Figure 39 for pastes and Figure 40 for mortars, consists of a preshear step, a stepwise decreasing rotational velocity profile, and the determination of a segregation point. A segregation point is needed to evaluate the degree of shear induced particle migration during the rheological test [393, 398-400]. Shear induced particle migration happens even at low shear rates and results in an underestimation of the yield stress and apparent viscosity at low shear rates [401]. The rheological test is invalid when the difference between the torque measured during the segregation point at about two thirds of the maximum rotational velocity differs more than 10% of the interpolated value from the actual measurement [398] or in case segregation was visually observed during testing.

The measured torque profile based on the last 5 seconds of each rotational velocity step was used to calculate the Modified Bingham constants (Equation 36) of pastes and the Bingham constants (Equation 37) of the mortars in which τ_0 is the yield stress and μ is the plastic viscosity. When the torque measured during a rotational velocity step was not in equilibrium, this data point was not used for the analysis. A plug flow correction at the lowest rotational velocities was performed if necessary [302]. Since the torque – rotational velocity diagram was linear and no segregation

occurred during the mortar tests, the Bingham model was applicable for mortars. The exponential decrease in torque measured during the pre-shear was used to calculate the breakdown speed $\alpha_{breakdown}$ and the exponential increase in torque measured during the last step at 5 rpm was used to calculate the buildup speed $\alpha_{buildup}$ fitting the curves to Equations 38 and 39.

$$\tau = \tau_{0,MB} + \mu_{MB} \cdot \dot{\gamma} + c_{MB} \cdot \dot{\gamma}^2 \quad \text{(Eq. 36)}$$

$$\tau = \tau_{0,B} + \mu_B \cdot \dot{\gamma} \quad \text{(Eq. 37)}$$

$$\tau_{80\,rpm} = C_1 + C_2 \cdot \exp(-\alpha_{breakdown} \cdot \dot{\gamma} \cdot t) \quad \text{(Eq. 38)}$$

$$\tau_{5\,rpm} = C_3 - C_4 \cdot \exp\left(-\alpha_{buildup} \cdot \dot{\gamma} \cdot t\right) \quad \text{(Eq. 39)}$$

Symbol	Unit	Definition
τ	[Pa]	Shear stress
$\dot{\gamma}$	[s^{-1}]	Shear rate
$\tau_{0,MB}$	[Pa]	Modified Bingham yield stress
μ_{MB}	[Pa.s]	Modified Bingham linear term
c_{MB}	[Pa.s^2]	Modified Bingham second order term
$\tau_{0,B}$	[Pa]	Bingham yield stress
μ_B	[Pa.s]	Bingham plastic viscosity
$\alpha_{breakdown}$	[-]	Breakdown speed
$\alpha_{buildup}$	[-]	Buildup speed
C_1, C_1, C_1, and C_1		Fitting parameters

Table 23: Symbols used in the Modified Bingham equation (Eq. 1)

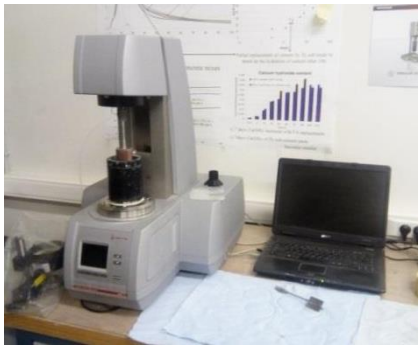

Figure 37: The Anton Paar MCR 201 rheometer configuration for rotational rheometry

Figure 38: The ribbed outer cylinder and sanded inner cylinder

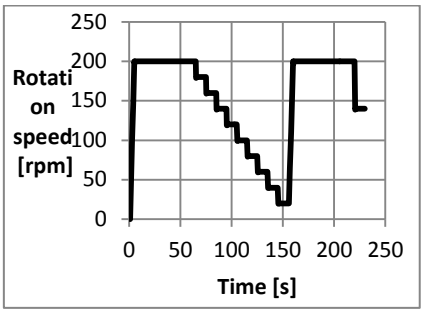

Figure 39: The rotational velocity profile for pastes

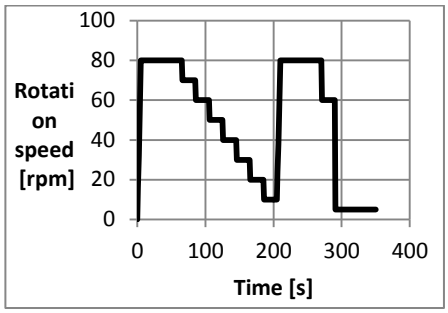

Figure 40: The rotational velocity profile for mortars

2.3.1.2. Oscillatory rheometry

Applying a small amplitude oscillatory shear or stress, the storage and loss modulus (Equations 40 to 43, abbreviations in Table 24) evolution in time can be measured [24, 25, 139, 227, 264, 265, 275, 288, 402, 403]. The storage modulus G' is responsible for the elastic part of the strain or stress response, the loss modulus G" for the viscous part.

$$\sigma = \sigma_0 \cdot \cos(\omega \cdot t) \quad \text{(Eq. 40)}$$

$$\gamma = \gamma_0 \cdot \cos(\omega \cdot t - \delta) \quad \text{(Eq. 41)}$$

$$G^* = \frac{\sigma_0}{\gamma_0} \cdot (\cos\delta + i \cdot \sin\delta) \quad \text{(Eq. 42)}$$

$$G^* = G' + i \cdot G'' \quad \text{(Eq. 43)}$$

Symbol	Definition
σ	Oscillatory stress [Pa]
σ_0	Amplitude of the applied stress [Pa]
ω	Angular velocity [1/s]
t	Time [s]
γ	Oscillatory strain [-]
γ_0	Amplitude of the oscillatory strain [-]
δ	Phase lag between the applied oscillatory stress and the resulting oscillatory strain [-] ($0 < \delta < \pi/2$)
G^*	Complex shear modulus [-]
G'	Storage modulus [-]
G''	Loss modulus [-]

Table 24: Abbreviations of Equations 40 to 43

In this project, oscillatory rheometry was used to monitor the structural buildup of the cement paste at rest. The storage modulus evolution in time under a constant small shear rate amplitude alternated with a breakdown step of two minutes was monitored using an Anton Paar MCR 201 rheometer with a vane in cylinder setup (Figure 41). A vane with a diameter of 15 mm and a height of 40 mm oscillates within a small angle and a frequency of 1 Hz in an outer cylinder with a radius of 35 mm. After destroying the structure in a 2 minutes time sweep with a strain of 50% (above the critical strain), the structural buildup inside the paste was monitored in a time sweep with a small strain of 0.1% (below the critical strain) for 20 minutes using the storage modulus G' [24, 227, 264]. A typical example of a measurement is shown in Figure 42.

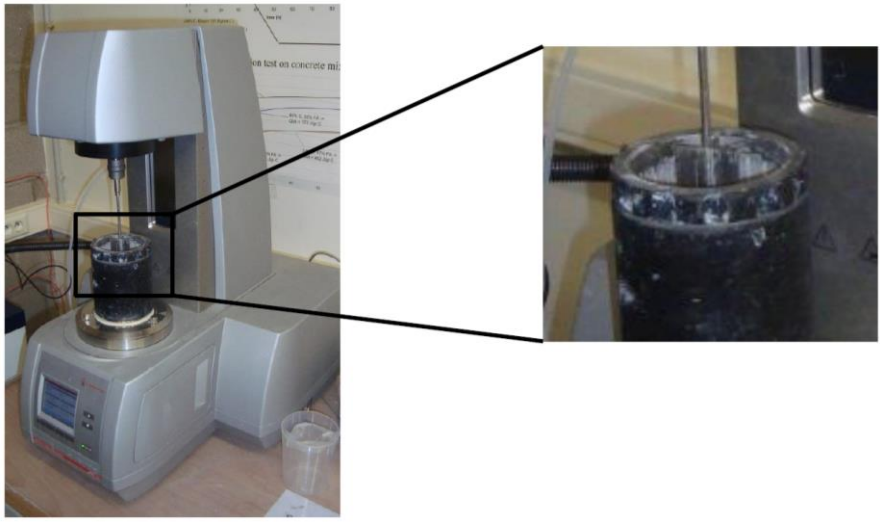

Figure 41: The Anton Paar MCR 201 rheometer configuration for oscillatory rheometry

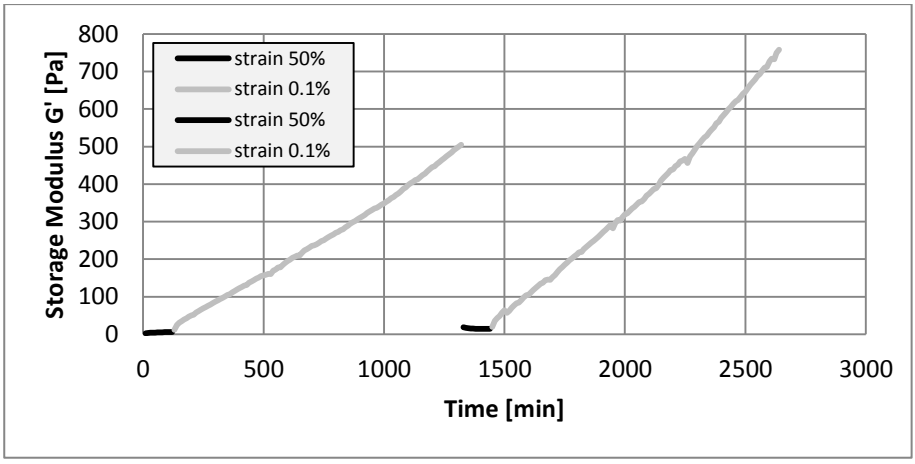

Figure 42: Monitoring of the Storage Modulus G' using oscillatory rheology

2.3.2. ICAR rheometer

2.3.2.1. Rotational rheometry

An ICAR rheometer was used in Section 3.3.2. to determine the rheological characteristics of SCC. The ICAR rheometer had a 6-bladed vane with a diameter of 127 mm and a height of 127 mm inserted in a ribbed cylindrical bucket with a diameter of 286 mm (Figure 43). The torque necessary to rotate the vane according to a fixed rotation speed profile including a segregation point, as illustrated in Figure 44, is measured. The data measured during the last 2 seconds of every rotational velocity step was used to calculate the Modified Bingham rheological parameters [397] (Equation 36). When plug flow occurred, a plug flow correction was applied during the analysis [397].

Figure 43: The ICAR rheometer

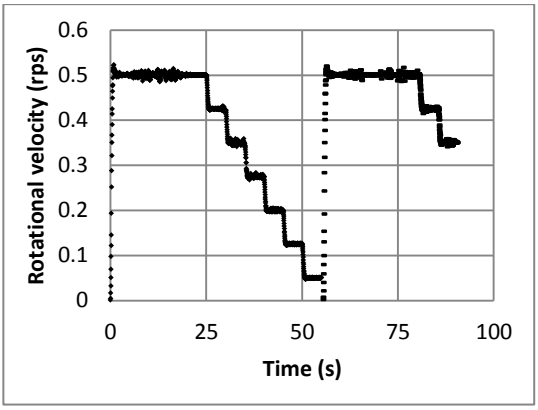

Figure 44: The rotational velocity profile used in an ICAR rheometer

2.3.2.2. Static yield stress measurements

An ICAR rheometer with a four-bladed vane was used for static yield stress measurements. The vane had a diameter of 127 mm and a height of 127 mm. Every ten minutes, a static yield stress was performed in a sample at rest. During such a measurement, the torque necessary to maintain a constant small rotational velocity of 0.001 rps is measured (Figure 45). Once a maximum peak torque is reached, the rotation is stopped to allow the continuation of the thixotropic buildup inside the sample. The peak torque is converted into the static yield stress assuming all the shearing happens across a cylindrical surface surrounding the vane. Experimental scatter is filtered out with a polynomial fit around the peak torque as shown in Figure 45.

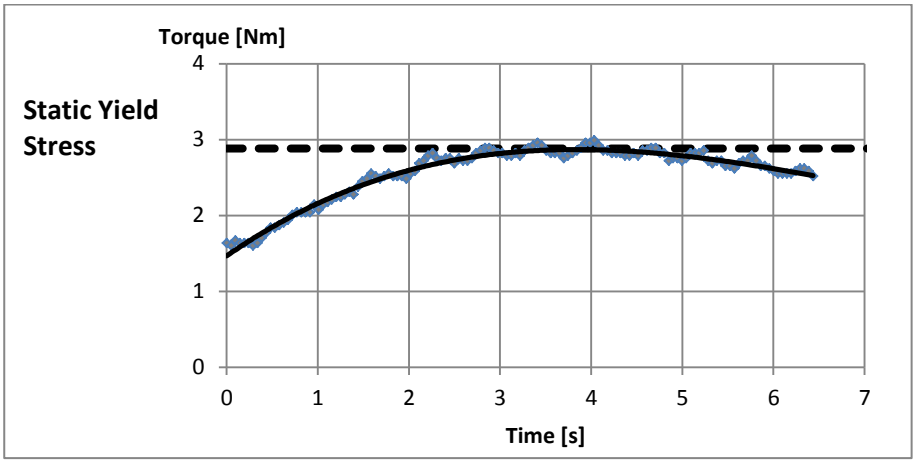

Figure 45: Torque measurement during the static yield stress test

2.3.3. Contec rheometer

A Contec viscometer 5 has also been used during the project. This wide gap concentric cylinder rheometer with an inner cylinder radius of 100 mm and an outer cylinder radius of 145 mm (Figure 46) only measures the torque on the top part of the inner cylinder, avoiding a complicated three dimensional bottom effect. Both the inner and outer cylinders are equipped with vertical ribs to prevent wall slip. The applied rotational velocity profile is shown in Figure 47: after a preshear step at a rotational velocity of 0.40 rps during 25 seconds, the samples were subjected to a stepwise decreasing rotational velocity profile from 0.40 to 0.025 rps in 10 steps of 5 s. When the torque measurement during a constant rotational velocity step was not in equilibrium, it was not considered in the analysis. A segregation point was measured after the test.

The Bingham model (Equation 37) was used to calculate the dynamic yield stress and plastic viscosity. For all mixtures, a linear torque – rotational velocity diagram was measured and the Bingham model was applicable. A plug flow correction was performed in case plug flow occurred [302].

Figure 46: The Contec rheometer

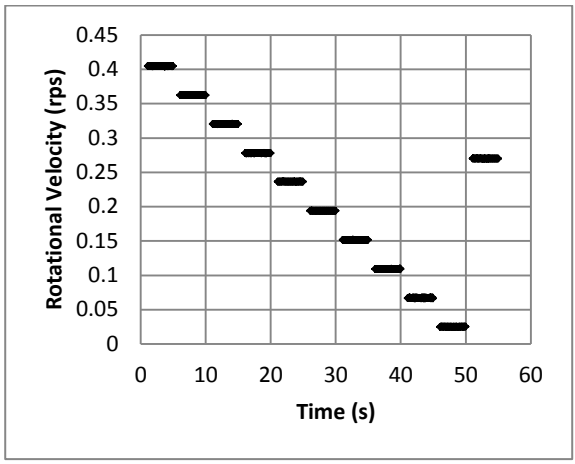

Figure 47: The rotational velocity profile used in an Contec rheometer

3. Experimental program: mix design and robustness

3.1. Paste volume and water-to-powder ratio

By varying the paste volume and the water-to-powder ratio of SCC mixtures, a wide range of rheological properties can be obtained. The optimal rheological properties of SCC, illustrated in the rheogram of Wallevik and Wallevik [404] (Figure 48), are situated in between two extreme situations: SCC mixtures with a relatively high yield stress and a very low plastic viscosity on the left side of the rheogram, and SCC mixtures with a zero yield stress and a high plastic viscosity on the right side of the rheogram.

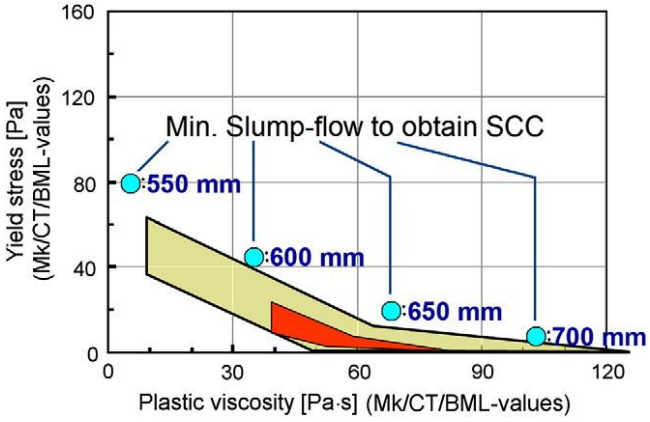

Figure 48: Range of suitable rheological characteristics of SCC [404]

As the workability demands depend on the application, different rheological parameters are needed for various applications. SCC mixtures with a relatively high yield stress and low plastic viscosity have a relatively small slump flow and low V-funnel flow time and therefore allow fast and convenient casting of large elements. A zero or near-zero yield stress combined with a high plastic viscosity flows more slowly but is able to fill all small edges in the formwork. The EFNARC guidelines [6] contain a table ranking the needed workability demands for certain applications (Figure 49).

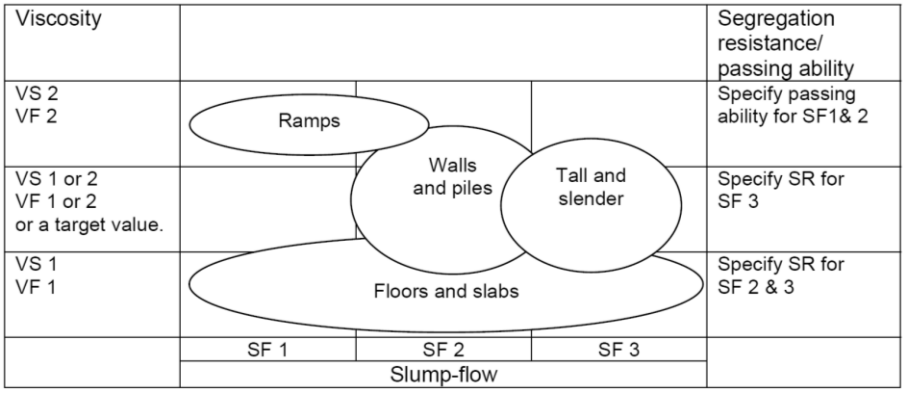

Figure 49: Workability demands for various types of applications [6]

By examining the impact of the two parameters which determine the rheological behavior of SCC, a possible link between the rheology and robustness can be investigated. The paste volume and water-to-powder ratio are varied within pragmatic ranges, the Sieve Stability Index (S.S.I.) is always kept in the range of 8-12% by adjusting the superplasticizer dosage of each mixture (Table 16 in Section 2). The paste volume of 350, 375, and 400 l/m³ and the volumetric water-to-powder ratios correspond with the 20%, 50%, and 80% fractals of a database summarizing the properties of SCC mixtures used in more than 175 papers [316, 405]. For every reference mixture, another mixture with 8 l/m³ water in excess and a mixture with 8 l/m³ water lacking was manufactured in order to test the robustness against changes in the water content.

The following mix procedure was used: (1) 1 minute mixing of all dry constituents; (2) 1 minute mixing after addition of the water; (3) 2 minutes mixing after addition of the superplasticizer. 3 minutes after mixing, the slump flow, V-funnel time, SSI, L-box ratio, density and air content were determined. Table 25 summarizes the fresh properties of the nine reference mixtures. The values for the reference mixtures are listed together with the change of the test response due to the presence of more or less water In Table 26. In this table, the robustness is expressed in two manners: the test response variations per liter water (e.g. the

change in slump flow: ΔSF / 16 l/m³, see Equation 44) and the ratio of the response interval (difference between the largest and the smallest test response) divided by the tests response of the reference mixture and the water variation (eg. $\Delta SF / SF_{ref} / 16\ l/m^3$, Equation 45). Both parameters reflect the slope of test response variation in Figures 50 to 59, once in absolute terms and once relative to the reference value. All workability tests except the L-box ratio gave a good picture of the impact of fluctuations of the water content on the fresh behaviour of the mixtures. The raw data is summarized in Appendix A.

$$\frac{\Delta SF}{16\frac{l}{m^3}} = \frac{SF_{+8\ l/m^3} - SF_{-8\ l/m^3}}{+8\ l/m^3 - (-8\ l/m^3)} \quad \text{(Eq. 44)}$$

$$\frac{\Delta SF}{SF_{ref} \cdot 16\ l/m^3} = \frac{SF_{+8l/m^3} - SF_{-8l/m^3}}{SF_{ref} \cdot (+8l/m^3 - (-8l/m^3))} \quad \text{(Eq. 45)}$$

Paste volume / water-to-powder ratio by volume [l/m³] / [-]	Slump flow [mm]	V-funnel time [s]	L-box ratio [-]	S.S.I. [%]	Density [kg/m³]	Air content [%]
400 / 0.75	673	13.7	0.82	9.4	2475	2.5
400 / 0.90	680	6.3	0.85	12.2	2369	1.6
400 / 1.05	688	3.5	0.83	12.0	2369	1.2
375 / 0.75	705	17.6	0.96	11.2	2394	1.9
375 / 0.90	680	8.0	0.91	10.1	2375	1.8
375 / 1.05	680	4.0	0.86	12.3	2372	1.4
350 / 0.75	865	15.9	1.00	10.5	2406	0.9
350 / 0.90	750	10.5	0.98	9.4	2375	1.5
350 / 1.05	675	5.3	0.80	8.0	2369	1.5

Table 25: Fresh state properties of reference mixtures

Paste volume (l/m3) /water-powder ratio by volume	400 / 0.75	400 / 0.90	400 / 1.05	375 / 0.75	375 / 0.90	375 / 1.05	350 / 0.75	350 / 0.90	350 / 1.05
Slump flow [mm]	673	680	688	705	680	680	865	750	675
ΔSF / 16 l/m³	16.3	10.2	13.1	9.7	8.6	8.3	5.6	8.1	9.2
ΔSF / SF_{ref} / 16 l/m³	0.024	0.015	0.019	0.014	0.013	0.012	0.006	0.011	0.014
V-funnel time [s]	13.7	6.3	3.5	17.6	8.0	4.0	15.9	10.5	5.3
ΔVF / 16 l/m³	0.71	0.24	0.24	1.15	0.34	0.14	1.36	0.34	0.18
ΔVF / VF_{ref} / 16 l/m³	0.052	0.038	0.067	0.065	0.043	0.035	0.086	0.032	0.033
L-box ratio [-]	0.82	0.85	0.83	0.96	0.91	0.86	1.00	0.98	0.80
ΔLB / 16 l/m³	0.049	0.012	0.022	0.004	0.017	0.009	0.001	0.002	0.012
ΔLB / LB_{ref} / 16 l/m³	0.059	0.014	0.026	0.004	0.018	0.011	0.001	0.001	0.001
S.S.I. [%]	9.4	12.2	12.0	11.2	10.1	12.3	10.5	9.4	8.0
ΔSSI / 16 l/m³	1.04	0.51	0.80	0.86	0.50	0.52	0.57	0.28	0.31
ΔSSI / SSI_{ref} / 16 l/m³	0.111	0.042	0.068	0.077	0.050	0.043	0.054	0.030	0.039

Table 26: Workability test responses and robustness

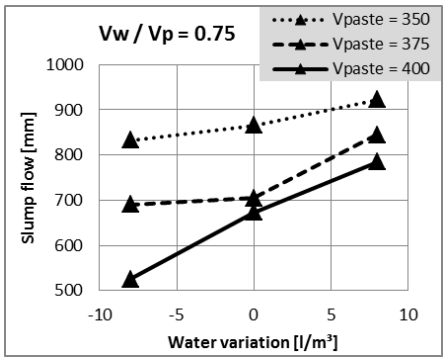

Figure 50: Influence of the paste volume and water-to-powder ratio on the slump flow

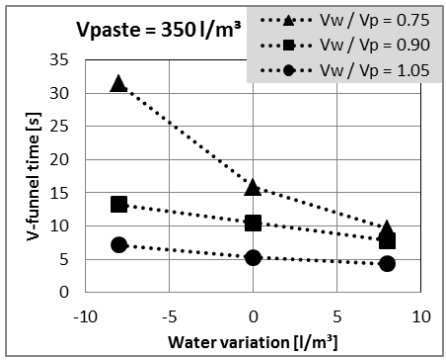

Figure 51: Influence of the paste volume and water-to-powder ratio on the V-funnel time

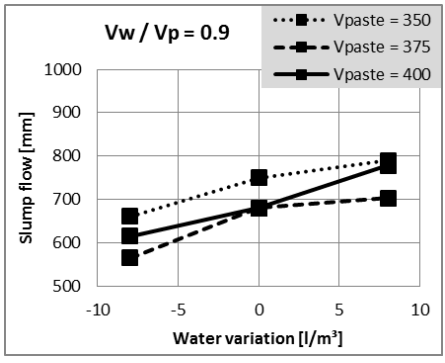

Figure 52: Influence of the paste volume and water-to-powder ratio on the slump flow

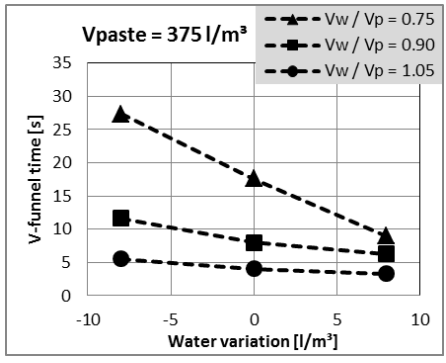

Figure 53: Influence of the paste volume and water-to-powder ratio on the V-funnel time

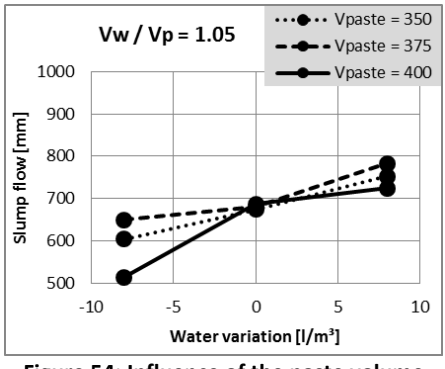

Figure 54: Influence of the paste volume and water-to-powder ratio on the slump flow

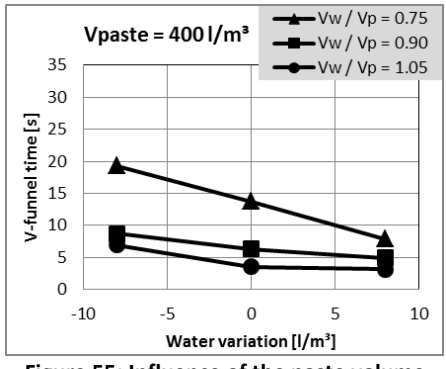

Figure 55: Influence of the paste volume and water-to-powder ratio on the V-funnel time

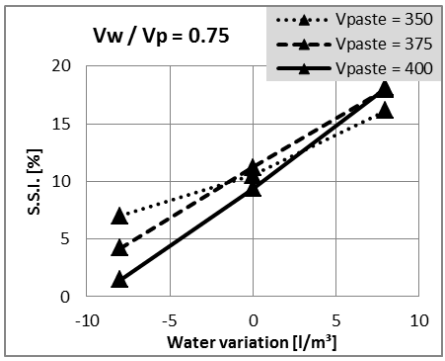

Figure 56: Influence of the paste volume and water-to-powder ratio on the sieve stability

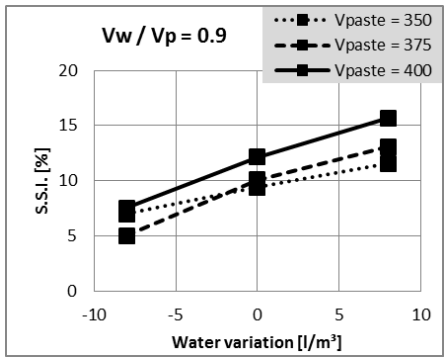

Figure 57: Influence of the paste volume and water-to-powder ratio on the sieve stability

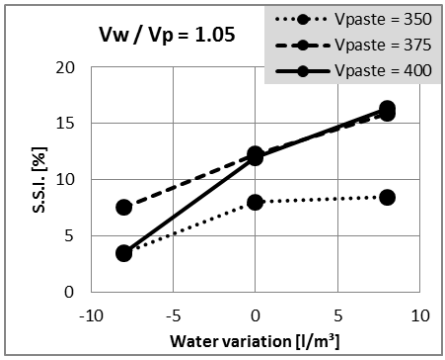

Figure 58: Influence of the paste volume and water-to-powder ratio on the sieve stability

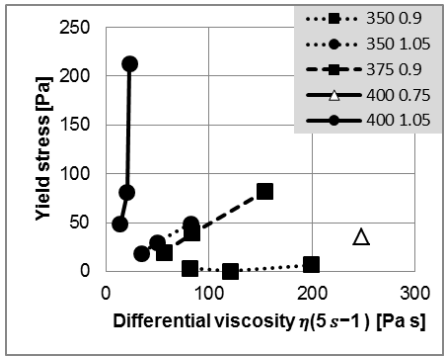

Figure 59: Influence of the paste volume and water-to-powder ratio on the rheology

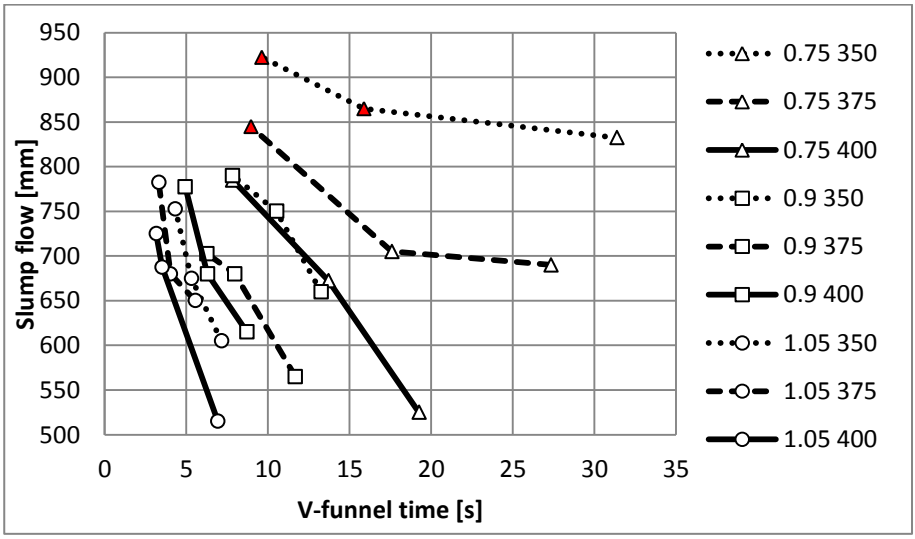

Figure 60: Impact of the paste volume and water-to-powder ratio on the robustness, illustrated in a workability box

Small changes in the water content almost never result in problems in the three key characteristics of SCC at the same time. As a result it is not evident to grasp the variations of the slump flow, V-funnel time, L-box ratio, and sieve stability index into one global 'robustness value' as suggested by Billberg et al. [31, 32]. A better approach is to evaluate the robustness of a mixture by investigating its most critical parameter, which also might depend on the application.

The observed impact of the paste volume and water-to-powder ratio is summarized in Table 27. The effect of the water-to-powder ratio on the robustness of the S.S.I. has been studied while varying both the water and powder contents in order to maintain the given paste volume. A different impact could have been obtained if the water or powder contents would have been kept constant.

Mixtures with a higher paste volume require a lower dosage of superplasticizer to reach a S.S.I. of 10±2%. Such mixtures have a lower slump flow value and are more sensitive to small reductions of the water content. the combined effect of a higher water-to-powder ratio and the associated reduction in superplasticizer dosage on the slump flow robustness is limited.

The robustness of the V-funnel time is mainly affected by the water-to-powder ratio. Mixtures with a higher water-to-powder ratio need a lower superplasticizer dosage in order to reach a S.S.I. of 10±2% and have a lower, more robust V-funnel time. The V-funnel time of more viscous SCC mixtures with a low water-to-powder ratio is very sensitive to a small decrease in the water content. The V-funnel time robustness of such mixtures can be enhanced with an increased paste volume, up to a limit at which the higher paste volume also negatively affects the robustness of the slump flow.

The L-box results are more difficult to interpret because of the poor flowability of the mixtures with 8 l/m³ less water, a paste volume of 400 l/m³ and volumetric water-to-powder ratios of 0.75 and 1.00, which had a slump flow of respectively 525 and 515 mm. As a result, no clear trends on the L-box ratio results could be observed.

	Impact paste volume	Impact water-to-powder ratio
Slump flow	As the paste volume increases, the robustness of the slump flow to water variations decreases.	The water-to-powder ratio has no clear influence on the robustness of the slump flow.
V-funnel time	When the paste volume increases, the robustness slightly increases.	A lower water-to-powder ratio increases the sensitivity to small variations of the water content. Especially a small decrease of the water content can result in a very sticky, unworkable mixture.
S.S.I.	An increase of the paste volume results in a less robust S.S.I.	A decrease in water-to-powder volumetric ratio seems to decrease the robustness of the S.S.I., but the effect is less significant than a change in paste volume.

Table 27: The influence of the paste volume and water-to-powder ratio on the robustness of SCC

3.2. Water Film Thickness (WFT)

In order to investigate the mechanisms behind the water-to-powder volumetric ratio more in depth, an additional series of tests was conducted in which the influence of the water content and the superplasticizer content is investigated independently from each other on paste level. The material properties are given in Section 2.1 (Cement 2 and Limestone filler 2), the mix compositions are summarized in Table 17 of Section 2.2.

In order to differentiate the water filling the voids from the water film actually lubricating the solid particles, the concept of the water film thickness (WFT) has been used (Section 7.5 of the literature review). The water film thickness is calculated using equations 46 to 48, using the abbreviations of Table 28. The maximum packing density ϕ_{max} is calculated based on the maximum possible density of the paste obtained by varying the water content [85, 327-329]. The determination of the maximum packing density is described in more detail in Appendix B. Using oscillatory rheometry, the impact of the WFT and the superplasticizer dosage on the structural buildup is monitored together with the robustness against small changes in the water content (±3% of the water content). The coefficient of variation of the WFT measurements is about 2%.

$$WFT = \frac{u_w - u_{min}}{A_s} \quad \text{(Eq. 46)}$$

$$u_{min} = \frac{1 - \phi_{max} - \varepsilon_a(\phi_{max})}{\phi_{max}} \quad \text{(Eq. 47)}$$

$$u_w = \frac{1 - \phi - \varepsilon_a(\phi)}{\phi} \quad \text{(Eq. 48)}$$

Symbol	Unit	Name	Definition
WFT	[m]	Water Film Thickness	Thickness of the excess water layer covering the solid particles.
ϕ	[%]	Packing density	The volume of solids divided by the bulk volume
ϕ_{max}	[%]	Maximum packing density	The maximum possible packing density possible for this mixture under varying water content.
$\varepsilon_a(\phi)$	[%]	Air content	The volume of air divided by the bulk volume.
u_w	[%]	Water ratio	The volume of water divided by the volume of solids.
u_{min}	[%]	Minimum voids ratio	The water ratio corresponding with the maximum packing density.
A_s	[m²/m³]	Specific surface area of the solids	The total surface of all solids in one volumetric unit.

Table 28: Definition of the parameters used in Equations 46 to 48

Figure 61 illustrates the ranges of water-to-powder volumetric ratio (0.85, 0.90, and 0.95) and superplasticizer dosage (0.118%, 0.159%, and 0.200% of the cement weight) tested during this experimental program. In order to cover a wider range of WFT (Figure 62), four additional mixtures were tested with water-to-powder / superplasticizer dosage combinations of respectively 0.75/0.200%, 0.80/0.200%, 1.00/0.159%, and 1.00/0.118%. The cement-to-powder ratio (by weight) was always kept at 0.6 .

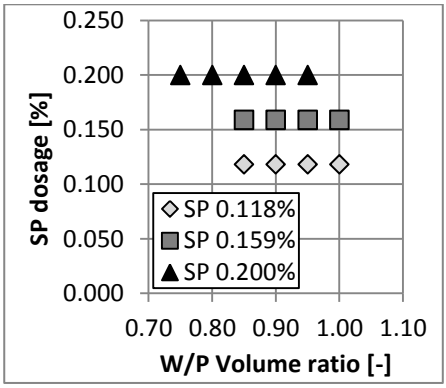

Figure 61: Range of water-to-powder volumetric ratios and superplasticizer dosages

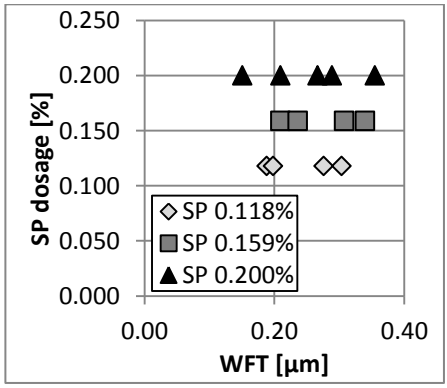

Figure 62: Corresponding range of WFT and superplasticizer dosages

The measured properties of the 13 reference mixtures were determined according to the time table in Table 29 and are listed in Table 29. The properties of the mixtures with ±3% water are given in Appendix A. The range of covered WFT values is illustrated in Figure 62. As illustrated in Figure 63, a higher superplasticer dosage

provides more free water in the paste mixture as indicated by the higher maximum packing densities, and thus results in a higher WFT.

Time	Duration	Step	Mixing speed
0 min	1 min	Mixing of cement, limestone powder and water	140 rpm
1 min	1 min	Adding the superplasticizer	140 rpm
2 min	1 min	Mixing	285 rpm
3 min	2 min	A thin layer of paste is scraped from the mixing arm and the walls and bottom of the mixing bowl	0 rpm
5 min	1 min	Mixing	285 rpm
6 min	11 min	Rest	0 rpm
17 min	1 min	Remixing	285 rpm
18 min	2 min	Rest	0 rpm
20 min	3 min	Rotational rheometry: determination of the Modified Bingham parameters	-
25 min	45 min	Start oscillatory rheometry: measurement of G' buildup	-
29 min	1 min	Remixing	285 rpm
30 min	5 min	Measuring the density and air content	-

Table 29: Timing of the test procedures

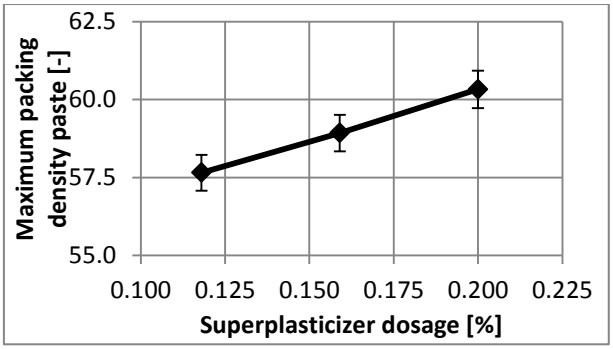

Figure 63: Impact of the superplasticizer dosage on the maximum packing density of pastes

A clear link between the WFT / superplasticizer dosage combination and the rheology of the mixture can be observed in Table 29 and Figures 65 to 67. Based on the shear stress at a shear rate of 20 s^{-1}, the impact of the WFT and superplasticizer is investigated more in detail in Figure 68. Similar conclusions can be drawn based on a shear rate of 10 s^{-1} or 50 s^{-1}.

Mix nr	Water-to-powder ratio	Super-plasticizer dosage	WFT	Yield stress	MB linear term	MB 2nd order term	Increase in G' (1)	Increase in G' (2)
	[-]	[%]	[µm]	[Pa]	[Pa.s]	[Pa.s²]	[Pa]	[Pa]
1	0.85	0.118	0.188	16.38	1.59	0.0000	1073	1873
2	0.90	0.118	0.198	7.05	0.85	0.0005	711	1218
3	0.95	0.118	0.276	2.55	0.39	0.0024	717	1665
4	1.00	0.118	0.304	2.17	0.30	0.0012	514	1220
5	0.85	0.159	0.209	2.68	0.41	0.0048	322	365
6	0.90	0.159	0.236	2.23	0.32	0.0034	306	364
7	0.95	0.159	0.308	0.62	0.28	0.0018	302	411
8	1.00	0.159	0.340	0.49	0.14	0.0031	225	521
9	0.75	0.200	0.151	8.71	0.68	0.0086	701	1007
10	0.80	0.200	0.209	3.22	0.28	0.0066	265	462
11	0.85	0.200	0.267	0.77	0.32	0.0047	206	202
12	0.90	0.200	0.289	0.00	0.22	0.0031	256	504
13	0.95	0.200	0.355	0.00	0.18	0.0022	382	2836

Table 29: Properties of the reference self-compacting paste mixtures

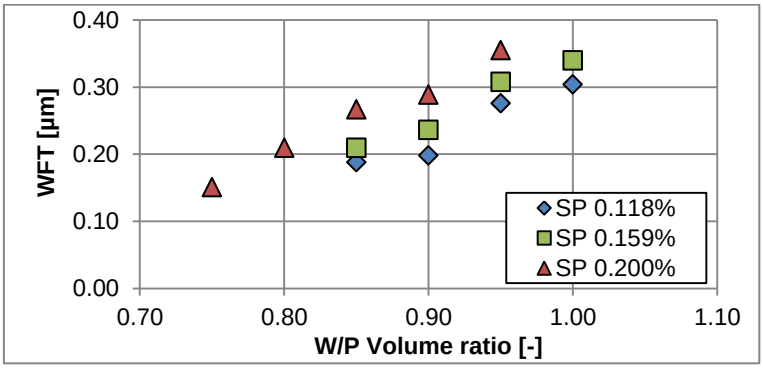

Figure 64: Influence of the superplasticizer dosage on the WFT

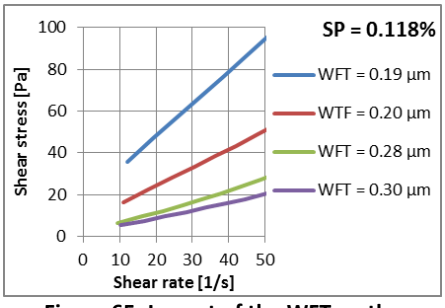

Figure 65: Impact of the WFT on the rheology (SP dosage of 0.118 %)

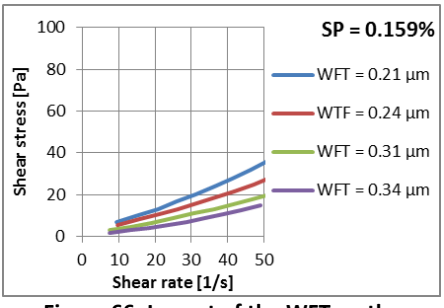

Figure 66: Impact of the WFT on the rheology (SP dosage of 0.159 %)

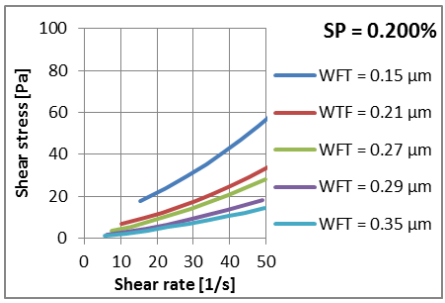

Figure 67: Impact of the WFT on the rheology (SP dosage of 0.200 %)

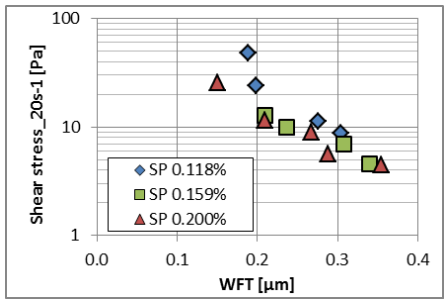

Figure 68: Impact of the WFT and superplasticizer dosage on the rheology

The robustness against small variations in the water content is tested by changing the water content with ±3%. Figures 69 to 72 illustrate the impact of variations in the water content on the rheology for 3 mixtures with a similar WFT. Table 30 summarizes the impact on the rheological characteristics. Because the variations in the test results should be compared with the value of the reference mixture, all changes are expressed as percentages.

Figure 73 illustrates that an increasing WFT or superplasticizer dosage, increases the robustness of the shear stress at a shear rate of 20 s^{-1} ($\tau(20\ s^{-1})$. A similar trend can be observed using the shear stress inclination at 20 s^{-1} ($\frac{d\tau}{d\dot{\gamma}}(20\ s^{-1})$. The effect on the yield stress seems to be independent of WFT (similar slopes are obtained).

Figures 69 and 74 to 76 show the changes in a rheogram. A logarithmic scale is used to illustrate the graphs because the impact of a change in the rheological parameters depends on the value of the parameter itself. A change of 0.1 Pa on the yield stress has a more pronounced impact on a mixture with a yield stress of 0.2 Pa than on a mixture with a yield stress of 50 Pa. Higher water-to-powder ratios resulted in a higher water film thicknesses (WFT), and in more robust mixtures. A higher superplasticizer dosage resulted in a higher WFT and also more robust mixtures. No clear influence of the yield stress τ_0, inclination of the shear stress at 20 s^{-1} $\frac{d\tau}{d\dot{\gamma}}(20\ s^{-1})$, or the shear stress at 20 s^{-1} $\tau(20\ s^{-1})$ on the robustness is observed.

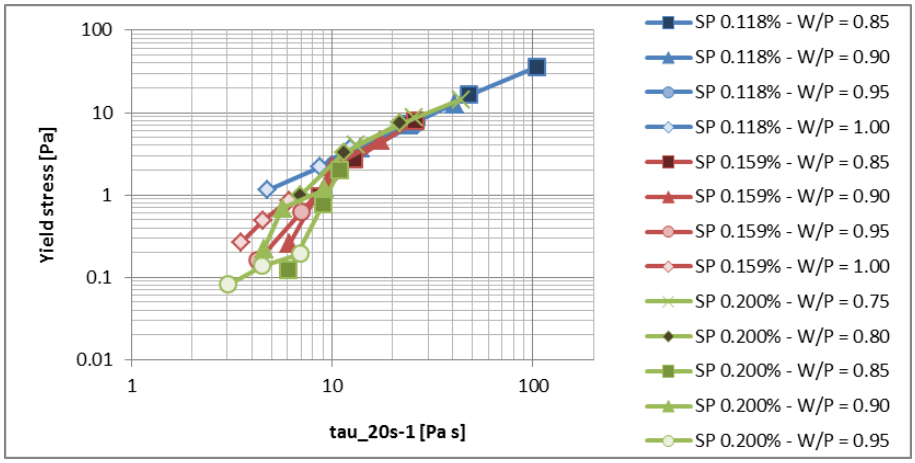

Figure 69: Impact of variations in the water content on the rheology

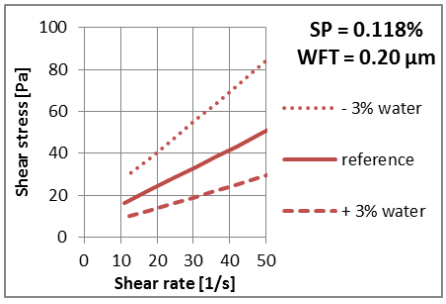

Figure 70: Impact of small changes in the water content on the rheology (WFT of 0.20 µm; SP dosage of 0.118 %)

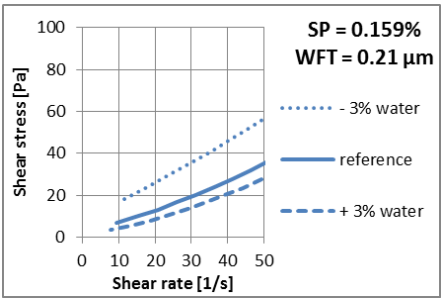

Figure 71: Impact of small changes in the water content on the rheology (WFT of 0.21 µm; SP dosage of 0.118 %)

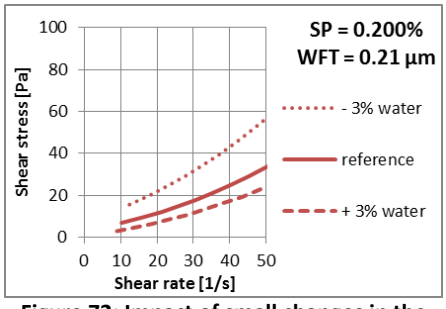

Figure 72: Impact of small changes in the water content on the rheology (WFT of 0.21 µm; SP dosage of 0.118 %)

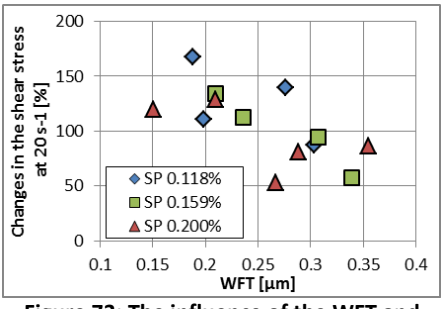

Figure 73: The influence of the WFT and superplasticizer dosage on the robustness

Mix nr	Water-to-powder ratio	Superplasticizer dosage	WFT	Changes in the shear stress at 20s-1	Changes in the yield stress	Changes in the shear stress inclination at 20s-1
	[-]	[%]	[µm]	[%]	[%]	[%]
1	0.85	0.118	0.188	167	176	160
2	0.90	0.118	0.198	111	126	105
3	0.95	0.118	0.276	140	201	115
4	1.00	0.118	0.304	87	118	73
5	0.85	0.159	0.209	134	257	77
6	0.90	0.159	0.236	112	196	91
7	0.95	0.159	0.308	94	313	75
8	1.00	0.159	0.340	57	121	51
9	0.75	0.200	0.151	120	118	95
10	0.80	0.200	0.209	128	199	89
11	0.85	0.200	0.267	53	245	48
12	0.90	0.200	0.289	81	248	57
13	0.95	0.200	0.355	86	90	73

Table 30: Robustness of the reference mixtures against small changes in the water content

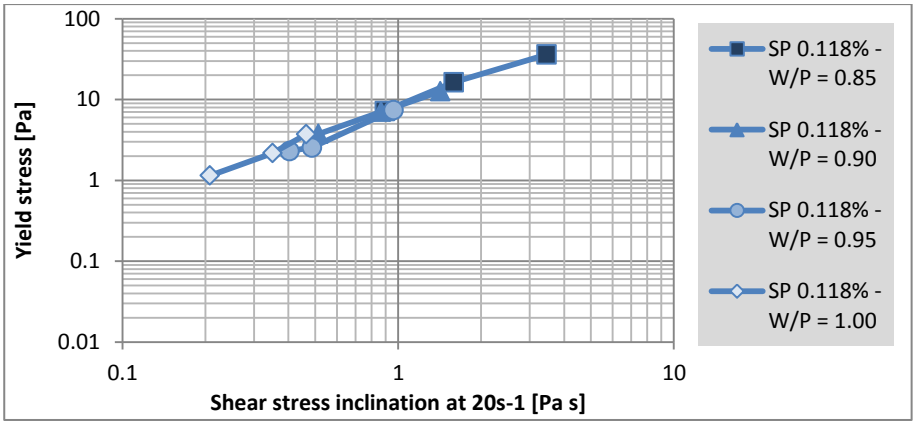

Figure 74: Robustness of the rheology illustrated in a rheogram (SP 0.118%)

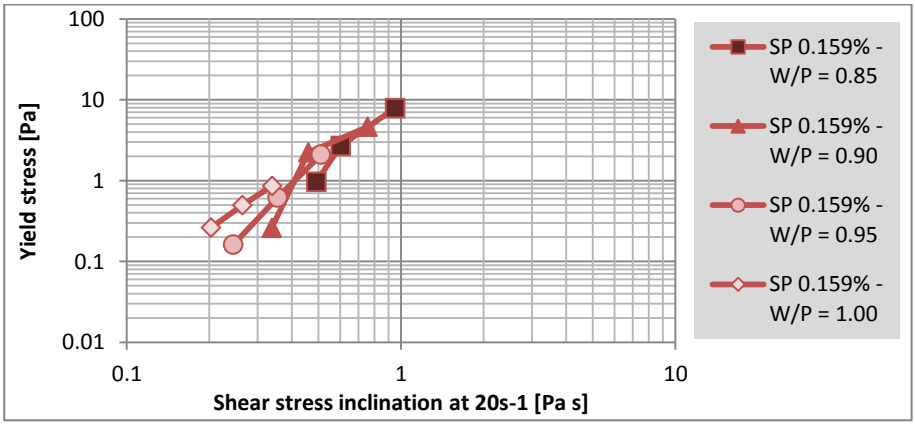

Figure 75: Robustness of the rheology illustrated in a rheogram (SP 0.159%)

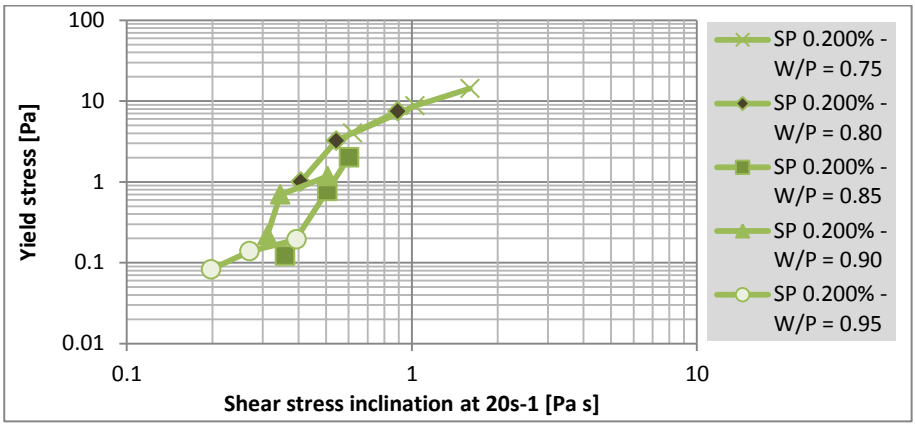

Figure 76: Robustness of the rheology illustrated in a rheogram (SP 0.200%)

Table 31 and Figure 76 summarize the storage modulus G' evolution during the first and second 20 min of structural buildup during oscillatory rheology measurements (G'_1 and G'_2) as described in Section 2.3.1.2. Mixtures with a higher early age structural buildup as measured by the increase in storage modulus G' at rest also were less robust. In Figures 77 to 80, the relation between the sensitivity of the rheology and the structural buildup as measured by the storage modulus G' buildup at rest is illustrated.

Mix nr	Water-to-powder ratio	Superplasticizer dosage	WFT	Yield stress	Inclination of the shear stress at 20s-1	Increase in G'_1	Increase in G'_2
	[-]	[%]	[µm]	[Pa]	[Pa s]	[Pa]	[Pa]
1	0.85	0.118	0.188	16.38	1.59	1073	1873
2	0.90	0.118	0.198	7.05	0.87	711	1218
3	0.95	0.118	0.276	2.55	0.49	717	1665
4	1.00	0.118	0.304	2.17	0.35	514	1220
5	0.85	0.159	0.209	2.68	0.60	322	365
6	0.90	0.159	0.236	2.23	0.46	306	364
7	0.95	0.159	0.308	0.62	0.35	302	411
8	1.00	0.159	0.340	0.49	0.26	225	521
9	0.75	0.200	0.151	8.71	1.03	701	1007
10	0.80	0.200	0.209	3.22	0.54	265	462
11	0.85	0.200	0.267	0.77	0.50	206	202
12	0.90	0.200	0.289	0.00	0.35	256	504
13	0.95	0.200	0.355	0.00	0.27	382	2836

Table 31: The robustness evaluation of all reference mixtures

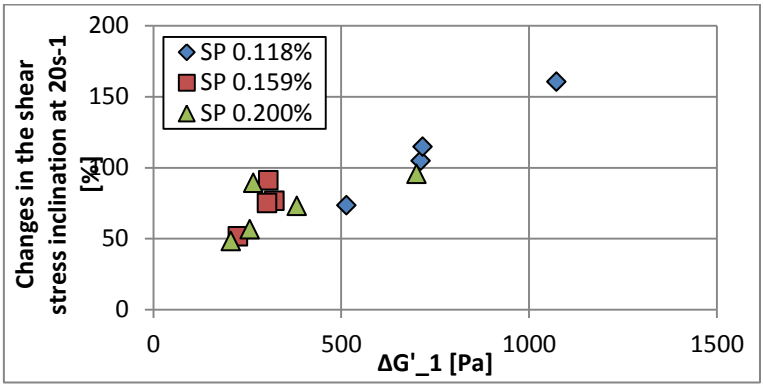

Figure 77: Influence of the structural buildup on the robustness of the shear stress at 20 s^{-1}

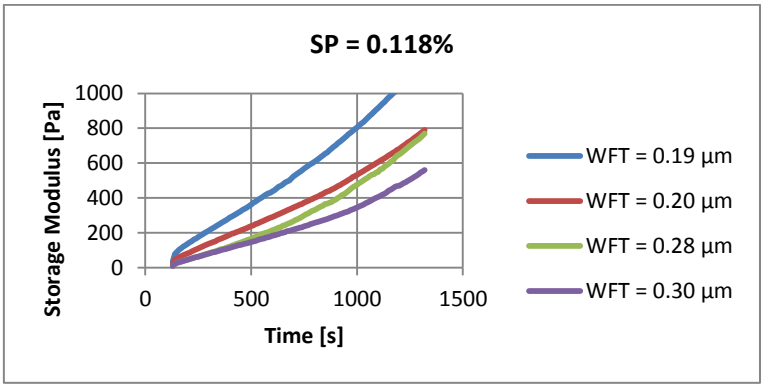

Figure 78: Impact of the WFT on the storage modulus G_1' evolution – SP dosage of 0.118%

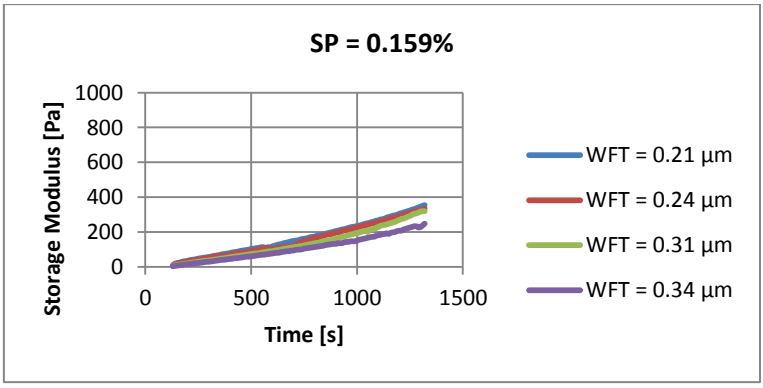

Figure 79: Impact of the WFT on the storage modulus G_1' evolution – SP dosage of 0.159%

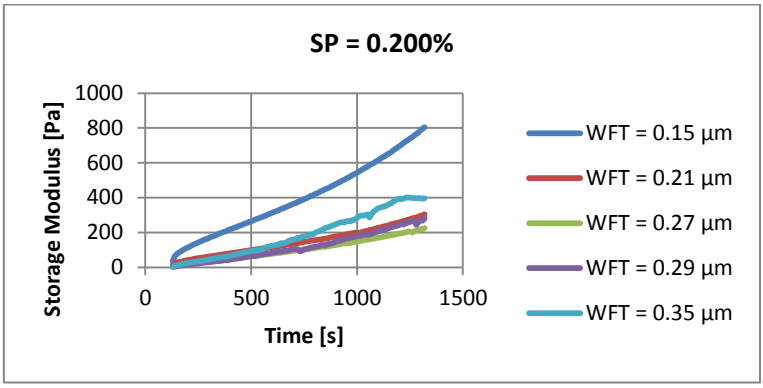

Figure 80: Impact of the WFT on the storage modulus G_1' evolution – SP dosage of 0.200%

3.3. Viscosity Modifying Admixtures (VMA's)

Many authors and admixtures manufacturers recommend the use of VMA's as a robustness enhancing product [31, 38, 79, 88, 93, 104-116]. In this section, the impact of VMA's on the rheology, structural buildup and robustness of self-compacting mortars and SCC is studied. The use of mortars allows testing a larger number of samples and simulates better the dispersion state of SCC compared to paste mixtures. Pastes, in which no aggregates are providing a ball bearing effect during the mixing process, differ in dispersion state and hydration rate compared to SCC.

3.3.1. Experiments on mortars

Obviously, not all types of VMA's were tested during this project. Only four types of VMA's were selected for an exploratory experimental program: purified attapulgite clay, diutan gum, corn starch, and propylene carbonate. Their properties are summarized in Table 32. The raw data of the experiments are summarized in Appendix A. The impact of small variations in the water content (±6.95 l/m³, corresponding with a variation of ±5 l/m³ water in the equivalent concrete) on the rheology and robustness of mortars was measured using the flow spread test, V-funnel flow time, and Bingham parameters as determined with an Anton Paar rheometer (Section 2.3.1). The thixotropic behaviour of the mortars was evaluated using the breakdown speed during the preshear step of the rheological test and a low shear rate buildup step. For each reference mixture (mix composition given in Table 18 of Section 2.2.), the VMA dosage was based on the manufacturers recommended dosage. The superplasticizer dosage of each reference mixture was adjusted to reach a flow spread of 240 – 260 mm.

	Attapulgite clay	Diutan gum	Starch	Propylene carbonate (PPC)
Description	Small clay needles with negative charges along its main axis and the pH-dependent charges at the ends [280]	High molecular weight microbial polysaccharide compatible with cement hydration products [105]	Natural polysaccharide. In this experimental program, corn starch is used.	A carbonate ester derived from propylene glycol, used as a polar, aprotic solvent.
Effect in concrete	A strong increase of the floc strength [289, 294]	Hydrogen bonds fix part of the water and increases the yield stress and plastic viscosity [78]. Polymer chains entangle at rest and align with the flow when sheared.	Increases the yield stress, but has only a small effect on the plastic viscosity [98]. Superplasticizer should be added before the starch to prevent adsorption onto cement particles [222].	The propylene glycol develops water bonds, inducing a network structure [406]. The carbonate anions might affect the cement hydratation process.
Effect robustness	Combined with a reduction of the amount of filler, it should improve the robustness.	Reported to enhance the robustness of SCC mixes [105].	Reported to enhance the robustness of SCC mixes [37, 104, 107, 113, 117].	Unknown
Application	- Stabilizing mineral suspensions - Slipform pavement SCC [293]	- Stabilizer in SCC	- Stabilizer in SCC	- Aprotic solvent - Thixotropy-enhancing admixture in SCC [406]

Table 32: Properties of the applied VMA's

Table 34 summarizes the rheological parameters and robustness of all mortars, tested according to the procedure given in Table 33. For each test, the result of the reference test (e.g. S), the difference between the maximum and the minimum values divided by the variation in water content (e.g. ΔS / 10 l/m³), and the difference divided by the test result of the reference mixture and the water variation (e.g. $\Delta S/S_{ref}$/10 l/m³) is listed. High values indicate a low robustness of the mortar. Figures 81 and 82 illustrate the thixotropic breakdown and buildup during the rheological test.

Time	Duration	Step	Mixing speed
0 min	1 min	Mixing of cement, limestone powder and water	140 rpm
1 min	1 min	Adding the superplasticizer	140 rpm
2 min	1 min	Adding of VMA	140 rpm
3 min	1 min	Mixing	285 rpm
4 min	2 min	A thin layer of paste is scraped from the mixing arm and the walls and bottom of the mixing bowl	0 rpm
6 min	1 min	Mixing	285 rpm
7 min	3 min	Rest	
10 min		Measurement flow spread and V-funnel time	
11 min		Measurement of the density, air content and rheological parameters	

Table 33: Timing of the test procedures

	No VMA	Diutan gum	Corn Starch	Attapulgite clay	Propylene carbonate
Flow spread S [mm]	248	240	243	250	250
ΔS / 10 l/m³	8.6	3.5	6.9	5.7	7.0
ΔS / S_{ref} / 10 l/m³	0.035	0.015	0.028	0.023	0.028
V-funnel time VF [s]	10.4	10.9	7.4	7.8	11.7
ΔVF / 10 l/m³	0.41	0.65	0.35	0.30	1.6
ΔVF/VF_{ref} / 10 l/m³	0.040	0.060	0.047	0.038	0.139
Yield stress YS [Pa]	17	26	14	12	11
ΔYS / 10 l/m³	1.2	2.0	2.4	1.4	1.7
ΔYS/YS_{ref} / 10 l/m³	0.069	0.076	0.176	0.117	0.150
Plastic viscosity PV [Pa.s]	8	13	8	7	10
ΔPV / 10 l/m³	0.7	0.6	0.6	0.5	0.5
ΔPV/PV_{ref} / 10 l/m³	0.084	0.046	0.076	0.073	0.050
Thixotropic breakdown speed $\alpha_{breakdown}$ [-]	0.0043	0.0051	0.0039	0.0041	0.0039
Thixotropic buildup speed $\alpha_{buildup}$ [-]	0.017	0.012	0.015	0.023	0.021

Table 34: Discussion of robustness for all tests

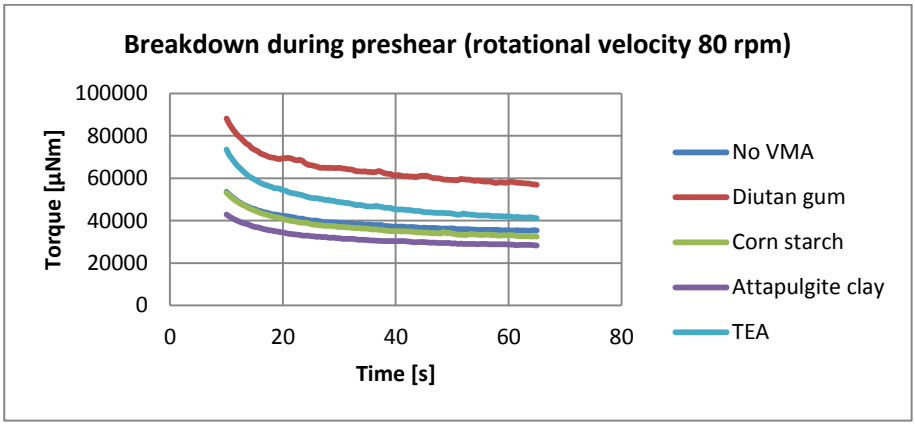

Figure 81: Thixotropic breakdown during the preshear step (80 rpm)

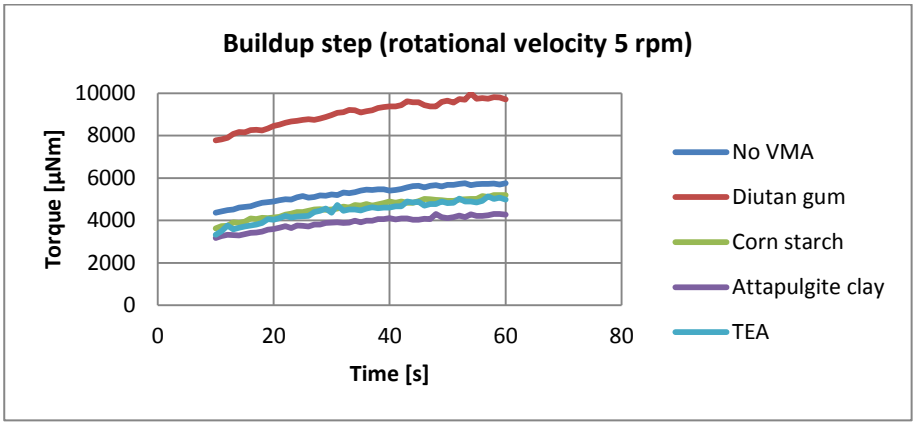

Figure 82: Thixotropic buildup step at a low shear rate (5 rpm)

Based on the flow spread and V-funnel time results (Figure 83), diutan gum provides a significantly larger robustness compared to attapulgite clay, being more robust than propylene carbonate and corn starch. The mixture without VMA had the least robust flow spread. The addition of diutan gum did not affect the V-funnel time in comparison to the reference mix without VMA. Corn starch and attapulgite clay decreased the V-funnel time, and propylene carbonate increased the V-funnel time. Because the variation in the V-funnel time depends on the V-funnel time of the reference mixture, the robustness of the V-funnel time of a mortar should be evaluated using the ratio of the differences in V-funnel time to the reference V-funnel time. Based on this parameter, the robustness of the mixture with attapulgite clay, corn starch, and no VMA are more robust than the mixture with diutan gum. Propylene carbonate caused the largest decrease in robustness.

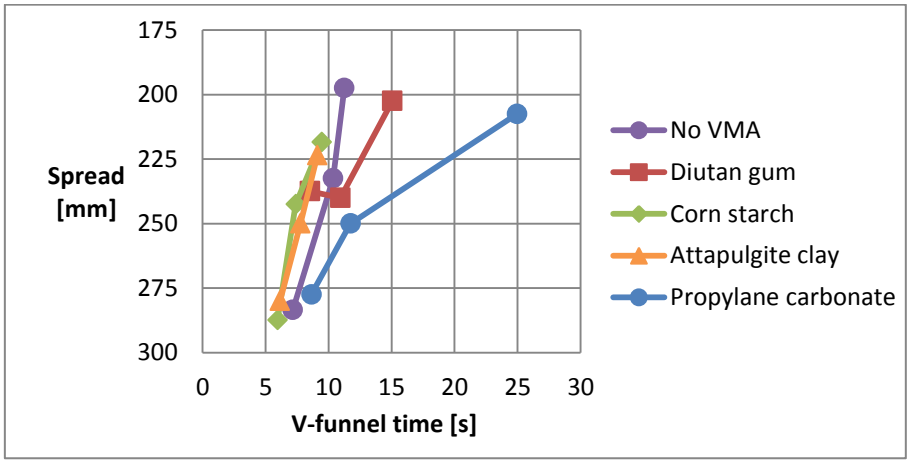

Figure 83: Impact of VMA's on the robustness in a workability box

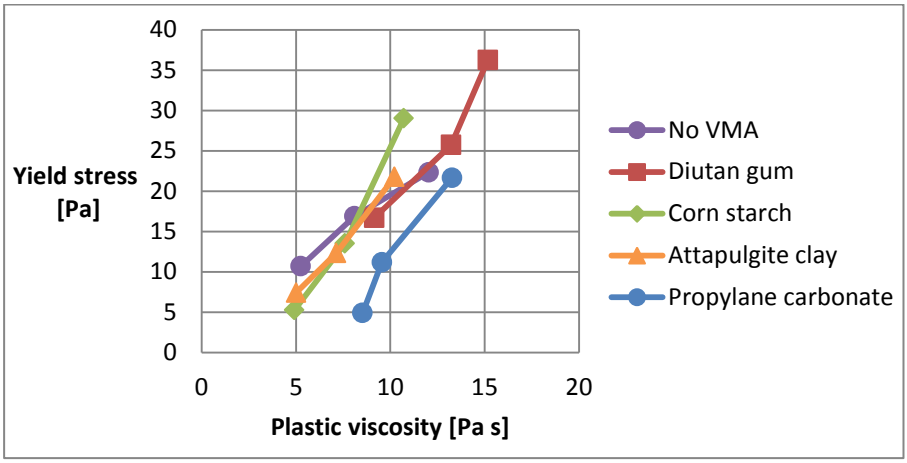

Figure 84: Impact of VMA's on the robustness in a rheogram

Although the flow spread of all mixtures was about the same, large differences were observed in the yield stress. The incorporation of diutan gum (with adjusted superplasticizer content) resulted in a higher yield stress, all other VMA's reduced the yield stress. Most probably, these variations are a result of differences in the strength of the thixotropic network built during three minutes rest between the mixing and performing the flow spread test. As is illustrated in Figure 51, the mixtures with higher yield stresses reached more rapidly their equilibrium state during the preshear step of the rheology test and therefore probably were able to reach the same flow spread as a mixture with half the yield stress. The mixtures without VMA and with attapulgite clay had the most robust yield stress, followed by the mixtures with propylene carbonate, diutan gum and corn starch. Although the yield stress of the mixtures with a VMA was less robust, all mortars showed a more robust flow spread behaviour. Changes in the buildup and breakdown speed of the thixotropic network alone cannot explain the observed ranking of robustness in this test program. Most probably, the large dependency of the thixotropic buildup to variations in the water content makes the final behaviour more complicated.

Attapulgite clay (SP dosage 6% higher) and corn starch (SP dosage 4% higher) decrease the yield stress and do not affect the plastic viscosity. Also the robustness of the plastic viscosity and V-funnel flow time are similar. Diutan gum (SP dosage 27% higher) and propylene carbonate (same SP dosage) enhance the plastic viscosity of the mortars (respectively +63% and +25%). The similar but less robust V-funnel time of both VMA's contradicts the more robust plastic viscosity of the mortars. Both diutan gum and propylene carbonate mainly affect the viscosity of the free water and do not adsorb onto the cement particles. Attapulgite clay and starch are reported to interact with cement particles and therefore affecting the

balance of flocculation and deflocculation inside the cement paste [78, 222, 289, 294, 406].

The plastic viscosity is somehow correlated with the V-funnel time, but it is not the only parameter determining the V-funnel time of a mixture. For example the addition of diutan gum resulted in a similar V-funnel time, although the plastic viscosity doubled. The robustness of the V-funnel time decreased as the plastic viscosity of the mixture increased by the addition of diutan gum or propylene carbonate. When corn starch or attapulgite clay were added, the plastic viscosity itself remained about the same, but both the robustness of the V-funnel time and the plastic viscosity increased. Probably, the sensitivity of the V-funnel time increases more than proportional for mixtures with a higher plastic viscosity.

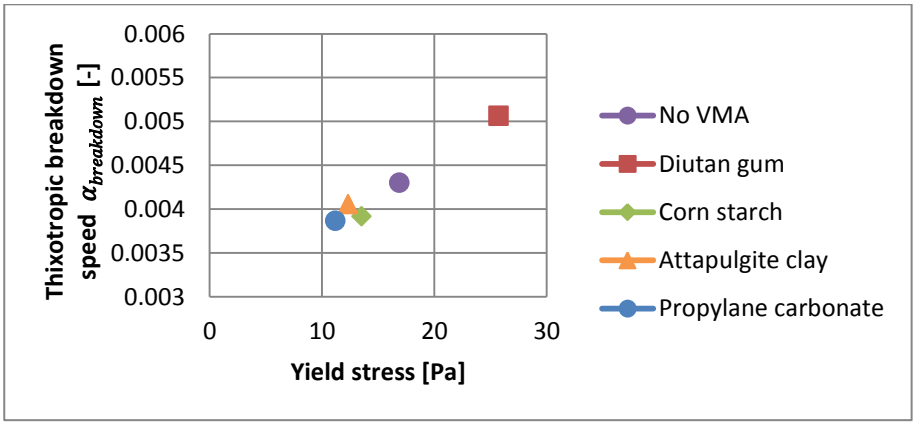

Figure 85: The relation between the thixotropic breakdown speed and the yield stress

The relation between the robustness of the workability parameters and the rheological parameters is unclear. Adding a VMA to the reference mixture increased the robustness of the flow spread test, decreased the robustness of the yield stress, and increased the robustness of the plastic viscosity. The robustness of the V-funnel time increased when corn starch or attapulgite clay were added, but decreased when diutan gum or propylene carbonate were added. The robustness of the V-funnel test decreased as the plastic viscosity increased.

The thixotropic breakdown speed of self-compacting mortars seems to affect the relation between the yield stress and the flow spread test, but has no clear influence on the robustness of the flow spread test. Most VMA's had a slower thixotropic breakdown (-7%) and therefore a lower yield stress (-27%) was obtained when the superplasticizer was set to reach a similar spread flow. The inclusion of diutan gum, however, resulted in a faster thixotropic breakdown speed (+19%), allowing a higher yield stress (+53%) to reach a similar spread flow.

3.3.2. Experiments on SCC

This section investigates whether the influence of VMA on the robustness of a SCC mixture with high yield stress and low plastic viscosity is the same as on a SCC mixture with low yield stress and high plastic viscosity. Two types of VMA are used in this experimental program: diutan gum (0.05% of the water weight) and purified attapulgite clay (0.15% of the cement weight). The fresh properties of the reference mixtures A and B (mix composition given in Table 19 of Section 2.2.) in which diutan gum, attapulgite clay, and no VMA were added are summarized in Table 35 and Figures 86 to 92. The following mix procedure was used: (1) 1 minute mixing of all dry constituents; (2) 1 minute mixing after addition of the water; (3) 1 minute mixing after addition of the superplasticizer; (4) 1 minute of mixing after adding the VMA. In case no VMA was present in the mixture, the same mixing procedure was followed. After mixing, the concrete rested for 3 minutes. The complete data is given in Appendix A. Two mixtures in which diutan gum is added to mix B were considered: one with a lower superplasticizer dosage which was very sensitive to a decrease of the water content, and one with a higher superplasticer dosage which was very sensitive to an increase of the water content and suffered from bleeding.

The robustness is evaluated by changes in the water content of ± 10 l/m³. Two parameters were used to describe the robustness: the change of the test response per liter water (e.g. ΔSF / 20 l/m³) and the ratio of this change per liter divided by the mean value (e.g. $\Delta SF / SF_{ref}$ / 20 l/m³). The rheological parameters listed in Table 35 were determined using an ICAR rheometer. The plastic viscosity listed is the first derivative of the shear stress to the shear rate at 5 s^{-1} for the mixtures having a Modified Bingham rheological behaviour (Equation 49).

$$\eta_{5\,s^{-1}} = \mu + 2 \cdot c \cdot 5\,s^{-1} \qquad \text{(Eq. 49)}$$

	Mix A No VMA	Mix A Diutan gum	Mix A Attapulgite clay	Mix B No VMA	Mix B Diutan gum 1	Mix B Diutan gum 2	Mix B Attapulgite clay
SP dosage [l/m³]	1.86	4.00	3.29	6.57	8.00	2.00	3.14
Slump flow [mm]	720	680	675	705	695	785	660
ΔSF / 20 l/m³	12.3	5.6	10.1	4.8	10.5	3.3	16.5
ΔSF / SF_{ref} / 20 l/m³	0.017	0.008	0.015	0.007	0.015	0.004	0.025
V-funnel time [s]	3.8	7.6	4.6	9.5	14.8	10.9	10.1
ΔVF / 20 l/m³	0.2	0.26	0.17	0.25	2.19	0.29	0.27
ΔVF / VF_{ref} / 20 l/m³	0.054	0.034	0.038	0.026	0.148	0.026	0.027
S.S.I. [%]	10.8	11.9	8.2	14.5	15	21.2	9.4
ΔSSI / 20 l/m³	0.53	0.55	0.59	0.4	1.06	0.24	1.12
ΔSSI / SSI_{ref} / 20 l/m³	0.049	0.047	0.071	0.028	0.071	0.011	0.120
Yield stress [Pa]	29	37	51	0	23	8	34
ΔYS / 20 l/m³	6.2	1.8	3.1	0.8	11.4	0.8	2.9
ΔYS / YS_{ref} / 20 l/m³	0.212	0.049	0.062	-	0.485	0.109	0.084
Differential viscosity at 1 s-1 $\boldsymbol{\eta_{5\,s^{-1}}}$ [Pa s]	38	69	45	55	94	57	87
ΔPV / 20 l/m³	2.5	2.7	2.0	3.5	15.6	2.6	7.3
ΔPV / PV_{ref} / 20 l/m³	0.066	0.039	0.045	0.064	0.166	0.045	0.085
Differential viscosity at 5 s-1 $\boldsymbol{\eta_{5\,s^{-1}}}$ [Pa s]	38	69	45	138	145	93	193
ΔPV / 20 l/m³	2.5	2.7	2.0	8.2	13.5	5.0	10.4
ΔPV / PV_{ref} / 20 l/m³	0.066	0.039	0.045	0.059	0.093	0.054	0.054
Density [kg/m³]	2350	2360	2350	2360	2370	2360	2370
Air content [%]	1.6	2	1.8	2	1.7	1.7	2.6
Modified Bingham parameters							
Yield stress $\tau_{0,MB}$ [Pa]	29	37	51	0	23	8	34
Modified Bingham linear term μ_{MB} [Pa s]	38	69	45	34	81	49	60
Modified Bingham 2nd order coefficient c_{MB} [Pa s²]	0	0	0	10	6	4	13
Differential viscosity at 1 s-1 $\boldsymbol{\eta_{5\,s^{-1}}}$ [Pa s]	38	69	45	55	94	57	87
Differential viscosity at 5 s-1 $\boldsymbol{\eta_{5\,s^{-1}}}$ [Pa s]	38	69	45	138	145	93	193

The "*differential viscosity*" is the first derivative of the shear stress to the shear rate (Eq. 17).

Table 35: Influence of VMA's on the sensitivity to changes in the water content.

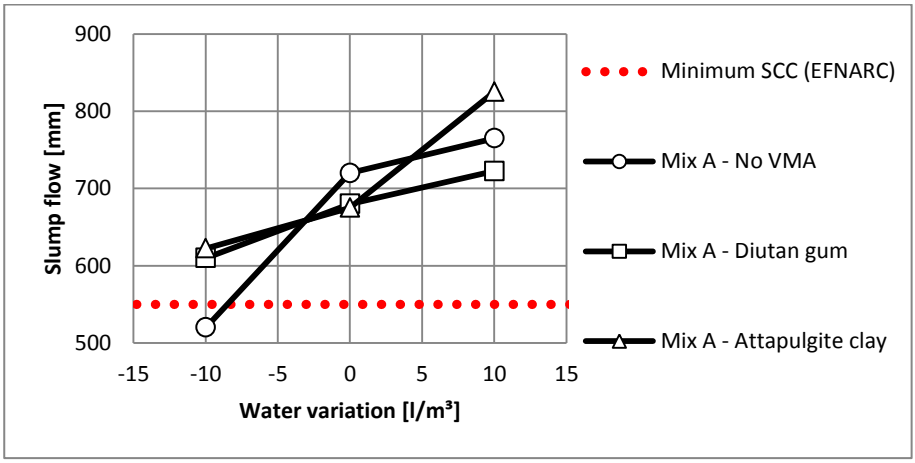

Figure 86: Mix A - the robustness of the slump flow test

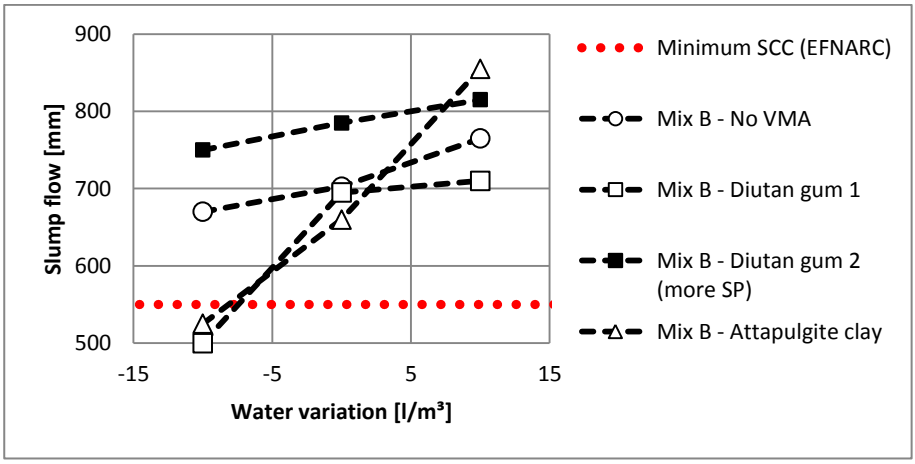

Figure 87: Mix B - the robustness of the slump flow test

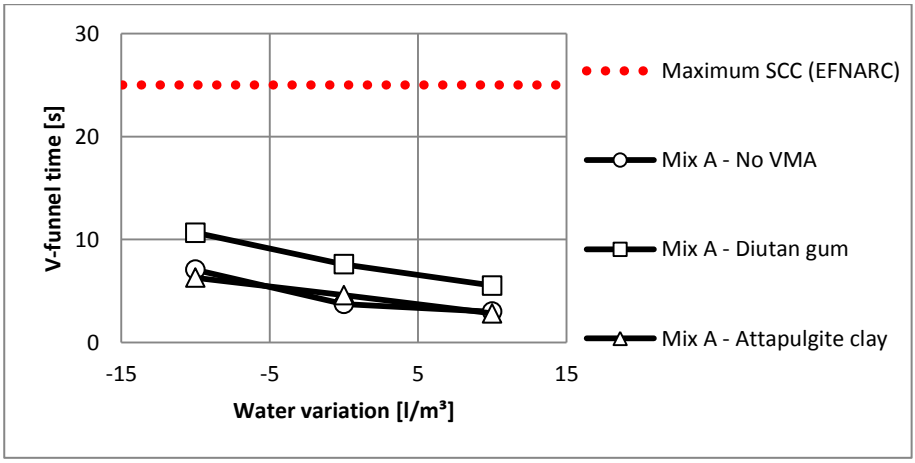

Figure 88: Mix A - the robustness of the V-funnel test

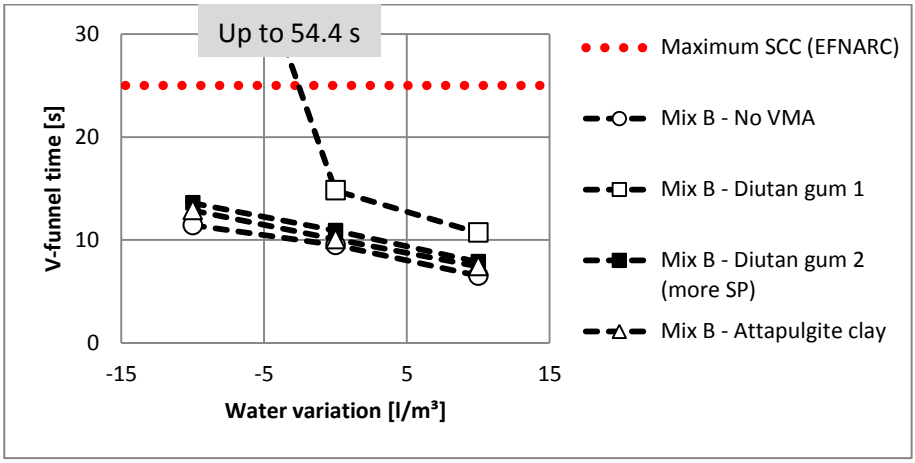

Figure 89: Mix B - the robustness of the V-funnel test

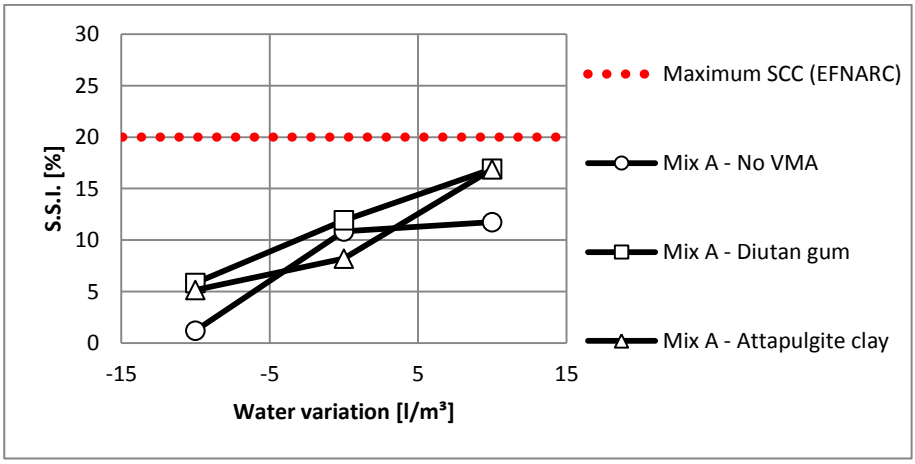

Figure 90: Mix A - the robustness of the S.S.I.

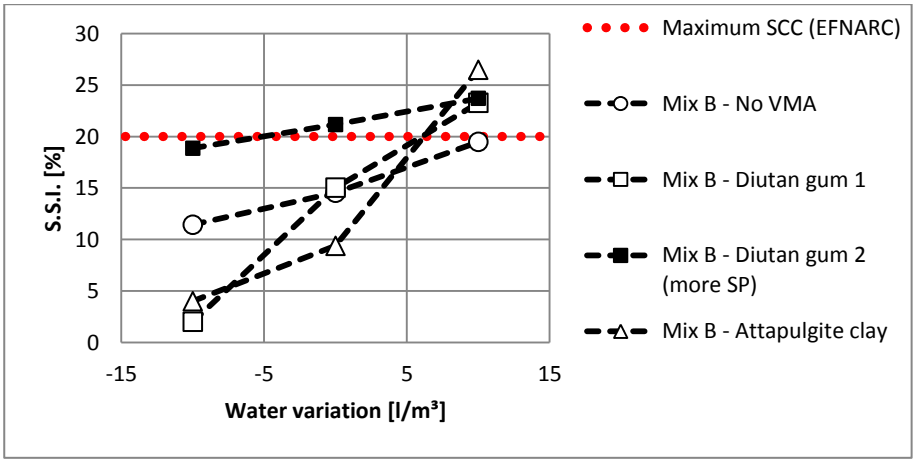

Figure 91: Mix B - the robustness of the S.S.I.

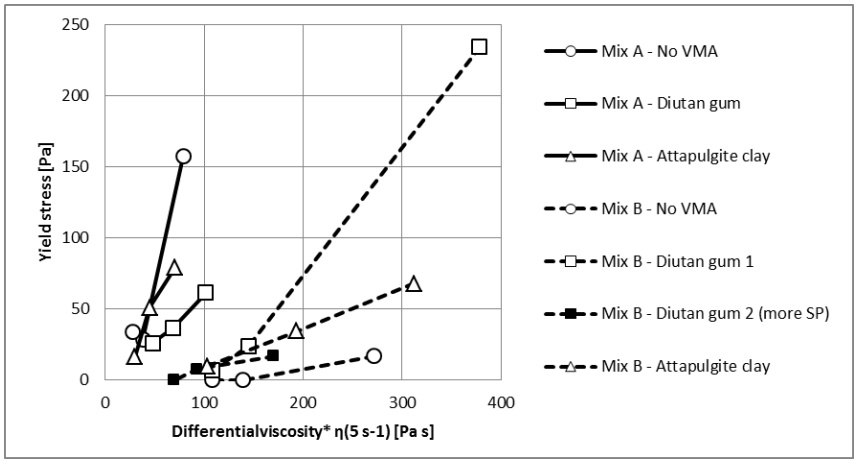

Figure 92: Robustness of the rheological parameters

Mix A, with a high yield stress and low plastic viscosity $\eta_{5\ s^{-1}}$ (the first derivative of the shear stress to the shear rate at 5 s^{-1}) reacts differently on the inclusion of a VMA in the mix design than the Mix B, with a high plastic viscosity and low yield stress. When a VMA is included in the mixture, the robustness of the yield stress of Mix A increases significantly, while the plastic viscosity maintained its original robustness. In Mix B, the addition of a VMA caused a decrease of the robustness. Because a part of the water was fixed by the VMA, a higher superplasticizer dosage was needed in these mixtures which were already on the limit of bleeding due to the low yield stress. As a result, the range of acceptable superplasticizer dosage limited by excessive bleeding and a too viscous mixture reduced, resulting in a reduction of the robustness against changes in the water content as these variations also affect this delicate equilibrium. Because especially a small decrease of the water content had a pronounced effect on the rheology of Mix B, another Mix B was tested, including diutan gum and a larger dose of superplasticizer (slump flow 785 mm). This mixture had an improved robustness of the Bingham parameters, but suffered from severe bleeding and segregation. Similar trends are observed for the workability tests.

Diutan gum and purified attapulgite clay have different working mechanisms in SCC. The diutan gum polysaccharide molecules dissolve in the mixing water, develop attractive forces, and intertwine with each other [78, 105]. This increases the viscosity of the mixing water at rest, resulting in an increased yield stress and plastic viscosity of the concrete mix. Attapulgite clay particles are charged needles which increase flocculation rate and yield stress of the concrete mixture [289, 294]. The influence of VMA's on the rheology is partly compensated by an increased superplasticizer dosage. Although diutan gum and attapulgite clay have different mechanisms affecting robustness, both VMAs had a similar impact on the

robustness. The positive impact of a VMA on a mixture with high yield stress and low plastic viscosity might be caused by fixing a part of the free water in these mixtures, reducing the sensitivity for segregation of the course aggregates. Because these mixtures are not sensitive to bleeding, a moderate increase of the superplasticizer dosage does not cause any problems. Diutan gum increases the plastic viscosity and yield stress, providing more resistance to changes of the water content compared to attapulgite clay which only affects the yield stress of SCC.

3.4. Cement replacement

In this section, the interactions in SCC mixtures with a low yield stress and high plastic viscosity are investigated more in depth. The impact of a replacement of part of the cement by silica fume, fly ash, or limestone powder on two reference mixtures was studied: one sensitive to bleeding and one sensitive to becoming a very sticky unworkable mixture. The composition of mixtures C and D is summarized in Table 20 and 21 of Section 2.2.

As summarized in the literature review, bleeding is the macroscopic result of a breakdown in the colloidal network inside cement paste, caused by repulsive steric forces dominating over the attractive Van Der Waals forces on the smallest colloidal particles in the cement paste. When repulsive forces are dominating over attractive Van Der Waals forces for small colloidal particles, syneresis occurs and a layer of water will be formed on top of the concrete surface. A possible solution has been proposed in Section 3.1: lowering the dosage of superplasticizer, for example by enhancing the water to powder ratio or paste volume. In this section, the influence of a cement replacement is studied.

As visible in the workability box and rheogram of both reference mixtures under small variations of the water content (Figures 93 and 94), excessive stickiness is not a synonym of a high plastic viscosity. The thixotropic buildup was not measured quantitatively, but based on visual observations during testing: based on the evolution in the workability and the buildup of a structure at rest after performing the slump flow, a distinction was made between a limited or no thixotropy, a moderate thixotropy and a strong thixotropic buildup. An excessive stickiness seemed to be more related to thixotropy compared to plastic viscosity.

The following mix procedure was used: (1) 1 minute mixing of all dry constituents; (2) 1 minute mixing after addition of the water; (3) 2 minutes mixing after addition of the superplasticizer.

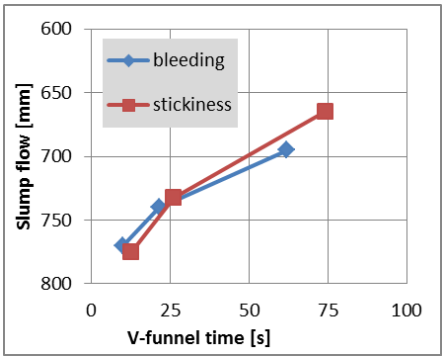

Figure 93: Workability box of mixture C and D

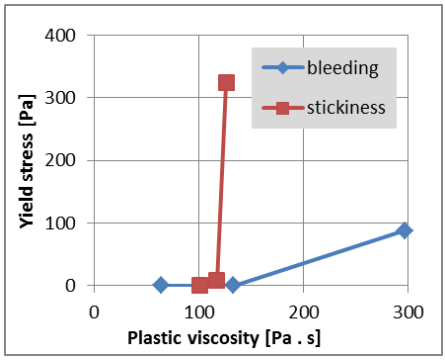

Figure 94: Rheogram of mixture C and D

3.4.1. Excessive bleeding

Tables 36 and 37 and Figures 95 and 96 summarize the fresh properties, visually observed bleeding and the robustness of mixture C, which is suffering from bleeding. The properties of the mixtures with ± 10 l/m³ water is given in Appendix A. Three bleeding classes were distinguished: no bleeding, light bleeding, and bleeding. A replacement of cement with silica fume helps to reduce the tendency to bleeding and enhances the robustness. Because the micro filling effects of silica fume are counteracted by the adsorption of part of the superplasticizer onto the large surface of silica fume, a similar packing density and a slightly higher needed superplasticizer dosage is reached. Fly ash decreases the needed superplasticizer content and plastic viscosity due to a higher packing density, but worsens the tendency for bleeding. The robustness of the yield stress reduces vastly (Figure 96).

The beneficial bleeding reducing effect of silica fume can be explained by its accelerating effect on the nucleation rate. Fine silica fume particles enhance the attractive Van Der Waals forces, strengthening the colloidal network in cement paste and thus reducing the tendency for bleeding. Although fly ash enhances the packing density and therefore reduces the required superplasticizer dosage and thus steric repulsive forces, it slows down the hydration reaction and the rate of structural buildup. As a result, less superplasticizer is consumed and repulsive forces are still dominating the attractive Van Der Waals forces.

	Mix C Reference	Mix C Replacement by silica fume	Mix C Replacement by fly ash
SP dosage [l/m³]	12.29	13.43	9.29
Slump flow [mm]	740	695	725
V-funnel flow [s]	21.5	36.4	21.7
S.S.I. [%]	2.7	1.8	3.6
Density [kg/m³]	2323	2313	2331
Yield stress [Pa]	0.0	63.3	200.0
Plastic viscosity [Pa . s]	133.2	152.8	117.0
Solid fraction in SCC [%]	81.6	81.7	82.3
Solid fraction in the paste [%]	52.3	52.7	53.7
Visual evaluation of bleeding	light bleeding	no bleeding	bleeding

Table 36: Fresh properties of Mix C, suffering from bleeding

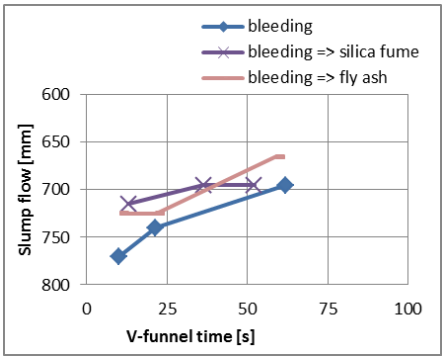

Figure 95: Workability box of Mix C

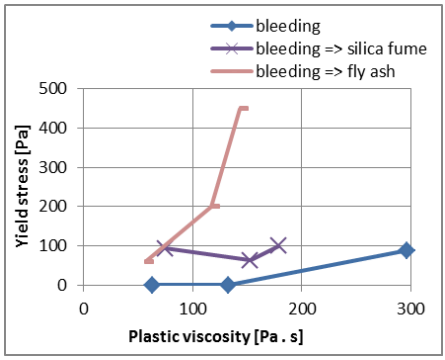

Figure 96: Rheogram of Mix C

	Mix C Reference	Mix C Replacement by silica fume	Mix C Replacement by fly ash
Slump flow [mm]	740	695	725
ΔSF / 20 l/m³	3.75	1.00	3.00
ΔSF / SF_{ref} / 20 l/m³	0.0051	0.0014	0.0041
V-funnel time [s]	21.5	36.4	21.7
ΔVF / 20 l/m³	2.59	1.95	2.42
ΔVF / VF_{ref} / 20 l/m³	0.120	0.053	0.111
S.S.I. [%]	2.7	1.8	3.6
ΔSSI / 20 l/m³	0.26	0.05	0.25
ΔSSI / SSI_{ref} / 20 l/m³	0.094	0.027	0.070
Yield stress [Pa]	0.0	63.3	200.0
ΔYS / 20 l/m³	4.40	0.29	19.4
ΔYS / YS_{ref} / 20 l/m³	-	0.005	0.097
Plastic viscosity [Pa s]	133.2	152.8	117.0
ΔPV / 20 l/m³	11.65	5.19	4.31
ΔPV / PV_{ref} / 20 l/m³	0.087	0.034	0.037

Table 37: Robustness of Mix C, suffering from bleeding

3.4.2. Excessive stickiness

Tables 38 and 39 and Figures 97 and 98 summarize the fresh properties and robustness of Mix D, in which the effect of cement replacement on the stickiness is studied. The properties of the mixtures with ± 10 l/m³ water is given in Appendix A. A cement replacement by silica fume increases the nucleation rate and enhances the thixotropic behaviour of the mixture, resulting in a more sticky mixture with a lower robustness. Vikan and Justness [407] suggested this thickening is a result of an increase of the attractive forces between solid particles, enhancing the flocculation.

The better packing density of the SCC with a fly ash replacement provides more free water and thus reduces the needed superplasticizer dosage, with a lower V-funnel flow time and plastic viscosity for a similar slump flow value. The particle morphology of fly ash reduces early age hydration rate, thixotropic behaviour and stickiness of the mixture [121]. A replacement of cement by limestone powder keeps a similar packing density, but enhances the water demand of the powder. As a result, the superplasticizer dosage reduces a bit and a mixture with a higher plastic viscosity and more thixotropic behaviour is obtained. The stickiness of the mixture with a cement replacement by limestone filler increases and its robustness decreases. Especially the sensitivity to a decrease of the water content increases. A replacement of cement by limestone filler also enhances the attractive forces inside fresh SCC.

The most efficient way to enhance the robustness of SCC with high stickiness is a reduction of this stickiness. A higher packing density reduces the plastic viscosity with more free water but does not necessarily have an impact on the stickiness. Not only a high plastic viscosity ensures stickiness, also the thixotropy of the mixture has an important contribution. A possible way to improve the packing density without enhancing the thixotropic buildup is the replacement of cement with fly ash.

	Mix D Reference	Mix D Replacement by silica fume	Mix D Replacement by fly ash	Mix D Replacement by limestone
SP dosage [l/m³]	14.29	14.57	8.57	11.43
Slump flow [mm]	733	700	750	715
V-funnel flow [s]	26.1	33.3	11.8	24.8
S.S.I. [%]	3.3	2.0	3.0	3.1
Density [kg/m³]	2328	2313	2331.25	2319
Yield stress [Pa]	8.3	68.0	0.0	3.0
Plastic viscosity [Pa . s]	116.8	160.5	96.8	135.7
Solid fraction in SCC [%]	81.5	81.4	82.4	81.8
Solid fraction in the paste [%]	52.4	52.2	53.9	52.8
Visual evaluation of stickiness	viscous and sticky	very viscous	normal SCC	viscous and sticky

Table 38: Fresh properties of Mix D, suffering from excessive stickiness

	Mix D Reference	Mix D Replacement by silica fume	Mix D Replacement by fly ash	Mix D Replacement by limestone
Slump flow [mm]	733	700	750	715
ΔSF / 20 l/m³	5.50	5.25	2.88	3.75
ΔSF / SF_{ref} / 20 l/m³	0.0075	0.0075	0.0038	0.0052
V-funnel time [s]	26.1	33.3	11.8	24.8
ΔVF / 20 l/m³	3.07	3.91	1.49	8.97
ΔVF / VF_{ref} / 20 l/m³	0.12	0.12	0.13	0.36
S.S.I. [%]	3.3	2.0	3.0	3.1
ΔSSI / 20 l/m³	0.16	0.15	0.36	0.27
ΔSSI / SSI_{ref} / 20 l/m³	0.049	0.074	0.119	0.088
Yield stress [Pa]	8.3	68.0	0.0	3.0
ΔYS / 20 l/m³	16.21	11.80	9.67	4.63
ΔYS / YS_{ref} / 20 l/m³	1.94	0.17	-	1.53
Plastic viscosity [Pa s]	116.8	160.5	96.8	135.7
ΔPV / 20 l/m³	1.25	4.86	5.26	6.30
ΔPV / PV_{ref} / 20 l/m³	0.011	0.030	0.054	0.046

Table 39: Robustness of Mix D, suffering from excessive stickiness

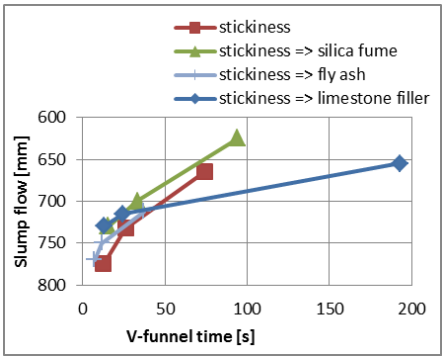

Figure 97: Workability box of Mix D

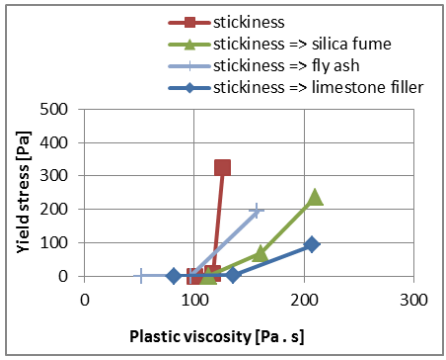

Figure 98: Rheogram of Mix D

3.5. Mixing procedure

The mixer type has an enormous impact on the hydration rate of paste and thus the rheology of cement paste [348]. In SCC, the ball bearing effect of coarse aggregates enhances the shear rates during mixing significantly, resulting in a better dispersion of the fines even at low velocities of mixing. In order to investigate the impact of various mixing procedures on concrete level, a series of experiments has been performed. Also the impact of the mixing sequence and moisture condition of aggregates was investigated. All mixtures had the same mix composition given in Table 21 of Section 2.2 and were mixed in an intensive Eirich mixer.

3.5.1. Reference: Water content

To assess the relative impact of variations in the mixing procedure, a comparison is made with changes in the water variation of ±10 l/m³. Table 40 and Figures 99 and 100 summarize the changes in the rheology and workability retention induced by variations of the water content. The rheological parameters were determined with a Contec rheometer (Section 2.3.2.) and the static yield stress shown in Figure 101 with an ICAR rheometer (Section 2.3.1.). This reference mixture was mixed according to the following procedure: (1) 1 min mixing of aggregates ; (2) after addition of cement and filler, 1 min mixing; (3) after adding the water, 1 min of mixing; (4) after addition of superplasticizer, 2.5 min of mixing.

The water content obviously had an impact on the workability of SCC. When 10 l/m³ water was lacking, the mixture had a slump flow of 464 mm and could even not be considered as an SCC. The evolution of the workability and static yield stress in time is greatly affected by variations in the water content.

	- 10 l/m³ water	Reference	+ 10 l/m³ water
Slump flow (mm)			
20 min	464	597	699
45 min	470	648	762
75 min	403	603	730
V-funnel time (s)			
20 min	12.5	5.1	4.5
45 min	17.3	7.7	5.0
75 min	-	7.1	4.6
S.S.I. (%)			
20 min	0.1	2.3	9.1
75 min	0.0	0.0	6.7
Yield stress (Pa)			
10 min	85.0	36.2	19.6
30 min	113.2	28.6	17.0
60 min	89.9	24.4	13.9
90 min	-	36.6	16.8
Plastic viscosity (Pa . s)			
10 min	52.3	31.0	16.6
30 min	55.4	36.5	19.2
60 min	81.2	47.7	24.2
90 min	-	67.4	33.0

Table 40: Impact of variations in the water content

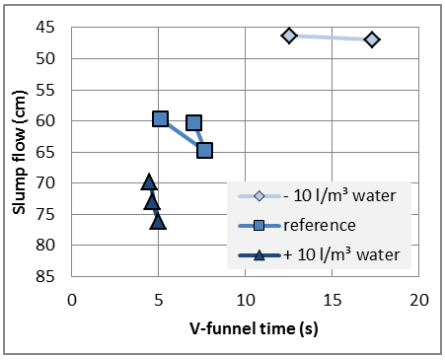

Figure 99: Impact of variations in the water content in a workability box

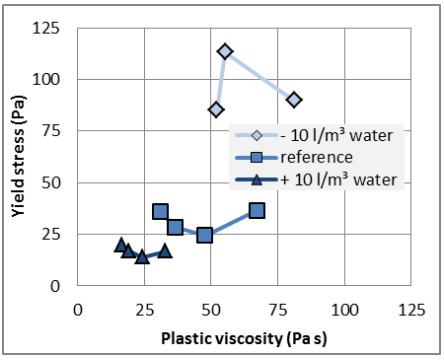

Figure 100: Impact of variations in the water content in a rheogram

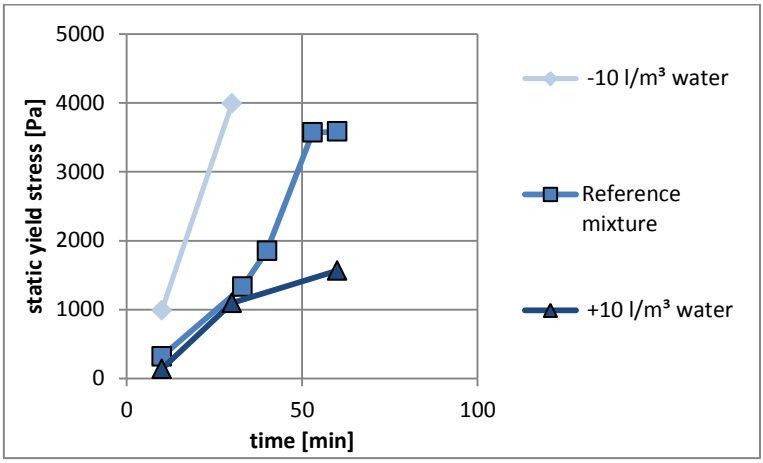

Figure 101: Impact of variations in the water content on the structural buildup

3.5.2. Mixing speed

Due to the impact of the mixing speed on the dispersion state of fines, changes of the workability are observed when the same mix composition is made with different mixing speeds. Table 41 and Figures 102 to 104, summarize the impact of variations in the rotator speed of an Eirich mixer. A lower mixing speed results in a larger slump flow and lower yield stress but a similar V-funnel time and plastic viscosity. Based on the power consumption curve shown in Figure 105, the reference mixture might be slightly overmixed as the mixing time exceeds its stabilization time with about half a minute. The stabilization time during mixing is defined as the time at which an exponential fit to the power consumption curve reaches its horizontal asymptote (a slope of -4 . 10-4 s-1). The stabilization time is presumed to be the moment of optimum dispersion [335, 341-343, 346]. Compared to the impact of variations in the water content, the impact of changes in the mixing speed is much smaller. However, this conclusion is only valid as the mixing speed does not differs too much. Another mixture, mixed at a high mixing speed, (Figure 101) was strongly overmixed, resulting in a much higher yield stress. This mixture is not taken into account for the analysis of the robustness, compared to other mixing parameters.

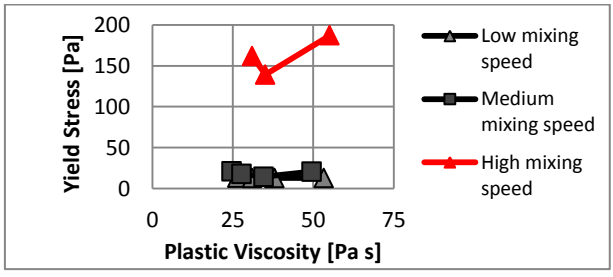

Figure 101: A mixture mixed at a high mixing speed was well overmixed and not considered during the analysis

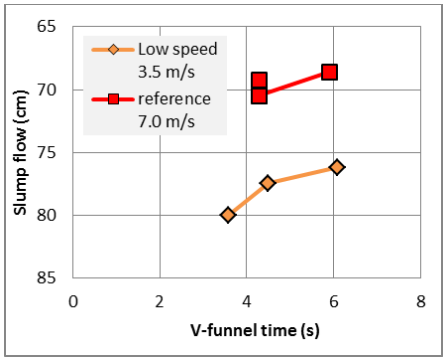

Figure 102: Impact of variations in the water content in a workability box

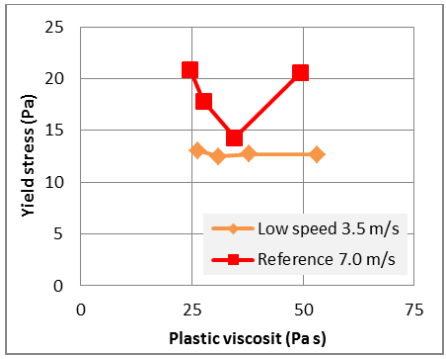

Figure 103: Impact of variations in the water content in a rheogram

	Low speed (rotor speed 3.5 m/s)	Reference (rotor speed 7.0 m/s)	High speed (rotor speed 13.7 m/s)
Slump flow (mm)			
20 min	800	692	406
45 min	775	705	387
75 min	762	686	-
V-funnel time (s)			
20 min	3.6	4.3	8.8
45 min	4.5	4.3	18.0
75 min	6.1	5.9	-
S.S.I. (%)			
20 min	8.5	5.2	0.0
75 min	4.6	3.5	0.0
Yield stress (Pa)			
10 min	13.1	20.8	162
30 min	12.5	17.8	139
60 min	12.7	14.3	187
90 min	12.7	20.6	-
Plastic viscosity (Pa . s)			
10 min	26.4	24.7	31
30 min	31.0	27.7	35
60 min	38.0	34.6	55
90 min	53.3	49.5	-

Table 41: Impact of the mixing speed

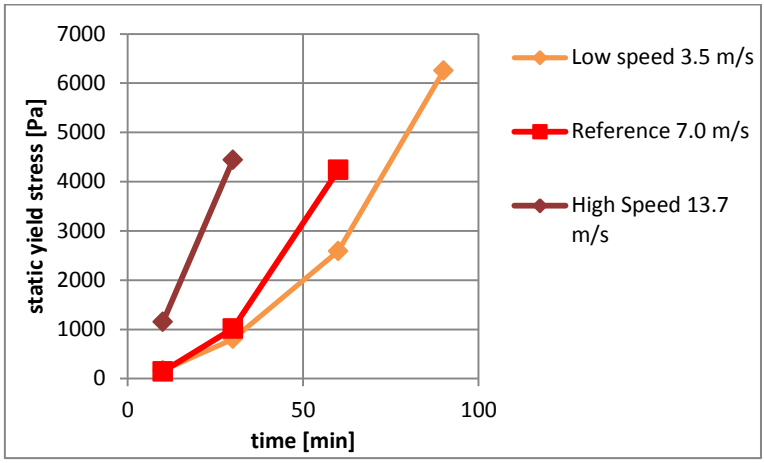

Figure 104: Impact of variations in the water content on the structural buildup

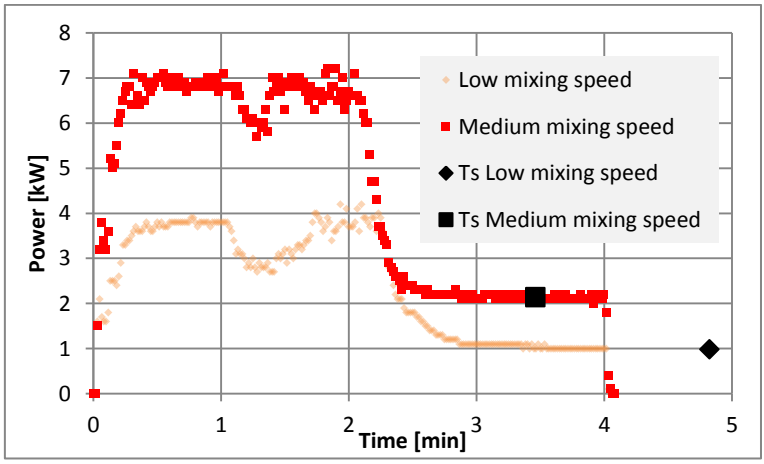

Figure 105: Power consumption during mixing

3.5.3. Mixing time

Table 42 and Figures 106 to 108 summarize the impact of the mixing time on the workability of SCC. Compared to the induced changes due to variations in the water content, only small changes in the workability, rheology, and structural buildup are observed. The mixture with a mixing time of 2.5 min has a slightly higher plastic viscosity and did not reach its stabilization time during mixing (Figures 109 to 111). Changes in the mixing time did not affect the workability evolution.

	Short mixing time (2.5 min)	Reference (3.5 min)	Long mixing time (4.5 min)
Slump flow (mm)			
20 min	762	705	730
45 min	768	743	762
75 min	743	724	737
V-funnel time (s)			
20 min	4.0	3.9	3.6
45 min	4.5	4.3	4.0
75 min	5.3	4.7	5.4
S.S.I. (%) 20 min	6.9	6.0	7.5
Yield stress (Pa)			
10 min	16.9	15.9	16.0
30 min	8.1	14.1	14.3
60 min	7.7	12.2	11.8
90 min	19.0	14.8	14.7
Plastic viscosity (Pa . s)			
10 min	38.0	26.8	22.0
30 min	44.4	31.3	25.7
60 min	50.9	37.4	32.0
90 min	64.1	50.7	43.7

Table 42: Impact of the mixing time

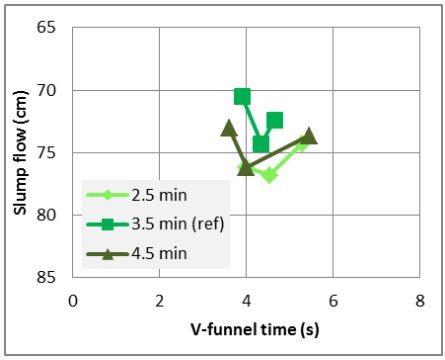

Figure 106: Impact of variations of the mixing time in a workability box

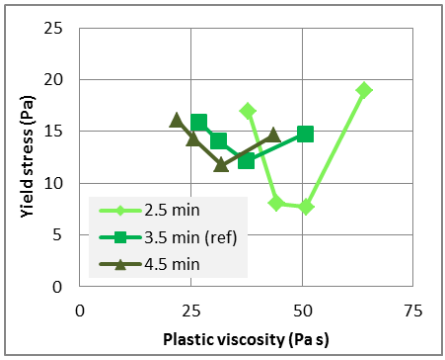

Figure 107: Impact of variations of the mixing time in a rheogram

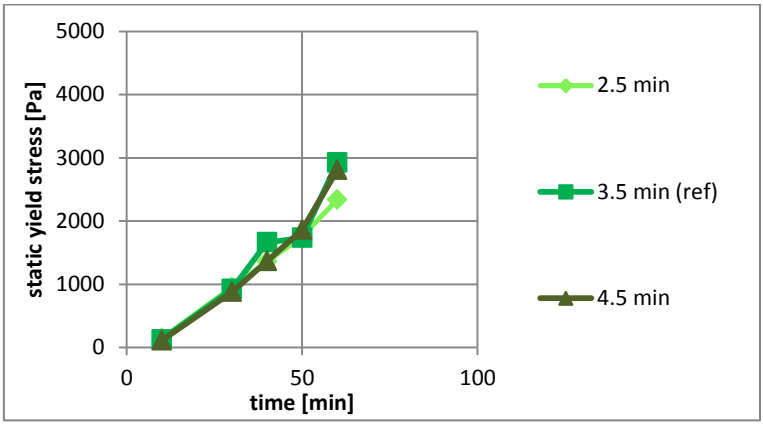

Figure 108: Impact of variations of the mixing time on the structural buildup

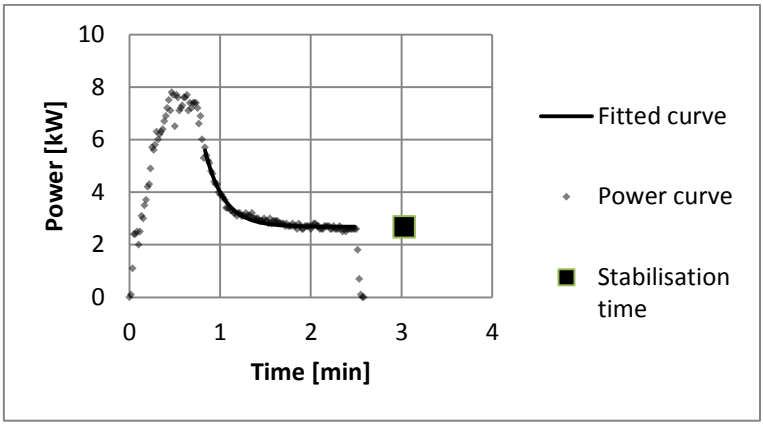

Figure 109: power consumption curve – mixing time of 2.5 min

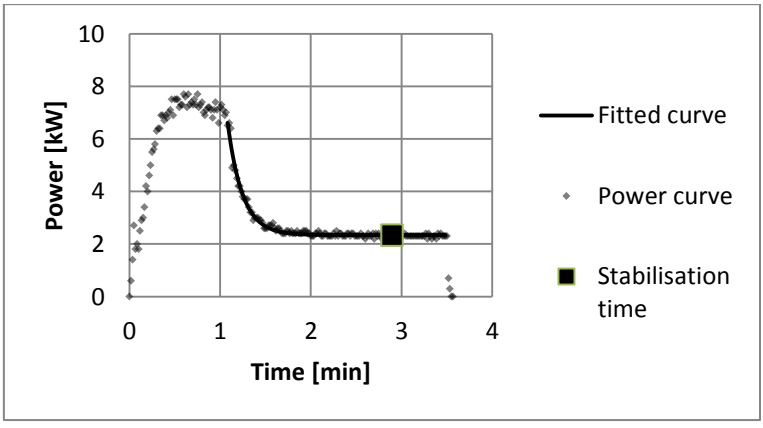

Figure 110: power consumption curve – mixing time of 3.5 min

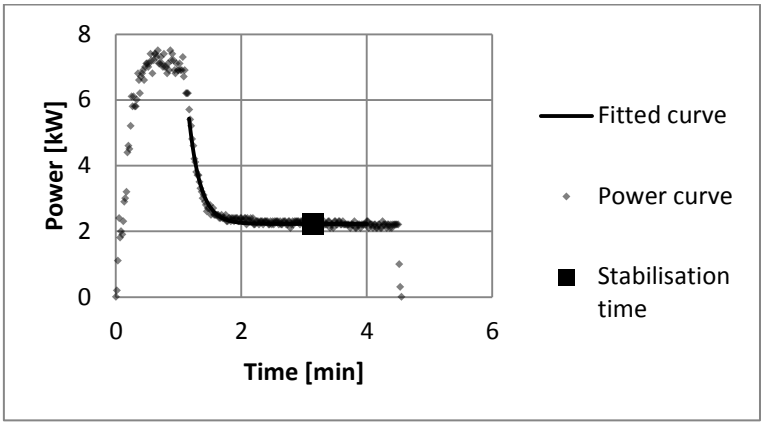

Figure 111: power consumption curve – mixing time of 4.5 min

3.5.4. Addition sequence of the aggregates

Four mixtures were made with the same composition, but different mixing sequences (Table 43 and 44). All mixtures were made with air-dried aggregates. Based on the workability box and rheogram plotted in Figures 112 and 113, SCC2 can be considered as the mixture with the lowest fluidity. The aggregates in this mixture were premixed with part of the water before adding cement and filler. Mixtures SCC3 and SCC4 are more fluid. In these mixtures, cement and water were first mixed together before adding the aggregates and superplasticizer. SCC1 in which the powder and aggregates are mixed together before adding the water, has an intermediate fluidity. Similar trends are observed for the structural buildup: premixing the aggregates with half of the mixing water delivers the largest increase of the static yield stress in time, premixing cement, filler and water before adding the aggregates resulted in the lowest increase of the static yield stress. No changes in the workability retention due to differences in the addition sequence were observed.

A possible explanation for the differences in the fluidity are differences in the absorption of water by the aggregates. During the premixing of aggregates and part of the water in SCC2, an amount of water will absorb into the aggregate pores and therefore not be available to lubricate the paste. When water, cement and limestone filler are mixed before adding the aggregates, as in SCC3 and SCC4, the paste is formed before any water can absorb into the aggregates. This paste covers the aggregates surface and obstructs the absorption of water. As a result, the paste contains more water and is more fluid. In SCC1, in which the cement, filler and aggregates are first mixed together before adding water, the adsorption of water by aggregates is in between both cases, and an intermediate situation occurs. The mixtures with less water available in the paste also had a stronger and faster structural buildup (Figure 114).

SCC1	SCC2	SCC3	SCC4
Aggregates 1 min	Aggregates 30 sec	Cement 1 min	Cement 1 min
	Half of water 30 sec		
Cement and filler 1 min	Cement and filler 1 min	All water 1 min	All water 1 min
All water 1 min	Half of water 1 min	SP 1 min	Aggregates 1 min
SP 2.5 min	SP 2 min	Aggregates 2.5 min	SP 2.5 min

Table 43: Variations in the mixing sequence

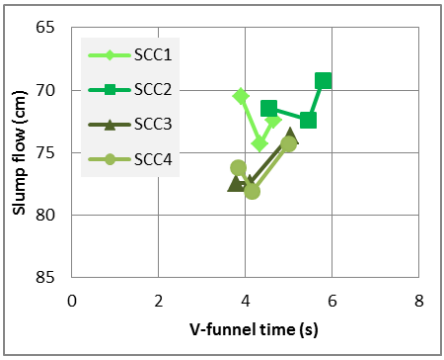

Figure 112: Impact of variations of the mixing time in a workability box

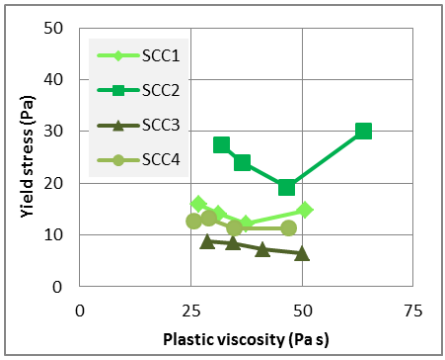

Figure 113: Impact of variations of the mixing time in a rheogram

	SCC1	SCC2	SCC3	SCC4
Slump flow (mm)				
20 min	705	714	775	762
45 min	743	724	775	781
75 min	724	692	737	743
V-funnel time (s)				
20 min	3.9	4.5	3.8	3.8
45 min	4.3	5.5	4.1	4.2
75 min	4.7	5.8	5.0	5.0
S.S.I. (%) 20 min	6.0	-	6.6	7.9
Yield stress (Pa)				
10 min	15.9	25.2	8.8	12.6
30 min	14.1	22.3	8.4	13.2
60 min	12.8	100.5	7.2	11.3
90 min	14.8	204.0	6.4	11.3
Plastic viscosity (Pa . s)				
10 min	26.8	33.3	28.9	25.8
30 min	31.2	38.6	34.5	29.0
60 min	37.4	35.8	41.3	34.9
90 min	50.7	41.7	50.1	47.1

Table 44: Impact of the mixing sequence

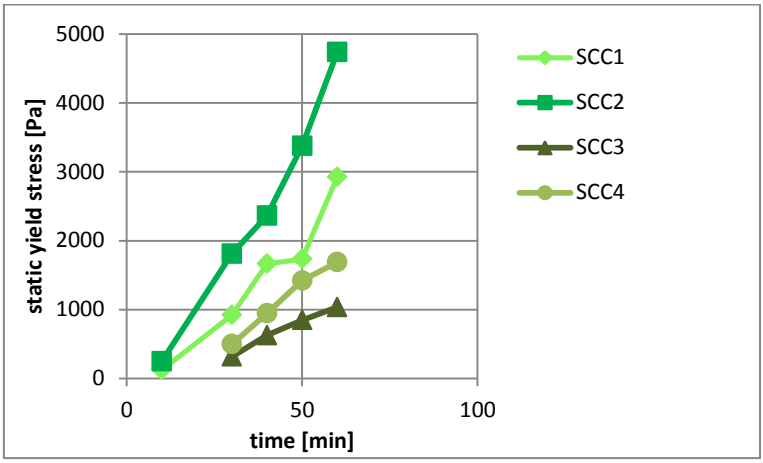

Figure 114: Impact of variations of the mixing time on the structural buildup

3.5.5. Moisture content of aggregates

To confirm the hypothesis stated in Section 3.5.4. two additional mixtures were made using the mixing sequence of Table 45: one with soaked aggregates and one with air dried aggregates. The soaked aggregates were prepared by pouring all water over buckets of aggregates and soaking them for one night. Any evaporation of water from the buckets with sand was prevented by closing them with a plastic cover.

Table 46 and Figures 115 to 117 summarize the experimental results. Because part of the water was absorbed during one night of soaking, the mixture made of soaked aggregates was less fluid compared to the mixture made with air dried aggregates (lower slump flow and higher yield stress, Figure 116). No influence on the V-funnel time, and plastic viscosity evolution was observed (Figure 115). During 30 seconds of mixing, no full absorption of the air dried aggregates is reached and more water is available to lubricate the paste. As a result, a more fluid mixture is obtained. The static yield stress evolution was slightly steeper when air dried aggregates were used instead of soaked aggregates (Figure 117).

SCC5	SCC6
Aggregates soaked with all water 30 sec	Dry aggregates and all water 30 sec
Cement 1 min	Cement 1 min
SP 2.5 min	SP 2.5 min

Table 45: Impact of the mixing sequence

	Air dried aggregates	Soaked aggregates
Slump flow (mm)		
20 min	761	692
45 min	760	714
75 min	740	699
V-funnel time (s)		
20 min	5.1	4.5
45 min	5.3	4.9
75 min	6.2	6.2
S.S.I. (%) - 20 min	3.1	4.6
Yield stress (Pa)		
10 min	14.9	18.7
30 min	9.4	13.7
60 min	5.8	10.5
90 min	8.2	14.1
Plastic viscosity (Pa . s)		
10 min	36.5	34.4
30 min	41.6	39.6
60 min	51.0	47.5
90 min	64.5	65.2

Table 46: Impact of moisture content of the aggregates

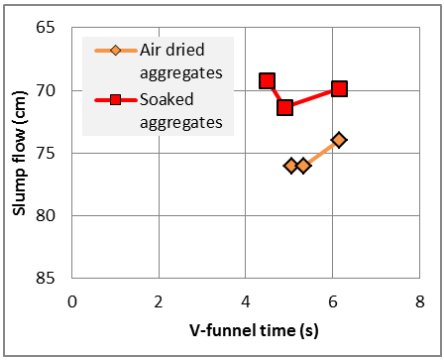

Figure 115: Impact of the aggregates moisture content in a workability box

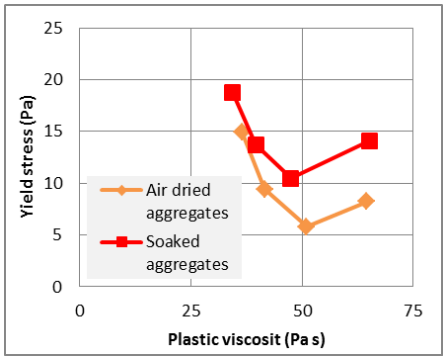

Figure 116: Impact of the aggregates moisture content in a rheogram

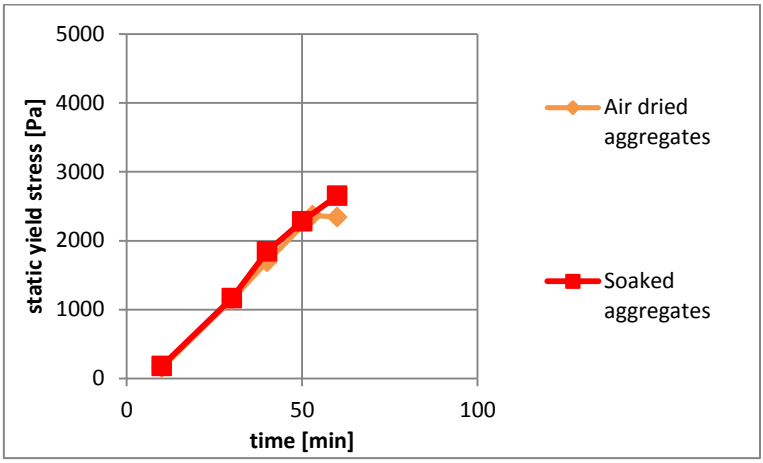

Figure 117: Impact of the moisture content on the structural buildup

4. Mechanisms governing the robustness of SCC

Robust SCC mixtures can resist small changes in the mix proportions, material properties, or mixing procedures without disproportional changes in the filling ability, passing ability or segregation resistance, resulting in failed concrete batches. Because most often, not all three key characteristics fail together, the most critical characteristic of the concrete mixture should be determined. When this parameter becomes less sensitive to small changes, the overall robustness of the mixture can be improved. The knowledge of mechanisms affecting this most critical property is essential in this respect.

The experiments described in Section 3.1 demonstrated a distinction between the failure mechanisms of SCC as illustrated in the rheogram of Wallevik and Wallevik [404] in Figure 118. Dependent on whether yield stress or plastic viscosity provide stability, other mechanisms should be considered. When the yield stress is providing stability, the mixture can display segregation of the coarse aggregates or a lack of flowability (slump flow < 550 mm). SCC mixtures in which the plastic viscosity is providing stability can have an excessive bleeding or become very viscous and unworkable due to small changes in the water content. SCC mixtures with intermediate characteristics can show a combination of several failure mechanisms.

- Lack of flowability versus segregation of coarse aggregates
    1) Lack of flowability: the mixture still meets most criteria for SCC (easy to process, self-consolidation, …), with the exception of sufficient flowability. A low slump flow (below 550 mm) and low L-box ratio (below 0.6) are inacceptable for most applications [6].
    2) Segregation of the coarse aggregates: due to segregation, the coarse aggregates of the mixtures are sinking. The Sieve Segregation Index (S.S.I.), an indicator of the segregation risk of the mixture, is high.
- Highly viscous mixture, difficult to process versus excessive bleeding
    1) Highly viscous mixture: although a sufficiently large slump flow is obtained, the casting of the mixture is difficult or even impossible because of the highly viscous and very sticky behavior (V-funnel flow time > 25 s). Thixotropic buildup at rest amplifies the stickiness of viscous SCC mixtures.
    2) Excessive bleeding: water migration can result in the formation of a water layer on the top surface of the fresh SCC [359, 360].

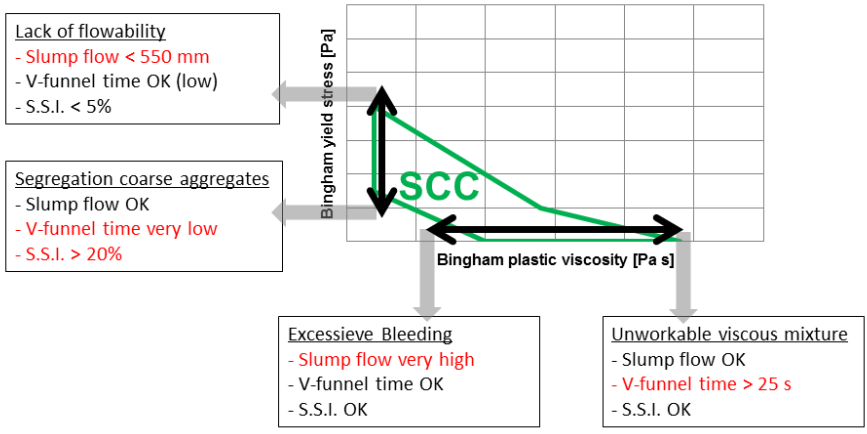

Figure 118: Failure mechanisms of self-compacting concrete

4.1. Relatively high yield stress, low plastic viscosity

The relatively high yield stress providing stability in these mixtures is a result of attractive Van Der Waals forces dominating the colloidal network of the paste [264]. The low plastic viscosity allows a convenient casting and is not susceptible to small changes in the water content. However, variations in the yield stress have a bigger impact: a too high yield stress jeopardises the filling ability and a too low yield stress is not able to prevent segregation of the coarse aggregates. As a result, the robustness of mixtures with a high yield stress and a low plastic viscosity (low slump flow class and V-funnel time class) mainly depends on the robustness of the yield stress of this mixture.

4.1.1. Robustness of the paste yield stress

Rheological models of the yield stress can be used to study the impact of small changes in the water content on the robustness of the yield stress. Although the Compressible Packing Model of de Larrard [260, 317] (Section 6.3. of the literature review) is the most accurate model predicting the yield stress of SCC, it is not suitable for a conceptual approach. Many parameters in the model, such as the superplasticizer saturation dosage and the maximum packing volume of the different fractions, depend on the global mix composition of the mixture complicating the study of small variations in one mix design parameter separately.

Consequently, the Yield stress model of Flatt (YODEL) [148, 266, 267] was used to study the impact on paste level (Equation 50 and 51, symbols summarized in Table 47). Due to the complicated chemical and physical processes happening in cement paste, YODEL does not provide an accurate prediction of the yield stress [142] and is only able to estimate the relative impact of certain changes in the mix design. Many influences of the impact of the properties of the fines and superplasticizer content are gathered in the prefactor m_1, which was arbitrary fixed to 1. Based on the experiments on pastes described in Section 3.2., the percolation treshhold is set at 0, the value which corresponded with the best fit of experimental results. The maximum packing densities used during the analysis were determined in wet condition during the experiments of Section 3.2, a different method as suggested in the work of Flatt [267], estimating the maximum packing density based on the Compressible Packing Model of de Larrard [260].

$$\tau_0 = m_1 \cdot \frac{\phi(\phi-\phi_0)^2}{\phi_{max}\cdot(\phi_{max}-\phi)} \quad \text{(Eq. 50)}$$

$$m_1 = \frac{1.8}{\pi^4} \cdot G_{max} \cdot a^* \cdot u_{k,k} \cdot \frac{F_{PSD}}{{R_{v,50}}^2} \quad \text{(Eq. 51)}$$

Symbol	Unit	Definition
τ_0	[Pa]	Yield stress
m_1	[-]	Prefactor accounting for the interparticle forces, particle size, and particle size distribution
ϕ	[-]	Volume fraction
ϕ_0	[-]	Percolation treshhold
ϕ_{max}	[-]	Volume fraction at maximum packing
G_{max}	[-]	Maximum attractive interparticle force, normalized by the radius of curvature at the contact points
a^*	[-]	Average fixed radius of curvature of the contact points
$u_{k,k}$	[-]	Normalization function $u_{k,k} = \frac{16\pi}{2-\sqrt{3}}$
F_{PSD}	[-]	A function accounting for the particle size distribution
$R_{v,50}$	[-]	Mean volume radius

Table 47: Abbreviations used in the YODEL model (Eq. 50 and 51)

A first parameter which has been used for a qualitative comparison is the impact of the superplasticizer dosage. In Section 3.2, the correlation between higher superplasticizers and higher maximum packing densities ϕ_{max} of the paste has been demonstrated (Figure 63 of Section 3.2). According to the YODEL model, higher maximum packing densities result in a more robust yield stress (Figure 119), which agrees with the experiments of Section 3.2 (Figure 120). The experimental results on SCC level, described in Section 3.1, and shown in Figure 121 also indicate a more robust slump flow of SCC with higher superplasticizer dosages of the paste: the sensitivity of the slump flow (ΔSF/ 16 l/m³) decreases as the superplasticizer dosage increases (lower paste volume) for all water-to-powder volumetric ratios. Another method to improve the maximum packing density of paste is the optimizing of the powder composition. However, this method has not been further investigated. Based on Figures 119 and 120, one would assume that a lower packing density also helps to improve the robustness of paste. However, lowering the particle density might result in an increase of the risk to segregation.

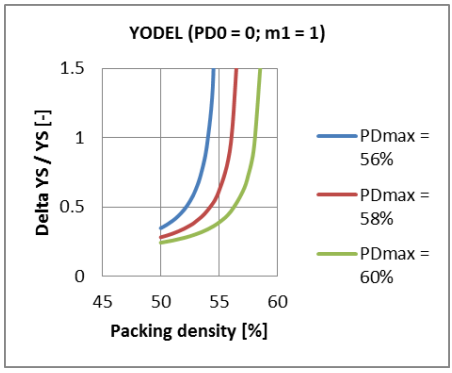

Figure 119: Impact of the maximum packing density on the robustness of the yield stress of cement paste (YODEL model)

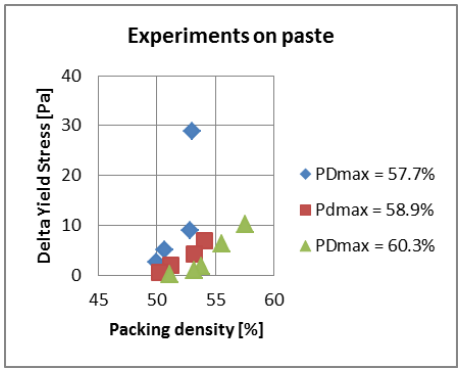

Figure 120: Impact of the maximum packing density on the robustness of the yield stress of cement paste (experiments Section 3.2)

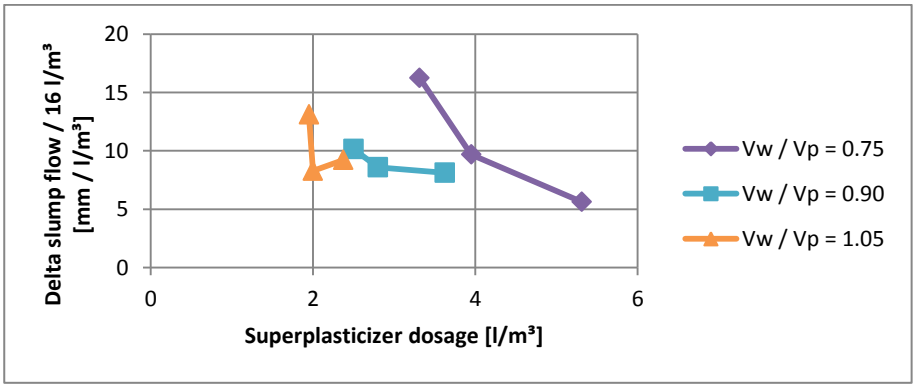

Figure 121: Impact of the superplasticizer dosage on the robustness of the slump flow (experiments Section 3.1.)

A second parameter investigated with the YODEL model is the yield stress value itself. Figure 122 illustrates that the robustness of the yield stress decreases with increasing yield stress value. Based on this trend, a possible approach to reduce the robustness of mixtures with a high yield stress and low plastic viscosity can be suggested: reducing the colloidal attractive Van Der Waals forces or providing more steric repulsive forces (higher superplasticizer dosage). Those measures manifest macroscopically as a lower yield stress of the paste.

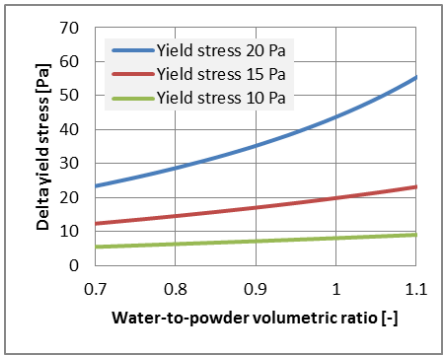

Figure 122: Impact of the yield stress value on the yield stress robustness (YODEL model)

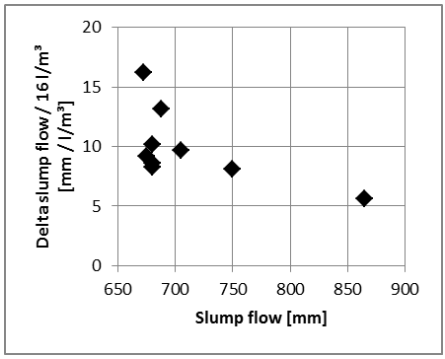

Figure 123: Relation between slump flow value and slump flow robustness (experiments of Section 3.1)

As shown in the model of Ferraris and de Larrard [320] (Equation 52, in which ϕ^* is a packing density parameter), aggregates amplify the yield stress of SCC. The impact of aggregates on the yield stress robustness is illustrated in Figures 124 and 125: the impact of changes in the maximum packing density of the aggregates is smaller when the aggregates packing density is lower.

$$\frac{\mu_{concrete}}{\mu_{paste}} = \exp\left(26.75\left(\frac{\phi}{\phi^*} - 0.7448\right)\right) \qquad \text{(Eq. 52)}$$

The contribution of aggregates to the yield stress can be limited using rounded aggregates instead of crushed aggregates or by an increase in the maximum aggregates packing density. Optimizing the aggregates packing with the compressible packing model of de Larrard [260] creates more free paste available to help lubricating the aggregate particles and thus reduces the risk of a lack of flowability. Other optimizations of the aggregate grading curves have been suggested in literature [91, 95]. Rounded aggregates have been recommended by Jonasson et al. [94].

The friction in between coarse aggregates should not be lowered with an increased paste content as this would lead to a lower superplasticizer dosage to keep the same slump flow. A reduction of the superplasticizer lowers the robustness of the paste yield stress and therefore worsens the robustness of the SCC. Only when suffering with a low quality control of the aggregates, a slightly higher paste volume can be justified to reduce the impact of variations in the aggregates [39, 91].

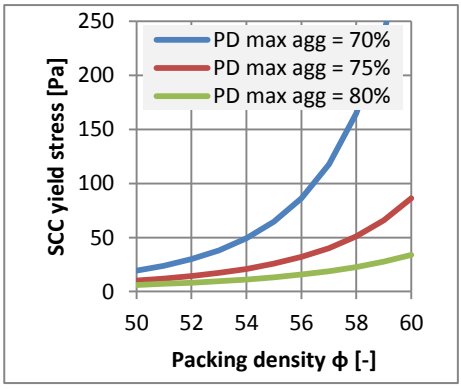

Figure 124: Impact of variations in the packing density on the yield stress of SCC

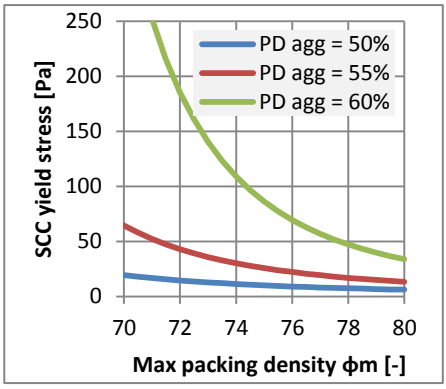

Figure 125: Impact of variations in the maximum packing density on the yield stress of SCC

4.1.2. Segregation of aggregates

Bleeding only rarely happens in SCC mixtures with a relative high yield stress. Relative high Van Der Waals forces provide a strong colloidal network in the cement paste and prevent the occurrence of bleeding. Segregation of coarse aggregates, on the other hand, is more likely to happen in SCC mixtures with a low plastic viscosity. The influence of mix proportions on the robustness of the segregation resistance can be estimated based on Equation 53 (abbreviations summarized in Table 48), describing the static segregation rate [91, 156] of the mixture. Gravity induced migration during flow is mainly affecting the coarsest particles [367].

$$u_a = \frac{\left(\frac{(\rho_S - \rho_L)\cdot g \cdot d}{18} - \tau_0\right)\cdot d}{\eta_{pl}} \cdot \left(1 - \frac{\phi}{\phi_m}\right)^{5.18} \qquad \text{(Eq. 53)}$$

Symbol	Definition
u_a	Segregation rate of the entire set of agggregates
ϕ	Volume fraction of aggregates
ϕ_m	Packing density of aggregates
ρ_s	Density of aggregates
ρ_L	Density of paste
g	Gravitational acceleration
d	Diameter of the representative aggregate
τ_0	Paste yield stress
η_{pl}	Paste plastic viscosity

Table 48: Abbreviations used in Equation 53

In case of a low paste plastic viscosity, small variations of this paste plastic viscosity have a large impact on the static segregation rate as it is the divisor of the quotient. The segregation resistance robustness of such a mixture can therefore be enhanced most effectively by slightly increasing the paste plastic viscosity η_{pl}:

- Decreasing the water-to-powder ratio. The superplasticizer dosage should also be adjusted in order to keep the same fluidity.
- The inclusion of a VMA in the mix design. The needed superplasticizer dosage to obtain a certain target fluidity may be affected by the inclusion of a VMA.

The term $\left(1-\frac{\phi}{\phi_m}\right)^{5.18}$ and d show the importance of a proper grading curve:

- A higher aggregate packing density can be obtained by lowering the paste volume. The superplasticizer content should be raised to compensate for the lower volume of paste lubricating the aggregates. The impact of the aggregate packing density is larger than the negative effect of lowering of the paste yield stress on the segregation resistance [91, 156].
- A reduction of the coarse aggregates size [33, 91, 93, 120, 156].
- Although a lower maximum aggregate packing density ϕ_m seems to affect the segregation resistance in a positive way, it would result in a significant increase of the needed superplasticizer dosage to keep the same fluidity. The global result is a decrease of the SCC robustness.

4.2. Low yield stress, high plastic viscosity

Section 3.1. demonstrated that the robustness of the rheology of SCC with a low or zero yield stress and high plastic viscosity depends on the mechanism providing stability: the robustness of the paste plastic viscosity. A low yield stress ensures a proper filling ability of the mixture. However, the slow flowing rate of SCC may endanger the workability of the mixture. A small change in the mix composition might even induce an extreme mode of a lack in workability: an excessive stickiness. The experiments described in Section 3.4. have shown that this extreme sticky concrete is not only caused by a high plastic viscosity, but also as a result of strong thixotropy.

In mixtures with a low yield stress, occasionally bleeding is observed. Bleeding occurs when the repulsive forces dominate the attractive Van Der Waals forces for small colloidal particles in the colloidal network of the paste. An upward displacement of water through the paste results in a thin layer of water on the SCC surface or at the edge of the slump flow test. Only when extreme bleeding occurs, the paste loses all cohesion and is not able to support the aggregates. In all other cases, segregation of the aggregates is prevented by the relative high paste viscosity.

4.2.1. Robustness of the paste plastic viscosity

The impact of small changes in the paste plastic viscosity is studied using the Krieger – Doherty equation for suspensions [86] (Equation 54, abbreviations in Table 49). The Krieger – Doherty equation cannot be used for an accurate prediction of the plastic viscosity of cement paste as it is developed for colloidal suspensions of spherical particles at a low concentration. Although this model is only an inaccurate approximation, it will be used in this thesis to study the relative impact of certain mixing parameters. Alternative models such as the Nielsen model [322, 323] and the Chan and Powell model [320] can only be used to determine the plastic viscosity on concrete level. The viscosity of the matrix was set at 8.9 . 10^{-4} Pa.s (viscosity of water), the intrinsic viscosity η_i was set at 4 to fit to the experimental results of Section 3.2.

$$\frac{\eta}{\eta_m} = \left(1 - \frac{\Phi}{\Phi_m}\right)^{-\eta_i \cdot \Phi_m} \qquad \text{(Eq. 54)}$$

Symbol	Unit	Definition
η	[Pa s]	Viscosity of the suspension
η_m	[Pa s]	Viscosity of the matrix
Φ	[-]	Packing density of solids
Φ_m	[-]	Maximum packing density allowing flow of the suspension
η_i	[-]	Intrinsic viscosity (2.5 for rigid uncharged spheres)

Table 49: Abbreviations used in the Krieger-Doherty model (Eq. 54)

When the higher packing density increases, the Krieger – Doherty equation becomes more steep, indicating a higher sensitivity to changes in the water content. This inclination can be explained using the concept of the Water Film Thickness (WFT): as less water is available in the mixture (higher packing density), the film of water lubricating the solid particles becomes thinner and more sensitive to small changes in the mix composition. The relative impact of a small increase in the Water Film Thickness is bigger when this Water Film Thickness is smaller.

This trend was confirmed by the experiments on paste of Section 3.2. As shown in Figures 126 to 131, an increase of the packing density (i.e. a decrease of the water-to-powder ratio) strongly decreases the robustness of the paste plastic viscosity.

The impact of changes in the packing density enlarges when the maximum packing density reduces (less superplasticizer).

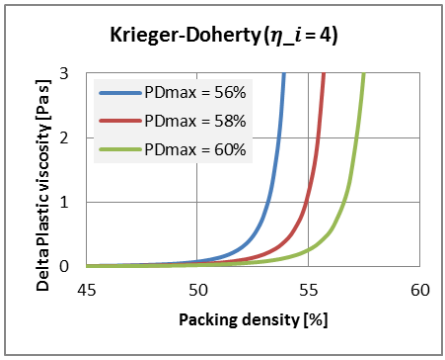

Figure 126: Impact of the packing density on the plastic viscosity robustness (Krieger – Doherty model)

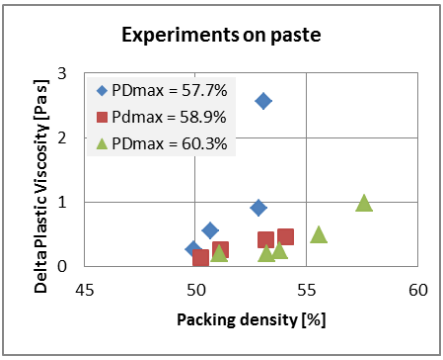

Figure 127: Impact of the packing density on the plastic viscosity robustness (experiments of Section 3.2)

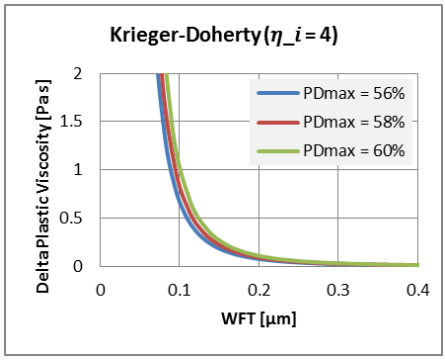

Figure 128: Impact of the WFT on the plastic viscosity robustness (Krieger – Doherty model)

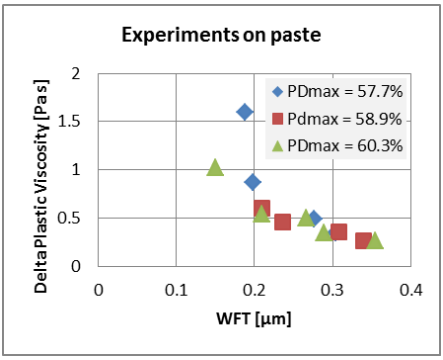

Figure 129: Impact of the WFT on the plastic viscosity robustness (experiments of Section 3.2)

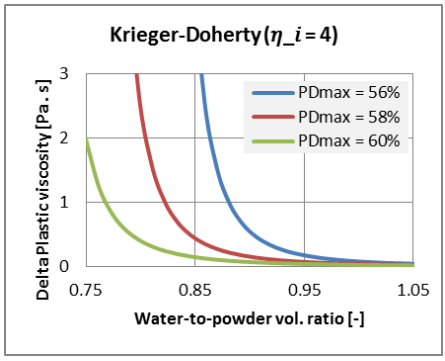

Figure 130: Impact of the water-to-powder ratio on the plastic viscosity robustnes (Krieger – Doherty model)

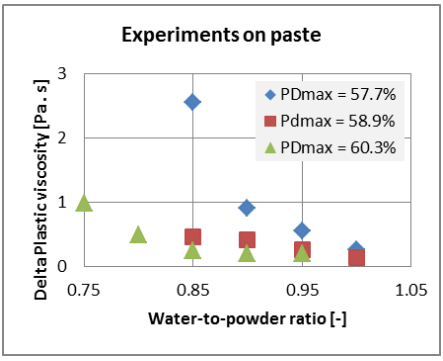

Figure 131: Impact of the water to powder ratio on the plastic viscosity robustnes (experiments of Section 3.2)

As shown in Figure 132, the plastic viscosity of mixtures with a higher plastic viscosity is less robust compared to mixtures with a lower plastic viscosity. For mixtures with a higher plastic viscosity, the impact of the water-to-powder ratio (and thus packing density) also becomes more important. Similar results were obtained on concrete level (Figure 133): the V-funnel flow time of a mixture with a water-to-powder volumetric ratio of 0.75 (more viscous) was less robust compared to the V-funnel flow time of mixtures with a water-to-powder volumetric ratio of 1.05 (less viscous).

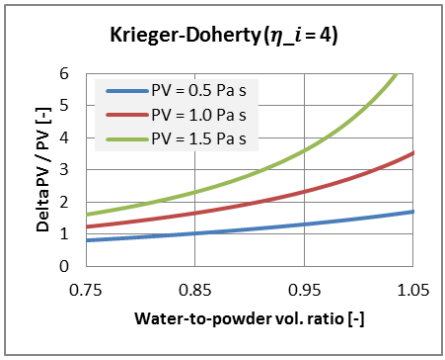

Figure 132: Impact of the plastic viscosity value on the plastic viscosity robustnes (Krieger – Doherty model)

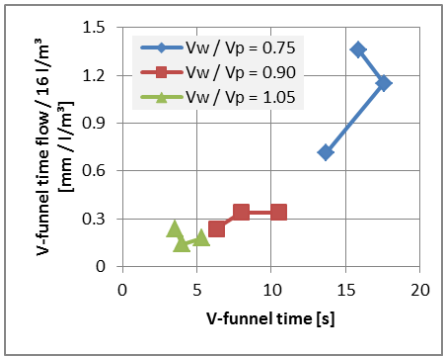

Figure 133: Impact of the water to powder ratio on the plastic viscosity robustnes (experiments of Section 3.1)

4.2.2. Robustness against excessive stickiness

A small decrease of the water content in a SCC mixture with high plastic viscosity can result in an excessive stickiness and therefore unworkable concrete mixture. Experiments in Section 3.4. have indicated that the origins of an excessive stickiness differ from the origins of a high plastic viscosity: the more sticky mixture had a lower plastic viscosity than the non sticky mixture and was rather related to the thixotropic buildup. An excessive stickiness, nevertheless, only happens in mixtures with a high plastic viscosity. Mixtures with a low plastic viscosity in general have a higher water-to-powder ratio and therefore a less thixotropic behaviour.

Possible methods to avoid an extreme stickiness are a reduction of the thixotropic buildup and a higher water-to-powder ratio. The experiments of Section 3.1. and the literature review [88, 408] indicated that a higher water-to-powder ratio is the most effective way. Because VMA either fixes part of the water or reduces the mobility of the water, a reduction of the VMA dosage or their removal from the mix design also helps to prevent an excessive stickiness.

The thixotropic buildup can be reduced with a cement replacement by fly ash (experiments Section 3.4.) or an increase of the Water Film Thickness (Figure 101, experiments Section 3.2.). When the distance separating the solid particles in a paste increases, fewer contact points can be connected to create a strong interparticle network inside the fresh paste.

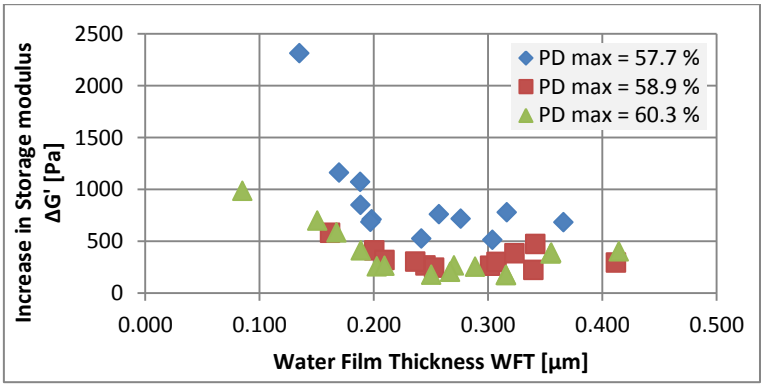

Figure 134: Impact of the Water Film thickness on the rate of structural buildup (experiments of Section 3.2.)

The type of superplasticizer also affects the tendency for an excessive stickiness of SCC. When the hydrophilic-lipophilic balance (HLB) value of a PCE molecule is above 18.5, the PCE molecules are very hydrophilic resulting in a lower plastic viscosity of the produced SCC [158, 186, 187]. As the steric repulsion force depends solely on the adsorbed amount and thickness of the polymer layer and is independent of the HLB value of the PCE polymers, the mechanism leading to an excessive stickiness are most probably independent of the mechanism governing the particle dispersion [186]. In mixtures with a high solid volume fraction, the energy dissipation during flow is concentrated in strongly sheared fluid layers of water in between the particles. PCE superplasticizers might affect the viscosity [177], surface tension [142], or anionic charge [185] of the of the pore water, cause weak hydrophobic Van Der Waals interactions in between the polymers absorbed on the cement surface [186], or non-adsorbed polymers may lubricate the shear flow [182, 183]. Further research into these possible mechanisms is needed. In Section 4.2.2. of the literature review, each possible mechanism was discussed briefly.

4.2.3. Robustness against bleeding

When the repulsive forces dominate the attractive forces for small colloidal particles, the colloidal network inside of SCC is broken and bleeding of the water occurs [271]. Problems related to such high repulsive forces in between small colloidal particles only occur when a high dosage of superplasticizer is present in the mix composition.

A higher paste volume (less aggregates), a higher water-to-powder ratio, and less VMA reduce the superplasticizer demand and thus the repulsive steric forces in the mixture. Consequently the tendency for bleeding reduces (experiments Section 3.1 and 3.3.). Another solution is an acceleration of the hydration process [385], for example by adding silica fume (experiments Section 3.4. or in [66, 386-388]). When the hydration process is accelerated, ettringite formation and CSH-nucleation increase the amount of small colloidal particles in fresh SCC, consuming part of the superplasticizer and thus countering bleeding.

5. Particle clustering

This section deals with the impact of particle clustering on the paste yield stress and plastic viscosity models. Particle clustering affects both the packing density and maximum packing density of the paste and the rate of cement hydration.

5.1. Mixing procedure

The duration and shear forces during the mixing procedure determine the balance between dispersion and clustering of particles in fresh SCC. An increase of the mixing time decreases the plastic viscosity, but does not affect the yield stress of the mixtures (Figures 135 and 136) and an increase in the mixing speed increases the yield stress but does not affect the plastic viscosity (Figures 137 and 138). The rate of structural buildup as measured by the increase in static yield stress is connected to the changes in the yield stress: the mixing time had no effect on the rate of structural buildup; the mixing speed did have an influence (Figures 139 and 140).

Because the observed results regarding the impact of the mixing time and mixing speed do not match, no general conclusions can be made about the impact of the shear history on the particle clustering and its impact on the rheology. As higher shear forces both enhance the dispersion and increase the hydration rate, its combined effect on the rheology of SCC is difficult to predict.

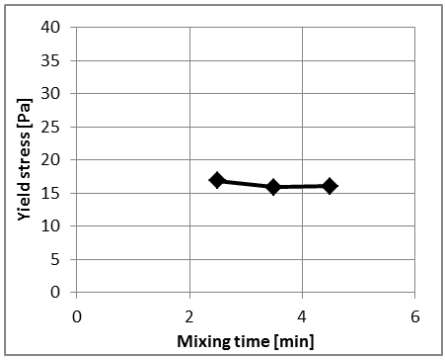

Figure 135: Impact of the mixing time on the yield stress (Experiments Section 3.5.)

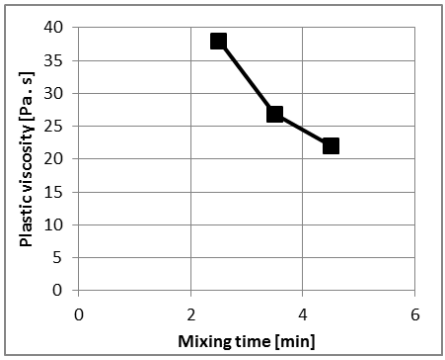

Figure 136: Impact of the mixing time on the plastic viscosity (Experiments Section 3.5.)

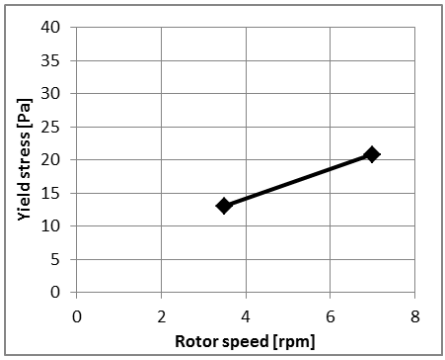

Figure 137: Impact of the mixing speed on the yield stress (Experiments Section 3.5.)

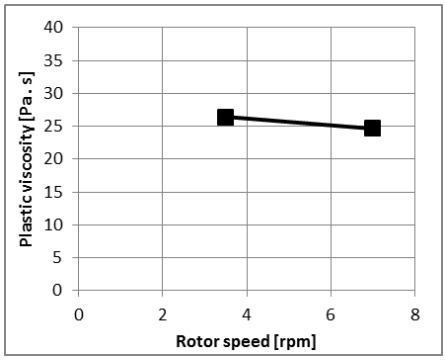

Figure 138: Impact of the mixing speed on the plastic viscosity (Experiments Section 3.5.)

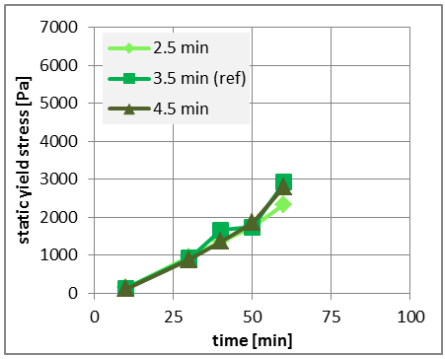

Figure 139: Impact of the mixing speed on the rate of structural buildup (Experiments Section 3.5.)

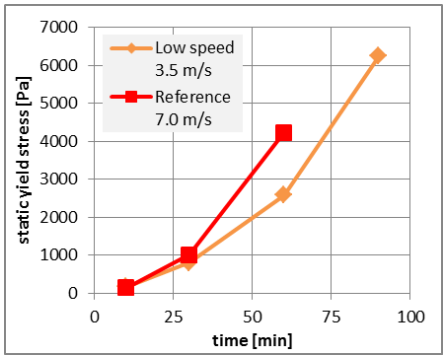

Figure 140: Impact of the mixing speed on the rate of structural buildup (Experiments Section 3.5.)

5.2. Steric repulsion forces

The impact of the superplasticizer dosage has already been discussed in Section 4. PCE superplasticizer disperses the fines in cement paste with steric repulsion forces. As a result, a higher maximum packing density and therefore higher water film thickness is observed with a similar water-to-powder ratio of the paste (Figure 141). Macroscopically, this higher water film thickness results in a lower yield stress and plastic viscosity of the paste (Figures 142 and 143).

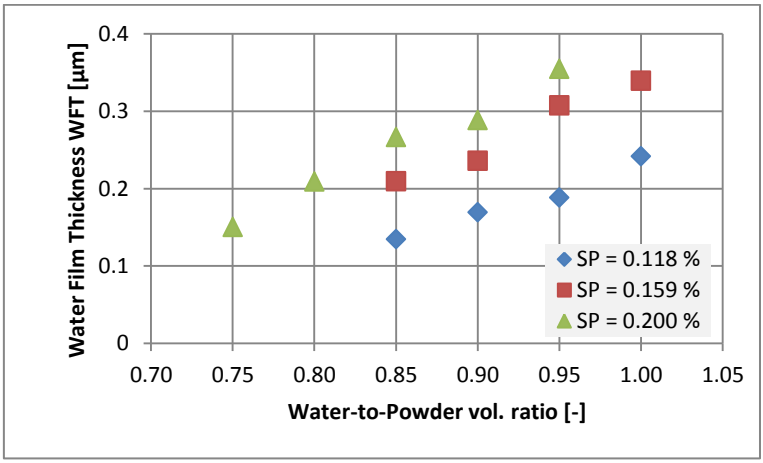

Figure 141: Impact of the superplasticizer dosage on the Water Film Thickness (experiments of Section 3.2)

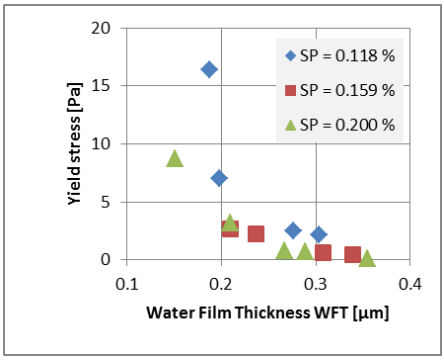

Figure 142: Impact of the superplasticizer dosage on the yield stress (experiments of Section 3.2.)

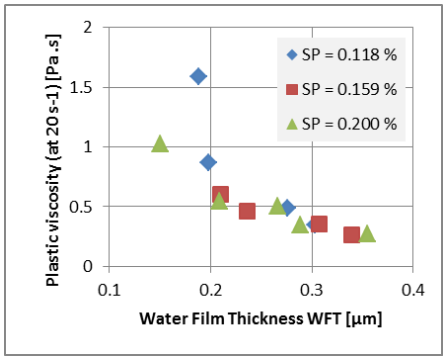

Figure 143: Impact of the superplasticizer dosage on the plastic viscosity (experiments of Section 3.2.)

5.3. Water Film Thickness and structural buildup

An increasing water film thickness (WFT) decreases the rate of structural buildup (Figures 144 to 146, experiments of Section 3.2.). As the distance between the solid particles increases, a longer time is needed to obtain a connection of ettringite or C-S-H hydrates between these particles. Because the WFT also has an effect on the rate of hydration, its impact is smaller compared to the impact of changes in the superplasticizer dosage. A larger superplasticizer dosage enhances the steric repulsive forces on the particles surface and thus results in a better dispersion state.

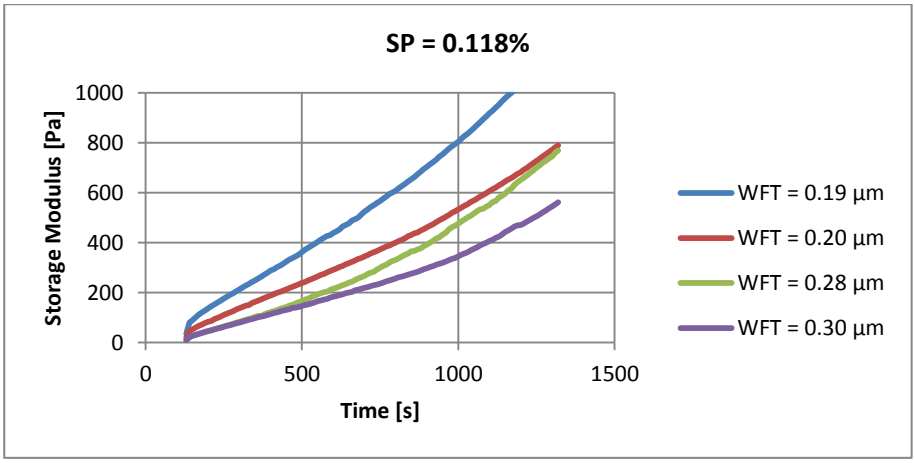

Figure 144: Impact of the WFT on the rate of structural buildup (superplasticizer dosage or 0.118%)

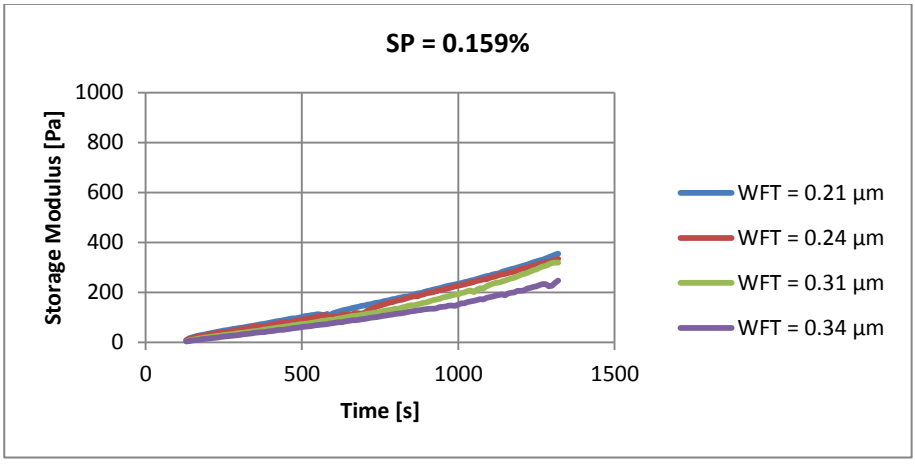

Figure 145: Impact of the WFT on the rate of structural buildup (superplasticizer dosage or 0.159%)

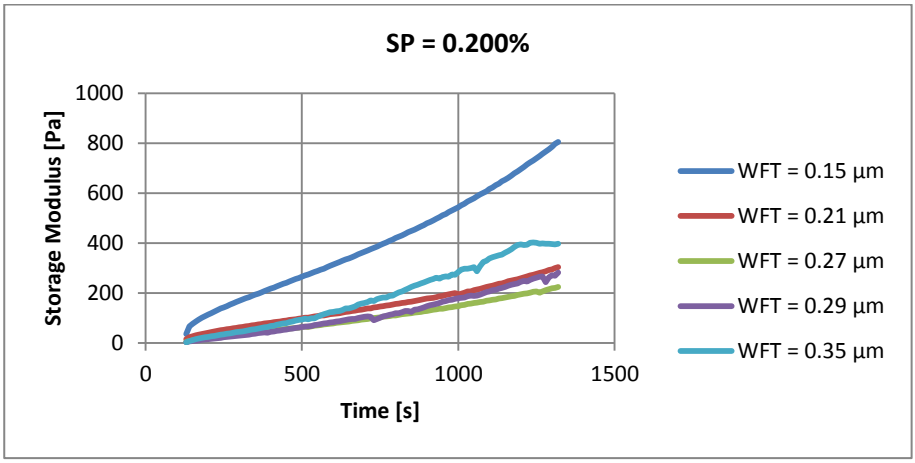

Figure 146: Impact of the WFT on the rate of structural buildup (superplasticizer dosage or 0.200%)

Figure 147 shows the rate of structural buildup measured by the increase in storage modulus as a function of the yield stress at the start of the storage modulus evolution for the reference paste mixtures of Section 3.2. Mixtures with a higher yield stress have a higher rate of structural buildup, a result of a stronger network of CSH and ettringite hydrates connecting the solid particles inside a cement paste. The higher yield stress indicates that stronger attractive Van Der Waals forces are present in the paste and is most probably a result of the formation of newly formed hydration products in the mixture. The link between the structural buildup and robustness of the yield stress is illustrated in Figures 148 to 150 (experiments Section 3.2.), in which the impact of small changes in the water content (±3% of the water content) on the yield stress and structural buildup is illustrated. Mixtures suffering from large variations in the yield stress most often also demonstrated large fluctuations in the rate of structural buildup.

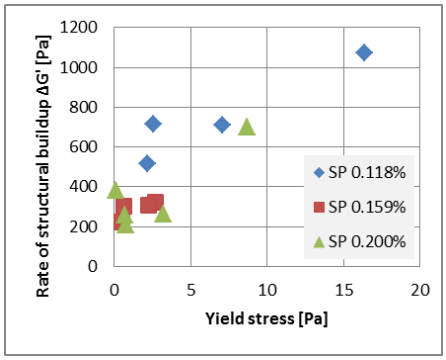

Figure 147: The rate of the structural buildup as a function of the yield stress

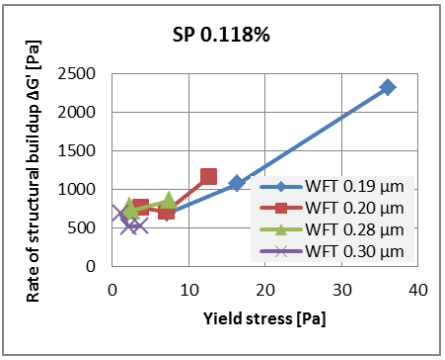

Figure 148: Robustness of the yield stress and rate of the structural buildup (SP dosage of 0.118%)

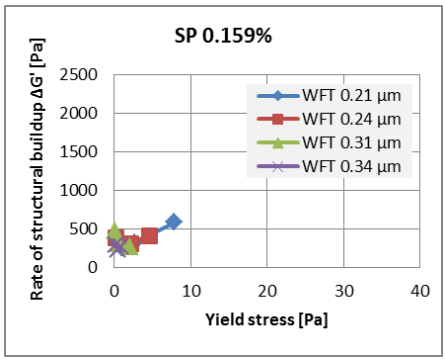

Figure 149: Robustness of the yield stress and rate of the structural buildup (SP dosage of 0.159%)

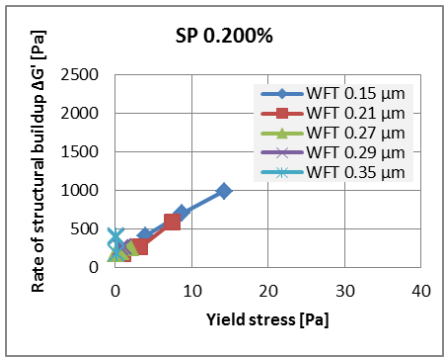

Figure 150: Robustness of the yield stress and rate of the structural buildup (SP dosage of 0.200%)

6. Guidelines

As different applications require different workability properties, other types of SCC should be used in different situations. Dependent on the type of SCC, another method should be applied to optimize the robustness. Table 50 summarizes the practical recommendations arising from this thesis[6]. Of course other requirements regarding the compressive strength, plastic shrinkage, and durability also have an impact on the mix design. As a result, the recommendations given in Table 50 should not be considered as strict regulations, but rather as an assistance to improve the robustness.

Application	Recommended paste volume	Recommended volumetric water-to-powder ratio	Superplasticizer dosage	Include a VMA?
Large horizontal elements (floors and slabs)	Low 350 to 375 l/m³	High 0.90 to 1.05	Low	Yes
Long horizontal elements (reinforced beams)	Low 350 to 375 l/m³	Intermediate 0.82 to 0.98	Intermediate	Yes
Long vertical elements (walls)	Intermediate 365 to 385 l/m³	Low 0.75 to 0.90	High	No
Slender vertical elements (columns)	High 375 to 400 l/m³	Low 0.75 to 0.90	High	No

Table 50: Recommendations for a maximum robustness[6]

[6] The recommendations assume a regular quality control on the all compounds. In case of a very low quality control on the aggregates grading curve, aggregate friction should be prevented from dominating the rheology of SCC by a sufficient high paste volume.

6.1. Large horizontal elements (floors and slabs)

A fast and convenient casting of large horizontal elements requires an SCC with a low plastic viscosity and to provide a sufficient segregation resistance of the coarsest aggregates, the mixture needs a sufficiently high yield stress. The robustness of such a mixture with a relatively high yield stress and low plastic viscosity can be improved by combining a high water-to-powder volume ratio with a low paste volume. A cement replacement by fly ash or the inclusion of diutan gum or attapulgite clay can further improve the robustness of such a mixture.

6.2. Long horizontal elements (reinforced beams)

In long horizontal elements such as reinforced concrete beams, a slow, but far flowing mixture is most convenient. This SCC with a low yield stress is stabilized by an intermediate plastic viscosity, obtained with a low water-to-paste ratio and relatively low paste volume. A sufficiently high but not too high water-to-powder ratio can enhance the robustness of such a mixture. An intermediate water-to-powder ratio is recommended.

6.3. Long vertical elements (walls)

A slowly flowing mixture with a high plastic viscosity will not suffer from dynamic segregation during the casting of long vertical elements. The high plastic viscosity is achieved with a low water-to-powder ratio. To ensure a proper filling of the space of the formwork and to flow around the reinforcement, a low or zero yield stress is needed. The robustness of this type of SCC can be enhanced with a higher paste volume, although it should not be too high, making the yield stress dominant and decreasing the robustness with regard to flowability. The robustness decreases when a VMA is included in the mix design of such a mixture. A replacement of part of the cement by silica fume can reduce the tendency to bleeding in case the mixture is prone to bleeding. In case an excessive stickiness is an issue, a cement replacement by fly ash may help.

6.4. Slender vertical elements (columns)

The stability of SCC made for casting high vertical elements such as columns should be guaranteed with a high plastic viscosity. A low yield stress allows the air bubbles to escape and a proper filling of the formwork. A combination of a low water-to-powder ratio and a high paste volume gives an optimum robustness. No VMA should be included in such a mix design. Just as in the previous section, a cement replacement by silica fume should be considered in case bleeding causes problems and a cement replacement by fly ash can help to reduce the tendency to an excessive stickiness.

7. Summary

This chapter investigates the mechanisms governing the robustness of fresh SCC. Based on a series of experiments exploring the impact of several mix parameters, a fundamental theory was developed to explain the observed experimental results. Practical guidelines were summarized in the Section 6.

The risk of disproportional changes in the workability due to small changes in the water content is related to the mechanism providing stability in the mixture. In SCC mixtures with a relative high yield stress and a low plastic viscosity, the sensitivity of this yield stress determines the robustness of the global mixture. In mixtures with a low yield stress and high plastic viscosity, the sensitivity of the plastic viscosity was the robustness determining factor. The best method to enhance the robustness of a SCC mixture is to reduce the sensitivity of the parameter providing stability.

Mixtures with a relatively high yield stress can be improved with a small increase of the paste plastic viscosity, for example by adding a VMA in the mix composition, or by an increase of the repulsive forces on the colloidal particles in the paste, for example due to an increase of the superplasticizer dosage combined with a lower paste volume. A higher superplasticizer dosage enhances the steric repulsion forces on the fines and thereby increases the maximum packing density of the mixture.

To enhance the robustness of mixtures with a high plastic viscosity, its plastic viscosity itself should be stabilized, and at the same time too much bleeding or an excessive stickiness should be avoided. A slightly higher water content helps to reduce the plastic viscosity itself and reduces the sensitivity of the plastic viscosity vastly. VMA's should be avoided in a mixture with a high plastic viscosity, as the use of VMA's raises the required superplasticizer dosage and thus repulsive forces in a mixture with a low yield stress. When the repulsive forces dominate the attractive Van Der Waals forces for the smallest colloidal particles, bleeding might occur. To enhance the attractive Van Der Waals forces in mixtures suffering from bleeding, a cement replacement by silica fume may help.

Mixtures with a high plastic viscosity sometimes suffer from an excessive stickiness, making them difficult to process. This excessive stickiness is mainly related to the thixotropic buildup inside SCC. The most effective method to reduce the thixotropy is an increase of the water-to-powder ratio. Another option is a replacement of cement by fly ash.

Using the YODEL model for the paste yield stress and the Krieger-Doherty model for the paste viscosity, a qualitative analyses of the mechanisms governing the robustness was performed. In addition to the confirmation of the experimental results, the mechanisms and origins could be clarified. The impact of the superplasticizer content on the yield stress could be explained by its impact on the maximum packing density of the paste and the effect of a higher water content on the robustness of the paste plastic viscosity was linked to the overall lower solid packing density of the paste.

As the clustering and hydration speed of paste mixtures is strongly affected by the mixing energy, experiments were performed on concrete level to assess the impact of the mixing procedure on SCC. General conclusions were not drawn as the changes on the mixing energy and the mixing time (both related to the mixing energy) did not follow the same trend. The influence of the addition sequence was remarkable: when air dried aggregates are premixed with water, part of the water is absorbed into the aggregate pores and not available to lubricate the paste. This results in a less flowable concrete compared to a mixture in which the powder and water were first mixed together before adding the aggregates.

Chapter 4: Monitoring of particle clustering and structural buildup

1. Introduction

The rheology and hence the robustness of SCC is not only dependent on the proportions and properties of the constituents, but also on the arrangement of the various particles in the fresh concrete. The balance between particle flocculation and deflocculation will determine the degree of particle clustering. An example of the importance of particle clustering is the use of superplasticizers: adsorbed PCE molecules provide steric repulsion forces on fine colloidal particles and thereby induce a more dispersed microstructure inside of the fresh concrete. As a result, an unworkable dry mixture can be transformed into a highly flowable concrete such as SCC.

During the dormant period, flocculation processes happen and hydration continues at a very slow rate. The resultant changes on microscopic level cause macroscopic changes in the rheology in time and sometimes a strong structural buildup at rest. Different theories have been proposed to model the observed macroscopic changes based on their microscopic origins, but lots of ambiguity still exist on what is exactly happening inside of the fresh concrete. In order to explore the particle clustering inside concrete on a more fundamental basis, the applicability of potential techniques to study the microstructure has been investigated in this chapter. An improved technique to study the particle clustering would help to understand the delicate equilibrium of clustering and dispersion during flow, the mechanisms inducing changes in the rheology by variations in the mixing process, and how particle clustering occurs at rest. In the study of robustness, it would be helpful to understand what effect small changes in for example the water content have on the microstructure and particle clustering of fresh concrete.

As concrete is a dense opaque solution of particles covering a very broad particle size distribution range, the study of the microstructure is not evident. On top of that, the constituents of concrete have an irregular non-spherical shape and consist of a combination of various minerals, each with other ultrasonic and optical properties. Some minerals have a purely crystalline form, others an amorphous form.

2. Modeling particle clustering

In Section 6.4. of the literature review (Chapter 2), an overview is given of the thixotropic models. Based on the structural kinetics model of Roussel [310] and the particle clustering model of Mewis [275], the evolution of the number of links can be modeled.

The structural kinetics model of Roussel [310] assumes that particle clustering only affects the yield stress of the material. In this model (Equation 55), λ is the structural parameter and the thixotropic parameters T, m and α should be experimentally determined. Assuming the Bingham model for cement paste, parameters $n = 1$ and k is the plastic viscosity μ_p. When the paste is subjected to a constant shear rate $\dot{\gamma}$, the differential equation can be solved into Equation 56.

$$\begin{cases} \tau = (1+\lambda)\cdot\tau_0 + k\cdot\dot{\gamma}^n \\ \frac{d\lambda}{dt} = \frac{1}{T\cdot\lambda^m} - \alpha\cdot\lambda\cdot\dot{\gamma} \end{cases} \quad \text{(Eq. 55)}$$

$$\lambda(t) = \left(\frac{1}{\alpha\cdot\dot{\gamma}\cdot T} + \left({\lambda_0}^{m+1} - \frac{1}{\alpha\cdot\dot{\gamma}\cdot T}\right)\cdot\exp(-\alpha\cdot\dot{\gamma}\cdot(m+1)\cdot t)\right)^{\frac{1}{m+1}} \quad \text{(Eq. 56)}$$

Mewis [275] proposed a model based on single-order kinetics (Equation 57) to estimate the number of links. The parameters c (assumed 0), d (assumed 2), k_1, k_2, α, and β (assumed 0) are constants and n_∞ is the limiting number of thixotropic links. If the assumptions in brackets are taken into account, Equation 58 shows the evolution under a constant shear rate. The relation between the number of links and the macroscopic rheology is not clear.

$$\frac{dn(t)}{dt} = -k_1\cdot n^c\cdot\left(\dot{\gamma}(t)\right)^\alpha + k_2\cdot\left(n_\infty - n(t)\right)^d\cdot\left(\dot{\gamma}(t)\right)^\beta \quad \text{(Eq. 57)}$$

$$\begin{cases} n(t) = n_\infty - \sqrt{\frac{k_1\cdot\dot{\gamma}^\alpha}{k_2}}\cdot\tanh\left(\sqrt{k_1\cdot k_2\cdot\dot{\gamma}^\alpha}\cdot(t+C_1)\right) \\ C_1 = \frac{1}{\sqrt{k_1\cdot k_2\cdot\dot{\gamma}^\alpha}}\cdot tanh^{-1}\left(\sqrt{\frac{k_2}{k_1\cdot\dot{\gamma}^\alpha}}\cdot\left(n_\infty - n(0)\right)\right) \end{cases} \quad \text{(Eq. 58)}$$

3. Static yield stress measurements

A direct measure of the macroscopic structuration at rest is the static yield stress evolution [25, 310, 398, 402, 409]. At different resting times, the peak stress τ_{0s} under a small constant rotational velocity is determined in a sample of SCC at rest as a measure of the structural buildup at rest (Figures 151 and 152). No direct information on what is happening at the microscopic level can be gathered using static yield stress tests. Static yield stress measurements are typically performed during a longer time span before setting begins. Based on the static yield stress measurements, SCC can be categorized in thixotropy classes as proposed by Roussel [310] (Equation 59, and Table 51). In the context of tests investigating the impact of variations in the mixing procedure, static yield stress tests have been reported in Section 3.5. of Chapter 3 of this thesis.

$$\tau_{0s} = \tau_{0i} + A_{thix} \cdot t \qquad \text{(Eq. 59)}$$

Flocculation rate A_{thix} (Pa/s)	SCC type
<0.1	Non-thixotropic SCC
0.1 – 0.5	Thixotropic SCC
>0.5	Highly thixotropic SCC

Table 51: The thixotropy classes based on static yield stress measurements [310]

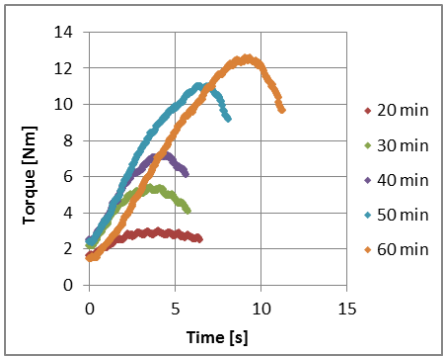

Figure 151: Peak torque evolution in time

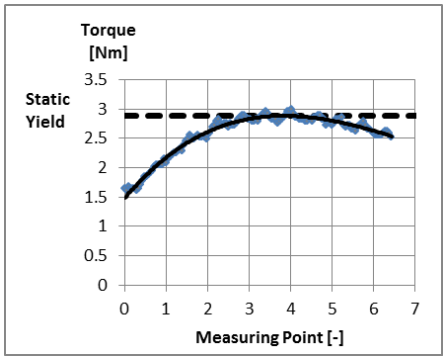

Figure 152: Measurement of the peak torque under a small constant rotational velocity

4. Oscillatory rheology

4.1. Experimental setup

The rate of structural buildup in cement pastes can be studied using oscillatory rheology [24, 25, 139, 227, 264, 265, 275, 402, 403]. A vane is subjected to oscillations in a sample of paste at rest. When the amplitude of oscillation is very

small (below the critical strain), the microscopic network inside the paste is not ruptured by the movement of the vane. As shown in Section 2.3.1.2. of Chapter 3, the corresponding torque curve can be analyzed using Equations 60 to 64, with abbreviations explained in Table 52. The storage modulus G' is the elastic response of the sample and the loss modulus is the viscous contribution to the measured shear stresses. Both G' and G" depend on the frequency used during the oscillatory rheometry.

$$\gamma = \gamma_0 \cdot \cos(\omega \cdot t - \delta) \quad \text{(Eq. 60)}$$

$$\sigma = \sigma_0 \cdot \cos(\omega \cdot t) \quad \text{(Eq. 61)}$$

$$G^* = \frac{\sigma_0}{\gamma_0} \cdot (\cos\delta + i \cdot \sin\delta) \quad \text{(Eq. 62)}$$

$$G^* = G' + i \cdot G" \quad \text{(Eq. 63)}$$

$$\tau_0 = \gamma_{critical} \cdot G' \quad \text{(Eq. 64)}$$

Symbol	Unit	Definition
γ	[-]	Oscillatory strain
γ_0	[-]	Amplitude of the strain
σ	[Pa]	Oscillatory stress
σ_0	[Pa]	Amplitude of the applied stress
ω	[1/s]	Angular velocity
t	[s]	Time
δ	[-]	Phase lag between the applied oscillatory strain and ($0 < \delta < \pi/2$)
G^*	[Pa]	Complex shear modulus
G'	[Pa]	Storage modulus
$G"$	[Pa]	Loss modulus

Table 52: Abbreviations used in Equations 60 to 64

4.2. Literature review

4.2.1. Time sweep

The procedure of oscillatory rheometry with a constant strain amplitude and frequency in time described above is referred to as a time sweep and used to measure the evolution of a material in time. The procedure can be used to monitor the buildup of a network in cement paste or mortars. As the increase of the storage modulus G' in time is related to the hydration heat produced, most probably the formation of CSH bridges is responsible for the increase of the elastic response [24].

4.2.2. Stress sweep

During a stress sweep, the shear stress amplitude is gradually increased under a constant frequency. At low stress amplitudes, the network inside cement paste can withstand the applied forces and a constant storage modulus is measured. As the shear stress amplitude continues to increase, the storage modulus decreases. The shear stress amplitude below which the storage modulus is larger than the loss modulus and above which the opposite is true, is called the critical stress limit, and corresponds with the breakdown of the microstructure inside the cement paste [410]. The critical stress is higher in mixtures with a higher water-to-powder ratio, a lower superplasticizer dosage, or a higher dosage of VMA (welan gum) [410].

4.2.3. Strain sweep

Under a constant frequency, the shear strain gradually increases during a strain sweep test. At a low shear strain amplitude, a linear elastic (solid) behaviour is observed as the flocculated particles recover elastically after each strain oscillation. Above the critical strain, an elastic recovery is not possible. As the water-to-powder ratio increases, the critical strain decreases. The linear elastic domain of cement paste is limited by a strain of around 10^{-4} [24, 227]: below this shear strain, the storage modulus is independent of the applied deformation. When a cellulose ether is included in the mix design, a higher critical strain is observed [227] because of the enhanced Van Der Waals forces and hydrogen bonds in the mixture, forming a three dimensional gel structure.

Dependent on the applied frequency and strain amplitude applied on cement paste, one can measure the short term thixotropy originating from colloidal flocculation/deflocculating or the long term thixotropy originating from hydrates nucleation, which is of practical interest for SCC (the very stiff elastic behavior of the material at very low strains) [240, 264]. The short term thixotropy has a characteristic time of several seconds, a critical strain of several % and the frequency needs to be above 5 Hz. The long term thixotropic behaviour has a characteristic time of several minutes, a critical strain of several 10^{-2} %, and can be monitored using a frequency of 1 Hz [264].

4.2.4. Frequency sweep

In order to investigate the influence of the speed of forces on the observed rheological behavior, a frequency sweep can be performed. The frequency decreases gradually applying a constant shear stress / shear strain. A solid like behavior is observed at high frequencies, and the fluid like behavior dominates at low frequencies, as the material relaxes in between two oscillations, and no residual energy of previous oscillation is remaining in the next one. At very high

frequencies (above 0.2 Hz), gel relaxing occurs, the residual energy of the past oscillation is still present during the following one [288].

4.3. Experimental results

The structural buildup in pastes has been monitored by oscillatory rheology in Section 3.2. of Chapter 3. A correlation was found between the rate of structural buildup and superplasticizer dosage (affecting the maximum packing density of solid particles) and the water film thickness (Figures 153 to 155). However, as this technique is only capable of monitoring the macroscopic response, only a conceptual description of the influence on particle clustering was possible.

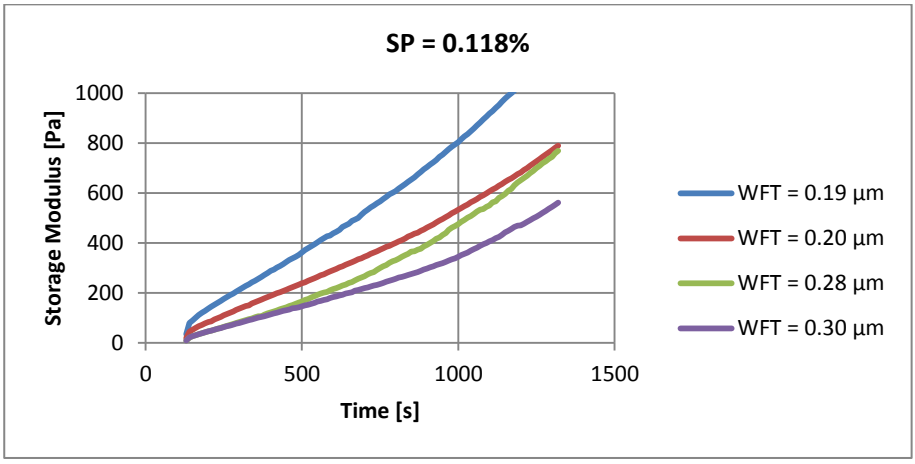

Figure 153: Impact of the WFT on the storage modulus G' evolution – SP dosage of 0.118%

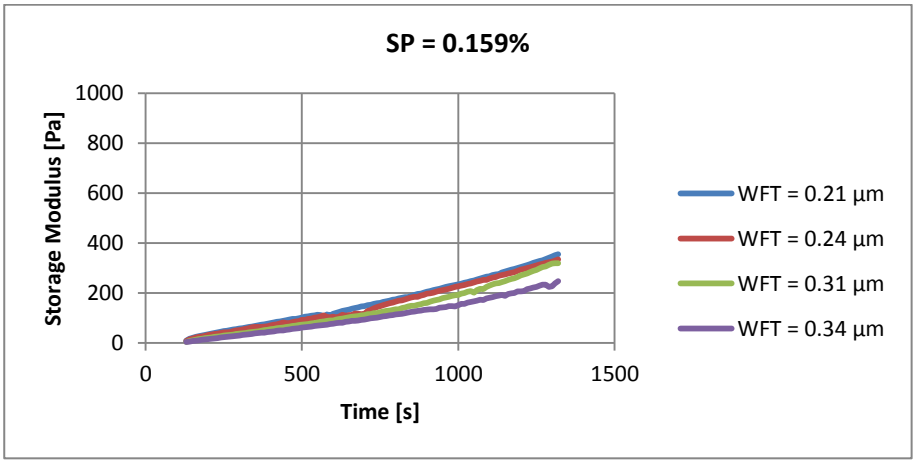

Figure 154: Impact of the WFT on the storage modulus G' evolution – SP dosage of 0.159%

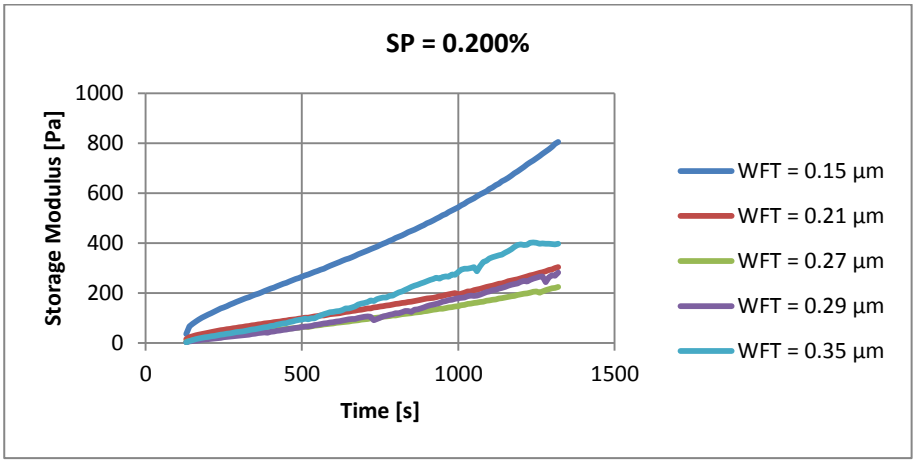

Figure 155: Impact of the WFT on the storage modulus G' evolution – SP dosage of 0.200%

5. Ultrasound attenuation

5.1. Introduction

Ultrasound attenuation is the amplitude loss of an ultrasound signal over the distance. Equation 65 describes the exponential decrease of the amplitude of the ultrasound signal. The attenuation coefficient α depends on the medium, the particle size, the particle concentration, the frequency of the signal, and the temperature. A higher attenuation coefficient indicates higher losses. The attenuation losses as a function of the frequency are displayed in an attenuation spectrum.

$$A(x) = A_0 \cdot \exp(-\alpha \cdot x) \qquad \text{(Eq. 65)}$$

Knowledge of the predominant loss mechanism allows to interpret the attenuation spectra. In case an attenuation model and a fitting method are available, it is even possible to calculate the particle size distribution of the suspended particles based on the measured attenuation spectrum [411, 412]. Acoustic spectroscopy has been successfully applied in colloid dispersions, emulsions, and dilute systems without particle-particle interactions [27-29, 413, 414]. However, no solid theory has been developed yet for dense, polydisperse systems [415].

Several mechanisms lead to attenuation losses of ultrasound signals [28, 411, 412, 415, 416]. Because of the large differences in critical frequencies for a certain particle size, most often only one mechanism is dominant. For broad particle size distributions such as cementitious materials, two or three mechanisms can contribute to the overall attenuation spectrum.

5.1.1. Intrinsic or bulk attenuation losses

The overall attenuation caused by the bulk homogeneous material of particles at molecular level causes intrinsic or bulk attenuation losses. The intrinsic attenuations should be considered when other attenuation losses are low, for example when small particles are suspended at a low volume fraction.

5.1.2. Viscous attenuation losses

When ultrasound waves pass over particles in suspension, differences in density between the particle and the medium cause a relative movement of the particle in the medium. The liquid flows around the particle and causes hydrodynamic drag and friction losses of the acoustic energy. The viscous attenuation losses are more pronounced for suspensions with large differences in density between the suspended particles and the suspending medium. Viscous attenuation losses are dominant for a suspension of small rigid particles with sizes smaller than 3 μm and should be taken into account when studying cement pastes.

5.1.3. Particle inertia attenuation losses

The oscillating movement caused by differences in the density between the particle and the medium also causes particle inertia losses. Especially for large particles at high frequencies, a correction for particle inertia losses should be implemented. Some authors consider the viscous and inertial attenuation losses as one mechanism, referred to as the visco-inertial losses.

5.1.4. Scattering attenuation losses

Because ultrasound waves are redirected and scattered on the particles surface, part of the ultrasound energy is lost by scattering losses. In strict sense, scattering does not induce energy losses. However, because part of the wave energy is redirected, part of the ultrasound energy does not reach the ultrasound transducer at the other side of the gap. Scattering losses, which are strongly dependent on the particle size distribution and the frequency of the signal, are very important for particles larger than 3 μm at frequencies above 10 MHz. Scattering losses should be taken into account for cement pastes.

5.1.5. Thermal attenuation losses

Small soft particles such as emulsions and latex beads are compressed when an ultrasound wave passes, generating temperature gradients near the particle surface. The thermodynamic coupling between pressure and temperature results in thermal attenuation losses. Thermal losses are negligible in high density contrast suspensions such as cement pastes.

5.1.6. Structural attenuation losses

In a network of particles, the oscillation caused by ultrasound waves is obstructed by network interactions and forces.

5.1.7. Electrokinetic attenuation losses

The oscillation of the double layer surrounding charged particles by ultrasound waves induces an alternating electric field and alternating electric currents in the sample. This mechanisms is the basis of electro-acoustics and can be used to determine the zeta potential. Electrokinetic attenuation losses are small compared to the other attenuation mechanisms.

5.2. Test setup

Two commercial apparatuses have been used to examine the potential use of ultrasound attenuation in cement paste: the DT-1202 system of Quantachrome and the OPUS system of Sympatec. Both systems are described in more detail below. In order to avoid bias in the attenuation spectra, the following issues should be dealt with carefully [27]:

- Misalignment of the transducers (especially for frequencies above 10 MHz).
- The use of an inadequate physical model. Non-linear concentration effects of particle concentrations happen above solid fractions of 5%.
- Gas bubbles in water have an impact on the attenuation for ultrasound frequencies below 10 MHz.
- An incorrect measurement of the intrinsic attenuation of water. A proper sample preparation is needed in order to evade the presence of air bubbles in the water.
- Temperature variations.

5.2.1. Quantachrome DT-1202

The DT-1202 system of Quantachrome, shown in Figure 156, measures the attenuation spectra for a range of 18 frequencies (3 to 100 MHz) over a range of 21 gaps. For each frequency the attenuation coefficient is calculated by linear interpolation over all gaps in which a proper signal-to-noise ratio was observed. According to the manufacturer, the system can determine the particle size distribution of particles in between 5 nm and 250 µm in opaque suspensions with high concentrations up to 70% by volume assuming a lognormal or bilognormal particle size distribution (Figure 157). The sample is pumped around during the measurement to prevent segregation of coarse particles. The DT-1202 system is

used for quality control in milling processes, crystallization processes, polymerization processes, precipitation processes, and emulsification processes.

In order to calculate the particle size distribution based on the measured attenuation spectra, the advanced coupled phase acoustic model of Dukhin and Goetz [415] with a sound scattering modification based on the Morse theory [417] is used. This theory is suitable because only the viscous, inertial, and scattering attenuation mechanisms are important for cement pastes. In order to simplify the conversion, the particle size distribution is assumed to be lognormal or bilognormal.

Figure 156: The DT-1202 ultrasound spectroscopy system of Quantachrome

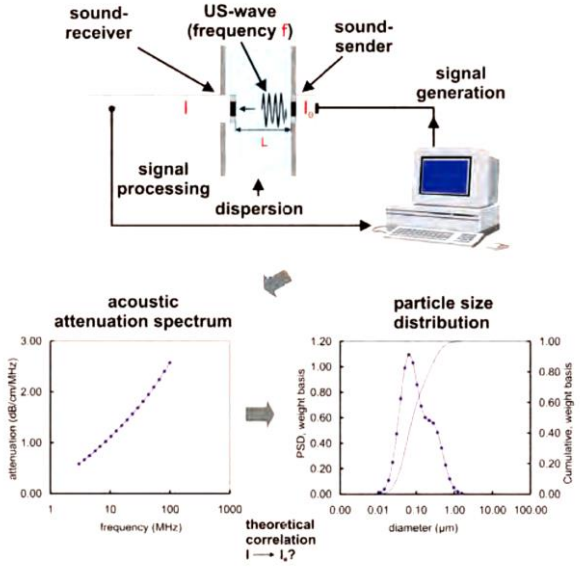

Figure 157: The measuring principle of the DT-1202

5.2.2. Sympatec OPUS system

The OPUS system of Sympatec (Figure 158) measures the ultrasound attenuation over 31 frequencies in a range of 100 kHz to 200 MHz on one single gap. The gap should be selected based on the sample (2 to 10 mm): a too large gap results in too much attenuation, a gap which is too small results in too little attenuation. In the tests described below, the gap was chosen 2 mm. Sympatec recommends the OPUS system, to monitor the particle size distribution during milling, crystallization, or other industrial processes using concentrated opaque suspensions.

The conversion of the measured attenuation spectra to the calculated particle size distribution is based on a calibration using a powder with known particle size distribution and physical properties, assuming this powder has a similar particle shape as the tested materials. The inversion problem is solved with linear algebra, generating a particle size distribution with 31 size classes. Most probably small changes in the measured attenuation will be amplified during this linear inversion. Although the apparatus cannot accurately measure attenuation losses above 150 dB, these measurements are not excluded when calculating the particle size distribution.

Figure 158: The OPUS ultrasound spectroscopy system of Sympatec

5.3. Literature review

Ultrasound attenuation has been used to determine the particle size distribution (PSD), disperse phase, volume fraction, phase transitions, particle interactions, and sedimentation in colloids, dispersions, and emulsions [27-29, 413, 414, 416, 418-420]. Ultrasound waves can penetrate into highly concentrated or optically opaque slurries and emulsions at full concentration, avoiding changes in the dispersion state when a dilution is needed.

5.3.1. Modelling attenuation losses

Several models exist to calculate the attenuation spectrum for a sample [28, 29, 418, 419] (Figure 159 [28]). For cement pastes, such a model should meet two requirements: (1) valid for a broad range of particle sizes, and (2) valid for concentrated particle suspensions with a high density contrast between the suspended particles and the medium [419]. Figure 159 provides an overview of the most cited attenuation losses theories [28]. Almost all theories describe the attenuation losses of spherical particles, which differs from the attenuation from irregular particles such as cement particles. In order to get around this problem, sometimes a calibration using particles with a known particle size distribution is used [27, 421]. However, because the particle shape used during calibration also differs from cement particles, such an approach might as well result in errors in the calculated particle size distributions.

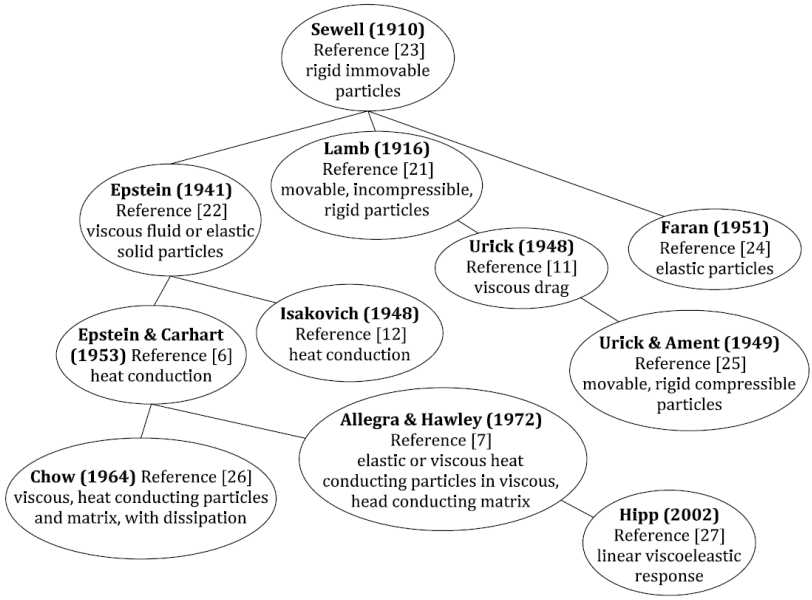

Figure 159: An overview of the theoretical models for attenuation losses [28]

The determination of the particle size distribution out of the measured attenuation spectra is a complicated ill-posed inverse problem [28]. For diluted suspensions (solid volume below 5% [27]), the attenuation spectrum is a superposition of individual uncorrelated attenuation spectra of all particles, and therefore results in a linear problem allowing linear algebra to calculate the particle size distribution [27]. However, for denser suspensions, a direct algebraic inversions does not always result in the correct solution. The inversion of an ill-posed problem is complicated by instability and non-uniqueness of the solution and the large influence of noise in the system [27, 28]. In order to solve this ill-posed problem, several approaches can be followed:

- Assume the suspended particles follow a certain particle size distribution model (for example a lognormal model). The parameters of the model can be determined using a nonlinear regression. Such an approach is used in the Quantachrome DT-1202 system.
- Add additional restraints to the shape of the particle size distribution in order to counteract the extreme magnification of signal noise. Such an approach is referred to as a regularization of the particle size distribution.

5.3.2. Applications on cementitious materials

Hackley et al. [412] used ultrasound attenuation to study changes in a cement suspension induced by hydration using a phenomenological approach. Changes in the attenuation spectra induced by the formation of CSH products during the first 7 hours of hydration were measured in samples with a solid fraction of 2% up to 20% using an Quantrachrome DT-1200 acoustic spectrometer. The attenuation spectrum below 30 MHz increases proportional with the volume fraction up to a volume fraction of 20% (Figure 160). The high frequency portion of the acoustic spectrum is more sensitive to the coarser components of the clinker (Figures 161 and 162). This section is also different when a chemical admixture was included in the mix composition of the paste (Figure 163). The p-wave acoustic velocity was not changing during early hydration.

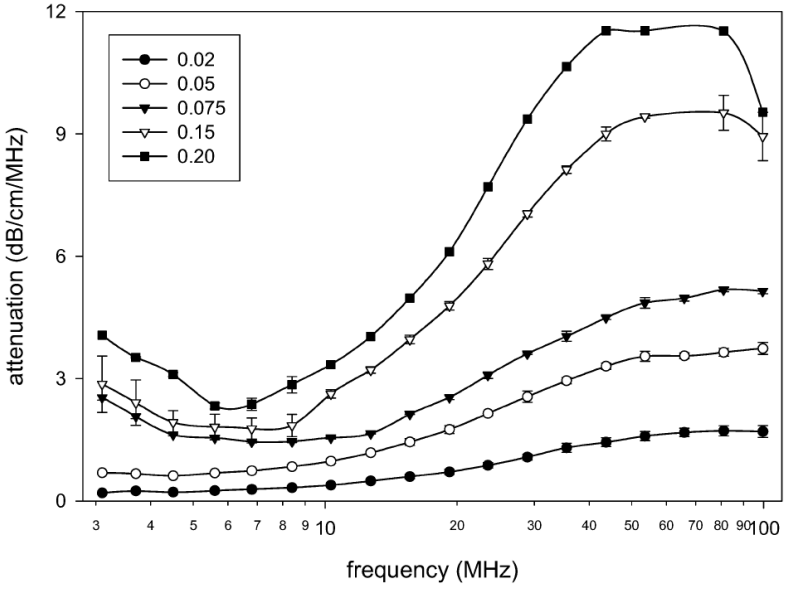

Figure 160: The attenuation spectrum as a function of the concentration in a suspension of cement particles [412]

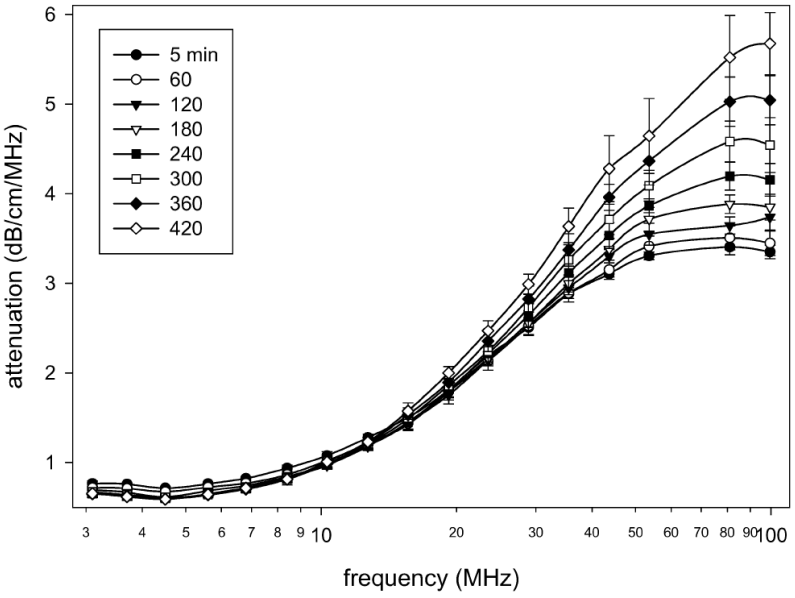

Figure 161: Evolution of the attenuation spectrum in time for a suspension of cement particles with a solid volume fraction of 5% [412]

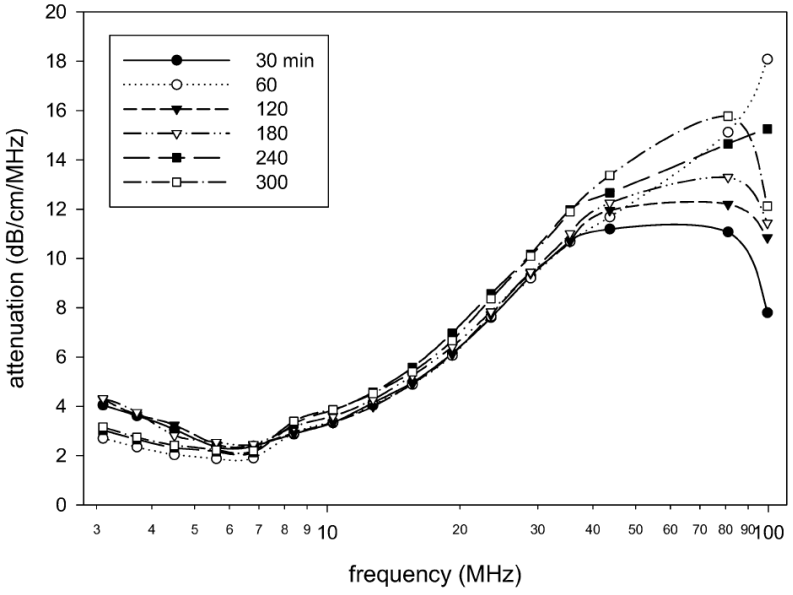

Figure 162: Evolution of the attenuation spectrum in time for a suspension of cement particles with a solid volume fraction of 20% [412]

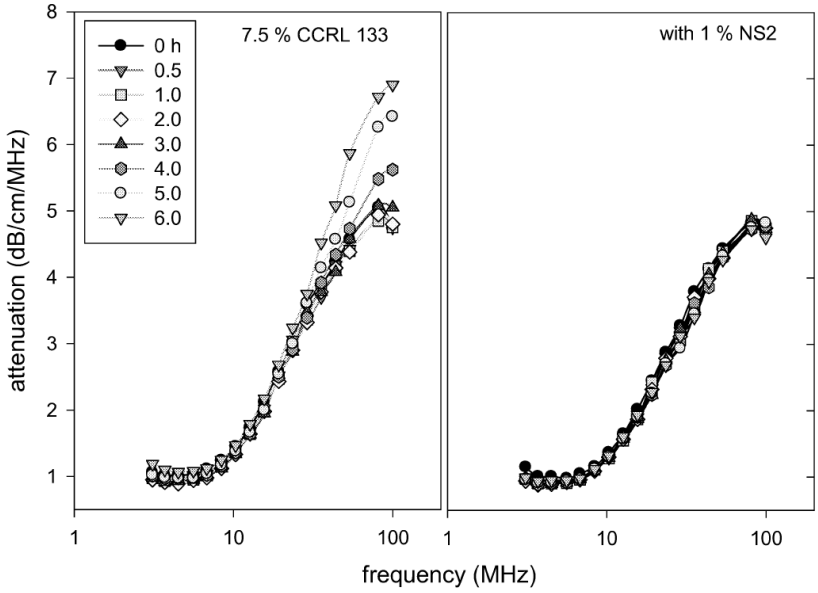

Figure 163: Impact of a superplasticizer on the attenuation spectrum of a suspension of cement particles [412]

5.4. Experimental results

5.4.1. Quantachrome DT-1202

The Quantachrome DT-1202 system is used for an explorative study on cement paste tests, which were performed on pastes with different solid fractions to study the impact of superplasticizers. The paste samples were moving during the tests in the Quantachrome DT-1202 apparatus.

As shown in Figure 164, the volume fraction has a major impact on the attenuation spectrum at low volume fractions, but hardly affects the attenuation spectrum at high volume fractions. The assumption of a lognormal or bilognormal particle size distribution leads to the calculation of unrealistic particle size distributions (Figure 165).

Experiments in which a volume fraction of 10% cement in water and in isopropanol was used resulted in a lognormal approximation of the particle size distribution as determined with a laser diffractometer in isopropanol (Figures 166 and 167). Using suspensions with a solid fraction of 10%, no influence of the superplasticizer on the measured particle size distribution was observed (Figures 168 and 169).

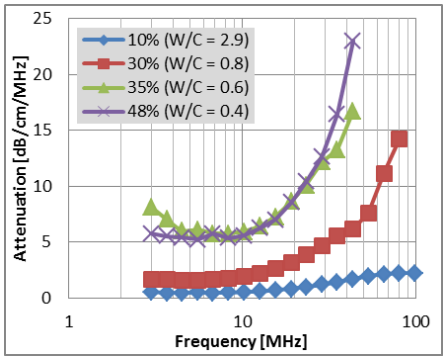

Figure 164: Influence of the solid fraction on ultrasonic spectrum

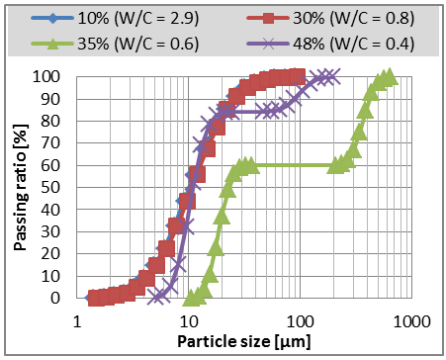

Figure 165: Influence of the solid fraction on the calculated particle size distribution

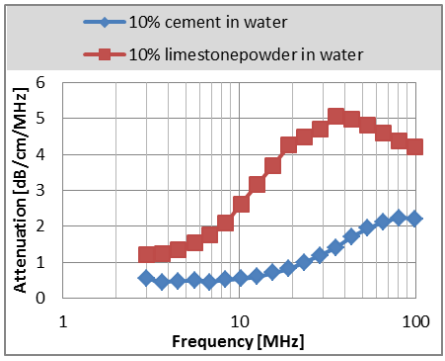

Figure 166: Attenuation spectra of limestone powder compared to cement (volume fraction of 10%)

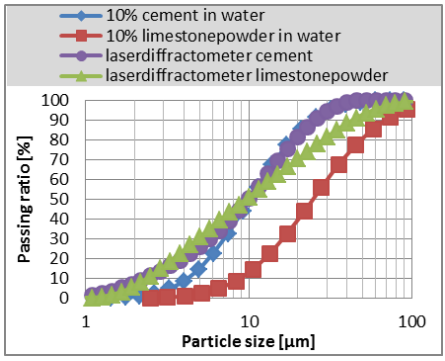

Figure 167: The calculated particle size distribution of cement and limestone powder compared to a laser diffractometer

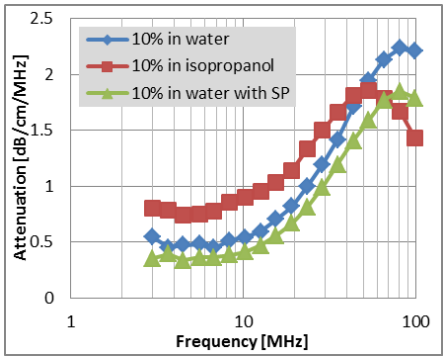

Figure 168: Influence of superplasticizer on the attenuation spectra

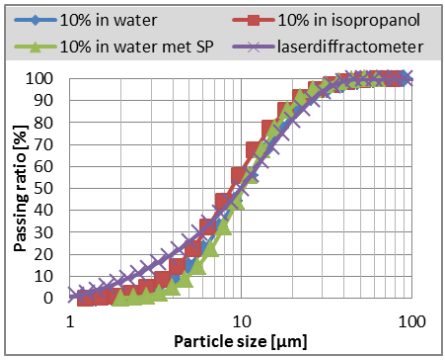

Figure 169: Influence of superplasticizer on the calculated particle size distribution

5.4.2. Sympatec OPUS system

Figure 170 shows the attenuation spectrum of a suspension of cement and limestone filler (volume fraction of 35%) in the OPUS system of Sympatec. Only the results below 150 dB are shown, as the accuracy of the measurement is limited above 150 dB. The chart can be devided into a declining trend up to 5000 kHz, resulting from viscous attenuation, and an inclining trend starting at 5000 kHz, resulting from scattering attenuation. The calculated particle size distribution based on this attenuation spectrum is shown in Figure 171.

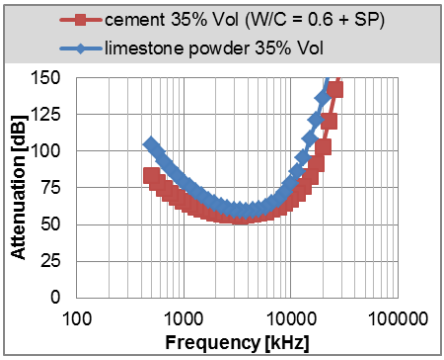

Figure 170: Attenuation spectra of cement and limestone filler suspension (vol fraction 35%)

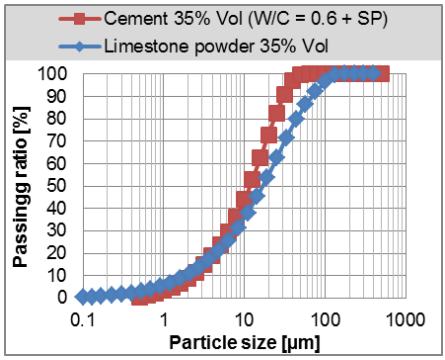

Figure 171: Calculated PSD of cement and limestone filler suspension (vol fraction 35%)

Because of the limited influence of small changes in the particle size distribution and solid volume fraction, no evolution of the attenuation spectra in time was observed (Figures 172 to 181). Only when severe segregation was happening, an impact was registered: the cement paste with a water-to-cement weight ratio of 0.6 and containing superplasticizer suffered from severe segregation at rest which resulted in a decrease of the attenuation for the larger frequencies (Figure 182).

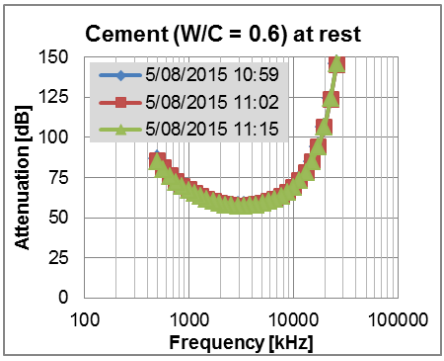

Figure 172: Evolution of the attenuation spectra - Cement paste (W/C = 0.6) at rest

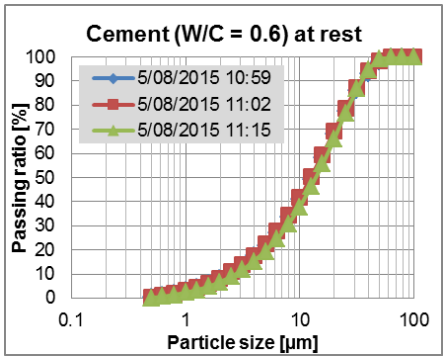

Figure 173: Calculated PSD Cement paste (W/C = 0.6) at rest

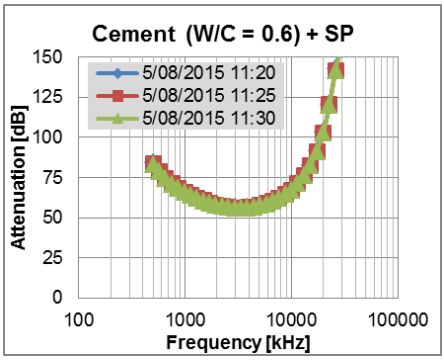

Figure 174: Evolution of the attenuation spectra - Cement paste (W/C = 0.6, with SP) agitated

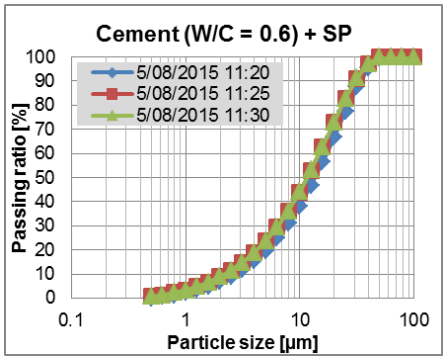

Figure 175: Calculated PSD - Cement paste (W/C = 0.6, with SP) agitated

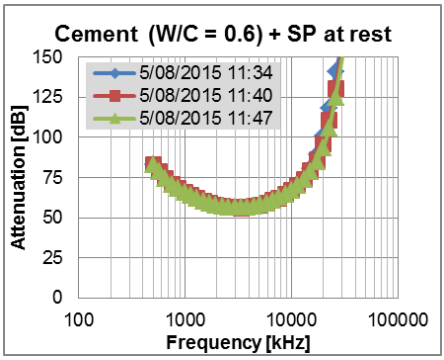

Figure 176: Evolution of the attenuation spectra - Cement paste (W/C = 0.6, with SP) at rest

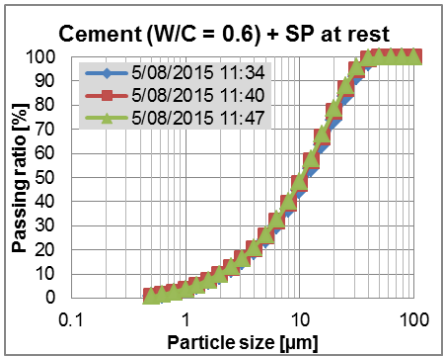

Figure 177: Calculated PSD - Cement paste (W/C = 0.6, with SP) at rest

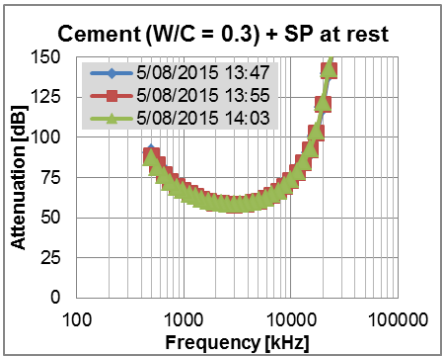

Figure 178: Evolution of the attenuation spectra - Cement paste (W/C = 0.3, with SP) at rest

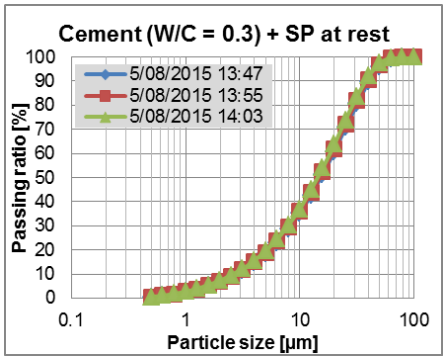

Figure 179: Calculated PSD - Cement paste (W/C = 0.3, with SP) at rest

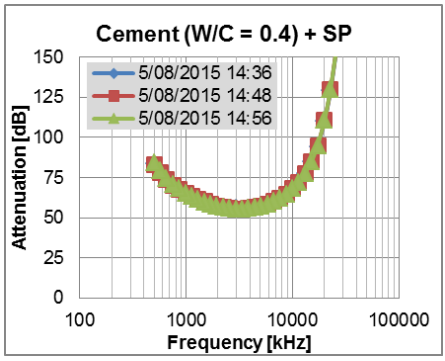

Figure 180: Evolution of the attenuation spectra - Cement paste (W/C = 0.4, with SP) at rest

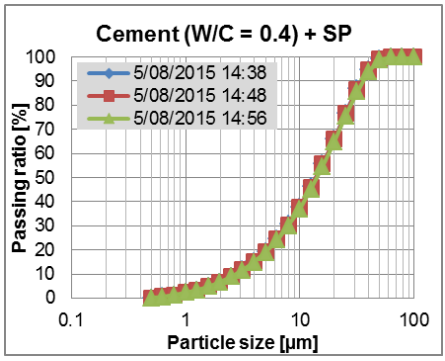

Figure 181: Calculated PSD - Cement paste (W/C = 0.4, with SP) at rest

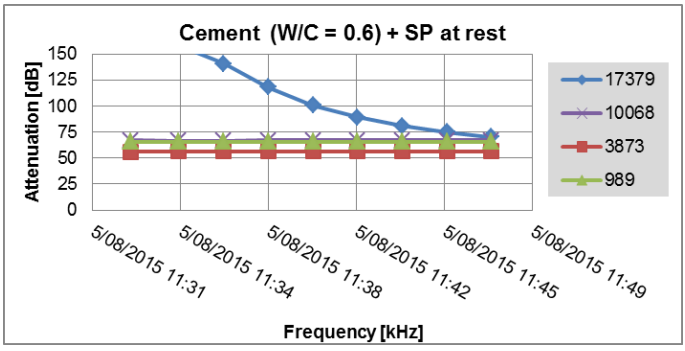

Figure 182: Changes in the attenuation spectra induced by severe segregation of the largest particles.

An increase of the volume fraction (water-to-powder weight ratio from 0.6 to 0.3) results in a small increase of the measured attenuation (Figure 183). This small difference in the attenuation spectra is not reflected in the calculated particle size distributions shown in Figure 184.

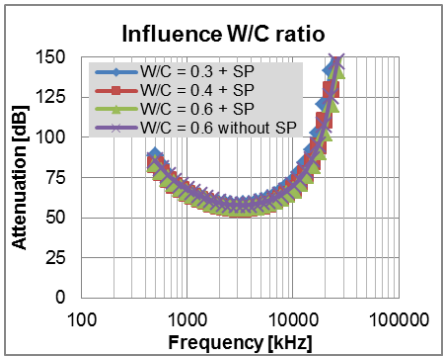

Figure 183: Influence of the solid volume fraction on the attenuation specra

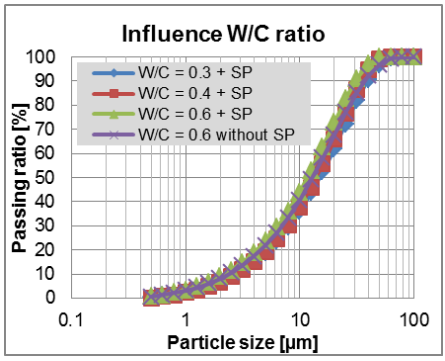

Figure 184: Influence of the solid volume fraction on the calculated PSD

Although the relation between the attenuation spectra and the particle size distribution of the cement paste is not completely founded on a theoretical basis, the OPUS system could deliver realistic particle size distributions compared to the particle size distribution as determined on a laser diffractometer (Figures 185 to 190). In the laser diffractometer, a sample of the paste was diluted in isopropanol. As the particle clustering changes when cement paste is diluted in isopropanol, the particle size distributions as determined on a laser diffractometer cannot be used to study the particle clustering in fresh SCC. In this section the laser diffractometer results are only used to evaluate whether the obtained particle size distribution from the OPUS system provides realistic values.

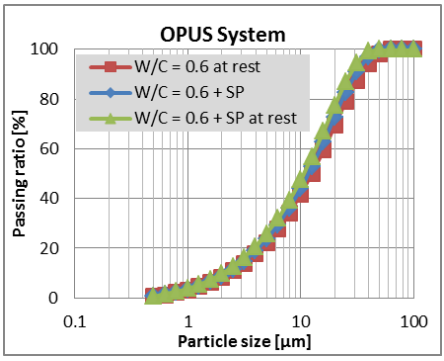

Figure 185: OPUS system: Influence superplasticizer

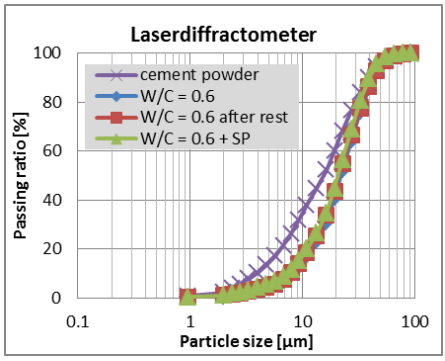

Figure 186: Laser diffractometer: Influence superplasticizer

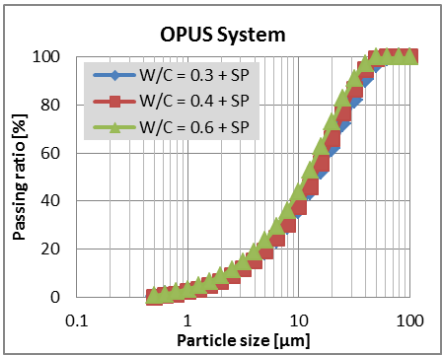

Figure 187: OPUS system: Influence volume fraction

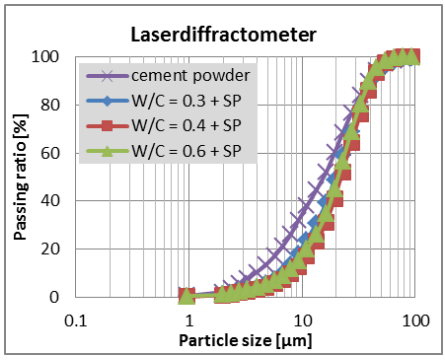

Figure 188: Laser diffractometer: Influence volume fraction

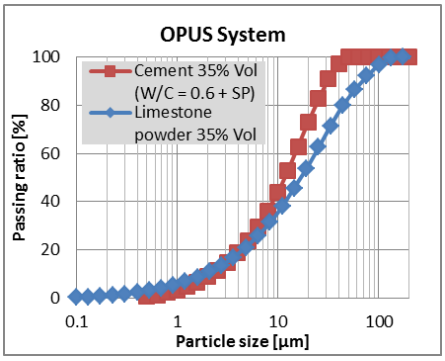

Figure 189: OPUS system: Cement and limestone powder

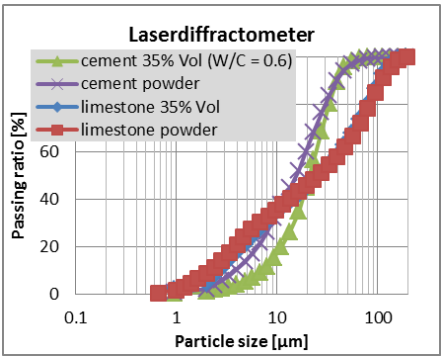

Figure 190: Laser diffractometer: Cement and limestone powder

6. Small Angle Light Scattering (SALS)

6.1. Experimental setup

Small Angle Light Scattering (SALS) images are the scattering pattern from radiation of a polarized laser beam through a sample collected in a narrow range of angles. Figures 191 and 192 illustrate the SALS extension equipped on an Anton Paar parallel plate rheometer used during this explorative research. An infrared laser beam with a wavelength of 658 nm is irradiated on a sheared sample in a parallel plate rheometer with glass plates having a diameter of 43 mm. The forward scattered light with scattering angles between 1° and 25° is recorded by a CCD camera below the lower glass plate while a beam stop protects the camera from the direct laser beam. Both the scattering pattern I_{VV} polarized in the same direction as the incident light, and the scattering pattern I_{VH} polarized perpendicular to the incident light can be measured.

Figure 191: The SALS equipment

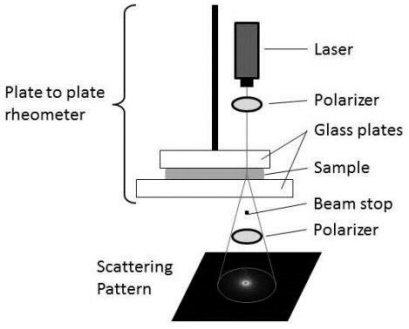

Figure 192: Schematic representation of the experimental setup

Because multiple scattering lowers the apparent anisotropy [422], this technique can only be used for a dilute concentration of particles. The SALS technique is used to study flow induced particle orientation in suspensions and the aggregation processes in solutions [26, 423-426]. This technique is also used in polymer science and to study cell structures. Considering the successful implementation of the SALS technique in the study of aggregation processes of protein solutions and polymers, the question raises whether this technique has a potential to investigate the clustering of cement particles under shear.

6.2. Literature review

6.2.1. Scattering patterns

6.2.1.1. Isotropic spherical particles

For isotropic spherical particles, the scattering pattern I_{VV} is a succession of dark and bright rings with nearly no azimuthal dependence and the scattering pattern I_{VH} has a fourfold symmetry and resembles a four-leaf clover [427]. These patterns have been experimentally observed for well-characterized monodisperse latex spheres (Figures 193 and 194 [428]). Particles with another shape or clusters of spherical particles will produce different scattering patterns [422, 427, 429, 430].

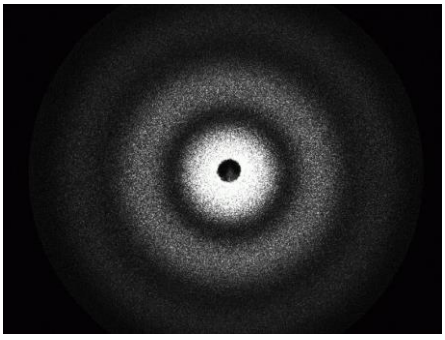

Figure 193: I_{VV} SALS images of a suspension of 5 µm Lattex spheres [427]

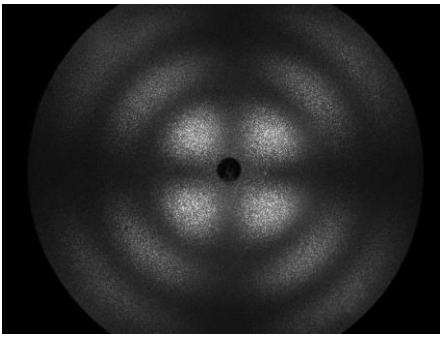

Figure 194: The I_{VH} SALS images of a suspension of 5 µm Lattex spheres [427]

6.2.1.2. Spherulitic scattering

Spherulites are used in polymer physics to describe spherical semicrystalline regions inside non-branched linear polymers. The I_{VV} and I_{VH} scattering pattern corresponding with spherulites typically have four lobes as illustrated in Figures 195 and 196 [427]. SALS images can be used to determine the spherulite size. The distance in between the centre and the spot of maximum intensity in the lobes can be converted into the polar angle of maximum intensity θ_{max}, which in turn can be related to the radius R_0 of the spherulites using Equation 66 [427].

$$R_0 = \frac{1.025}{\pi} \cdot \frac{\lambda}{\sin\left(\frac{\theta max}{2}\right)} \quad \text{(Eq. 66)}$$

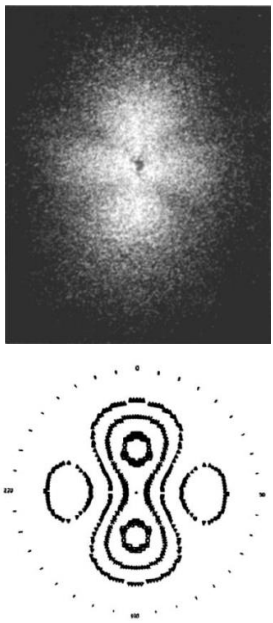

Figure 195: SALS I_{VV} pattern resulting from spherulitic scattering [427]

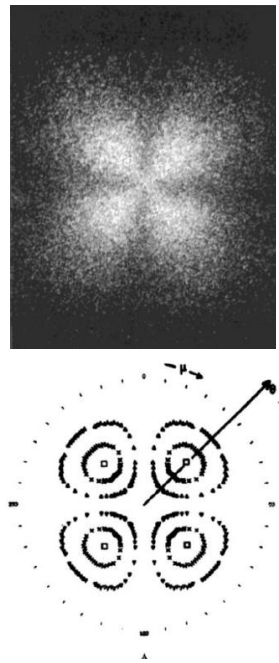

Figure 196: SALS I_{VH} pattern resulting from spherulitic scattering [427]

6.2.1.3. Scattering of oriented rods

In contrast to sphere and disk scattering theories, the scattering of assemblies of oriented rods results in I_{VH} SALS images with a maximum intensity in the center and an uniformly decreasing intensity further from this center [430]. Scattering of oriented rods is observed in polymers with folded chain lamella as a fundamental unit. Figures 197 to 199 are examples of SALS images of oriented rods.

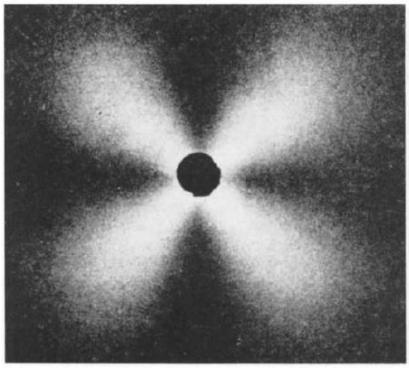

Figure 197: The SALS I_{VV} pattern of rods with random orientation [427]

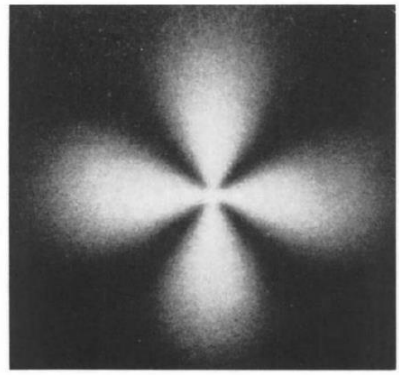

Figure 198: The SALS I_{VH} pattern of rods with random orientation [427]

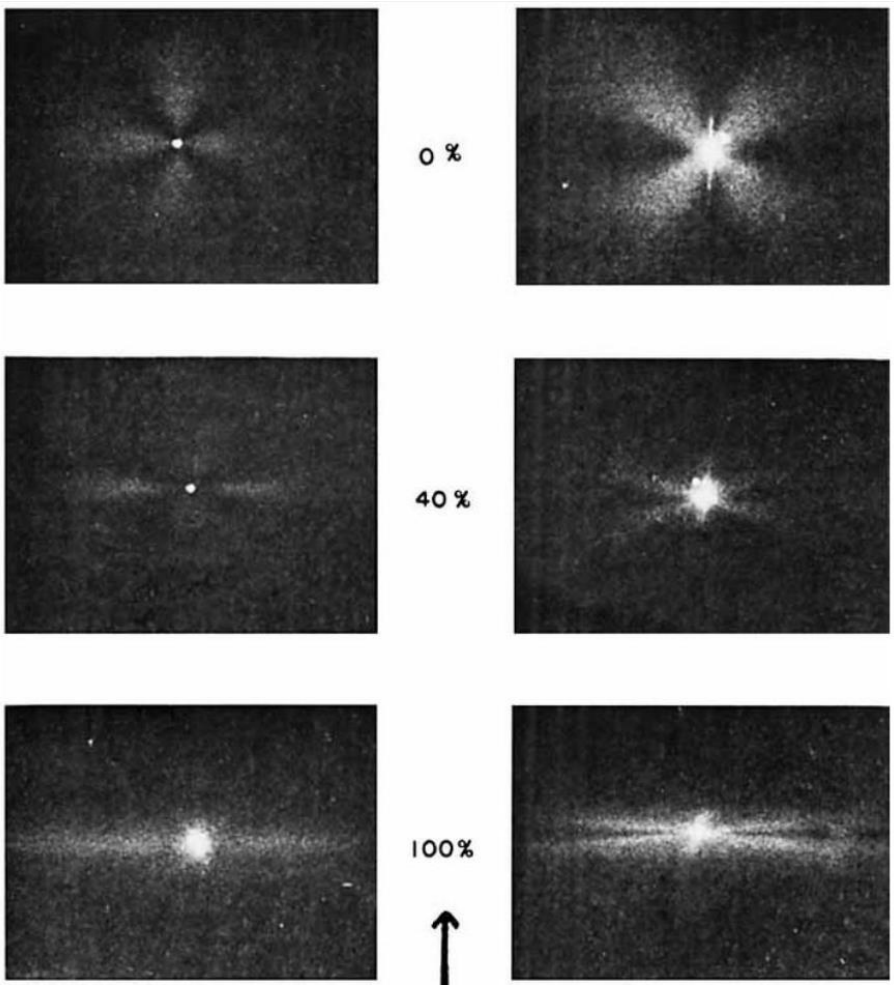

a) The I_{VH} pattern b) The I_{VV} pattern

Figure 199: SALS patterns of rods with increasing orientation [430]

6.2.1.4. Shear induced structures: polymer and latex suspensions

Anisotropy in the SALS images often indicates the existence of shear induced structures in the sample. The following sections describe three types of flow induced structures observed in polymer and latex suspensions [422].

6.2.1.4.1. Small distortion of the equilibrium structure at rest

In stable colloidal dispersions, emulsions, and polymer blends, small shear rates can cause only a small distortion of the equilibrium structure at rest and result in a deformed liquid like structure during small shear rates [422].

6.2.1.4.2. Particle orientation into shear flow direction

When particles in the suspension are migrating from the bulk to the walls of the sample under flow, elongated string-like structures of spheres can be created in the flow direction of latex particles or polystyrene particles near the walls [422, 431]. These strings of spherical particles result in a more elliptical scattering pattern as shown in Figure 200 [422]. The alignment increases as the gap becomes smaller and the shear rate increases.

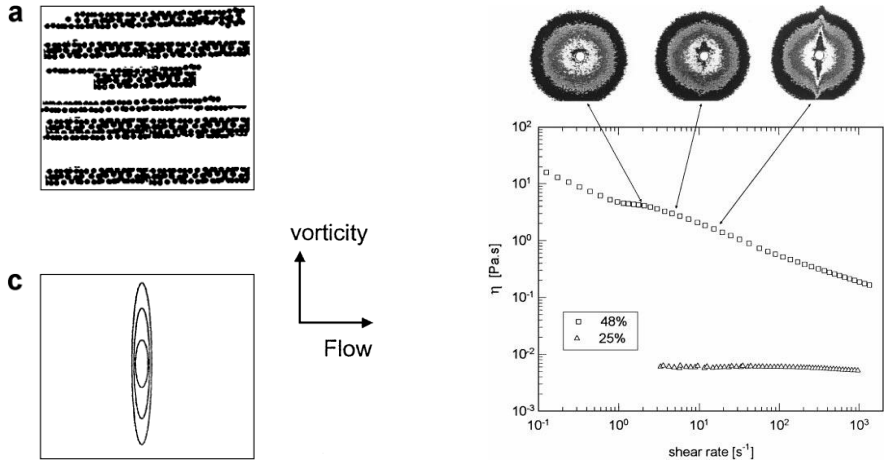

Figure 200: The influence of particle orientation into shear flow direction on the SALS images [422]

6.2.1.4.3. Fluctuations in particle concentration in the shear flow direction

When the shear rate in a dense suspension exceeds a certain critical shear, an anisotropic structure with orientation into flow direction is created, resulting in fluctuations in the particle concentration in shear flow direction. Figure 201 illustrates the origin of these fluctuations [432]. This shear induced structure results in a shear thinning behavior and butterfly SALS diffraction patterns for latex particles as shown in Figure 202 [422]. The volume fraction of the sample should be sufficiently high in order to observe this phenomenon.

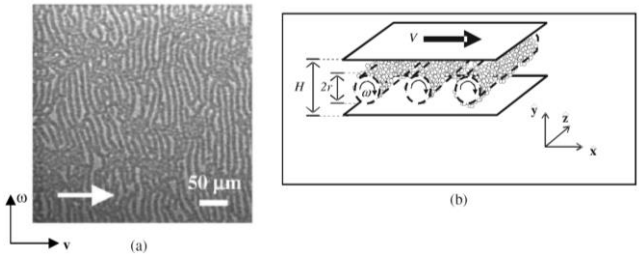

Figure 201: Mechanism causing fluctuations in particle concentration in the shear flow direction [432]

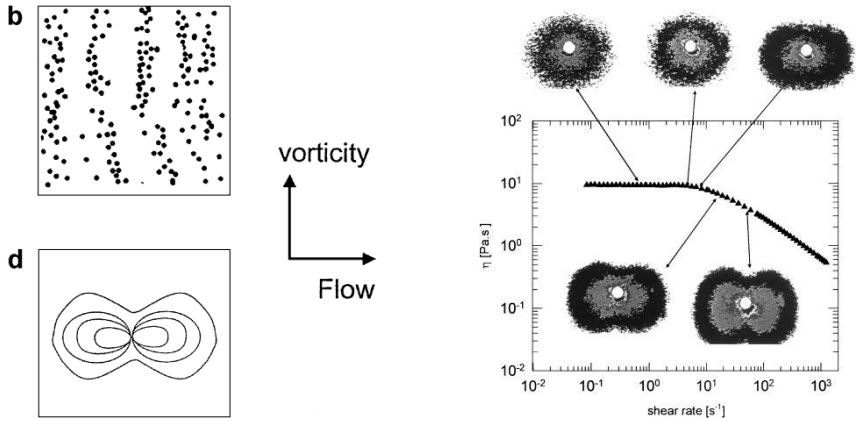

Figure 202: The influence of fluctuations in particle concentration in shear flow direction on the SALS images [422]

6.2.2. Modelling of unpolarized light scattering

Dependent on the dimensionless size parameter α (Equation 67, in which α is the dimensionless size parameter; D is the particle diameter; and λ is the wavelength of the incident radiation), light scattering is described by three different theories. Rayleigh scattering is applied when $\alpha \ll 1$, Mie scattering when $\alpha \approx 1$, and geometric scattering should be applied when $\alpha \gg 1$.

$$\alpha = \frac{\pi \cdot D}{\lambda} \qquad \text{(Eq. 67)}$$

6.2.2.1. Rayleigh scattering ($\alpha < 0.1$)

When the size of the particles is much smaller than the wavelength of the incident light, the theory of Rayleigh scattering [433] can be applied (Equation 68). An example of Rayleigh scattering is the scattering of sunlight by gas molecules in the atmosphere, causing a blue color of the Earth's sky coming from all directions on a clear day. The shorter violet and blue wavelengths are scattered more strongly than the longer yellow and red wavelengths. The spectrum of the Sun contains little violet and the Earth's atmosphere absorbs wavelengths in the ultra-violet region. Therefore, the sky is blue and the Sun is colored with a combination of the not scattered wavelengths: red and yellow. Observed from space, the sky is black and the sun is white.

$$I_{scat} = I_0 \cdot \frac{1+cos^2\theta}{2\,R^2} \cdot \left(\frac{2\pi}{\lambda}\right)^4 \cdot \left(\frac{n^2-1}{n^2+2}\right)^2 \cdot \left(\frac{d}{2}\right)^6 \qquad \text{(Eq. 68)}$$

6.2.2.2. Mie scattering ($0.1 < \alpha < 100$)

The scattering by particles with about the same size as the incident light is described in the theory of Mie scattering [434]. Mie scattering is applied in meteorological optics, medical applications, the paint industry, particle sizing, etc. . For example, due to the Mie scattering of sunlight by water droplets with a similar size of the wavelength, all wavelengths of visible light are scattered comparable, resulting in a white color of the clouds.

The following symbols and formulas can be used to calculate the scattering pattern of a spherical particle according to the Mie theory [435, 436]. Although the Mie scattering is very dependent on the shape of the particles, most theories assume spherical particles. An overview of light scattering theories considering non-spherical particles is given by Smith [437].

Relative scattering wavelength $$\lambda = \frac{\lambda_0}{m_0} \quad \text{(Eq. 69)}$$

Dimensionless size parameter $$\alpha = \frac{\pi \cdot D}{\lambda} \quad \text{(Eq. 70)}$$

Intensity of scattered unpolarized light with wavelength λ

$$I_{scat} = \frac{I_0 \cdot \lambda^2}{2 \cdot \pi^2 \cdot D^2} \cdot (\|I_{VV}\|^2 + \|I_{HH}\|^2) \quad \text{(Eq. 71)}$$

Intensity functions $$I_{VV} = \sum_{n=1}^{\infty} \frac{2n+1}{n(n+1)} \cdot (a_n \cdot \pi_n + b_n \cdot \tau_n) \quad \text{(Eq. 72)}$$

$$I_{HH} = \sum_{n=1}^{\infty} \frac{2n+1}{n(n+1)} \cdot (a_n \cdot \tau_n + b_n \cdot \pi_n) \quad \text{(Eq. 73)}$$

Angular dependent functions $$\pi_n = \frac{P_n^{(1)}(\cos\theta)}{\sin\theta} \quad \text{(Eq. 74)}$$

$$\tau_n = \frac{dP_n^{(1)}(\cos\theta)}{d\theta} \quad \text{(Eq. 75)}$$

Mie coefficients $$a_n = \frac{\Psi_n(\alpha) \cdot \Psi'_n(m \cdot \alpha) - m \cdot \Psi_n(m \cdot \alpha) \cdot \Psi'_n(\alpha)}{\xi_n(\alpha) \cdot \Psi'_n(m \cdot \alpha) - m \cdot \Psi_n(m \cdot \alpha) \cdot \xi'_n(\alpha)} \quad \text{(Eq. 76)}$$

$$b_n = \frac{m \cdot \Psi_n(\alpha) \cdot \Psi'_n(m \cdot \alpha) - \Psi_n(m \cdot \alpha) \cdot \Psi'_n(\alpha)}{m \cdot \xi_n(\alpha) \cdot \Psi'_n(m \cdot \alpha) - \Psi_n(m \cdot \alpha) \cdot \xi'_n(\alpha)} \quad \text{(Eq. 77)}$$

Ricatti-Bessel functions $$\Psi_n(z) = \left(\frac{\pi \cdot z}{2}\right)^{1/2} \cdot J_{n+1/2}(z) \quad \text{(Eq. 78)}$$

$$\xi_n(z) = \left(\frac{\pi \cdot z}{2}\right)^{1/2} \cdot H_{n+1/2}(z) \quad \text{(Eq. 79)}$$

Symbol	Name	Unit
α	Dimensionless size parameter	[-]
a_n and b_n	Mie coefficients	[-]
D	Particle diameter	[m]
I_{VV} and I_{HH}	Intensity functions. The subscript VV refers to both the vertically polarized incident light and vertically polarized scattered light. The subscript HH refers to both horizontally polarized incident and scattered light.	[-]
I_0	Intensity incident light	[cd]
I_{scat}	Intensity scattered light	[cd]
$H_{n+1/2}$	Half integer order Hankel function of the second kind	[-]
$J_{n+1/2}$	Half integer order Bessel function of the first kind	[-]
λ	Relative scattering wavelength	[m]
λ_0	Incident wavelength with respect to vacuum	[m]
m	Complex refractive index of the scattering particle	[-]
m_0	Refractive index of the surrounding medium	[-]
θ	Scattering angle	[rad]
π_n and τ_n	Angular dependent functions	[-]
Ψ and ξ	Ricatti-Bessel functions	[-]
$P_n^{(1)}$	nth degree Legendre polynomial	[-]

Table 53: Symbols used in Mie equations (Eq. 69 to 79)

6.2.2.3. Fraunhofer scattering ($\alpha > 100$, $|m - 1| \gg 1$)

The Fraunhofer scattering theory is a simplification of the Mie theory, applicable for far field scattering in which the scattered and incident waves are quite separate and do not interfere with each other. Two conditions must be met: scattering happens around the particles ($|m - 1| \gg 1$) and the particles are significant larger than the wavelength ($\alpha > 100$) [438]. The calculation of the scattered light is independent of the refractive index of the particles and can be calculated using the Fraunhofer scattering theory (Equation 80) [438, 439]. For a laser beam with a wavelength of 500 nm, these restrictions mean the particles diameter needs to be larger than 15 µm.

$$I_{scat} = I_0 * \frac{\pi^2 * D^4}{16 * \lambda^2} * \left(\frac{2 * J_1\left(\frac{\pi\, D\, sin(\theta)}{\lambda}\right)}{\frac{\pi\, D\, sin(\theta)}{\lambda}} \right)^2 \qquad \text{(Eq. 80)}$$

Symbol	Name	Unit
D	Particle diameter	[m]
I_0	Intensity incident light	[cd]
I_{scat}	Intensity scattered light	[cd]
J_1	Bessel function of the first kind and first order	[-]
λ	Relative scattering wavelength	[m]
θ	Scattering angle	[rad]

Table 54: Symbols used in the Fraunhofer scattering equation (Eq. 80)

6.2.2.4. Multiple scattering

Multiple scattering by particles with an non-spherical shape can be computed with the T-matrix method, also referred to as the null field method and the extended boundary technique method (EBCM) [429]. However, because of difficulties with implementing in Matlab, this method was not further investigated.

6.2.2.5. Geometric scattering

The behaviour of light in combination with large macroscopicobjects can be described using geometric optics.

6.2.3. Mie scattering of polarized light

Using polarized light, two scattering patterns can be measured: the scattering pattern I_{VV} polarized in the same direction as the incident light, and the scattering pattern I_{VH} polarized perpendicular to the incident light. Both scattering patterns I_{VV} and I_{VH} are functions of the polar and azimuthal angle and any scatterer can be described by the scattering matrix B, using Equations 81 to 83 [427] (symbols summarized in Table 55).

$$B = \begin{bmatrix} S_2 & S_3 \\ S_4 & S_1 \end{bmatrix} \quad \text{(Eq. 81)}$$

$$I_{VV} = I_0 * \left(\frac{\lambda}{2\pi}\right)^2 \cdot \frac{1}{{r_0}^2} \cdot |S_1 \cdot sin^2\mu + S_2 \cdot cos^2\mu + (S_3 - S_4) \cdot \sin\mu \cdot \cos\mu|^2 \quad \text{(Eq. 82)}$$

$$I_{VH} = I_0 * \left(\frac{\lambda}{2\pi}\right)^2 \cdot \frac{1}{{r_0}^2} \cdot |S_3 \cdot sin^2\mu - S_4 \cdot cos^2\mu + (S_2 - S_1) \cdot \sin\mu \cdot \cos\mu|^2 \quad \text{(Eq. 83)}$$

Symbol	Name	Unit
B	The scattering matrix of a scatterer	[-]
I_0	Intensity incident light	[cd]
I_{VV}	The intensity pattern of the scattered light polarized in the same direction as the incident light	[cd]
I_{VH}	The intensity pattern of the scattered light polarized in the opposite direction as the incident light	[cd]
λ	Relative scattering wavelength	[m]
μ	The azimuthal angle	[rad]
r_0	The distance from the scatterer	[m]
S_1, S_2, S_3, S_4	The components of the scattering matrix B	[-]
θ	The polar angle	[rad]

Table 55: Symbols used in the Mie scattering equations (Eq. 81 to 83)

For an isotropic sphere, $S_3 = S_4 = 0$, the Mie theory (Equations 84 and 85) can be used to calculate the other components of the scattering matrix, S_1 and S_2. The Mie coefficients a_n and b_n and angular dependent functions π_n and τ_n are given in Equations 75 to 78 [427].

$$S_1 = \sum_{n=1}^{\infty} \frac{2n+1}{n(n+1)} \cdot (a_n \cdot \pi_n + b_n \cdot \tau_n) \quad \text{(Eq. 84)}$$

$$S_2 = \sum_{n=1}^{\infty} \frac{2n+1}{n(n+1)} \cdot (b_n \cdot \pi_n + a_n \cdot \tau_n) \quad \text{(Eq. 85)}$$

The scattering pattern I_{VV} is a succession of dark and bright rings with nearly no azimuthal dependence, the scattering pattern I_{VH} has a fourfold symmetry and resembles a four-leaf clover [427]. Figures 203 and 204 illustrate the calculated scattering patterns for a suspension of polystyrene spheres with a diameter of 3 µm in water.

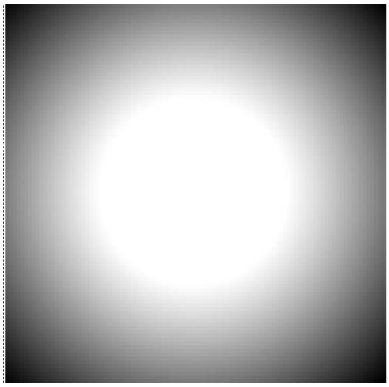

Figure 203: The calculated I_{VV} scattering pattern of polystyrene particles in water with a diameter of 3 µm

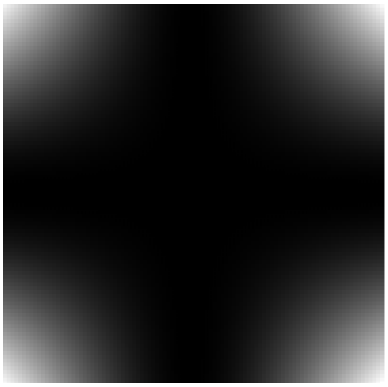

Figure 204: The calculated I_{VH} scattering pattern of polystyrene particles in water with a diameter of 3 µm

6.2.4. Calculating the particle size distribution

Assuming spherical particles, the Mie theory (Equation 86) can be used to calculate the scattering pattern of the individual particles. For a certain particle size distribution f(D), the superposition of all individual scattering patterns results into the global scattering pattern of the material.

$$I(\theta) = \int_0^{\infty} I(q, D) \cdot \frac{f(D)}{\frac{4}{3} \cdot \pi \cdot \frac{D^3}{8} \cdot \rho} \cdot dD \quad \text{(Eq. 86)}$$

The determination of the particle size distribution f(D) based on a measured scattering pattern I(θ) is a complicated inversion problem: a classical Fredholm

integral equation of the first kind with $\frac{I(q,R)}{\frac{4}{3}*\pi*\frac{D^3}{8}*\rho}$ as a Kernel function. The integration in Equation 86 has a smoothening effect on influence of the particle size distribution f(D) on the scattering pattern. Most high frequency components of f(D) are filtered out. As a result, the experimental scatter is magnified in the reverse process [440], creating an ill-posed problem. The inversion problem is very sensitive to small perturbations of the system, incomplete information, the non-continuous dependence of the solution to the data, and the non-uniqueness of the solution. As a result, traditional methods fail to obtain meaningful particle size distributions based on a measured scattering pattern.

Substituting the continuous particle size distribution f(D) by an approximate sum of N functions (Equation 87), the integration is replaced by a discrete sum (Equation 88). After discretizing the measured scattering pattern $I(\theta)$, the scattering problem can be rewritten into matrix form as shown in Equation 89[7]. The high conditioning number κ (Equation 90) of the Kernel matrix K warns the failing of classical numerical solution methods to obtain meaningful results. Many different solutions can approach the measured signal because of the low backward stability of the problem. The particle size distribution corresponding with the best approximation of the measured signal including noise most often differs substantially from the real particle size distribution. Many options exist to discretize the particle size distribution (rectangular, triangular, wavelet, lognormal, …). During this analysis in this report, the particle size distribution function is approximated by consecutive logarithmically spaced rectangular functions.

$$f(D) = \sum_{i=1}^{N} f_i(D) \qquad \text{(Eq. 87)}$$

$$I(\theta) = \sum_{i=1}^{N} \int_0^{\infty} I(q,D) \cdot \frac{f_i(D)}{\frac{4}{3}*\pi*\frac{D^3}{8}*\rho} \cdot dD \qquad \text{(Eq. 88)}$$

$$b = K \cdot F \qquad \text{(Eq. 89)}$$

$$\kappa = \|H\| \cdot \|H^{-1}\| \qquad \text{(Eq. 90)}$$

The Tikhonov regularization of ill-posed minimization problems such as $\|K \cdot F - b\|$ gives a preference to a particular solution with desirable properties by adding a regularization term to the original problem. This technique can be used to minimize the influence of noise (Equation 91) [440-443]. Most often, the Tikhonov matrix Γ is

[7] The intensity matrix is named b in order to avoid confusion with the identity matrix

the product of a constant and the identity matrix or a differential operator, giving a preference to smaller or smoother solutions ($\Gamma = \alpha \cdot \mathrm{L}$). The effect of the regularization can be varied by the parameter α. Different methods exist to solve this minimization problem and to determine the optimum regularization parameter α.

$$\|K \cdot F - b\| + \|\Gamma \cdot F\| \qquad \text{(Eq. 91)}$$

Because negative values are not excluded, a direct numerical solution cannot calculate the particle size distribution $\hat{F}$ (Equation 92). A better approach is a non-negative least squares iterative solution of Equation 86 using the Nelder–Mead simplex algorithm implemented in the Matlab function fminsearch [444]. Although this method requires a long computing time, a proper minimization of the problem is obtained. In order to exclude negative values, the square of the minimization problem is applied as the particle size distribution in the algorithm.

$$\hat{F} = \left(K^T \cdot K + \alpha^2 \cdot \mathrm{L}^T \cdot \mathrm{L}\right)^{-1} \cdot K^T \cdot b \qquad \text{(Eq. 92)}$$

Several methods exist to determine the optimum weight of the regularization α. In this experimental program, only the L-curve method has been used (Figure 205 [445]), in which $\frac{\|\Gamma \cdot F\|}{\alpha}$ is plotted as a function of $\|K \cdot F - b\|$ for various values of the regularization parameter α. The steep beginning of the L-curve corresponds with too small α values and a large influence of perturbation errors. Corresponding with the larger α values, the L-curve has a flat part and is dominated by regularization errors: useful data is filtered out with the noise. As shown in Figure 205, the optimum solution is a compromise between a good fit to the measured signal and a smoothing by the regularization can be found in the corner of the L-curve. Appendix C to F summarize the Matlab code used during this experimental program.

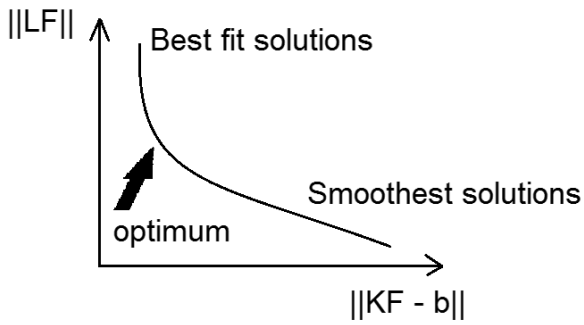

Figure 205: Determining the optimal regularization parameter α using the L-curve

6.3. Experimental results

6.3.1. Experiments on monodisperse polystyrene microspheres

Experiments on dilute concentrations of monodisperse polystyrene microspheres with a diameter of 1 µm and 75.7 µm have been performed. The scattering patterns, shown in Figures 206 to 209, were observed with a polarization in the same and opposite direction of the incident light. The I_{VV} images of the particles with a diameter of 75.7 µm have a succession of rings. The central core of the I_{VV} SALS pattern of a particle with size 1 µm has a larger diameter than the SALS pattern of a particle with diameter 75.7 µm. Figures 210 and 211 illustrate the corresponding calculated Fraunhofer scattering I_{VV} patterns. The measured I_{VH} images differ from the expected clover-leaf pattern. The I_{VH} SALS images are completely black, even for an image taken on a sample with the highest concentration of particles ($7 . 10^6$ particles / ml). The intensity of the scattered light in opposite polarization of the incident light is insufficient and therefore not detected.

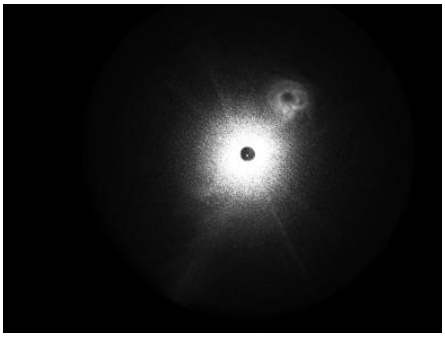

Figure 206: The measured I_{VV} SALS image of Polystyrene spheres with diameter 1 µm

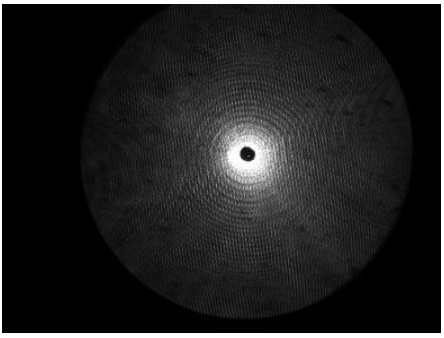

Figure 207: The measured I_{VV} SALS image of Polystyrene spheres with diameter 75.7 µm

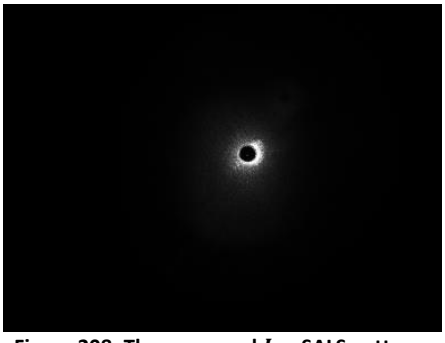

Figure 208: The measured I_{VH} SALS patterns of polystyrene spheres with diameter 1 µm

Figure 209: The measured I_{VH} SALS patterns of polystyrene spheres with diameter 75.7 µm

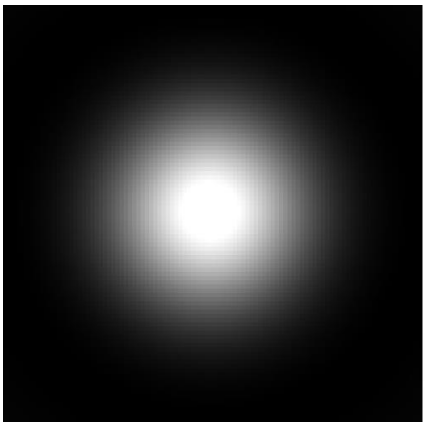

Figure 210: A calculated I_{VV} SALS image of Polystyrene spheres with diameter 1 µm

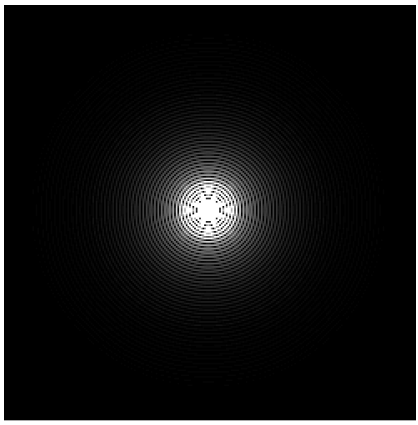

Figure 211: A calculated I_{VV} SALS image of Polystyrene spheres with diameter 75.7 µm

Using the Matlab code given in Appendix C to F, the SALS images have been converted into calculated particle size distributions. The calculated particle size distributions shown in Figures 212 and 213 differ significantly from the actual size of the monodisperse polystyrene microspheres. The origin of this failed calculation can be found in the impossibility to model the SALS images using the 30 hood functions. As shown in Figures 214 and 215 the alternating bright and dark rings are filtered out when during fitting. Below, only a qualitative analysis of the SALS images will be performed. As a calculation of the particle size distribution fails for spherical particles with known optical properties using this technique, no reliable estimate can be performed for cement particles having irregular shapes and only approximately known optical properties.

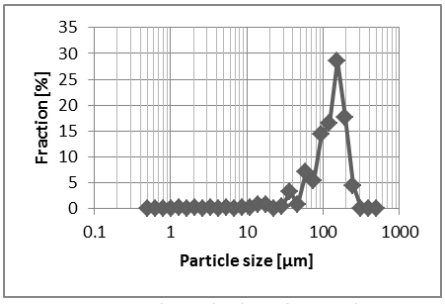

Figure 212: The calculated particle size distribution based on an SALS image of polystyrene spheres with diameter 1 µm

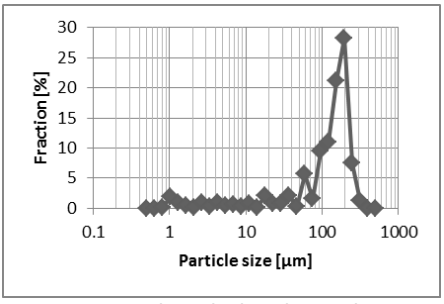

Figure 213: The calculated particle size distribution based on an SALS image of polystyrene spheres with diameter 75.7 µm

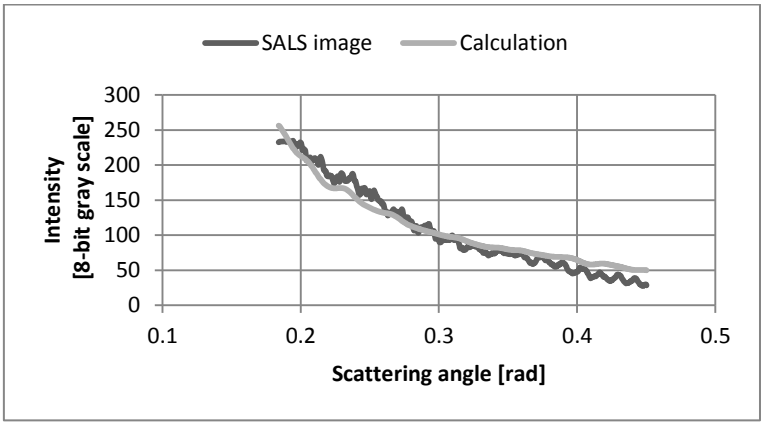

Figure 124: Comparison of the SALS image and its approximation based on 30 hood functions (polystyrene spheres with diameter 1 µm)

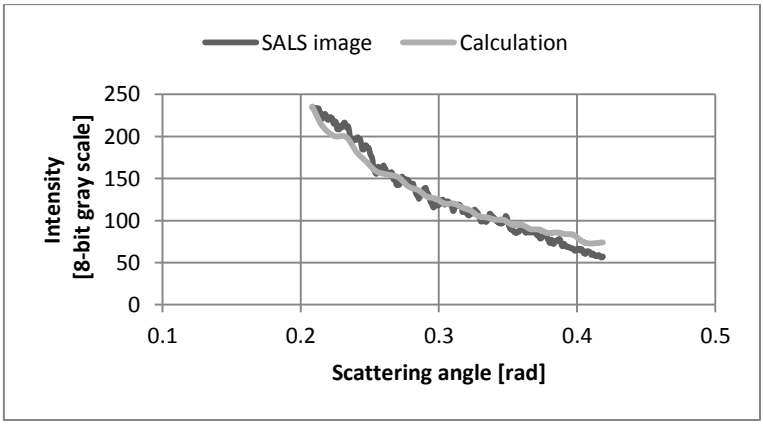

Figure 125: Comparison of the SALS image and its approximation based on 30 hood functions (polystyrene spheres with diameter 75.7 µm)

6.3.2. Experiments on corn starch

In this section, shear induced structures of corn starch are studied by measuring the SALS patterns under increasing shear rates (rotation speed of 0, 0.005, 0.05, 0.5, 5, and 50 rpm in steps of 10 sec). A solution of 0.2% corn starch in water by weight produces the I_{VV} and I_{VH} SALS patterns shown in Figures 216 and 217.

The I_{VV} SALS pattern is independent on the rotation speed: each time exactly the same intensity profile over the scattering angles is observed (Figure 218). The I_{VH} images have characteristics of spherulitic scattering [427]: four identical lobes around a centrum with zero intensity. The images become less bright when the rotation speed of the rheometer increases, but the radius of maximum intensity remains about the same, indicating no large changes in the spherulitic size.

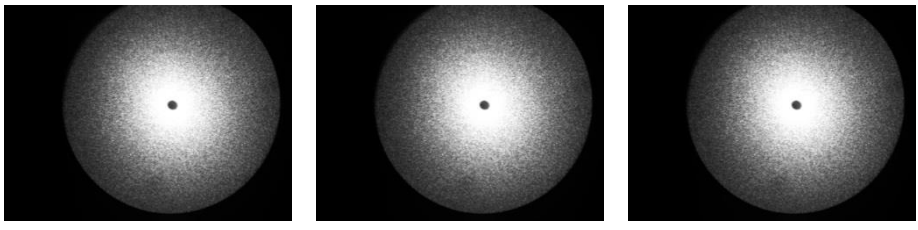

a) 0 rpm b) 0.005 rpm c) 0.05 rpm

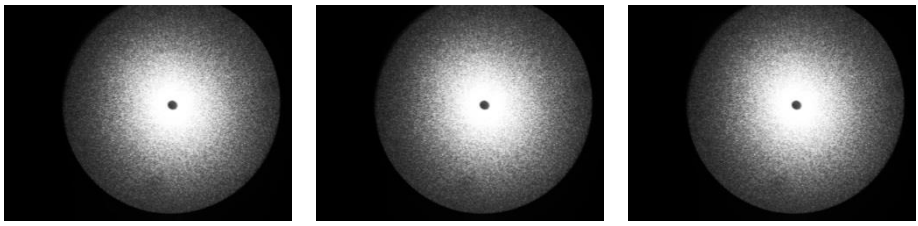

d) 0.5 rpm e) 5 rpm f) 50 rpm

Figure 216: The I_{VV} SALS patterns of corn starch in water at different shear rates

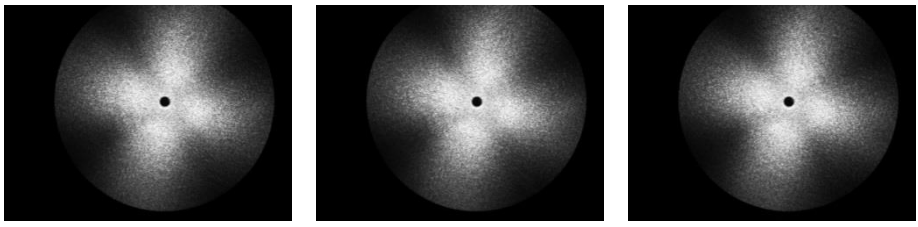

a) 0 rpm b) 0.005 rpm c) 0.05 rpm

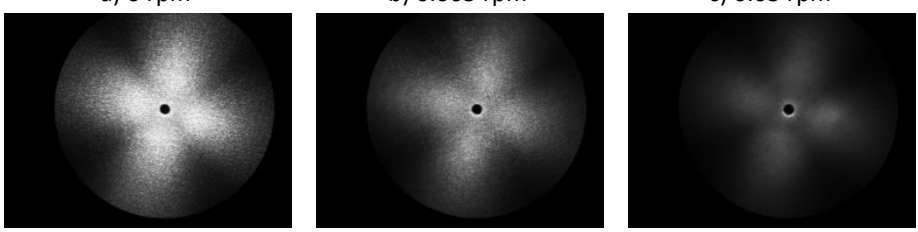

d) 0.5 rpm e) 5 rpm f) 50 rpm

Figure 217: The I_{VH} SALS patterns of corn starch in water at different shear rates

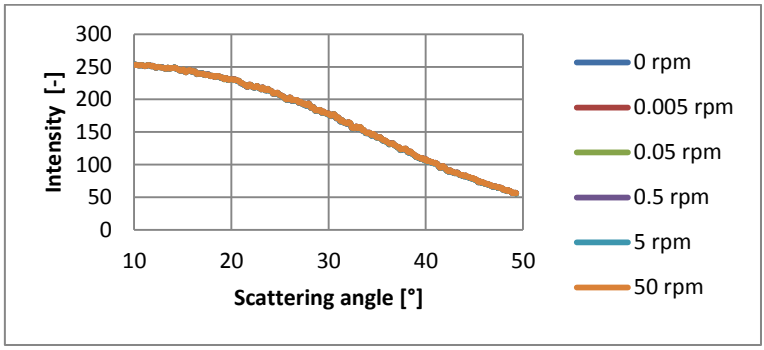

Figure 218: The I_{VV} intensity as a function of the scattering angle

6.3.3. Measurements on attapulgite clay, montmorillonite clay, and superplasticizer

Figures 219 to 226 illustrate the scattering patterns from attapulgite clay, montmorillonite clay, and two types of superplasticizer (BASF MasterGlenium 51, 35% and BASF MasterGlenium 27, 20%). Under different shear rates, no changes in the scattering patterns were observed.

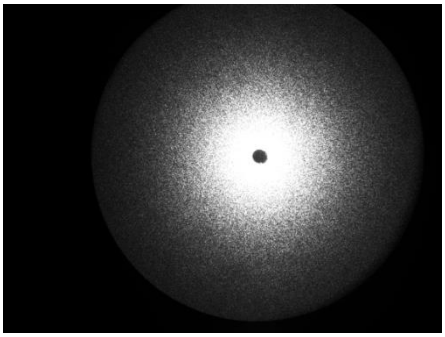

Figure 219: I_{VV} pattern of attapulgite clay

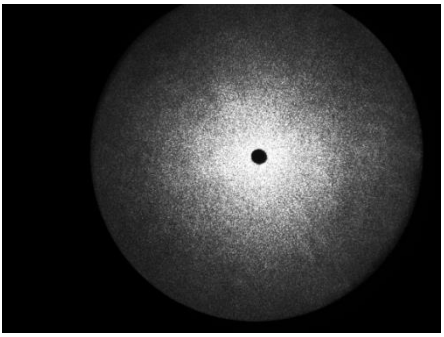

Figure 220: I_{VH} pattern of attapulgite clay

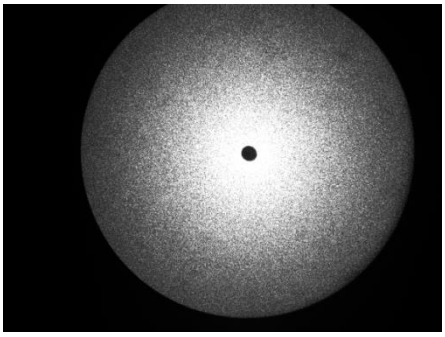

Figure 221: I_{VV} pattern of montmorillonite clay

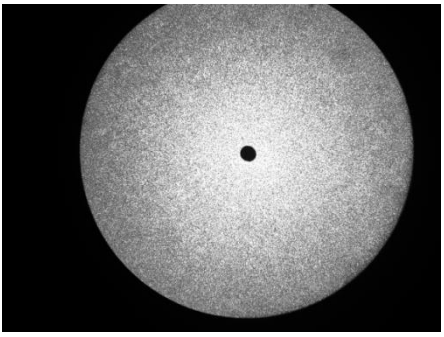

Figure 222: I_{VH} pattern of montmorillonite clay

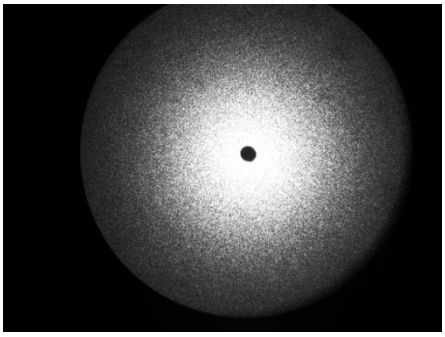

Figure 223: I_{VV} pattern of superplasticizer A

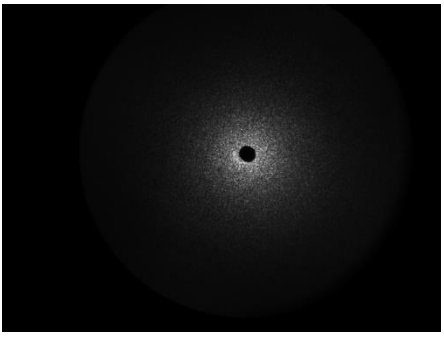

Figure 224: I_{VH} pattern of superplasticizer A

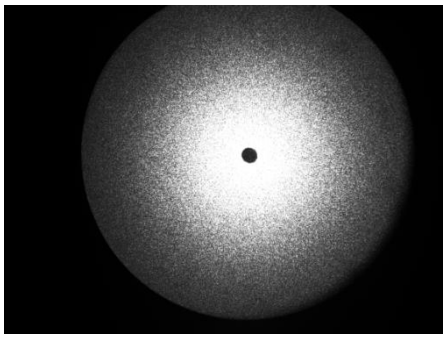

Figure 225: I_{VV} pattern of superplasticizer B

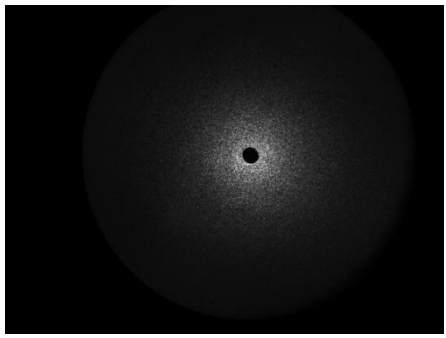

Figure 226: I_{VH} pattern of superplasticizer B

6.3.4. Measurements on cement

To verify the applicability of the technique for cementitious materials, experiments on cement have been performed (Figures 227 to 230). In a very dilute solution, a problem with the hydration speed of cement arises: the hydration speed increases as the concentration decreases and below a certain threshold concentration, completely different hydration kinetics apply [334].

The I_{VH} SALS images of a solution of 0.2% cement are given in Figure 227. The SALS images are similar except from the sharp line in one specific azimuthal angle, developing above a rotation speed of 0.5 rpm. When 0.1% superplasticizer (BASF MasterGlenium 51 35%) is included in a solution of cement, a more outspread intensity distribution, indicating a smaller scattering particle size. No influence of the shear rate is observed.

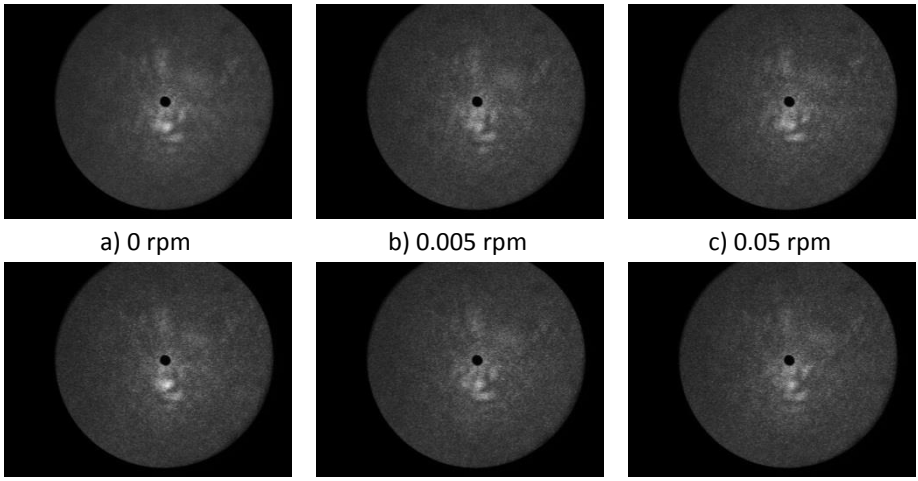

a) 0 rpm b) 0.005 rpm c) 0.05 rpm

d) 0.5 rpm e) 5 rpm f) 50 rpm

Figure 227: The I_{VH} SALS patterns of a 0.02% cement solution in water at different shear rates

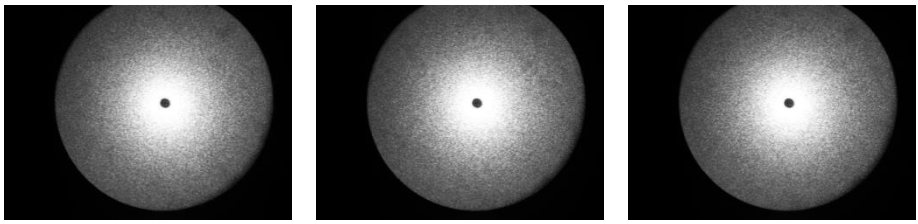

a) 0 rpm b) 0.005 rpm c) 0.05 rpm

d) 0.5 rpm e) 5 rpm f) 50 rpm

Figure 228: The I_{VV} SALS patterns of a 0.02% cement solution in water at different shear rates

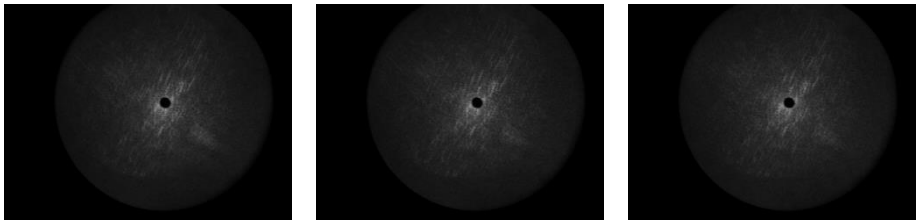

a) 0 rpm b) 0.005 rpm c) 0.05 rpm

d) 0.5 rpm e) 5 rpm f) 50 rpm

Figure 229: The I_{VH} SALS patterns of a cement and superplasticizer solution at different shear rates

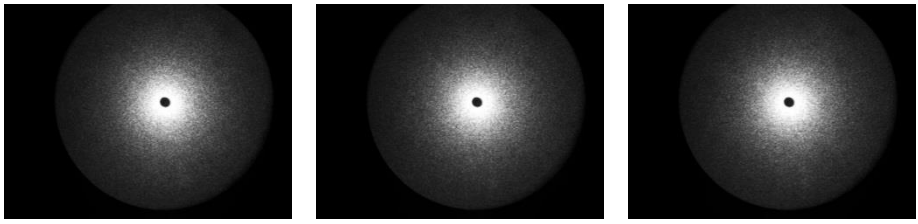

a) 0 rpm b) 0.005 rpm c) 0.05 rpm

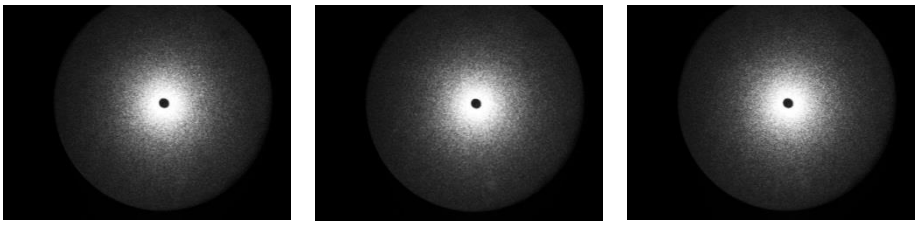

d) 0.5 rpm e) 5 rpm f) 50 rpm

Figure 230: The I_{VV} SALS patterns of a cement and superplasticizer solution at different shear rates

7. Summary

In this chapter, different techniques to study the structural buildup and particle clustering in materials have been investigated. The intention was to get a better view on the mechanisms governing particle clustering and dispersion inside fresh cement paste. Because of the dense packing density and very broad particle size distribution, only the static yield stress measurement and oscillatory rheometry were found to be suitable to study the macroscopic structural buildup in time. The static yield stress can be used on concrete level, the oscillatory rheology on paste and mortar level. The possibility of a direct view on the particle clustering inside the fresh concrete was also investigated using ultrasound attenuation and Small Angle Light Scattering (SALS), but none of those techniques was successful for the application on cement paste.

Ultrasound attenuation could be used for cement suspension with a low volume fraction (10%). As long as the volume fraction was low enough, the attenuation spectrum was sensitive to small changes in the particle clustering. However, at realistic solid volume fractions, the attenuation losses are so large, a small variation in the particle clustering or particle size distribution is unnoticed. The OPUS system could generate realistic particle size distributions on pastes with a water-to-cement mass ratio of 0.3, 0.4, and 0.6. However, no differences in particle size distribution were observed.

Although Small Angle Light Scattering (SALS) techniques have been successfully applied in polymer science, no major progress has been made from the application on cement. The addition of superplasticizer affected the images, but no shear induced structures were observed on cement solutions. The conversion of measured scattering images into particle size distributions of the sample was complicated by the complexity of the mathematical problem and the large impact of experimental noise.

Chapter 5: Conclusions & Perspectives

1. Research context

As predicted during the First International RILEM Symposium on Self-Compacting Concrete in 1999 [446], the worldwide use of self-compacting concrete (SCC) is steadily increasing in time. Because no external compaction is needed, the production process in precast factories can be accelerated and organized more efficiently. The highly flowable SCC also allows a further automation of the production process. In onsite applications, the usage of SCC avoids errors during the external compaction of concrete and allows a more dense reinforcement network and the application of a more complex shaped formwork.

However, SCC has a lower robustness; SCC is more sensitive to small changes in the mix proportions, material properties, and mixing and casting procedures. As the costs of failed batches and delays in the work plan are enormous, a severe quality control and experienced staff is needed. If the robustness of fresh SCC could be improved, its cost and labor saving characteristics can be applied in an even broader range of applications and circumstances.

Not only practical hints and guidelines to improve the robustness of SCC were established in this project, but also the origins and mechanisms of the robustness of SCC were investigated. By uncovering the mechanisms governing the robustness, the problem of a high sensitivity can be addressed in a fundamental way instead of with quick fixes. Understanding why a particular parameter has an influence allows to draw general conclusions and to extrapolate the observed experimental results to other situations or parameters, not investigated during this project.

2. Summary

A concise overview of the fundamental mechanisms and interactions governing the microstructure of fresh SCC is given in the literature review (Chapter 3). The chemical reactions during the first hours of hydration, the forces and interactions in between particles, the working mechanisms of admixtures, and the impact of shear stresses are explained in more detail in order to obtain a better understanding of the microstructure of fresh SCC

Based on the experimental results, methods to improve the robustness of fresh SCC were developed. Dependent on the mechanism providing stability in SCC, another strategy should be used.

When the yield stress is providing stability, the sensitivity of this yield stress to small changes is determining the robustness of the mixture. Because such mixtures generally have a low plastic viscosity, changes in this plastic viscosity due to small variations have no major impact. Based on the experimental program and a qualitative analysis using the yield stress model (YODEL) of Flatt [266], possible solutions to enhance the yield stress robustness of SCC have been proposed. A higher maximum packing density results in a more robust yield stress and can be achieved with a higher superplasticizer dosage, which can be reached with a lower paste volume. An alternative solution is the combination of a lower paste yield stress and a slightly higher plastic viscosity, for example by adding a VMA and a higher superplasticizer dosage.

In mixtures with a low or zero yield stress and the paste plastic viscosity providing stability, the sensitivity of the paste plastic viscosity is determining the robustness of the global mixture. A small decrease in the amount of water can result in an unworkable, sticky mixture; a small excess in water can result in bleeding. The best approach to improve the robustness of such a mixture is to enhance the robustness of the paste plastic viscosity. Based on a set of experiments and considering the Krieger-Doherty model, specific measures have been proposed: lowering the paste packing density, for example by raising the water-to-powder ratio. Also lowering the paste plastic viscosity helps to enhance the robustness against small variations in the mix composition. Mixtures prone to an excessive stickiness can be improved by reducing the thixotropic buildup, for example by increasing the water-to-powder ratio, a cement replacement by fly ash, or reducing the content of silica fume.

In case the risk of bleeding is limiting the applicability of SCC, a different approach is needed. Bleeding is a result of an imbalance in the intermolecular forces. When steric repulsion forces dominate over attractive Van Der Waals forces for small

colloidal particles, the colloidal network is broken and syneresis will manifest itself as a layer of water floating on top of SCC. To eliminate the origin of bleeding, two methods exist: reducing the steric repulsive forces with a reduction of the superplasticizer dosage (higher water-to-powder ratio, higher paste volume), or increasing the attractive Van Der Waals forces inside the fresh concrete, for example by a replacement of cement by silica fume.

All of this has been summarized in simple guidelines given in Table 50 of Chapter 3. As different applications have different workability demands, SCC with proper rheological properties customized to the application should be used. As the mixing procedure has a large impact on the rheology of SCC, a fixed mixing procedure should be used during the manufacturing of SCC.

An attempt was made to investigate particle clustering and the structural buildup more fundamentally using innovative experimental techniques. Due to the very broad particle size distribution and the non-transparent opaque nature of cement paste, monitoring the flocculation and deflocculation of the individual cement particles is not evident. Two techniques have been selected for a more thorough examination of their applicability: ultrasound attenuation and Small Angle Light Scattering (SALS).

When ultrasound amplitude losses are measured over a range of ultrasound frequencies, attenuation spectra can be used to characterize an opaque dense solution. As no evolution in the attenuation spectra was observed on samples of cement paste at rest, the flocculation at rest cannot be evaluated using the ultrasound attenuation technique. Different water-to-powder ratios caused variations in the measured attenuation spectra. However, in an apparatus in which the particle size distributions were calculated based on a theory taking into account the viscous attenuation losses and the scattering attenuation losses, no realistic particle size distribution could be generated. Using another apparatus, in which the particle size distribution was calculated based on a calibration with a powder with known properties, realistic particle size distributions were obtained. As paste mixtures varying in water-to-powder ratio all generated similar particle size distributions, no effects of particle clustering could be observed using ultrasound attenuation.

When Small Angle Light Scattering (SALS) was used on diluted samples of a solution of cement in water, the influence of adding a superplasticizer of the scattering patterns could be observed. Because the SALS images were independent on the shear rate applied on the samples, the flocculation / deflocculation mechanisms in cement paste cannot be studied more in depth using this technique. A calculation

of the particle size distribution based on the SALS images was not successful. Although this technique is useful in polymer science, its application on cement paste is less promising.

3. Perspectives for future research

Recently, an important progress in uncovering the mechanisms governing the structural buildup at rest has been made [149]. However, still not all mysteries surrounding the thixotropy of SCC are uncovered. Ambiguity exists concerning the role of flocculation of fines and the impact of admixtures. Up to now, no thixotropy model exists which is easy to implement and is still founded on a simple hypothesis of the mechanisms governing thixotropy.

In order to investigate the origins of thixotropy more in depth, a method has to be developed which is able to observe the structural buildup at rest and breakdown of the thixotropic network under shear on a more fundamental level. Oscillating rheology is useful when monitoring the macroscopic changes in fresh SCC, but does not expose what exactly is happening inside the microstructure of the sample. This thesis describes an explorative study of possible techniques observing the flocculation and deflocculation of fines directly, but no practical solution was established. Continued research using a combination of the Focused Beam Reflection Measurements (FBRM) [235] and cryo-FIB and cryo-SEM images [142] might help to study this aspect. FBRM measurements can be used to count the individual clusters of particles under shear and establish a measure of the cluster size distribution. Cryo-FIB and cryo-SEM images allow to study the microstructure of a sample prepared by high pressure freezing based on a direct observation of the microstructure. Using a combination of these techniques, it might be possible to observe directly the buildup of a thixotropic network and to study the impact of hydration more fundamentally.

This better understanding of the thixotropy, and by extension the entire microstructure of fresh SCC, has to be incorporated in rheological models. Improved rheological models could help to study the impact of small variations in the mix composition more easily. For a specific application, for example, it might be possible to use improved rheological models to examine whether the pumpability can be compromised by the inevitable inaccuracies occurring during the dosing of superplasticizers. A further optimization of the mix composition based on such a risk analysis will facilitate the use of SCC even further.

A further optimization of the mix design of SCC will require a better understanding of the links between the plastic viscosity, thixotropy and stickiness of SCC. The microstructural origins of the stickiness of SCC are not fully known yet and most probably linked to the thixotropic buildup of SCC. More research on the working mechanisms VMA's and their effects on the rheology can help to obtain a deeper understanding of the microstructure. A more consistent classification of the very broad range of commercial available VMA's would help to reduce the existing uncertainties and thereby facilitate their application inside SCC.

Appendix A

This appendix summarizes the raw data of the robustness experiments of Chapter 3.

1. Paste volume and water-to-powder ratio (section 3.1. in Chapter 3)

Paste volume [l/m³]	**400**	**400**	**400**
water-to-powder ratio [-]	**0.75**	**0.90**	**1.05**
Slump flow [mm] Ref – 8 l/m³ water	525	615	515
Slump flow [mm] Reference	673	680	688
Slump flow [mm] Ref + 8 l/m³ water	785	778	725
V-funnel time [s] Ref – 8 l/m³ water	19.3	8.7	6.9
V-funnel time [s] Reference	13.7	6.3	3.5
V-funnel time [s] Ref + 8 l/m³ water	7.8	4.9	3.2
L-box ratio [-] Ref – 8 l/m³ water	-	0.75	0.58
L-box ratio [-] Reference	0.82	0.85	0.83
L-box ratio [-] Ref + 8 l/m³ water	0.86	0.93	0.93
S.S.I. [%] Ref – 8 l/m³ water	1.5	7.5	3.5
S.S.I. [%] Reference	9.4	12.2	12.0
S.S.I. [%] Ref + 8 l/m³ water	18.1	15.7	16.3

Paste volume [l/m³]	**400**	**400**	**400**
water-to-powder ratio [-]	**0.75**	**0.90**	**1.05**
Yield stress [Pa] Ref – 8 l/m³ water	-	-	212
Yield stress [Pa] Reference	36	-	81
Yield stress [Pa] Ref + 8 l/m³ water	-	-	48
MB linear term [Pa. s] Ref – 8 l/m³ water	-	-	23
MB linear term [Pa. s] Reference	72	-	21
MB linear term [Pa. s] Ref + 8 l/m³ water	-	-	14
MB 2nd order term [Pa. s²] Ref – 8 l/m³ water	-	-	0
MB 2nd order term [Pa. s²] Reference	18	-	0
MB 2nd order term [Pa. s²] Ref + 8 l/m³ water	-	-	0

Paste volume [l/m³]	**400**	**400**	**400**
water-to-powder ratio [-]	**0.75**	**0.90**	**1.05**
Density [kg/m³] Ref – 8 l/m³ water	2381	2356	2350
Density [kg/m³] Reference	2475	2369	2369
Density [kg/m³] Ref + 8 l/m³ water	2369	2375	2350
Air content [%] Ref – 8 l/m³ water	2.3	2.0	1.7
Air content [%] Reference	2.5	1.6	1.2
Air content [%] Ref + 8 l/m³ water	1.8	1.1	1.2

Paste volume [l/m³]	**375**	**375**	**375**
water-to-powder ratio [-]	**0.75**	**0.90**	**1.05**
Slump flow [mm] Ref – 8 l/m³ water	690	565	650
Slump flow [mm] Reference	705	680	680
Slump flow [mm] Ref + 8 l/m³ water	845	703	783
V-funnel time [s] Ref – 8 l/m³ water	27.3	11.7	5.6
V-funnel time [s] Reference	17.6	8.0	4.0
V-funnel time [s] Ref + 8 l/m³ water	9.0	6.3	3.3
L-box ratio [-] Ref – 8 l/m³ water	0.90	0.76	0.76
L-box ratio [-] Reference	0.96	0.91	0.86
L-box ratio [-] Ref + 8 l/m³ water	0.96	1.02	0.91
S.S.I. [%] Ref – 8 l/m³ water	4.3	5.0	7.5
S.S.I. [%] Reference	11.2	10.1	12.3
S.S.I. [%] Ref + 8 l/m³ water	18.0	13.1	15.9

Paste volume [l/m³]	**375**	**375**	**375**
water-to-powder ratio [-]	**0.75**	**0.90**	**1.05**
Yield stress [Pa] Ref – 8 l/m³ water	12	82	-
Yield stress [Pa] Reference	20	39	-
Yield stress [Pa] Ref + 8 l/m³ water	10	19	-
MB linear term [Pa. s] Ref – 8 l/m³ water	57	90	-
MB linear term [Pa. s] Reference	75	44	-
MB linear term [Pa. s] Ref + 8 l/m³ water	25	29	-
MB 2nd order term [Pa. s²] Ref – 8 l/m³ water	44	6	-
MB 2nd order term [Pa. s²] Reference	37	4	-
MB 2nd order term [Pa. s²] Ref + 8 l/m³ water	9	3	-

Paste volume [l/m³]	**375**	**375**	**375**
water-to-powder ratio [-]	**0.75**	**0.90**	**1.05**
Density [kg/m³] Ref – 8 l/m³ water	2388	2369	2375
Density [kg/m³] Reference	2394	2375	2372
Density [kg/m³] Ref + 8 l/m³ water	2400	2369	2369
Air content [%] Ref – 8 l/m³ water	2.0	2.4	1.5
Air content [%] Reference	1.9	1.8	1.4
Air content [%] Ref + 8 l/m³ water	0.9	1.6	0.7

Paste volume [l/m³]	**350**	**350**	**350**
water-to-powder ratio [-]	**0.75**	**0.90**	**1.05**
Slump flow [mm] Ref – 8 l/m³ water	833	660	605
Slump flow [mm] Reference	865	750	675
Slump flow [mm] Ref + 8 l/m³ water	923	790	753
V-funnel time [s] Ref – 8 l/m³ water	31.4	13.3	7.2
V-funnel time [s] Reference	15.9	10.5	5.3
V-funnel time [s] Ref + 8 l/m³ water	9.6	7.8	4.3
L-box ratio [-] Ref – 8 l/m³ water	0.96	0.92	0.74
L-box ratio [-] Reference	1.05	0.98	0.80
L-box ratio [-] Ref + 8 l/m³ water	0.98	0.95	0.92
S.S.I. [%] Ref – 8 l/m³ water	7.0	7.0	3.4
S.S.I. [%] Reference	10.5	9.4	8.0
S.S.I. [%] Ref + 8 l/m³ water	16.2	11.6	8.4

Paste volume [l/m³]	**350**	**350**	**350**
water-to-powder ratio [-]	**0.75**	**0.90**	**1.05**
Yield stress [Pa] Ref – 8 l/m³ water	0	7	49
Yield stress [Pa] Reference	0	0	29
Yield stress [Pa] Ref + 8 l/m³ water	0	3	18
MB linear term [Pa. s] Ref – 8 l/m³ water	95	66	50
MB linear term [Pa. s] Reference	26	43	32
MB linear term [Pa. s] Ref + 8 l/m³ water	13	31	19
MB 2nd order term [Pa. s²] Ref – 8 l/m³ water	60	13	3
MB 2nd order term [Pa. s²] Reference	32	8	2
MB 2nd order term [Pa. s²] Ref + 8 l/m³ water	11	5	2

Paste volume [l/m³]	**350**	**350**	**350**
water-to-powder ratio [-]	**0.75**	**0.90**	**1.05**
Density [kg/m³] Ref – 8 l/m³ water	-	2381	2375
Density [kg/m³] Reference	2406	2375	2369
Density [kg/m³] Ref + 8 l/m³ water	2406	2381	2375
Air content [%] Ref – 8 l/m³ water	-	2.2	2.2
Air content [%] Reference	0.9	1.5	1.5
Air content [%] Ref + 8 l/m³ water	0.7	1.2	1.1

2. Water Film Thickness (section 3.2. in Chapter 3)

Water-to-powder ratio [-]	**0.85**	**0.90**	**0.95**	**1.00**
Superplasticizer dosage [%]	**0.118**	**0.118**	**0.118**	**0.118**
Water Film Thickness [μm] Ref – 3% water	0.135	0.170	0.189	0.242
Water Film Thickness [μm] Reference	0.188	0.198	0.276	0.304
Water Film Thickness [μm] Ref + 3% water	0.197	0.257	0.316	0.366
Yield stress [Pa] Ref – 3% water	36.09	12.64	7.41	3.72
Yield stress [Pa] Reference	16.38	7.05	2.55	2.17
Yield stress [Pa] Ref + 3% water	7.20	3.75	2.30	1.14
MB linear term [Pa. s] Ref – 3% water	3.45	1.39	0.91	0.40
MB linear term [Pa. s] Reference	1.59	0.85	0.39	0.30
MB linear term [Pa. s] Ref + 3% water	0.83	0.50	0.39	0.15
MB 2nd order term [Pa. s^2] Ref – 3% water	0.00000	0.00082	0.00127	0.00165
MB 2nd order term [Pa. s^2] Reference	0.00082	0.00049	0.00238	0.00123
MB 2nd order term [Pa. s^2] Ref + 3% water	0.00164	0.00035	0.00025	0.00134
Increase in G' (1) [Pa] Ref – 3% water	2311	1162	852	528
Increase in G' (1) [Pa] Reference	1073	711	717	514
Increase in G' (1) [Pa] Ref + 3% water	687	762	779	685
Increase in G' (2) [Pa] Ref – 3% water	4079	1752	1725	1468
Increase in G' (2) [Pa] Reference	1873	1218	1665	1220
Increase in G' (2) [Pa] Ref + 3% water	1282	1902	2567	1826

Water-to-powder ratio [-]	**0.85**	**0.90**	**0.95**	**1.00**
Superplasticizer dosage [%]	**0.159**	**0.159**	**0.159**	**0.159**
Water Film Thickness [µm] Ref – 3% water	0.162	0.201	0.245	0.302
Water Film Thickness [µm] Reference	0.209	0.236	0.308	0.340
Water Film Thickness [µm] Ref + 3% water	0.253	0.323	0.341	0.412
Yield stress [Pa] Ref – 3% water	7.87	4.62	2.09	0.86
Yield stress [Pa] Reference	2.68	2.23	0.62	0.49
Yield stress [Pa] Ref + 3% water	0.96	0.26	0.16	0.26
MB linear term [Pa. s] Ref – 3% water	0.84	0.52	0.37	0.19
MB linear term [Pa. s] Reference	0.41	0.32	0.28	0.14
MB linear term [Pa. s] Ref + 3% water	0.28	0.25	0.16	0.12
MB 2nd order term [Pa. s^2] Ref – 3% water	0.00268	0.00581	0.00363	0.00381
MB 2nd order term [Pa. s^2] Reference	0.00481	0.00344	0.00181	0.00305
MB 2nd order term [Pa. s^2] Ref + 3% water	0.00530	0.00221	0.00199	0.00203
Increase in G’ (1) [Pa] Ref – 3% water	583	414	268	265
Increase in G’ (1) [Pa] Reference	322	306	302	225
Increase in G’ (1) [Pa] Ref + 3% water	247	386	474	296
Increase in G’ (2) [Pa] Ref – 3% water	749	529	392	430
Increase in G’ (2) [Pa] Reference	365	364	411	521
Increase in G’ (2) [Pa] Ref + 3% water	343	448	-	789

Water-to-powder ratio [-]	**0.75**	**0.80**	**0.85**	**0.90**	**0.95**
Superplasticizer dosage [%]	**0.200**	**0.200**	**0.200**	**0.200**	**0.200**
Water Film Thickness [µm] Ref – 3% water	0.085	0.167	0.203	0.270	0.315
Water Film Thickness [µm] Reference	0.151	0.209	0.267	0.289	0.355
Water Film Thickness [µm] Ref + 3% water	0.189	0.250	0.316	0.355	0.414
Yield stress [Pa] Ref – 3% water	14.25	7.43	2.00	1.17	0.19
Yield stress [Pa] Reference	8.71	3.22	0.77	0.69	0.14
Yield stress [Pa] Ref + 3% water	4.00	1.00	0.12	0.22	0.08
MB linear term [Pa. s] Ref – 3% water	1.37	0.53	0.29	0.29	0.28
MB linear term [Pa. s] Reference	0.68	0.28	0.32	0.22	0.18
MB linear term [Pa. s] Ref + 3% water	0.29	0.19	0.24	0.12	0.10
MB 2nd order term [Pa. s^2] Ref – 3% water	0.00569	0.00905	0.00787	0.00533	0.00294
MB 2nd order term [Pa. s^2] Reference	0.00864	0.00664	0.00465	0.00312	0.00224
MB 2nd order term [Pa. s^2] Ref + 3% water	0.00823	0.00548	0.00306	0.00469	0.00249
Increase in G’ (1) [Pa] Ref – 3% water	987	585	259	268	175
Increase in G’ (1) [Pa] Reference	701	265	206	256	382
Increase in G’ (1) [Pa] Ref + 3% water	415	178	176	391	404
Increase in G’ (2) [Pa] Ref – 3% water	-	911	237	227	266
Increase in G’ (2) [Pa] Reference	1007	462	202	504	2836
Increase in G’ (2) [Pa] Ref + 3% water	596	204	252	2014	4628

3. Viscosity Modifying Admixtures – experiments on mortars (section 3.3.1. in Chapter 3)

	No VMA	Diutan gum	Corn starch	Attapulgite clay	Propylene carbonate
Flow spread [mm] Ref – 5 l/m³ water	198	203	219	224	208
Flow spread [mm] Reference	248	240	243	250	250
Flow spread [mm] Ref + 5 l/m³ water	284	238	288	280	278
V-funnel time [s] Ref – 5 l/m³ water	11.3	15.1	9.5	9.1	25.0
V-funnel time [s] Reference	10.4	10.9	7.4	7.8	11.7
V-funnel time [s] Ref + 5 l/m³ water	7.2	8.5	6.0	6.1	8.6
Yield stress [Pa] Ref – 5 l/m³ water	22.3	36.3	29.0	21.8	21.7
Yield stress [Pa] Reference	16.9	25.7	13.5	12.3	11.2
Yield stress [Pa] Ref + 5 l/m³ water	10.7	16.7	5.3	7.4	4.9
Plastic viscosity [Pa s] Ref – 5 l/m³ water	12.0	15.2	10.7	10.2	13.3
Plastic viscosity [Pa s] Reference	8.1	13.2	7.6	7.1	9.6
Plastic viscosity [Pa s] Ref + 5 l/m³ water	5.2	9.1	4.9	5.0	8.5
Breakdown speed [-] Ref – 5 l/m³ water	0.0064	0.0066	0.0042	0.0047	0.0064
Breakdown speed [-] Reference	0.0043	0.0051	0.0039	0.0041	0.0039
Breakdown speed [-] Ref + 5 l/m³ water	0.0036	0.0029	0.0032	0.0038	0.0037
Buildup speed [-] Ref – 5 l/m³ water	0.017	0.011	0.015	0.016	0.012
Buildup speed [-] Reference	0.017	0.012	0.015	0.023	0.021
Buildup speed [-] Ref + 5 l/m³ water	0.016	0.010	0.015	0.022	0.010

	No VMA	Diutan gum	Corn starch	Attapulgite clay	Propylene carbonate
Air content [%] Ref – 5 l/m³ water	1.8	2.7	2.8	2.5	2.3
Air content [%] Reference	2.3	2.6	2.3	2.3	2.7
Air content [%] Ref + 5 l/m³ water	1.8	2.1	-	1.8	1.7
Density [kg/m³] Ref – 5 l/m³ water	2273	2305	2278	2240	2274
Density [kg/m³] Reference	2273	2276	2294	2304	2246
Density [kg/m³] Ref + 5 l/m³ water	2261	2280	2257	2259	2257

4. Viscosity Modifying Admixtures – experiments on SCC (section 3.3.2. in Chapter 3)

	Mix A No VMA	Mix A Diutan gum	Mix A Attapulgite clay	Mix B No VMA	Mix B Diutan gum 1	Mix B Diutan gum 2	Mix B Attapulgite clay
Slump flow [mm] Ref – 10 l/m³ water	520	610	623	670	750	500	525
Slump flow [mm] Reference	720	680	675	703	785	695	660
Slump flow [mm] Ref + 10 l/m³ water	765	723	825	765	815	710	855
V-funnel time [s] Ref – 10 l/m³ water	7.1	10.7	6.3	11.4	13.6	54.4	12.9
V-funnel time [s] Reference	3.8	7.6	4.6	9.5	10.9	14.8	10.1
V-funnel time [s] Ref + 10 l/m³ water	3.0	5.5	2.8	6.5	7.9	10.7	7.4
S.S.I. [%] Ref – 10 l/m³ water	1.2	5.8	5.2	11.4	18.9	2.0	4.0
S.S.I. [%] Reference	10.8	11.9	8.2	14.5	21.2	15.0	9.4
S.S.I. [%] Ref + 10 l/m³ water	11.7	16.9	16.9	19.5	23.7	23.3	26.5

	Mix A No VMA	Mix A Diutan gum	Mix A Attap ulgite clay	Mix B No VMA	Mix B Diutan gum 1	Mix B Diutan gum 2	Mix B Attap ulgite clay
Yield stress [Pa] Ref – 10 l/m³ water	157	61	79	17	17	234	68
Yield stress [Pa] Reference	29	37	51	0	8	23	34
Yield stress [Pa] Ref + 10 l/m³ water	34	26	16	0	0	7	10
MB linear term [Pa. s] Ref – 10 l/m³ water	79	102	70	68	76	378	163
MB linear term [Pa. s] Reference	38	69	45	34	49	81	60
MB linear term [Pa. s] Ref + 10 l/m³ water	28	48	30	21	37	55	32
MB 2nd order term [Pa. s²] Ref – 10 l/m³ water	0.0	0.0	0.0	20.3	9.4	0.0	14.9
MB 2nd order term [Pa. s²] Reference	0.0	0.0	0.0	10.4	4.4	6.3	13.3
MB 2nd order term [Pa. s²] Ref + 10 l/m³ water	0.0	0.0	0.0	8.7	3.3	5.3	7.1

	Mix A No VMA	Mix A Diutan gum	Mix A Attapulgite clay	Mix B No VMA	Mix B Diutan gum 1	Mix B Diutan gum 2	Mix B Attapulgite clay
Density [kg/m³] Ref – 10 l/m³ water	2350	2341	2348	2375	2375	2400	2369
Density [kg/m³] Reference	2350	2350	2359	2363	2369	2356	2369
Density [kg/m³] Ref + 10 l/m³ water	2323	2326	2332	2350	2375	2356	2381
Air content [%] Ref – 10 l/m³ water	2.6	2.7	2.3	2.5	1.9	2.5	-
Air content [%] Reference	1.6	1.8	1.7	2.0	1.7	2.0	2.6
Air content [%] Ref + 10 l/m³ water	1.5	1.7	1.1	1.6	1.4	1.8	1.1

5. Cement replacement (section 3.4. in Chapter 3)

	Mix C Reference	Mix C Replacement by silica fume	Mix C Replacement by fly ash
Slump flow [mm] Ref – 10 l/m³ water	695	695	665
Slump flow [mm] Reference	740	695	725
Slump flow [mm] Ref + 10 l/m³ water	770	715	725
V-funnel time [s] Ref – 10 l/m³ water	62.0	52.1	59.2
V-funnel time [s] Reference	21.54	36.4	21.7
V-funnel time [s] Ref + 10 l/m³ water	10.18	13.1	10.8
S.S.I. [%] Ref – 10 l/m³ water	0.7	0.4	0.7
S.S.I. [%] Reference	2.7	1.8	3.6
S.S.I. [%] Ref + 10 l/m³ water	5.9	1.4	5.7

	Mix C Reference	Mix C Replacement by silica fume	Mix C Replacement by fly ash
Bingham yield stress [Pa] Ref – 10 l/m³ water	88	99	449
Bingham yield stress [Pa] Reference	0	63	200
Bingham yield stress [Pa] Ref + 10 l/m³ water	0	93	60
Bingham plastic viscosity [Pa. s] Ref – 10 l/m³ water	297	179	143
Bingham plastic viscosity [Pa. s] Reference	133	153	117
Bingham plastic viscosity [Pa. s] Ref + 10 l/m³ water	64	75	57

	Mix C Reference	Mix C Replacement by silica fume	Mix C Replacement by fly ash
Density [kg/m³] Ref – 10 l/m³ water	2336	2330	2335
Density [kg/m³] Reference	2323	2314	2331
Density [kg/m³] Ref + 10 l/m³ water	2339	2305	2323
Air content [%] Ref – 10 l/m³ water	3.6	2.7	2.7
Air content [%] Reference	2.7	2.4	1.8
Air content [%] Ref + 10 l/m³ water	1.8	2.0	1.2

	Mix D Reference	Mix D Replacement by silica fume	Mix D Replacement by fly ash	Mix D Replacement by limestone
Slump flow [mm] Ref – 10 l/m³ water	665	625	713	655
Slump flow [mm] Reference	733	700	750	715
Slump flow [mm] Ref + 10 l/m³ water	775	730	770	730
V-funnel time [s] Ref – 10 l/m³ water	74.0	94.0	37.3	192.6
V-funnel time [s] Reference	26.1	33.3	11.8	24.8
V-funnel time [s] Ref + 10 l/m³ water	12.6	15.8	7.4	13.1
S.S.I. [%] Ref – 10 l/m³ water	0.3	0.1	1.4	0.0
S.S.I. [%] Reference	3.3	2.0	3.0	3.1
S.S.I. [%] Ref + 10 l/m³ water	3.5	3.1	8.7	5.5

	Mix D Reference	Mix D Replacement by silica fume	Mix D Replacement by fly ash	Mix D Replacement by limestone
Bingham yield stress [Pa] Ref – 10 l/m³ water	324	236	193	93
Bingham yield stress [Pa] Reference	8	68	0	3
Bingham yield stress [Pa] Ref + 10 l/m³ water	0	0	0	0
Bingham plastic viscosity [Pa. s] Ref – 10 l/m³ water	126	210	157	208
Bingham plastic viscosity [Pa. s] Reference	117	160	97	136
Bingham plastic viscosity [Pa. s] Ref + 10 l/m³ water	101	113	52	82

	Mix D Reference	Mix D Replacement by silica fume	Mix D Replacement by fly ash	Mix D Replacement by limestone
Density [kg/m³] Ref – 10 l/m³ water	2335	2340	2370	2328
Density [kg/m³] Reference	2328	2313	2331	2319
Density [kg/m³] Ref + 10 l/m³ water	2332	2305	2315	2313
Air content [%] Ref – 10 l/m³ water	4.2	2.8	2.4	0.2
Air content [%] Reference	3.3	2.5	1.7	2.2
Air content [%] Ref + 10 l/m³ water	3.6	2.0	1.3	1.5

Appendix B

In Section 3.2. of Chapter 3, the Water Film Thickness (WFT) of paste mixtures was determined and used to study the mechanisms governing the influence of the water-to-powder volumetric ratio on the robustness against small variations in the water content. This appendix clarifies the calculation of the maximum packing density ϕ_{max} according to the wet method, originally described in [85, 327-329].

The packing density of a mix composition is calculated using the wet method, based on the mix proportions used while weighing the various constituents and the measured density of the fresh mixture. An example is shown in Table B.1 in which the packing density of a mixture with known mix composition and a measured mass density of 2193 kg/m³ is calculated.

	Mix composition	**Weighted quantity for 1.5 l**	**Mass in a sample of 1 liter with a mass density of 2193 kg/m³**	**Volume in a sample of 1 liter with a mass density of 2193 kg/m³**
Cement	923 kg/m³	1384 g	933 g	0.300 l
Limestone powder	615 kg/m³	923 g	622 g	0.233 l
Water	474 kg/m³	705 g [1]	476 g	0.476 l
Superplasticizer	0.200%	7.11 ml		
			Solid concentration:	53.2%

[1]) The weighted quantity of water was corrected for the water present in the superplasticizer.

Table B.1: Calculation of the packing density

Using this method, the packing density of mixtures varying in the mix composition can be determined using formulas B.1 to B.3. The maximum packing density in wet condition of a mix composition is the maximum packing density which can be achieved by varying the water content. Figures B.1 to B.6 summarize the calculation of the maximum packing densities of the mix compositions used in Section 3.2. of Chapter 3.

$$WFT = \frac{u_w - u_{min}}{A_s} \qquad \text{(Eq. B.1)}$$

$$u_{min} = \frac{1-\phi_{max}-\varepsilon_a(\phi_{max})}{\phi_{max}} \quad \text{(Eq. B.2)}$$

$$u_w = \frac{1-\phi-\varepsilon_a(\phi)}{\phi} \quad \text{(Eq. B.3)}$$

Symbol	Unit	Name	Meaning
WFT	[m]	Water Film Thickness	Thickness of the excess water layer covering the solid particles.
ϕ	[%]	Packing density	The volume of solids divided by the bulk volume
ϕ_{max}	[%]	Maximum packing density	The maximum possible packing density possible for this mixture under varying water content.
$\varepsilon_a(\phi)$	[%]	Air content	The volume of air divided by the bulk volume.
u_w	[%]	Water ratio	The volume of water divided by the volume of solids.
u_{min}	[%]	Minimum voids ratio	The water ratio corresponding with the maximum packing density.
A_s	[m²/m³]	Specific surface area of the solids	The total surface of all solids in one volumetric unit.

Table B.2: Definition of the parameters used in Equations B.1 to B.3

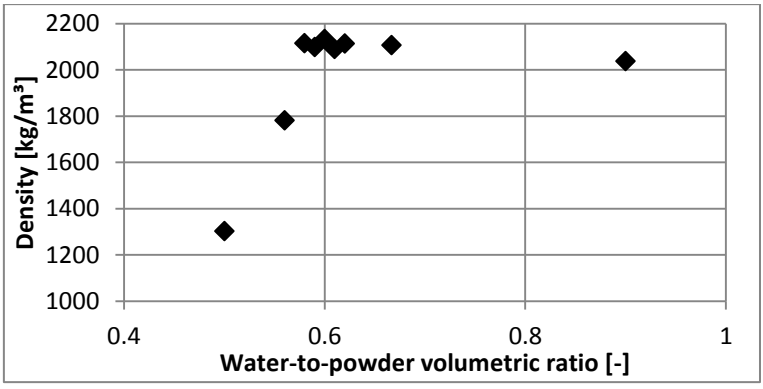

Figure B.1: Changes in the density induced by variations of the water content Superplasticizer dosage of 0.200%

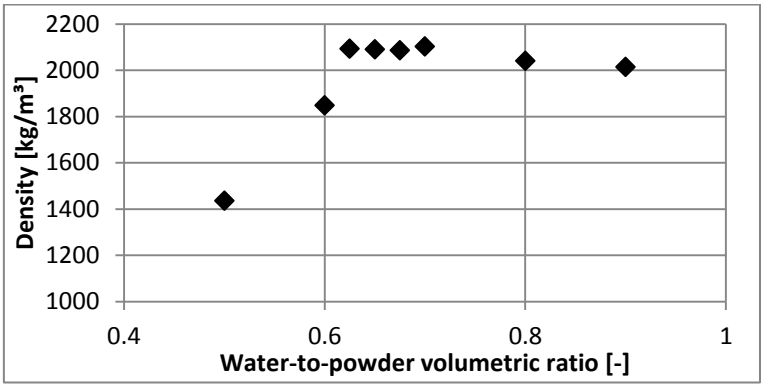

Figure B.2: Changes in the density induced by variations of the water content
Superplasticizer dosage of 0.159%

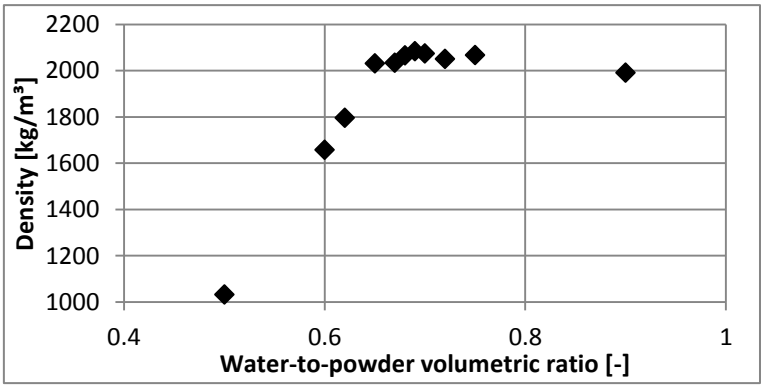

Figure B.3: Changes in the density induced by variations of the water content
Superplasticizer dosage of 0.118%

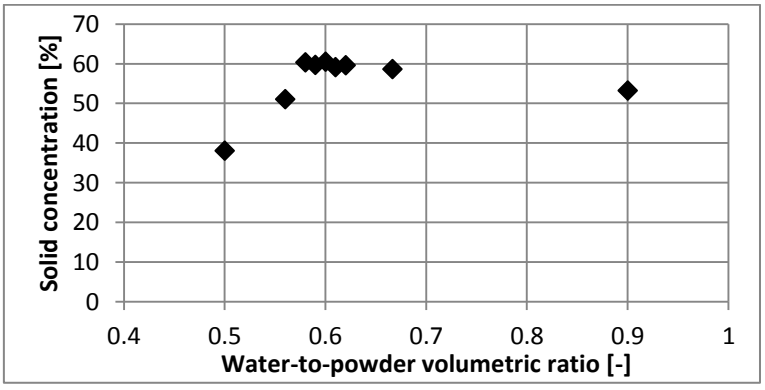

Figure B.4: Changes in the solid concentration induced by variations of the water content
Superplasticizer dosage of 0.200%

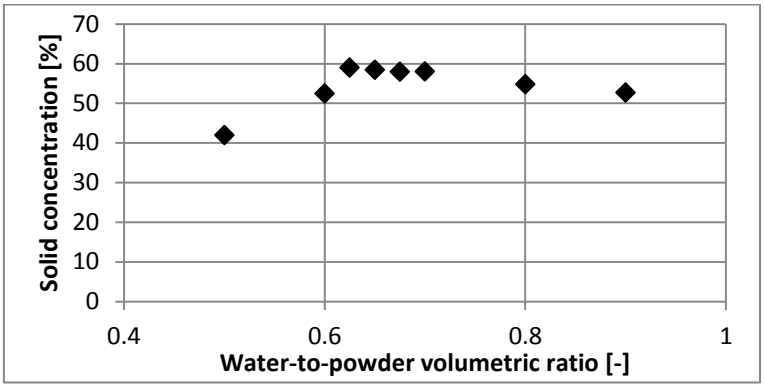

Figure B.5: Changes in the solid volume fraction induced by variations of the water content Superplasticizer dosage of 0.159%

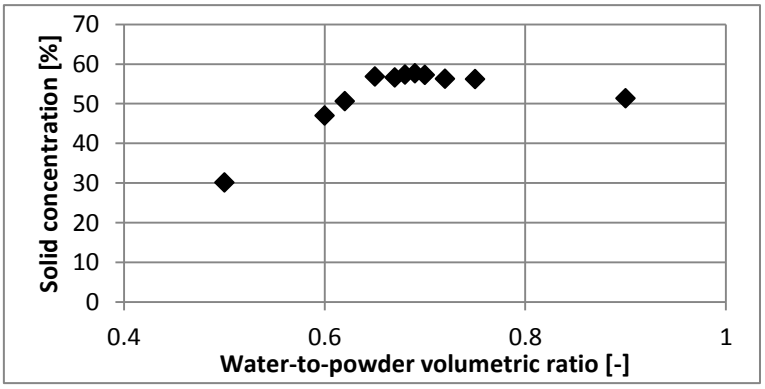

Figure B.6: Changes in the solid concentration induced by variations of the water content Superplasticizer dosage of 0.118%

Appendix C

The code used to convert the SALS images into intensity values as a function of the scattering vector. This code can be runned in the program newSalsBatsch.exe developed by Dr. Frank Vanden Berghen and Prof. Dr. Jan Vermant [447].

```
<?xml version="1.0" encoding="ISO-8859-1"?>
<SALS>
<block name='Top'>
        <operation name='Global Rheology Parameters' service='Global Rheology
        Parameters'>
                <p x="" y="" dss="11" pp="37,7950" wavelength="658"/>
        </operation>

        <operation name='BeamStop computation(C:/Users/…/image.bmp)'
        service='Automatic BeamStop position'>
                <p filename=" C:/Users/…/image.bmp" wsVar="beamstop"
                treshold="60" phase2="1"/>
        </operation>

        <fori name='for(i=100 ; i&lt;101 ; i+=1)' startv='100' endv='101' incv='1'
        wsVar='i'>
                <Print name='Print on status bar' toPrint='loop {i}'/>
                <operation name='Pie Intensity' service='Pie Intensity'>
                        <p filename="C:/Users/…/image.bmp"
                        wsvar="PieIntensity" x="{beamstop.x}" y="{beamstop.y}"
                        angle="360" direction="0" a="1" b="1"
                        dss="{GlobalParameters.DistScreenSample}"
                        pp="{GlobalParameters.PixelPerCM}"
                        wavelength="{GlobalParameters.Wavelength}" ca="0"/>
                </operation>
                <WSadd name='Update inside &apos;PieIntensity&apos; all the
                tags &apos;p&apos;' addTo='PieIntensity' tagName='p'
                text='&lt;time&gt;{i}&lt;/time&gt;' op='3' textIsXML='1'/>
```

```
            <MoveWS name='Move Vars in WS' fromTag='PieIntensity'
            toTag='results' tagName='' duplicate='0'/>
        </fori>

        <WSsave name='save tags Results.p' baseTag='Results' iterateTag='p'
        filename='C:/Users/…/resultsIntensityPie.txt' header='time,x,y'
        text='{time},{x},{y}'/>
</block>
</SALS>
```

Appendix D

Main Matlab file calculating the particle size distribution corresponding with the SALS images

```
%% LOAD THE DATA
% loading the txt file with the experimental data (no
heading, collumns
% separated by comma's)
experiment = load('polystyrene 1 µm IVV2.txt');

% number of images in the txt file
aantalfotos=1;

% the number of the image to analyse
fotonr = 1;

%% NUMBER OF ROWS

% Open the matrix 'experiment' and verify how many rows
are used for each
% image. This number of rows is N2.
N2=1050;

%% PARAMETERS

% Number of particle sizes
PSD=30;
% Diameters in micrometers
Rmin = log10(0.5);
Rmax=log10(500);
R = logspace(Rmin,Rmax,PSD);

%wavelength in nm
lambda = 658;

%refractive index
    % polystyrene = 1.57+1i*5e-4
    % cement = (1.6 - 1.8) + 1i* 0.1
refractiveindexparticle = 1.57+1i*5e-4;
```

```
refractiveindexmedium = 1.33; % water

%intensity incident light. This value is unknown and
fixed as 1
I0 = 1;

% This section analyses how many rows are useful in the
analysis.
% Because the intensities are expressed in the 8-bit
grayscale, only
% intensities in between 20 and 235 are considered to be
proportional to
% the acual inensities scattered by the sample.
% First the number of useful rows are counted and an
inventory is made of
% these rows.
teller=zeros(aantalfotos,N2);
for foto=1:aantalfotos
    for i=1:N2
        if experiment(i+(foto-1)*N2,3) > 20
            if experiment(i+(foto-1)*N2,3) <235
                if experiment(i+(foto-1)*N2,2)>0
                    teller(foto,1)=teller(foto,1)+1;

teller(foto,teller(foto,1)+1)=i+(foto-1)*N2;
                end
            end
        end
    end
end

% Collecting the usefull intensities IR and
corresponding scattering
% vectors q. The scattering vectors are converted into
the polar angles
% teta
IR = zeros(N2,aantalfotos);
for i=1:aantalfotos
    for k = 2:teller(i,1)+1
        IR(k-1,i) = experiment(teller(i,k),3);
    end
end
xlswrite('Measured intensities.xlsx',IR);

q = zeros(N2,aantalfotos);
for i=1:aantalfotos
    for k = 2:teller(i,1)+1
        q(k-1,i) = experiment(teller(i,k),2);
    end
end
```

```
teta = zeros(N2,aantalfotos);
for i=1:aantalfotos
    for k = 1:teller(i,1)
        teta(k,i) = asin(lambda*q(k,i)/4000/pi);
    end
end

%% CALCULATION OF THE SCATTERING MATRIX

% integrals are calculated as a summation
% => first a large matrix with points is calculated

% veelvoud = multiplication to determine the additional
points in the matrix. Or 1, or an even number
veelvoud = 20;
Rintegratie = logspace(Rmin,Rmax,PSD*veelvoud);

% for each point (a particle size), the scattering
intensities are
% calculated in the matrix 'veldvanpunten'
% This loop is a time-consuming process
veldvanpunten = zeros(teller(fotonr,1),PSD*veelvoud);
for j=1:teller(fotonr,1)
    tekstvoorscherm = ['angle nr ', num2str(j), ' of ',
num2str(teller(fotonr,1))];
    disp(tekstvoorscherm);
    for i = 1:PSD*veelvoud
        % Calculation of the Mie scatttering functions
S1 and S2
        S12 = Mie_S12(refractiveindexparticle,
(lambda/1000)*(Rintegratie(i)), cos(teta(j,fotonr)));
        veldvanpunten(j,i) = (lambda * 1e-9)^2 / 16 /
pi^2 * (abs(3 * S12(1)^2 + 2 * S12(1) * S12(2) + 3 *
S12(2)^2))^2;
    end
end

% matrix B is the matrix which needs to be inverted
B = zeros(teller(fotonr,1),PSD-4);
for j=1:teller(fotonr,1)
    for i = 3:PSD-2
        if veelvoud <2
            B(j,i-2)= veldvanpunten(j,i);
        else
            optelling = zeros(veelvoud,1);
            for k = 1:veelvoud
                optelling(k)=veldvanpunten(j,veelvoud*i-
1.5*veelvoud+k);
```

```
            end
            B(j,i-2)=sum(optelling)/veelvoud;
        end
    end
end
% matrix B is saved in an excell file
xlswrite('B.xls',B);
disp(['matrix B is calculated']);

% Condition number kappa
% a large kappa indicats an ill conditioned problem
kappa = norm(B)*norm(pinv(B));

%% CALIBRATION OF TEST SETUP OR A MEASUREMENT
% 1 = calculation of the particle size distrubution
based on a measurement
% 2 = calibration of test setup

kalibratie = 2;

%% SOLVING MINIMALISATION PROBLEM WITH REGULARISATION
% This sections uses a long calculation time

% Part 1: Finding the optimum alpha

% interval of alphas
mina=log10(0.001);
maxa=log10(0.1);
aantala=6;
alphas=logspace(mina,maxa,aantala);

% number of iterative calculations of a solution for
each alpha
% I recommend 4 to 6 in order to get a proper L-curve
aantalberekeningen = 5;

% Regularisation matrix L
% One option is the identity matrix
L = zeros(PSD,PSD);
for i=1:PSD
    L(i,i)=1;
end

% Iterative calculation of the solution
% The first and last two PSD points are set to zero.
This is to force the
% calculated PSD curve to go smoothly to zero when a
second order
% derivative regularization matrix is used.
```

```
oplvoorgegalpha = zeros(PSD-4,aantalberekeningen);
for tellera=0:aantala
    for iteratie = 1:aantalberekeningen
         if iteratie <2          % for the first
iteration
            if kalibratie <2     % if its not a
calibration
                goedeinB=round(PSD*2/3);     % start with
calculating the smallest particles distribution
            else
                goedeinB = PSD-4;            % for a
calibration, all the particles are considered from the
first iteration
            end
            xexp = [1:1:goedeinB];
            % first the PSD is determined without
regularization. This
            % solution is then used as initial value
with regularization
            if tellera>0
                for i = 1:goedeinB
                    xexp(i)= oplvoorgegalpha(i,tellera);
                end
            else
                for i=1:goedeinB
                    xexp(i)=0;               % without
regularization: alpha = 0
                end
            end
         else
            goedeinB=PSD-4;      % not the first
iteration => consider all particle sizes
            for i = 1:PSD-4
                xexp(i)=oplvoorgegalpha(i,tellera+1);    %
initial value = result previous iteration
            end
        end

        % iteration itself
        if tellera>0             % with regularization,
alpha is not zero
            options = optimset('MaxFunEvals',
1000000000,'MaxIter', 1000000000,
'PlotFcns',@optimplotfval);
            [oplminimalisatie,fval] = fminsearch(@(y)
teminimaliseren(y,IR,B,alphas(tellera),L,PSD,teller(foto
nr,1),fotonr,goedeinB),xexp,options);
            tekstvoorscherm = ['alpha ',
num2str(alphas(tellera)), ' yet to do ',
num2str((aantala-
```

```
tellera)*aantalberekeningen+aantalberekeningen-iteratie),
' funval ', num2str(fval)];
            disp(tekstvoorscherm);
        else
            % alpha is 0, no reularization
            options = optimset('MaxFunEvals',
1000000000,'MaxIter', 1000000000,
'PlotFcns',@optimplotfval);
            [oplminimalisatie,fval] = fminsearch(@(y)
teminimaliseren(y,IR,B,0,L,PSD,teller(fotonr,1),fotonr,g
oedeinB),xexp,options);
            tekstvoorscherm = ['alpha ', num2str(0), '
yet to do ', num2str((aantala-
tellera)*aantalberekeningen+aantalberekeningen-iteratie),
' funval ', num2str(fval)];
            disp(tekstvoorscherm);
        end

        % writing solution to matrix 'oplvoorgegalpha'
        for i=1:goedeinB
            oplvoorgegalpha(i,tellera+1) =
sqrt(oplminimalisatie(i))^2;     % sqrt^2 in order to
cancel out negative values
        end
    end
end

%% 2) WRITING TO OUTPUT FILE
% output file = to be exported to excel
output = zeros(PSD+10+teller(fotonr,1)+10,aantala+2);

% first column = particle sizes
for i=1:PSD
    output(i,1)=R(1,i);
end
% second to ... column = calculated PSD for each
corresponding alpha
for tellera=0:aantala
    % 2a) The PSD
    for i=3:PSD-2
        output(i,tellera+2)=(oplvoorgegalpha(i-
2,tellera+1))^2;
    end

    % 2b) The corresponding alpha
    if tellera>0
        output(PSD+2,tellera+2) = alphas(tellera);
    else
        output(PSD+2,2) = 0;
    end
```

```
    % 2c) norm(I-B*x)
    tijdelijkevector = zeros(PSD-4,1); % vector with PSD
    for i=3:PSD-2
        tijdelijkevector(i-2,1)=output(i,tellera+2);
    end
    tijdelijkevector2 = zeros(teller(fotonr,1),1); %
vector with measured image at first column
    for i=1:teller(fotonr,1)
        tijdelijkevector2(i,1)=IR(i,fotonr);
    end
    tijdelijkevector3 = B*tijdelijkevector; % vector
with calculated image at other columns
    for i=1:teller(fotonr,1)
        tijdelijkevector3(i,1)=tijdelijkevector3(i,1);
    end
    output(PSD+3,tellera+2) = norm(tijdelijkevector2-
tijdelijkevector3);

    % 2d) norm(L*x)
    tijdelijkevector = zeros(PSD,1);
    for i=1:PSD
        tijdelijkevector(i,1)=output(i,tellera+2);
    end
    output(PSD+4,tellera+2) = norm(L*tijdelijkevector);
end
% The optimum solution is at the corner of the L-curve:
the plot of
% norm(L*x) as a function of norm(I-B*x)

% 2e) calculated approximation of images (overwriting
first ones)
beelden = B*(oplvoorgegalpha.^2);
for i=1:teller(fotonr,1)
    output(PSD+10+i,1)=IR(i,fotonr);
    for j=0:aantala
        output(PSD+10+i,2+j)=beelden(i,j+1);
    end
end
% scattering angles
for i=1:teller(fotonr,1)
    output(PSD+10+i,3+aantala)=teta(i,fotonr);
end

% output exported in excel
xlswrite('output PSD.xlsx',output);
disp('Output file is ready');
```

Appendix E

This function is the number which needs to be minimized in the fminsearch function used in Annex B.

```
function uitkomst =
teminimaliseren(xexp,IR,B,alpha,L,PSD,aantalI,fotonr,goe
deinB)
% This function is the number which needs to be
minimized in the fminsearch function

x1=zeros(PSD-4,1);
for i=1:goedeinB
    x1(i,1)=(xexp(i))^2;            % The PSD we are
looking for is xexp^2. This is implemented to evade
negative values in the PSD
end

x2 = zeros(PSD,1);
for i=3:2+goedeinB
    x2(i,1)=(xexp(i-2))^2;
end

meting = zeros(aantalI,1);
berekening1 = B*x1;                 % The SALS image
corresponding with PSD x1
berekening2 = zeros(aantalI,1);
for i=1:aantalI
    meting(i,1)=IR(i,fotonr);       % The measured SALS
image
    berekening2(i,1)=berekening1(i,1)-
berekening1(1,1);     % The diffference between the
calculated and the measured image
end

% uitkomst = difference measured image & calculated
image + regularization
uitkomst = norm(meting-berekening1)+alpha^2*norm(L*x2);

end
```

Appendix F

The Matlab code Mie_S12, Mie_abcd, and Mie_pt are used to calculate the Mie scattering functions S1 and S2. The code was written by Christian Mätzler [436].

```
function result = Mie_S12(m, x, u)

% Computation of Mie Scattering functions S1 and S2
% for complex refractive index m=m'+im",
% size parameter x=k0*a, and u=cos(scattering angle),
% where k0=vacuum wave number, a=sphere radius;
% s. p. 111-114, Bohren and Huffman (1983) BEWI:TDD122
% C. Mätzler, May 2002

% uses Mie_abcd
% uses Mie_pt

nmax=round(2+x+4*x^(1/3));
abcd=Mie_abcd(m,x);
an=abcd(1,:);
bn=abcd(2,:);
pt=Mie_pt(u,nmax);
pin =pt(1,:);
tin=pt(2,:);
n=(1:nmax);
n2=(2*n+1)./(n.*(n+1));
pin=n2.*pin;
tin=n2.*tin;
S1=(an*pin'+bn*tin');
S2=(an*tin'+bn*pin');
result=[S1;S2];


function result = Mie_abcd(m,x)

% Computes a matrix of Mie coefficients, a_n, b_n, c_n,
d_n,
% of orders n=1 to nmax, complex refractive index
m=m'+im",
% and size parameter x=k0*a, where k0= wave number
% in the ambient medium, a=sphere radius;
```

```
% p. 100, 477 in Bohren and Huffman (1983) BEWI:TDD122
% C. Maetzler, June 2002

nmax=round(2+x+4*x^(1/3));
n=(1:nmax); nu = (n+0.5); z=m.*x; m2=m.*m;
sqx= sqrt(0.5*pi./x); sqz= sqrt(0.5*pi./z);
bx = besselj(nu, x).*sqx;
bz = besselj(nu, z).*sqz;
yx = bessely(nu, x).*sqx;
hx = bx+i*yx;
b1x=[sin(x)/x, bx(1:nmax-1)];
b1z=[sin(z)/z, bz(1:nmax-1)];
y1x=[-cos(x)/x, yx(1:nmax-1)];
h1x= b1x+i*y1x;
ax = x.*b1x-n.*bx;
az = z.*b1z-n.*bz;
ahx= x.*h1x-n.*hx;
an = (m2.*bz.*ax-bx.*az)./(m2.*bz.*ahx-hx.*az);
bn = (bz.*ax-bx.*az)./(bz.*ahx-hx.*az);
cn = (bx.*ahx-hx.*ax)./(bz.*ahx-hx.*az);
dn = m.*(bx.*ahx-hx.*ax)./(m2.*bz.*ahx-hx.*az);
result=[an; bn; cn; dn];


function result=Mie_pt(u,nmax)

% pi_n and tau_n, -1 <= u= cos? <= 1, n1 integer from 1
to nmax
% angular functions used in Mie Theory
% Bohren and Huffman (1983), p. 94 - 95

p(1)=1;
t(1)=u;
p(2)=3*u;
t(2)=3*cos(2*acos(u));
for n1=3:nmax,
p1=(2*n1-1)./(n1-1).*p(n1-1).*u;
p2=n1./(n1-1).*p(n1-2);
p(n1)=p1-p2;
t1=n1*u.*p(n1);
t2=(n1+1).*p(n1-1);
t(n1)=t1-t2;
end;
result=[p;t];
```

References

[1] EFNARC, "Specifications and Guidelines for Self-compacting Concrete," EFNARC, Farnham, England, UK2002.

[2] G. De Schutter, P. J. M. Bartos, P. Domone, and J. Gibbs, *Self-compacting concrete*. Dunbeath, Scotland, UK: Whittles Publishing, 2008.

[3] K. Ozawa, K. Maekawa, M. Kunishima, and H. Okamura, "Development of high performance concrete based on the durability design of concrete structures," presented at the Second East-Asia and Pacific Conference on Structural Engineering and Construction, Chiang-Mai, Thailand, 1989.

[4] Z. Li, *Advanced Concrete Technology*. Hoboken, New Jersey: Jon Wiley & Sons, 2011.

[5] K. H. Khayat, C. Hu, and H. Monty, "Stability of self-consolidating concrete, advantages, and potential applications," presented at the First International RILEM Symposium on Self-Compacting Concrete, Stockholm, Sweden, 1999.

[6] BIBM - CEMBUREAU - EFCA - EFNARC - ERMCO, "The European Guidelines for Self-Compacting Concrete - Specification, Production and Use," 2005.

[7] D. Constantiner and J. A. Daczko, "Not all applications are created equal; selecting the appropriate SCC performance targets," presented at the First North American Conference on the Design and Use of Self-Consolidating Concrete, Evanston, IL, USA, 2002.

[8] C. Shi, Z. Wu, K. Lv, and L. Wu, "A review on mixture design methods for self-compacting concrete," *Construction and Building Materials,* vol. 84, pp. 387-398, 2015.

[9] H. Okamura and K. Ozawa, "Mix design method for self-compacting concrete," *Concrete Library of Japan Society of civil Engineers,* vol. 25, pp. 107-120, 1995.

[10] P. Domone, "Proportioning of self-compacting concrete - the UCL method," University College London (UCL), Department of Civil, Environmental and Geomatic Engineering, London, UK2009.

[11] G. F. Kheder and R. S. AL Jadiri, "New method for proportioning self-consolidating concrete based on compressive strength requirements.," *ACI Materials Journal,* vol. 107, pp. 490-497, 2010.

[12] C. Hwang and C. Tsai, "The effect of aggregate packing types on engineering properties of self-consolidating concrete," presented at the 1st International Symposium on Design, Performance and Use of Self-Consolidating Concrete (SCC'2005), Changsha, China, 2005.

[13] N. Su, K.-C. Hsu, and H.-W. Chai, "A simple mix design method for self-compacting concrete," *Cement and Concrete Research,* vol. 31, pp. 1799-1807, 2001.

[14] T. Sedran and F. De Larrard, "Optimization of self compacting concrete thanks to packing model," presented at the First International RILEM Symposium on Self-Compacting Concrete, Stockholm, Sweden, 1999.

[15] K. H. Khayat, A. Ghezal, and M. S. Hadriche, "Factorial design model for proportioning self-consolidating concrete," *Materials and Structures,* vol. 32, pp. 679-686, 1999.

[16] A. W. Saak, H. M. Jennings, and S. P. Shah, "New methodology for designing self-compacting concrete," *ACI Materials Journal,* vol. 98, pp. 429-439, 2001.

[17] L. Ferrara, Y.-D. Park, and S. P. Shah, "A method for mix-design of fiber-reinforced self-compacting concrete," *Cement and Concrete Research,* vol. 37, pp. 957-971, 2007.

[18] L. Martinie, P. Rossi, and N. Roussel, "Rheology of fiber reinforced cementitious materials: classification and prediction," *Cement and Concrete Research,* vol. 40, pp. 226-234, 2010.

[19] L. Ferrara, P. Bamonte, A. Caverzan, A. Musa, and I. Sanal, "A comprehensive methodology to test the performance of Steel Fibre Reinforced Self-Compacting Concrete (SFR-SCC)," *Construction and Building Materials,* vol. 37, pp. 406-424, 2012.

[20] S. Grünewald, F. Laranjeira, J. C. Walraven, A. Aguado, and C. Molins, "Improved Tensile Performance with Fiber Reinforced Self-compacting Concrete," in *High Performance Fiber Reinforced Cement Composites 6*. vol. 2, G. J. Parra-Montesinos, H.-W. Reinhardt, and A. E. Naaman, Eds., ed: Springer, 2012, pp. 51-58.

[21] J. Yammine, M. Chaouche, M. Guerinet, M. Moranville, and N. Roussel, "From ordinary rheology concrete to self-compacting concrete: A transition between frictional and hydrodynamic interactions," *Cement and Concrete Research,* vol. 38, pp. 890-896, 2008.

[22] S. Kubens, "Interaction of cement and admixtures and its effect on rheological properties," Doctoral thesis, Bauhaus-Universität Weimar, Götingen, 2010.

[23] W. Schmidt, "Design concepts for the robustness improvement of self-compacting concrete - Effects of admixtures and mixture components on the rheology and early hydration at varying temperatures," Doctoral thesis, Eindhoven University of Technology, Eindhoven, The Netherlands, 2014.

[24] K. Lesage, "Interactions between cement and combined concrete admixtures - The influence on cement paste rheology," Doctoral thesis, Department of Civil Engineering, University of Leuven, Leuven, Belgium, 2014.

[25] H. A. Barnes, J. F. Hutton, and K. Walters, *An introduction to rheology*. Amsterdam, The Netherlands: Elsevier Science Publishers B.V., 1989.

[26] B. D. Fitz and S. Andjelic, "Real-time monitoring of segmental dynamics during crystallization of poly(L(–)-lactide) by simultaneous DRS/SALS technique," *Polymer,* vol. 44, pp. 3031-3036, 2003.

[27] International Organization for Standardization, "ISO 20998-1: Measurement and characterization of particles by acoustic methods - Part 1: Concepts and procedures in ultrasonic attenuation spectroscopy," ed. Geneva, Switzerland: ISO, 2006.

[28] International Organization for Standardization, "ISO 20998-2: Measurement and characterization of particles by acoustic methods - Part 2: Guidelines for linear theory," ed. Geneva, Switzerland: ISO, 2013.

[29] A. Richter, F. Babick, and S. Ripperger, "Polydisperse particle size characterization by ultrasonic attenuation spectroscopy for systems of diverse acoustic contrast in the large particle limit," *The Journal of the Acoustical Society of America,* vol. 118, pp. 1394-1405, 2005.

[30] S. Nunes, H. Figueiras, P. M. Oliveira, J. S. Coutinho, and J. Figueiras, "A Methodology to assess robustness of SCC mixtures," *Cement and Concrete Research,* vol. 36, pp. 2115-2122, 2006.

[31] P. Billberg and M. Westerholm, "Robustness of fresh VMA-modified SCC to varying aggregate moisture," *NCR Journal,* vol. 38, pp. 103-119, 2008.

[32] P. Billberg, "Increase of SCC robustness to varying aggregate moisture content using VMA," presented at the Second International Symposium on Design, Performance and Use of Self Consolidating Concrete, Beijing, China, 2009.

[33] A. K. H. Kwan and I. Y. T. Ng, "Optimum superplasticiser dosage and aggregate proportions for SCC," *Magazine of Concrete Research,* vol. 61, pp. 281-292, 2009.

[34] W. Schmidt, H. J. H. Brouwers, H.-C. Kühne, and B. Meng, "Influences of superplasticizer modification and mixture composition on the performance of self-compacting concrete at varied ambient temperatures," *Cement & Concrete Composites,* vol. 49, pp. 111-126, 2014.

[35] W. Brameshuber and S. Uebachs, "The influence of the temperature on the rheological properties of self-compacting concrete," presented at the 3rd International RILEM Symposium on Self Compacting Concrete, Reykjavik, Iceland, 2003.

[36] D. Bonen, Y. Deshpande, J. Olek, L. Shen, L. Struble, D. A. Lange, and K. H. Khayat, "Chapter 1. Robustness of SCC," in *Self-consolidating concrete*, D. A. Lange, Ed., ed Urbana, IL, U.S.A.: The Center for Advanced Cement Based Materials (ACBM), 2007, pp. 4-22.

[37] S. Naji, S.-D. Hwang, and K. H. Khayat, "Robustness of self-consolidating concrete incorporating different viscosity-enhancing admixtures," *ACI Materials Journal,* vol. 108, pp. 432-438, 2011.

[38] H. Höveling, "Robustheit von selbstverdichtendem Beton (SVB) - Robustness of self-compacting concrete (SCC), in German," Doctoral thesis, Faculty of Civil Engineering and Geodesy, University of Hannover, Hannover, Germany, 2006.

[39] M. Westerholm, B. Lagerblad, J. Silfwerbrand, and E. Forssberg, "Influence of fine aggregate characteristics on the rheological properties of mortars," *Cement & Concrete Composites,* vol. 30, pp. 274-282, 2008.

[40] D. H. Bager, M. R. Geiker, and R. M. Jensen, "Rheology of self-compacting mortars - Influence of particle grading," *Nordic Concrete Research,* vol. 26, 2001.

[41] P. F. G. Banfill, "Rheological methods for assessing the flow properties of mortar and related materials," *Construction and Building Materials,* vol. 8, pp. 43-50, 1994.

[42] K. Obla, "Variation in concrete performance due to aggregates," *Concrete in Focus,* vol. 10, pp. 9-14, 2011.

[43] L. F. Kristensen, "Influence of different Danish glacial deposited sands on SCC properties," presented at the Fifth North American Conference on the Design and Use of Self-Consolidating Concrete, Chicago, IL, USA, 2013.

[44] L. Lei and J. Plank, "A study on the sensibility of conventional vinyl ether-based polycarboxylate superplasticizers towards diferent clay minerals," presented at the Third International Symposium on Design, Performance and Use of Self-Consolidating Concrete, Xiamen, China, 2014.

[45] K. Juvas, A. Käppi, K. Salo, and E. Nordenswan, "The effects of cement variations on concrete workability," *Nordic Concrete Research,* vol. 26, pp. 39-46, 2001.

[46] S. Kubens and O. Wallevik, "Interaction of cement and admixtures - the influence of cement deliveries on rheological properties," presented at the Ibausil - Internationale Baustofftagung, Weimar, Germany, 2006.

[47] S. Nunes, P. M. Oliveira, J. S. Coutinho, and J. Figueiras, "Rheological characterization of SCC mortars and pastes with changes induced by cement delivery," *Cement and Concrete Composites,* vol. 33, pp. 103-115, 2011.

[48] O. H. Wallevik, S. Kubens, and F. Müller, "Influence of cement-admixture interaction on the stability of production properties of SCC," presented at the 5th International RILEM Symposium on Self-Compacting Concrete, Ghent, Belgium, 2007.

[49] S. Kubens, H. Peng, S. Oesterheld, and O. H. Wallevik, "Some effects of silica fume on variations in rheology of mortar due to production date of cement," *Annual Transactions of the Nordic Rheology Society,* vol. 16, p. 4, 2008.

[50] H. Vikan, H. Justnes, F. Winnefeld, and R. Figi, "Correlating cement characteristics with rheology of paste," *Cement and Concrete Research,* vol. 37, pp. 1502-1511, 2007.

[51] S. Nunes, P. Milheiro-Oliveira, J. Sousa Coutinho, and J. Figueiras, "Rheological characterization of SCC mortars and pastes with changes induced by cement delivery," *Cement & Concrete Composites,* vol. 33, pp. 103-115, 2011.

[52] P.-C. Aïtcin and R. J. Flatt, *Science and technology of concrete admixtures*. Amsterdam: Elsevier, 2016.

[53] K. Yamada, S. Ogawa, and T. Takahashi, "Improvement of the compatibility between cement and superplasticizer by optimizing the chemical structure of the polycarboxylate-type superplasticizer," presented at the Second International Symposium on Self-Compacting Concrete, Tokyo, Japan, 2001.

[54] K. Yamada and S. Hanehara, "Interaction mechanism of cement and superplasticizers - The roles of polymer adsorption and ionic conditions of aqueous phase," *Concrete Science and Engineering,* vol. 3, pp. 135-145, 2001.

[55] K. Yoshioka, E. Sakai, M. Daimon, and A. Kitahara, "Role of steric hindrance in the performance of superplasticizers for concrete," *Journal of the American Ceramic Society,* vol. 80, pp. 2667-2671, 1997.

[56] E. Sakai, K. Yamada, and A. Ohta, "Molecular structure and dispersion-adsorption mechanisms of comb-type superplasticizers used in Japan," *Journal of Advanced Concrete Technology,* vol. 1, pp. 16-25, 2003.

[57] Ö. Petersson, "Part VII - Mixing," in *Self-Compacting Concrete - State-of-the-Art Report of RILEM TC 174-SCC*, A. Skarendahl and Ö. Petersson, Eds., ed: RILEM, 2000, pp. 69-75.

[58] P. Billberg, "Form pressure generated by self-compacting concrete - Influence of thixotropy and structural behaviour at rest," Doctoral thesis, School of Architecture and the Built Environment Division of Concrete Structures, Royal Institute of Technology, Stockholm, Sweden, 2006.

[59] J. W. Rigueira, E. García-Taengua, and P. Serna-Ros, "Robustness of SCC dosages and its implications on large-scale production," presented at the 5th International RILEM Symposium on Self-Compacting Concrete, Ghent, Belgium, 2007.

[60] J. W. Rigueira, E. García-Taengua, and P. Serna-Ros, "Self-consolidating concrete robustness in continuous production regarding fresh and hardened state properties," *ACI Materials Journal,* vol. 106, pp. 301-307, 2009.

[61] D. Gálvez-Moreno, A. Durán-Herrera, J. R. González-López, and K. H. Khayat, "Robustness of powder-type SCC with fly ash and limestone crushed aggregates," presented at the 8th International RILEM Symposium on Self-Compacting Concrete, Washington D.C., USA, 2016.

[62] K. Obla and C. L. Lobo, "Mixing water control," *Concrete in Focus,* vol. 10, pp. 23-27, 2011.

[63] ACI Committee 117, "Standard specification for tolerances for concrete construction and materials (ACI 117-90)," ed. Farmington Hills: American Concrete Institute, 1990.

[64] ASTM, "ASTM C94/C94M-04 Standard specification for ready-mixed concrete," ed. West Consohocken, PA, USA: ASTM, 2004.

[65] European Committee for Standardization, "EN 206-1 Concrete - part 1: Specification, performance, production and conformity," ed. Brussels, Belgium: CEN, 2000.

[66] A. K. H. Kwan and I. Y. T. Ng, "Improving performance and robustness of SCC by adding supplementary cementitious materials," *Construction and Building Materials,* vol. 24, pp. 2260-2266, 2010.

[67] J. Ortiz, A. Aguado, L. Agullo, T. García, and M. Zermeño, "Influence of environmental temperature and moisture content of aggregates on the workability of cement mortar," *Construction and Building Materials,* vol. 23, pp. 1808-1814, 2009.

[68] L. Huanjian, H. Fali, T. Yanbin, L. Linxiang, Y. Zhonglai, and X. Yongjiang, "Coupled effect of temperature and time on rheology of SCC used in CRTSIII slab ballastless track," presented at the 8th International RILEM Symposium on Self-Compacting Concrete, Washington D.C., USA, 2016.

[69] J.-Y. Petit, K. Khayat, H., and E. Wirquin, "Coupled effect of time and temperature on variations of yield value of highly flowable mortar," *Cement and Concrete Research,* vol. 36, pp. 832-841, 2006.

[70] K. Yamada, T. Yanagisawa, and S. Hanehara, "Influence of temperature on the dispersibility of polycarboxylate type superplasticizer for highly fluid concrete," presented at the First International RILEM Symposium on Self-Compacting Concrete, Stockholm, Sweden, 1999.

[71] C. Jolicoeur and M.-A. Simard, "Chemical admixture-cement interactions: phenomenology and physico-chemical concepts," *Cement and Concrete Composites,* vol. 20, pp. 87-101, 1998.

[72] J. Roncero, R. Gettu, E. Vazquez, and J. M. Torrents, "Effect of superplasticizer content and temperature on the fluidity and settings of cement pastes," presented at the International RILEM Conference on the Role of Admixtures in High Performance Concrete, Monterrey, Mexico, 1999.

[73] H. G. Svavarasson and O. H. Wallevik, "Ceothermal well cementing: the effect of temperature and time on workability loss," *Annual Transactions of the Nordic Rheology Society,* vol. 12, pp. 123-126, 2004.

[74] M. Nehdi and S. Al Martini, "Estimating time and temperature dependent yield stress of cement paste using oscillatory rheology and genetic algorithms," *Cement and Concrete Research,* vol. 39, pp. 1007-1016, 2009.

[75] C. Jolicoeur, J. Sharman, N. Otis, A. Lebel, M.-A. Simard, and M. Pagé, "The influence of temperature on the rheological properties of superplasticized cement pastes," *ACI Special Publication,* vol. SP 173-20, pp. 379-406, 1997.

[76] J.-Y. Petit, E. Wirquin, K. H. Khayat, and Y. Vanhove, "Coupled effect of temperature and superplasticizer on rheological properties of SCC mortar," presented at the 5th International RILEM Symposium on Self-Compacting Concrete, Ghent, Belgium, 2007.

[77] F. Göller, S. Dikty, and D. Hamada, "The relationship between retention stability and chemical structure of PCE," presented at the 9th ACI International Conference on Superplasticizers and Other Chemical Admixtures in Concrete, Seville, Spain, 2009.

[78] W. Schmidt, J. Brouwers, H.-C. Kühne, and B. Meng, "Effects of superplasticizer and viscosity-modifying agent on fresh concrete performance of SCC at varied ambient temperatures," presented at the Design, Production and Placement of Self-Consolidating Concrete, Montreal, Canada, 2010.

[79] M. Yurugi, G. Sakai, and N. Sakata, "Viscosity agent and mineral admixtures for highly fluidized concrete," presented at the International Conference on Concrete Under Severe Conditions: Environment and Loading, 1995.

[80] S. Al-Martini and M. Nehdi, "Coupled effects of time and high temperature on rheological properties of cement pastes incorperating various

superplasticizers," *Journal of Materials in Civil Engineering,* vol. 21, pp. 392-401, 2009.

[81] J.-Y. Petit, K. H. Khayat, and E. Wirquin, "Methodology to couple time-temperature effects on rheology of mortar," *ACI Materials Journal,* vol. 105, pp. 342-349, 2008.

[82] D. Feys, R. Verhoeven, and G. De Schutter, "Non-reversible time-dependent rheological properties of fresh SCC," presented at the 5th International RILEM Symposium on Self-Compacting Concrete, Ghent, Belgium, 2007.

[83] D. Feys, R. Verhoeven, and G. De Schutter, "Steady-state rheological properties of fresh self-compacting concrete and their evolution in time," *Annual Transactions of the Nordic Rheology Society,* vol. 15, pp. 35-41, 2007.

[84] A. A. Asghari, A. M. Ley Hernandez, D. Feys, and G. De Schutter, "Which parameters, other than the water content, influence the robustness of cement paste with SCC consistency?," *Construction and Building Materials,* vol. 124, pp. 95-103, 2016.

[85] L. G. Li and A. K. H. Kwan, "Concrete mix design based on water film thickness and paste film thickness," *Cement and Concrete Composites,* vol. 39, pp. 33-42, 2013.

[86] I. M. Krieger, "Rheology of monodisperse latices," *Advances in Colloid and Interface Science,* vol. 3, pp. 111-136, 1972.

[87] D. Lowke and P. Schiessl, "Robustness of cement suspensions - superplasticizer adsorption, particle separation and interparticle forces," presented at the 3rd International RILEM Symposium on Rheology of Cement Suspensions such as Fresh Concrete, Reykjavik, Iceland, 2009.

[88] P. H. Billberg, "Influence of powder type and VMA combination on certain key fresh properties of SCC," in *9th International Symposium on High Performance Concrete*, Rotorua, New Zealand, 2011.

[89] D. Lowke, "Sedimentationsverhalten und Robustheit Selbstverdichtender Betone (Segregation resistance and robustness of self-compacting concrete, in german)," Doctoral thesis, Fakultät für Bauingenieur- und Vermessung, Technical University Munich, Munich, Germany, 2012.

[90] F. V. Müller, O. H. Wallevik, and K. H. Khayat, "Considerations for designing low-powder self-compacting concrete, ECO-SCC," presented at the International Symposium on Environmentally Friendly Concrete - ECO-Crete, Reykjavik, Iceland, 2014.

[91] L. Shen, H. B. Jovein, S. Shen, and M. Li, "Effects of aggregate properties and concrete rheology on stability robustness of self-consolidating concrete," *Journal of Materials in Civil Engineering,* vol. 27, p. 04014159, 2015.

[92] S. Nunes, P. M. Oliveira, J. S. Coutinho, and J. Figueiras, "Evaluation of SCC Mixture Robustness," presented at the 5th International RILEM Symposium on Self-Compacting Concrete, Ghent, Belgium, 2007.

[93] D. Bonen, Y. Deshpande, J. Olek, L. Shen, L. Struble, D. A. Lange, and K. Khayat, "Robustness of self-consolidating concrete," presented at the 5th

International RILEM Symposium on Self-Compacting Concrete, Ghent, Belgium, 2007.

[94] J.-E. Jonasson, M. Nilsson, S. Utsi, P. Simonsson, and M. Emborg, "Designing robust SCC for industrial construction with cast in place concrete," presented at the Second North American Conference on the Design and Use of Self-Consolidating Concrete; Fourth International RILEM Symposium on Self-Compacting Concrete, Chicago, IL, USA, 2005.

[95] L. Shen, H. B. Jovein, and M. Li, "Measuring static stability and robustness of self-consolidating concrete using modified segregation probe," *Construction and Building Materials,* vol. 70, pp. 210-216, 2014.

[96] P.-C. Nkinamubanzi and P.-C. Aïtcin, "Cement and superplasticizer combinations: Compatibility and robustness," *Cement, Concrete and Aggregates,* vol. 26, pp. 102-109, 2004.

[97] A. S. Georgiadis, K. K. Sideris, and N. S. Anagnostopoulos, "Properties of SCC produced with limestone filler or viscosity modifying admixture," *Journal of Materials in Civil Engineering,* vol. 22, pp. 352-360, 2010.

[98] R. Bouras, M. Chaouche, and S. Kaci, "Influence of viscosity-modifying admixtures on the thixotropic behaviour of cement pastes," *Applied Rheology,* vol. 18, pp. 45604-1 - 45604-8, 2008.

[99] S.-D. Hwang and K. H. Khayat, "Performance of hardened self-consolidating concrete designed for repair applications," in *SP-233: Workability of SCC: Roles of its Constituents and Measurement Techniques*, C. Shi and K. H. Khayat, Eds., ed: American Concrete Institute, 2006.

[100] R. Haldenwang and V. G. Fester, "The influence of different superplasticisers on the flowability and reproducibility of a SCC mix," presented at the 9th International Symposium on High Performance Concrete, Rotorua, New Zealand, 2011.

[101] V. B. Bosiljkov, N. Gasperic, and L. Zevnik, "New type of superplasticizer for SCC mixtures with increased robustness," presented at the 7th International RILEM Symposium on Self-Compacting Concrete, Paris, France, 2013.

[102] M. Gruber, P. Chuah, and S. Kalahasti, "Robustness of lignosulfonate- versus polycarboxylate ether based chemical admixtures in concrete," presented at the 14th International Congress on the Chemistry of Cement (ICCC 2015), Beijing, China, 2015.

[103] L. Zevnik and M. Bellotto, "Influence of the mixing order procedure on the workability of concrete," presented at the 7th International RILEM Symposium on Self-Compacting Concrete, Paris, France, 2013.

[104] S. Grünewald and J. C. Walraven, "Robust flowable concrete with viscosity agents," presented at the International RILEM Conference on Application of superabsorbent polymers and other new admixtures in concrete construction, Dresden, Germany, 2014.

[105] N. Sakata, S. Yanai, M. Yoshizaki, A. Phyfferoen, and H. Monty, "Evaluation of S-657 Biopolymer as a new viscosity-modifying admixture for self-compacting concrete," presented at the Second International Symposium on Self-Compacting Concrete, Tokyo, Japan, 2001.

[106] A. Phyfferoen, H. Monty, B. Skags, N. Sakata, S. Yanai, and M. Yoshizaki, "Evaluation of the biopolymer, diutan gum, for use in self-compacting concrete," presented at the First North American Conference on the Design and Use of Self-Consolidating Concrete, Evanston, IL, USA, 2002.

[107] S. Grünewald and J. C. Walraven, "The effect of viscosity agents on the characteristics of self-compacting concrete," presented at the Second North American Conference on the Design and Use of Self-consolidating Concrete / 4th International RILEM Symposium on Self-Compacting Concrete, Addison, IL, USA, 2005.

[108] P. L. Domone, "Self-compacting concrete: An analysis of 11 years of case studies," *Cement & Concrete Composites,* vol. 28, pp. 197-208, 2006.

[109] N. S. Berke, C. R. Cornman, A. A. Jeknavorian, G. F. Knight, and O. Wallevik, "The effective use of superplasticizers and viscosity-modifying agents in self-consolidating concrete," presented at the First North American Conference on the Design and Use of Self-Consolidating Concrete, Evanston, IL, USA, 2002.

[110] N. Sakata, S. Yanai, K. Yokozeki, and K. Maruyama, "Study on new viscosity agent for combination use type of self-compacting concrete," *Journal of Advanced Concrete Technology,* vol. 1, pp. 37-41, 2003.

[111] L. Garcia, M. Valcuende, S. Balasch, and J. Fernández-Lebrez, "Study of robustness of self-compacting concretes made with low fines content," *Journal of Materials in Civil Engineering,* vol. 25, pp. 497-503, 2013.

[112] R. Gettu, S. N. Shareef, and K. J. D. Ernest, "Evaluation of the robustness of SCC," *The Indian Concrete Journal,* vol. 83, pp. 13-19, 2009.

[113] T. H. Phan, "Thixotropic behaviour of self-compacting pastes (in french)," presented at the XXIVèmes Rencontres Universitaires de Génie Civil 2006, 2006.

[114] N. Sakata, K. Maruyama, and M. Minami, "Basic properties and effects of welan gum on self-consolidating concrete," presented at the International RILEM Conference on Production Methods and Workability of Concrete, Glasgow, UK, 1996.

[115] T. Shindoh and Y. Matsouka, "Development of combination-type self-compacting concrete and evalation test methods," *Journal of Advanced Concrete Technology,* vol. 1, pp. 26-36, 2003.

[116] M. Yurugi and G. Sakai, "A Proven QA System for Flowable Concrete," *Concrete International,* vol. 20, pp. 44-48, 1998.

[117] A. Leemann and F. Winnefeld, "The effect of viscosity modifying agents on mortar and concrete," *Cement & Concrete Composites,* vol. 29, pp. 341-349, 2007.

[118] F. Van Der Vurst and G. De Schutter, "Improving the robustness of fresh self-compacting concrete using small quantities of fine additions," presented at the Third International Symposium on Design, Performance and Use of Self-Consolidating Concrete, Xiamen, China, 2014.

[119] H. J. H. Brouwers and H. J. Radix, "Self-compacting concrete: The role of the particle size distribution," presented at the First International Symposium on Design, Performance and Use of Self-Consolidating Concrete, Changsha, Hunan, China, 2005.

[120] L. Lohaus and P. Ramge, "Robustness of UHPC - A new approach for mixture proportioning," presented at the 2nd International Symposium on Ultra High Performance Concrete, Kassel, Germany, 2008.
[121] S. Joseph, S. Bishnoi, K. Van Balen, and Ö. Cizer, "Modeling the effect of fineness and filler in early-age hydration of tricalcium silicate," *Journal of the American Ceramic Society,* 2016.
[122] K. L. Scrivener and A. Nonat, "Hydration of cementitious materials, present and future," *Cement and Concrete Research,* vol. 41, pp. 651-665, 2011.
[123] W. Schmidt, L. Weba, D. Silbernagl, B. Mota, P. Höhne, H. Sturm, J. Pauli, U. Resch-Genger, and G. Steinborn, "Influences of nano effects on the flow phenomena of self-compacting concrete," presented at the 8th International RILEM Symposium on Self-Compacting Concrete, Washington D.C., USA, 2016.
[124] J. W. Bullard, H. M. Jennings, R. A. Livingston, A. Nonat, G. W. Scherer, J. S. Schweitzer, K. L. Scrivener, and J. J. Thomas, "Mechanisms of cement hydration," *Cement and Concrete Research,* vol. 41, pp. 1208-1223, 2011.
[125] J. W. Bullard, "A determination of hydration mechanism for tricalcium silicate using a kinetic cellular automaton model," *Journal of the American Ceramic Society,* vol. 91, pp. 2088-2097, 2008.
[126] S. Garrault, E. Finot, E. Lesniewska, and A. Nonat, "Study of C-S-H growth on C3S surface during its early hydration," *Materials and Structures,* vol. 38, pp. 435-442, 2005.
[127] P. Juilland, E. Gallucci, R. J. Flatt, and K. L. Scrivener, "Dissolution theory applied to the induction period in alite hydration," *Cement and Concrete Research,* vol. 40, pp. 831-844, 2010.
[128] J. S. Schweitzer, J. M. Livingston, C. Rolfs, H. W. Becker, S. Kubsky, T. Spillane, M. Castellote, and P. G. de Viedma, "In situ measurements of the cement hydration profile during the induction period," presented at the 12th International Congress on the Chemistry of Cement, Montreal, Canada, 2007.
[129] K. L. Scrivener, P. Juilland, and P. J. M. Monteiro, "Advances in understanding hydration of Portland cement," *Cement and Concrete Research,* vol. 78, pp. 38-56, 2015.
[130] D. Ménétrier, I. Jawed, T. S. Sun, and J. Skalny, "ESCA and SEM studies on early C3S hydration," *Cement and Concrete Research,* vol. 9, pp. 473-482, 1979.
[131] J. M. Makar and G. W. Chan, "End of induction period in ordinary portland cement as examined by high-resolution scanning electron microscopy," *Journal of the American Ceramic Society,* vol. 91, pp. 1292-1299, 2008.
[132] A. Nonat, "Modelling hydration and setting of cement," *Ceramics,* vol. 92, pp. 247-257, 2005.
[133] J. J. Thomas, "The instantaneous apparent activation energy of cement hydration measured using a novel calorimetry-based method," *Journal of the American Ceramic Society,* vol. 95, pp. 3291-3296, 2012.
[134] E. M. Gartner, J. F. Young, D. A. Damidot, and I. Jawed, "Hydration of portland cement," in *Structure and Performance of Cements*, J. Bensted and P. Barnes, Eds., ed New York, USA: Spon Press, 2002, pp. 57-113.

[135] S. Gauffinet, É. Finot, E. Lesniewska, and A. Nonat, "Observation directe de la croissance d'hydrosilicate de calcium sur des surfaces d'alite et de silice par microscopic à force atomique " *Comptes Rendus de l'Académie des Sciences - Series IIA - Earth and Planetary Science,* vol. 327, pp. 231-236, 1998.

[136] C. Plassard, E. Lesniewska, I. Pochard, and A. Nonat, "Nanoscale experimental investigation of particle interactions at the origin of the cohesion of cement," *Langmuir,* vol. 21, pp. 7263-7270, 2005.

[137] S. Garrault and A. Nonat, "Hydrated Layer Formation on Tricalcium and Dicalcium Silicate Surfaces: Experimental Study and Numerical Simulations," *Langmuir,* vol. 17, pp. 8131-8138, 2001.

[138] S. P. Jiang, J. C. Mutin, and A. Nonat, "Studies on mechanism and physico-chemical parameters at the origin of the cement setting. II. Physoci-chemical parameters determining the coagulation process," *Cement and Concrete Research,* vol. 26, pp. 491-500, 1996.

[139] L. Nachbaur, J. C. Mutin, A. Nonat, and L. Choplin, "Dynamic mode rheology of cement and tricalcium silicate pastes from mixing to setting," *Cement and Concrete Research,* vol. 31, pp. 183-192, 2001.

[140] E. Gallucci, P. Mathur, and K. L. Scrivener, "Microstructural development of early age hydration shells around cement grains," *Cement and Concrete Research,* vol. 40, pp. 4-13, 2010.

[141] A. Bazzoni, "Study of early hydration mechanisms of cement by means of electron microscospy," Doctoral Thesis, Laboratoire des Matériaux de Construction, École Polytechnique Fédérale de Lausanne, Lausanne, Switzerland, 2014.

[142] A. Zingg, "Cement - superplasticizer interaction: Link between macroscopic phenomena and microstructural data of the early cement hydration," Doctoral thesis, Department of Materials Science, Swiss Federal Institute of Technology Zurich, Rapperswil, Zurich, 2008.

[143] L. Holzer, P. Gasser, A. Kaech, M. Wegmann, A. Zingg, R. Wepf, and B. Muench, "Cryo-FIB-nanotomography for quantitative analysis of particle structures in cement suspesions," *Journal of Microscopy,* vol. 227, pp. 216-228, 2007.

[144] A. Zingg, L. Holzer, A. kaech, F. Winnefeld, J. Pakusch, S. Becker, and L. Gauckler, "The microstructure of dispersed and non-dispersed fresh cement pastes — New insight by cryo-microscopy," *Cement and Concrete Research,* vol. 38, pp. 522-529, 2008.

[145] F. Dalas, S. Pourchet, D. Rinaldi, A. Nonat, s. Sabio, and M. Mosquet, "Modification of the rate of formation and surface area of ettringite by polycarboxylate ether superplasticizers duing early C3A-CaSO4 hydration," *Cement and Concrete Research,* vol. 69, pp. 105-113, 2015.

[146] L. Holzer, F. Winnefeld, B. Lothenbach, and D. Zampini, "The early cement hydration: a multi-method approach," presented at the 11th International Congress on the Chemistry of Cement (ICCC'2003), Durban, South-Africa, 2003.

[147] K. Kovler and N. Roussel, "Properties of fresh and hardened concrete," *Cement and Concrete Research,* vol. 41, pp. 775-792, 2011.

[148] R. J. Flatt, "Towards a prediction of superplasticized concrete rheology," *Materials and Structures,* vol. 37, pp. 289-300, 2004.
[149] N. Roussel, A. Lemaître, R. J. Flatt, and P. Coussot, "Steady state flow of cement suspensions: A micromechanical state of the art," *Cement and Concrete Research,* vol. 40, pp. 77-84, 2010.
[150] P. Coussot and C. Ancey, "Rheophsical classification of concentrated suspensions and granular pastes," *Physical Review,* vol. 59, pp. 4445-4457, 1999.
[151] J. Mewis and A. J. B. Spaull, "Rheology of concentrated dispersions," *Advances in Colloid and Interface Science,* vol. 6, pp. 173-200, 1976.
[152] Z. Li, T.-a. Ohkubo, and Y. Tanigawa, "Theoretical analysis of time-dependence and thixotropy of fluidity for high fluidity concrete," *Journal of Materials in Civil Engineering,* vol. 16, pp. 247-256, 2004.
[153] R. H. Ottewill and T. Walker, "Influence of particle size on stability of polystyrene latices with an adsorbed layer of nonionic surface-active agent," *Journal of the Chemical Society, Faraday Transactions 1: Physical Chemistry in Condensed Phases,* vol. 70, pp. 917-926, 1974.
[154] S. Damodaran and A. Paraf, *Food proteins and their applications*. New York, NY, USA: Marcel Dekker, 1997.
[155] L. Shen, H. B. Jovein, and Q. Wang, "Correlating agregate properties and concrete rheology to dynamic segregation of self-consolidating concrete," *Journal of Materials in Civil Engineering,* p. 04015067, 2015.
[156] L. Shen, L. Struble, and D. A. Lange, "Modeling static segregation of self-consolidating concrete," *ACI Materials Journal,* vol. 106, pp. 367-374, 2009.
[157] D. Feys, "Interactions between rheological properties and pumping of self-compacting concrete," Doctoral thesis, Department of Civil Engineering, Ghent University, Ghent, Belgium, 2009.
[158] J. Plank, "Concrete admixtures - Where are we now and what can we expect in the future," presented at the Tagungsbericht 19. Internationale Baustofftagung IBAUSIL, Weimar, Germany, 2015.
[159] W. Schmidt, C. Weimann, and L. C. Weba, "Influences of hydration effects on the flow phenomena of concrete with admixtures," presented at the 2nd International Conference on Advances in Cement and Concrete Technology in Africa, Dar es Salaam, Tanzania, 2016.
[160] P.-C. Aïtcin and P. K. Mehta, "Effect of coarse-aggregate characteristics on mechanical properties of high-strength concrete," *ACI Materials Journal,* vol. 87, pp. 103-107, 1990.
[161] F. Winnefeld, S. Becker, J. Pakusch, and T. Götz, "Effects of the molecular architecture of comb-shaped superplasticizers on their performance in cementitious systems," *Cement & Concrete Composites,* vol. 29, pp. 251-262, 2007.
[162] T. M. Vickers, S. A. Farrington, J. R. Bury, and L. E. Brower, "Influence of dispersant structure and mixing speed on concrete slump retention," *Cement and Concrete Research,* vol. 35, pp. 1882-1890, 2005.
[163] T. Nawa, "Effect of chemical structure on steric stabilization of polycarboxylate-based superplasticizer," *Journal of Advanced Concrete Technology,* vol. 4, pp. 225-232, 2006.

[164] K. Yamada, T. Takahashi, S. Hanehara, and M. Matsuhisa, "Effects of the chemical structure on the properties of polycarboxylate-type superplasticizer," *Cement and Concrete Research,* vol. 30, pp. 197-207, 2000.

[165] J. Plank, H. Keller, P. R. Andres, and Z. Dai, "Novel organo-mineral phases obtained by intercalation of maleic anhydride-allyl ether copolymers into layered calcium aluminum hydrates," *Inorganica Chemica Acta,* vol. 359, pp. 4901-4908, 2006.

[166] L. Ferrari, J. Kaufmann, F. Winnefeld, and J. Plank, "Multi-method approach for the characterization of the behavior of superplasticizer in cement suspensions," *Cement and Concrete Research,* vol. 41, pp. 1058-1066, 2011.

[167] J. Plank and C. Hirsch, "Impact of zeta potential of early cement hydration phases on superplasticizer adsorption," *Cement and Concrete Research,* vol. 37, pp. 537-542, 2007.

[168] A. Griesser, "Cement-superplasticizer interactions at ambient temperatures," Doctoral thesis, Swiss Federal Institute of Technology, Zurich, Switzerland, 2002.

[169] J. Plank, B. Sachsenhauser, and J. de Reese, "Experimental determination of the thermodynamic parameters affecting the adsorption behaviour and dispersion effectiveness of PCE superplasticizers," *Cement and Concrete Research,* vol. 40, pp. 699-709, 2010.

[170] K. Yamada, S. Ogawa, and S. Hanehara, "Controlling of the adsorption and dispersing force of polycarboxylate-type superplasticizer by sulfate ion concentration in aqueous phase," *Cement and Concrete Research,* vol. 31, pp. 375-383, 2001.

[171] R. J. Flatt, Y. F. Houst, P. Bowen, and H. Hofmann, "Electrosteric repulsion by superplasticizers between cement particles - An overlooked mechanism?," presented at the 6th CANMET/ACI International Conference on Superplasticizers and Other Chemical Admixtures in Concrete, Nice, France, 2000.

[172] R. J. Flatt, I. Schober, E. Raphael, C. Plassard, and E. Lesniewska, "Conformation of adsorbed comb copolymer dispersants," *Langmuir,* vol. 25, pp. 845-855, 2009.

[173] T. Nawa, H. Ichiboji, and M. Kinoshita, "Influence of Temperature on Fluidity of Cement Paste Containing Superplasticizer with Polyethylene Oxide Graft Chains," presented at the 6th CANMET/ACI International Conference on Superplasticizers and Other Chemical Admixtures in Concrete, Nice, France, 2000.

[174] O. H. Wallevik, *Introduction to rheology of fresh concrete*. Reykjavik, Iceland: ICI Rheocenter, 2009.

[175] O. H. Wallevik, "Rheology - A scientific approach to develop self-compacting concrete," presented at the 3rd International Symposium on Self-Compacting Concrete, Reykjavik, Iceland, 2003.

[176] G. Heirman, L. Vandewalle, D. Van Gemert, D. Feys, G. De Schutter, B. Desmet, and J. Vantomme, "Influence of mineral additions and chemical admixtures on the rheological behaviour of powder-type SCC," presented

at the 5th International RILEM Symposium on Self-Compacting Concrete, Ghent, Belgium, 2007.
[177] J. Hot, H. Bessaies Bey, C. Brumaud, M. Duc, C. Castella, and N. Roussel, "Adsorbing polymers and viscosity of cement pastes," *Cement and Concrete Research,* vol. 63, pp. 12-19, 2014.
[178] T. H. Phan, M. Chaouche, and M. Moranville, "Influence of organic admixtures on the rheological behaviour of cement pastes," *Cement and Concrete Research,* vol. 36, pp. 1807-1813, 2006.
[179] M. Cyr, C. Legrand, and M. Mouret, "Study of the shear thickening effect of superplasticizers on the rheological behaviour of cement pastes containing or not mineral additives," *Cement and Concrete Research,* vol. 30, pp. 1477-1483, 2000.
[180] A. Papo and L. Piani, "Effect of various superplasticizers on the rheological properties of Portland cement pastes," *Cement and Concrete Research,* vol. 34, pp. 2097-2101, 2004.
[181] I. M. Krieger and T. J. Dougherty, "A mechanism for non-Newtonian flow in suspensions of rigid spheres," *Transactions of the Society of Rheology,* vol. 3, pp. 137-152, 1959.
[182] M. Ilg and J. Plank, "Improvement of SCC flow properties through addition of non-adsorbing small molecule co-dispersants," presented at the 8th International RILEM Symposium on Self-Compacting Concrete SCC2016, Washington D. C., USA, 2016.
[183] A. Lange and J. Plank, "Contribution of non-adsorbing polymers to cement dispersion," *Cement and Concrete Research,* vol. 79, pp. 131-136, 2016.
[184] A. Lange, T. Hirata, and J. Plank, "The role of non-adsorbed PCE molecules in cement dispersion: experimental evidence for a new dispersion mechanism," presented at the 10th International Conference on Superplasticizers and Other Chemical Admixtures, Prague, Czech Republic, 2012.
[185] J. Stecher and J. Plank, "Phosphated comb polymers - A new generation of highly effective superplasticizers," presented at the 8th International RILEM Symposium on Self-Compacting Concrete SCC2016, Washington D.C., USA, 2016.
[186] A. Lange, T. Hirata, and J. Plank, "Influence of the HLB value of polycarboxylate superplasticizers on the flow behavior of mortar and concrete," *Cement and Concrete Research,* vol. 60, pp. 45-50, 2014.
[187] A. Lange and J. Plank, "Optimization of comb-shaped polycarboxylate cement dispersants to achieve fast-flowing mortar and concrete," *Journal of Applied Polymer Science,* vol. 132, p. 42529, 2015.
[188] N. Roussel, "Personal communication," ed, 2016.
[189] B. Lothenbach, F. Winnefeld, and R. Figi, "The influence of superplasticizers on the hydration of Portland cement," presented at the 12th International Congress on the Chemistry of Cement, Montreal, Canada, 2007.
[190] D. Jansen, F. Goetz-Neunhoeffer, J. Neubauer, W.-D. hergeth, and R. Haerzschel, "Studies on the interactions between superplasticizers and

hydrating OPC," presented at the 13th International Congress on the Chemistry of Cement, Madrid, Spain, 2011.

[191] D. Jansen, J. Neubauer, F. Goetz-Neunhoeffer, R. Haerzschel, and W.-D. Hergeth, "Change in reaction kinetics of a Portland cement caused by a superplasticizer - Calculation of heat flow curves from XRD data," *Cement and Concrete Research,* vol. 42, pp. 327-332, 2012.

[192] F. Puertas, H. Santos, M. Palacios, and S. Martinez-Ramirez, "Polycarboxylate superplasticiser admixtures: Effect on hydration, microstructure and rheological behaviour in cement pastes," *Advances in Cement Research,* vol. 17, pp. 77-89, 2005.

[193] J. Cheung, A. A. Jeknavorian, L. Roberts, and D. A. Silva, "Impact of admixtures on the hydration kinetics of Portland cement," *Cement and Concrete Research,* vol. 41, pp. 1289-1309, 2011.

[194] F. Ridi, L. Dei, E. Fratini, S.-H. Chen, and P. Baglioni, "Hydration kinetics of tri-calcium silicate in the presence of superplasticizers," *The Journal of Physical Chemistry B,* vol. 107, pp. 1056-1061, 2003.

[195] J. Rieger, J. Thieme, and C. Schmidt, "Study of precipitation reactions by X-ray microscopy: CaCO3 precipitation and the effect of polycarboxylates," *Langmuir,* vol. 16, pp. 8300-8305, 2000.

[196] N. Robeyst, G. De Schutter, C. Grosse, and N. De Belie, "Monitoring the effect of admixtures on early-age concrete behaviour by ultrasonic, calorimetric, strength and rheometer measurements," *Magazine of Concrete Research,* vol. 63, pp. 707-721, 2011.

[197] K. Lesage, Ö. Cizer, L. Vandewalle, B. Desmet, J. Vantomme, and G. De Schutter, "Influence of plasticizer type on hydration kinetics of self-compacting concrete," presented at the 13th International Congress on the Chemistry of Cement, Madrid, Spain, 2011.

[198] H. Uchikawa, D. Sawaki, and S. Hanehara, "Influence of kind and adding timing of organic admixture on the composition, structure and property of fresh cement paste," *Cement and Concrete Research,* vol. 25, pp. 353-364, 1995.

[199] F. Winnefeld, A. Zingg, L. Holzer, R. Figi, J. Pakusch, and S. Becker, "Interaction of polycarboxylate-based superplasticizers and cements: Influence of polymer structure and C3A content of cement," presented at the 12th International Congress on the Chemistry of Cement, Montréal, Canada, 2007.

[200] J. Roncero, S. Valls, and R. Gettu, "Study of the influence of superplasticizers on the hydration of cement paste using nuclear magnetic resonance and X-ray diffraction techniques," *Cement and Concrete Research,* vol. 32, pp. 103-108, 2002.

[201] C. Giraudeau, J.-B. d'Espinose de Lacaillerie, Z. Souguir, A. Nonat, and R. J. Flatt, "Surface and intercalation chemistry of polycarboxylate copolymers in cementitious systems," *Journal of the American Ceramic Society,* vol. 92, pp. 2471-2488, 2009.

[202] S. Ng and J. Plank, "Formation of organo-mineral phases incorporating PCE superplasticizers during early hydration of calcium aluminate cement,"

presented at the 13th International Congress on the Chemistry of Cement, Madrid, Spain, 2011.
[203] A. Habbaba, Z. Dai, and J. Plank, "Formation of organo-mineral phases at early addition of superplasticizers: The role of alkali sulfates and C3A content," *Cement and Concrete Research,* vol. 59, pp. 112-117, 2014.
[204] J. Plank, Z. Dai, and H. Keller, "Organo-mineral phases formed during cement hydration," presented at the 12th International Congress on the Chemistry of Cement, Montreal, Canada, 2007.
[205] J. Plank, D. Zhimin, H. Keller, F. V. Hössle, and W. Seidl, "Fundamental mechanisms for polycarboxylate intercalation into C3A hydrate phases and the role of sulfate present in cement," *Cement and Concrete Research,* vol. 40, pp. 45-57, 2010.
[206] R. J. Flatt and Y. F. Houst, "A simplified view on chemical effects perturbing the action of superplasticizers," *Cement and Concrete Research,* vol. 31, pp. 1169-1176, 2001.
[207] F. Dalas, A. Nonat, S. Pourchet, M. Mosquet, D. Rinaldi, and S. Sabio, "Tailoring the anionic function and the side chains of comb-like superplasticizers to improve their adsorption," *Cement and Concrete Research,* vol. 67, pp. 21-30, 2015.
[208] S. Hanehara and K. Yamada, "Interaction between cement and chemical admixture from the point of cement hydration, absorption behaviour of admixture, and paste rheology," *Cement and Concrete Research,* vol. 29, pp. 1159-1165, 1999.
[209] I. Y. T. Ng, P. L. Ng, W. W. S. Fung, and A. K. H. Kwan, "Optimizing mixing sequence and mixing time for SCC," presented at the Second International Symposium on Design, Performance and Use of Self-Consolidating Concrete, Beijing, China, 2009.
[210] V. Fernàndez-Altable and I. Casanova, "Influence of mixing sequence and superplasticiser dosage on the rheological response of cement pastes at different temperatures," *Cement and Concrete Research,* vol. 36, pp. 1222-1230, 2006.
[211] J. Zimmermann, C. Hampel, C. Kurz, L. Frunz, and R. J. Flatt, "Effect of polymer structure on the sulfate-polycarboxylate competition," presented at the 9th ACI International Conference on Superplasticizers and Other Chemical Admixtures in Concrete, Detroit, USA, 2009.
[212] S. Grünewald and J. C. Walraven, "Self-compacting concrete with viscosity agents in the fresh state," Stevin Laboratory, Delft University of Technology, Delft, The Netherlands2005.
[213] CAA, "CAA guidelines for establishing the suitability of viscosity-modifying admixtures for self-compacting concrete," UK Cement Admixture Association (CAA)2004.
[214] T. Kawai, "Non-dispersible underwater concrete using polymers - The production, performance and potential of polymers in concrete," presented at the 5th International Congress on Polymers, Brighton, UK, 1987.

[215] T. Nawa, T. Izumi, and Y. Edamatsu, "State-of-the-art report on materials and design of self-compacting concrete," presented at the International Workshop on Self-Compacting Concrete, Kochi, Japan, 1998.

[216] K. H. Khayat, "Viscosity-enhancing admixtures for cement-based materials - an overview," *Cement and Concrete Composites,* vol. 20, pp. 171-188, 1998.

[217] V. S. Ramachandran, *Concrete admixtures handbook - Properties, science, and technology*. Ottawa, Canada: Noyes Publications, 1995.

[218] N. P. Mailvaganam, "Miscellaneous Admixtures," in *Concrete Admixtures Handbook*, V. S. Ramachandran, Ed., ed Park Ridge, NJ, USA: Noyes Publications, 1995.

[219] S. Grünewald and J. C. Walraven, "Viscosity agents in self-compacting concrete: A state-of-the-art," Delft University of Technology, Delft, The Netherlands2004.

[220] N. Mikanovic, J. Sharman, C. Jolicoeur, K. Khayat, and M. Pagé, "Compatibility of viscosity-enhancing agents and superplasticizers in cementitious and model systems: Rheology, bleeding, and segregation," presented at the SP-262: Ninth ACI International Conference on Superplasticizers and Other Chemical Admixtures, Seville, Spain, 2009.

[221] E. Knapen and D. Van Gemert, "Cement hydration and microstructure formation in the presence of water-soluble polymers," *Cement and Concrete Research,* vol. 39, pp. 6-13, 2009.

[222] M. Palacios, R. J. Flatt, F. Puertas, and A. Sanchez-Herencia, "Compatibility between polycarboxylate and viscosity-modifying admixtures in cement pastes," *ACI Special Publication,* vol. 288, pp. 29-42, 2012.

[223] M. Sonebi, "Rheological properties of grouts with viscosity modifying agents as diutan gum and welan gum incorporating pulverised fly ash," *Cement and Concrete Research,* vol. 36, pp. 1609-1618, 2006.

[224] K. H. Khayat, "Effects of antiwashout admixtures on fresh concrete properties," *ACI Structural Journal,* vol. 92, pp. 164-171, 1995.

[225] R. Rixom and N. P. Mailvaganam, *Chemical admixtures for concrete*. London, U.K.: E & FN Spon, 1999.

[226] A. Phyfferoen, Y. Boland, and J. Naudts, "CP Kelco, Personal Communication, April 17th, 2014," ed, 2014.

[227] A. M. Betioli, P. J. P. Gleize, D. A. Silva, V. M. John, and R. G. Pileggi, "Effect of HMEC on the consolidation of cement pastes: isothermal calorimetry versus oscillatory rheometry," *Cement and Concrete Research,* vol. 39, pp. 440-445, 2009.

[228] L. Patural, P. Porion, H. Van Damme, A. Govin, P. Grosseau, B. Ruot, and O. Devès, "A pulsed field gradient and NMR imaging investigations of the water retention mechanism by cellulose ethers in mortars," *Cement and Concrete Research,* vol. 40, pp. 1378-1385, 2010.

[229] D. Bülichen, J. Kainz, and J. Plank, "Working mechanism of methyl hydroxyelthyl cellulose (MHEC) as water retention agent," *Cement and Concrete Research,* vol. 42, pp. 953-959, 2012.

[230] C. Brumaud, H. Bessaies Bey, C. Mohler, R. Baumann, M. Schmitz, M. Radler, and N. Roussel, "Cellulose ethers and water retention," *Cement and Concrete Research,* vol. 53, pp. 176-184, 2013.

[231] C. Brumaud, R. Baumann, M. Schmitz, and N. Roussel, "Influence of high molar mass polymers on the rheological behavior of fresh cement pastes," presented at the 13th International Congress on the Chemistry of Cement, Madrid, Spain, 2011.

[232] M. Cappellari, A. Daubresse, and M. Chaouche, "Influence of organic thickening admixtures on the rheological properties of mortars: Relationship with water-retention," *Construction and Building Materials,* vol. 38, pp. 950-961, 2013.

[233] H. Yammamuro, T. Izumi, and T. Mizunuma, "Study of non-adsorptive viscosity agents applied to self-compacting concrete," presented at the Fifth CANMET/ACI International Conference: Superplasticizers and Other Chemical Admixtures in Concrete, Rome, Italy, 1997.

[234] C. Negro, L. M. Sánchez, E. Fuente, A. Blanco, and J. Tijero, "Polyacrylamide induced flocculation of a cement suspension," *Chemical Engineerin Science,* vol. 61, pp. 2522-2532, 2006.

[235] R. D. Ferron, S. P. Shah, E. Fuente, and C. Negro, "Aggregation and breakage kinetics of fresh cement paste," *Cement and Concrete Research,* vol. 50, pp. 1-10, 2013.

[236] H. Bessaies Bey, R. Baumann, M. Schmitz, M. Radler, and N. Roussel, "Organic admixtures and cement particles: Competitive adsorption and its macroscopic rheological consequences," *Cement and Concrete Research,* vol. 80, pp. 1-9, 2016.

[237] H. Bessaies Bey, J. Hot, R. Baumann, and N. Roussel, "Consequences of competitive adsorption between polymers on the rheological behaviour of cement pastes," *Cement & Concrete Composites,* vol. 54, pp. 17-20, 2014.

[238] H. Bessaies, R. Baumann, and N. Roussel, "Consequences of competitive adsorption between polymers on the rheological behaviour of cement pastes," presented at the Fifth North American Conference on the Design and Use of Self-Consolidating Concrete, Chicago, IL, USA, 2013.

[239] H. J. Kong, S. G. Bike, and V. C. Li, "Electrosteric stabilization of concentrated cement suspensions imparted by a strong anionic polyelectrolyte and a non-ionic polymer," *Cement and Concrete Research,* vol. 36, pp. 842-850, 2006.

[240] C. Brumaud, R. Baumann, M. Schmitz, M. Radler, and N. Roussel, "Cellulose ethers and yield stress of cement pastes," *Cement and Concrete Research,* vol. 55, pp. 14-21, 2014.

[241] J. Plank, N. R. Lummer, and F. Dugonjic-Bilic, "Competitive adsorption between an AMPS-based fluid loss polymer and welan gum biopolymer in oil well cement," *Journal of Applied Polymer Science,* vol. 116, pp. 2913-2919, 2010.

[242] R. I. Feigin and D. H. Napper, "Depletion stabilisation and depletion flocculation," *Journal of Colloid and Interface Science,* vol. 75, pp. 525-541, 1980.

[243] C. Brumaud, "Origines microscopiques des conséquences rhéologiques de l'ajout d'éthers de cellulose dans une suspension cimentaire (Microscopic origins of rheological phenomena in cement suspensions caused by the addition of cellulose ether, in french)," Doctoral thesis, Department of Sciences, Engineering, and Environment, Université Paris-Est, Paris, France, 2011.

[244] K. De Weerdt and H. Vikan, "COIN Project report 38: Rheological properties of stabilized SCC - using fillers, admixtures or a combination," SINTEF Building and Infrastructure, Oslo, Norway2011.

[245] J. Pourchez, A. Peschard, P. Grosseau, R. Guyonnet, B. Guilhot, and F. Vallée, "HPMC and HEMC influence on cement hydration," *Cement and Concrete Research,* vol. 36, pp. 288-294, 2006.

[246] D. A. Silva and P. J. M. Monteiro, "The influence of polymers on the hydration of portland cement phases analyzed by soft X-ray transmission microscopy," *Cement and Concrete Research,* vol. 36, pp. 1501-1507, 2006.

[247] F. Ridi, E. Fratini, F. Mannelli, and P. Baglioni, "Hydration process of cement in the presence of a cellulosic additive. A calorimetric investigation," *Journal of Physical Chemistry B,* vol. 109, pp. 14727-14734, 2005.

[248] A. Peschard, A. Govin, P. Grosseau, B. Guilhot, and R. Guyonnet, "Effect of polysaccharides on the hydration of cement paste at early ages," *Cement and Concrete Research,* vol. 34, pp. 2153-2158, 2004.

[249] H. J. Weyer, I. Müller, B. Schmitt, D. Bosbach, and A. Putnis, "Time-resolved monitoring of cement hydration: influence of cellulose ethers on hydration kinetics," *Nuclear Instruments and Methods in Physics Research B,* vol. 238, pp. 102-106, 2005.

[250] J. Pourchez, P. Grosseau, R. Guyonnet, and B. Ruot, "HEC influence on cement hydration measured by conductometry," *Cement and Concrete Research,* vol. 36, pp. 1777-1780, 2006.

[251] A. Peschard, A. Govin, J. Pourchez, E. Fredon, L. Bertrand, S. Maximilien, and B. Guilhot, "Effect of polysaccharides on the hydration of cement suspension," *Journal of the European Ceramic Society,* vol. 26, pp. 1439-1445, 2006.

[252] T. Poinot, A. Govin, and P. Grosseau, "Impact of hydroxypropylguars on the early age hydration of Portland cement," *Cement and Concrete Research,* vol. 40, pp. 179-188, 2013.

[253] P. F. G. Banfill and D. C. Saunders, "The relationship between the sorption of organic compounds on cement and the retardation of hydration," *Cement and Concrete Research,* vol. 16, pp. 399-410, 1986.

[254] N. L. Thomas and J. D. Birchall, "The retarding action of sugars on cement hydration," *13,* vol. 6, 1983.

[255] M. C. G. Juenger and H. M. Jennings, "New insights into the effects of sugar on the hydration and microstructure of cement pastes," *Cement and Concrete Research,* vol. 32, pp. 393-399, 2002.

[256] J. F. Young, "Effect of organic compounds on the interconversions of calcium aluminate hydrates: hydration of tricalcium aluminate," *Journal of the American Ceramic Society,* vol. 53, pp. 65-69, 1970.

[257] D. A. Silva, H. Roman, and V. John, "Effects of EVA and HEC polymers on the Portland cement hydration," presented at the 11th Congress on Polymers in Concrete, Berlin, Germany, 2004.

[258] J. F. Young, "A review of the mechnaisms of set-retardation in Portland cement pastes containing organic admixtures," *Cement and Concrete Research,* vol. 2, pp. 415-433, 1972.

[259] J. Pourchez, A. Govin, P. Grosseau, B. Guilhot, and B. Ruot, "Alkaline stability of cellulose ethers and impact of their degradation products on cement hydration," *Cement and Concrete Research,* vol. 36, pp. 1252-1256, 2006.

[260] F. De Larrard, *Concrete mixture proportioning: a scientific approach*. New York, NY: E & Fn Spon, 1999.

[261] J. Dils, "Influence of vacuum mixing, air entrainment of heat curing on the properties of hardened and fresh (ultra) high performance mortar," Doctoral thesis, Department of Civil Engineering, Ghent University, Ghent, Belgium, 2015.

[262] H. F. W. Taylor, *Cement chemistry*. London, U.K.: Thomas Telford, 1997.

[263] J. Hot and N. Roussel, "Influence of adsorbing polymers on the macroscopic viscosity of concentrated cement pastes (ACI SP-288)," *ACI Special Publication,* pp. 223-233, 2012.

[264] N. Roussel, G. Ovarlez, S. Garrault, and C. Brumaud, "The origins of thixotropy of fresh cement pastes," *Cement and Concrete Research,* vol. 42, pp. 148-157, 2012.

[265] N. Roussel, *Understanding the rheology of concrete*. Cornwall, UK: Woodhead Publishing in Materials, 2012.

[266] R. J. Flatt and P. Bowen, "Yodel: a yield stress model for suspensions," *Journal of the American Ceramic Society,* vol. 89, pp. 1244-1256, 2006.

[267] R. J. Flatt and P. Bowen, "Yield stress of multimodal powder suspensions: An extension of the YODEL (Yield stress model)," *Journal of the American Ceramic Society,* vol. 90, pp. 1038-1044, 2007.

[268] M. R. Geiker, M. Brandl, L. N. Thrane, and L. F. Nielsen, "On the effect of coarse aggregate fraction and shape on the rheological properties of self-compacting concrete," *Cement, Concrete and Aggregates,* vol. 24, pp. 3-6, 2002.

[269] F. Mahaut, S. Mokéddem, X. Chateau, N. Roussel, and G. Ovarlez, "Effect of coarse particle volume fraction on the yield stress and thixotropy of cementitious materials," *Cement and Concrete Research,* vol. 38, pp. 1276-1285, 2008.

[270] L. J. Struble and W.-G. Lei, "Rheological changes associated with setting of cement paste," *Advanced Cement Based Materials,* vol. 2, pp. 224-230, 1995.

[271] A. Perrot, T. Lecompte, H. Khelifi, C. Brumaud, J. Hot, and N. Roussel, "Yield stress and bleeding of fresh cement pastes," *Cement and Concrete Research,* vol. 42, pp. 937-944, 2012.

[272] S. Jarny, N. Roussel, R. Le Roy, and P. Coussot, "Modelling thixoropic behavior of fresh cement pastes from MRI measurements," *Cement and Concrete Research,* vol. 38, pp. 616-623, 2008.

[273] S. Jarny, N. Roussel, S. Rodts, F. Bertrand, R. Le Roy, and P. Coussot, "Rheological behavior of cement pastes from MRI velocimetry," *Cement and Concrete Research,* vol. 35, pp. 1873-1881, 2005.

[274] A. W. Saak, H. M. Jennings, and S. P. Shah, "The influence of wall slip on yield stress and viscoelastic measurements of cement paste," *Cement and Concrete Research,* vol. 31, pp. 205-212, 2001.

[275] J. Mewis, "Thixotropy - A general review," *Journal of Non-Newtonian Fluid Mechanics,* vol. 6, pp. 1-20, 1979.

[276] L. Nachbaur, V. Waller, O. Haddad, and M. Vachon, "Extension of concrete equivalent mortar (CEM) method to self-compacting concrete," presented at the Second North American Conference on the Design and Use of Self-Consolidating Concrete; Fourth International RILEM Symposium on Self-Compacting Concrete, Chicago, IL, USA, 2005.

[277] Z. Quanji, "Thixotropic behavior of cement-based materials: effect of clay and cement types," Master thesis, Department of Civil, Construction, and Environmental Engineering, Iowa State University, Ames, Iowa, 2010.

[278] L. Reiter, T. Wangler, N. Roussel, and R. J. Flatt, "Distinguishing flocculation and hydration effects on the thixotropy of cement pastes," presented at the 8th International RILEM Symposium on Self-Compacting Concrete, Washington D.C., USA, 2016.

[279] J. Assaad, K. H. Khayat, and H. Mesbah, "Assessment of thixotropy of flowable and self-consolidating concrete," *ACI Materials Journal,* vol. 100, pp. 99-107, 2003.

[280] Z. Quanji, K. Wang, G. R. Lomboy, and S. P. Shah, "Influence of nano-clay addition and clay replacement on thixotropic behavior of fresh cement paste," presented at the 7th International RILEM Symposium on Self-Compacting Concrete, Paris, France, 2013.

[281] A. M. Mostafa and A. Yahia, "Effect of cement type and solid concentration on kinetics of structural build-up of cement suspensions," presented at the 8th International RILEM Symposium on Self-Compacting Concrete, Washington D.C., USA, 2016.

[282] R. P. Ferron, A. Gregori, Z. Sun, and S. P. Shah, "Rheological method to evaluate structural buildup in self-consolidating concrete cement pastes," *ACI Materials Journal,* vol. 104, pp. 242-250, 2007.

[283] R. P. Douglas, Z. Sun, D. Bonen, S. P. Shah, and A. Gregori, "The effect of ingredients and shear history on the thixotropic rate of the rebuilding of SCC," presented at the Second North American Conference on the Design and Use of Self-consolidating Concrete / 4th International RILEM Symposium on Self-Compacting Concrete, Chicago, IL, USA, 2005.

[284] R. P. D. Ferron, "Formwork pressure of self-consolidating concrete: influence of flocculation mechanism, structural rebuilding, thixotropy, and rheology," Doctoral thesis, Department of Civil and Environmental Engineering, Northwestern University, Evanston, IL, USA, 2008.

[285] D. Lowke, T. Kränkel, C. Gehlen, and P. Schiessl, "Effect of cement on superplasticizer adsorption, yield stress, thixotropy and segregation resistance," presented at the 6th International RILEM symposium on self-

compacting concrete; Design, Production and Placement of Self-Consolidating Concrete, Montreal, Canada, 2010.
[286] D. Lowke, "Interparticle forces and rheology of cement based suspensions," presented at the 3th Symposium on Nanotechnology in Construction, Prague, Czech, 2009.
[287] A. F. Omran, K. H. Khayat, and Y. M. Elaguab, "Effect of SCC mixture composition on thixotropy and formwork pressure," *Journal of Materials in Civil Engineering,* vol. 24, pp. 876-888, 2012.
[288] A. Kaci, M. Chaouche, and P.-A. Andréani, "Influence of bentonite clay on the rheological behaviour of fresh mortars," *Cement and Concrete Research,* vol. 41, pp. 373-379, 2011.
[289] S. Kawashima, M. Chaouche, D. J. Corr, and S. P. Shah, "Rate of thixotropic rebuilding of cement pastes modified with highly purified attapulgite clays," *Cement and Concrete Research,* vol. 53, pp. 112-118, 2013.
[290] R. Jarabo, E. Fuente, A. Moral, Á. Blanco, L. Izquierdo, and C. Negro, "Effect of sepiolite on the flocculation of suspensions of fibre-reinforced cement," *Cement and Concrete Research,* vol. 40, pp. 1524-1530, 2010.
[291] J. H. Kim, M. Beacraft, and S. P. Shah, "Effect of mineral admixtures on formwork pressure of self-consolidating concrete," *Cement & Concrete Composites,* vol. 32, pp. 665-671, 2010.
[292] M. Schellhorn. (2014, March, 3th 2014). *Quality clay solutions*. Available: http://www.schmidt-tone.de/cms/en/products/mineral-products/concrete-products.html
[293] T. Voigt, J.-J. Mbele, K. Wang, and S. P. Shah, "Using fly ash, clay and fibres for simultaneous improvement of concrete green strength and consolidatability for slip-form pavement," *Journal of Materials in Civil Engineering,* vol. 22, pp. 196-206, 2010.
[294] N. A. Tregger, M. E. Pakula, and S. P. Shah, "Influence of clays on the rheology of cement pastes," *Cement and Concrete Research,* vol. 40, pp. 384-391, 2010.
[295] K. Wang and G. R. Lomboy, "Thixotropic bahavior of frsh cement paste with highly purified magnesium alumino-silicate clay: measurements and interpretation," presented at the 8th International RILEM Symposium on Self-Compacting Concrete, Washington D.C., USA, 2016.
[296] K. G. Kuder and S. P. Shah, "Rheology of extruded cement-based materials," *ACI Materials Journal,* vol. 104, pp. 283-290, 2007.
[297] T. Voigt, T. Malonn, and S. P. Shah, "Green and early age compressive strength of extruded cement mortar monitored with compression tests and ultrasonic techniques," *Cement and Concrete Research,* vol. 36, pp. 858-867, 2006.
[298] P. Jarvis, B. Jefferson, J. Gregory, and S. A. Parsons, "A review of floc strength and breakage," *Water Research,* vol. 39, pp. 3121-3137, 2005.
[299] H. J. Yim, J. H. Kim, and S. P. Shah, "Cement particle flocculation and breakage monitoring under Couette flow," *Cement and Concrete Research,* vol. 53, pp. 36-43, 2013.
[300] D. N. Thomas, S. F. Judd, and N. Fawcett, "Flocculation modelling: a review," *Water Research,* vol. 33, pp. 1579-1592, 1999.

[301] C. Negro, Á. Blanco, E. Fuente, L. M. Sánchez, and J. Tijero, "Influence of flocculant molecular weight and anionic charge on flocculant behaviour and on the manufacture of fibre cement composites by the Hatschek process," *Cement and Concrete Research,* vol. 35, pp. 2095-2103, 2005.

[302] J. E. Wallevik, "Rheology of particle suspensions - Fresh concrete, mortar and cement paste with various types of lignosulfonates," Doctoral thesis, Department of Structural Engineering, The Norwegian University of Science and Technology (NTNU), Trondheim, Norway, 2003.

[303] J. E. Wallevik, "Thixotropic investigation on cement paste: Experimental and numerical approach," *Journal of Non-Newtonian Fluid Mechanics,* vol. 132, pp. 86-99, 2005.

[304] J. E. Wallevik, "Rheological properties of cement paste: Thixotropic behavior and structural breakdown," *Cement and Concrete Research,* vol. 39, pp. 14-29, 2009.

[305] K. Hattori and K. Izumi, "A rheological expression of coagulation rate theory - Part 3: Calculation of hysteresis and theoretical summary," *Journal of Dispersion Science and Technology,* vol. 3, pp. 169-193, 1982.

[306] E. J. W. Verwey and J. T. G. Overbeek, *Theory of the stability of lyophobic colloids*. Amsterdam, The Netherlands: Elsevier, 1948.

[307] M. Smoluchowski, "Versuch einer Mathematischen Theorie der Koagulationkinetik Kolloider Lösungen," *Zeltschrin für Physikalische Chemie,* vol. 92, pp. 129-168, 1917.

[308] A. Papo, "The thixotropic behavior of white Portland cement pastes," *Cement and Concrete Research,* vol. 18, pp. 595-603, 1988.

[309] P. Coussot, Q. D. Nguyen, H. T. Huynh, and D. Bonn, "Viscosity bifurcation in thixotropic, yielding fluids," *Journal of Rheology,* vol. 46, pp. 573-589, 2002.

[310] N. Roussel, "A thixotropy model for fresh fluid concretes: Theory, validation and applications," *Cement and Concrete Research,* vol. 36, pp. 1797-1806, 2006.

[311] D. C.-H. Cheng and F. Evans, "Phenomenological characterization of the rheological behaviour of inelastic reversible thixotropic and antithixotropic fluids," *British Journal of Applied Physics,* vol. 16, pp. 1599-1617, 1965.

[312] S. H. Lee, H. J. kim, E. Sakai, and M. Daimon, "Effect of particle size distribution of fly ash-cement system on the fluidity of cement pastes," *Cement and Concrete Research,* vol. 33, pp. 763-768, 2003.

[313] A. Yahia, M. Tanimura, and Y. Shimoyama, "Rheological properties of highly flowable mortar containing limestone filler-effect of powder content and W/C ratio," *Cement and Concrete Research,* vol. 35, pp. 532-539, 2005.

[314] A. K. H. Kwan and L. G. Li, "Combined effects of water film thickness and paste film thickness on rheology of mortar," *Materials and Structures,* vol. 45, pp. 1359-1374, 2012.

[315] L. G. Li and A. K. H. Kwan, "Mortar design based on water film thickness," *Construction and Building Materials,* vol. 25, pp. 2381-2390, 2011.

[316] P. Desnerck, P. Van Itterbeeck, V. Boel, B. Craeye, and G. De Schutter, "Survey on the mechanical properties of SCC: 20 years of research,"

presented at the 36th Conference on Our World in Concrete & Structures : 'Recent Advances in the Technology of Fresh Concrete', Singapore, Singapore, 2011.

[317] F. De Larrard and T. Sedran, "Mixture-proportioning of high-performance concrete," *Cement and Concrete Research,* vol. 32, pp. 1699-1704, 2002.

[318] F. De Larrard, "Concrete optimisation with regard to packing density and rheology," presented at the Third RILEM International Symposium on Rheology of Cement Suspensions such as Fresh Concrete, France, 2009.

[319] R. J. Farris, "Prediction of the viscosity of multimodal suspensions from unimodal viscosity data," *Transactions of the Society of Rheology,* vol. 12, pp. 281-301, 1968.

[320] C. F. Ferraris and F. De Larrard, "NISTIR 6094: Testing and Modelling of Fresh Concrete Rheology," National Institute of Standards and Technology, Gaithersburg, MD, USA1998.

[321] D. P. Bentz, C. F. Ferraris, M. A. Galler, A. S. Hansen, and J. M. Guynn, "Influence of particle size distributions on yield stress and viscosity of cement - fly ash pastes," *Cement and Concrete Research,* vol. 42, pp. 404-409, 2012.

[322] L. F. Nielsen, "Self-compacting concrete - modelled as a Bingham composite," *Nordic Concrete Research,* vol. 39, 2009.

[323] L. F. Nielsen, "A Bingham material mixed with stiff particles - some theoretical aspects," DTU Orbit2007.

[324] C. Chang and R. L. Powell, "Effect of particle size distributions on the rheology of concentrated bimodal suspensions," *Journal of Rheology,* vol. 38, pp. 85-98, 1994.

[325] N. S. Martys and R. D. Mountain, "Velocity Verlet algorithm for dissipative-particle-dynamics-based models of suspensions," *Physical Review E,* vol. 59, pp. 3733-3736, 1999.

[326] C. F. Ferraris and N. S. Martys, "Relating fresh concrete viscosity measureements from different rheometers," *Journal of research of the National Institute of Standards and Technology,* vol. 108, pp. 229-234, 2003.

[327] A. K. H. Kwan and H. H. C. Wong, "Packing density of cementitious materials: Part 2 - Packing and flow of OPC + PFA + CSF," *Materials and Structures,* vol. 41, pp. 773-784, 2008.

[328] H. H. C. Wong and A. K. H. Kwan, "Packing density of cementitious materials: Part 1 - Measurement using a wet packing method," *Materials and Structures,* vol. 41, pp. 689-701, 2008.

[329] A. K. H. Kwan, L. G. Li, and W. W. S. Fung, "Wet packing of blended fine and coarse aggregate," *Materials and Structures,* vol. 45, pp. 817-828, 2012.

[330] H. H. C. Wong and A. K. H. Kwan, "Rheology of cement paste: role of excess water to solid surface area ratio," *Journal of Materials in Civil Engineering,* vol. 20, pp. 189-197, 2008.

[331] A. K. H. Kwan and W. W. S. Fung, "Roles of water film thickness and SP dosage in rheology and cohesiveness of mortar," *Cement & Concrete Composites,* vol. 34, pp. 121-130, 2012.

[332] G. De Schutter, "Self-compacting concrete after two decades of research and practice," presented at the 9th International Symposium on High performance Concrete, Rotorua, new Zealand, 2011.

[333] P.-C. Aïtcin, C. Jolicoeur, and J. G. MacGregor, "Superplasticizers: How they work and why they occasionally don't," *Concrete International,* vol. 16, pp. 45-52, 1994.

[334] D. Han and R. D. Ferron, "Effect of mixing method on microstructure and rheology of cement paste," *Construction and Building Materials,* vol. 93, pp. 278-288, 2015.

[335] D. Lowke and P. Schiessl, "Effect of mixing energy on fresh properties of SCC," presented at the Second North American Conference on the Design and Use of Self-consolidating Concrete / 4th International RILEM Symposium on Self-Compacting Concrete, Chicago, IL, USA, 2005.

[336] P. Schiessl, O. Mazanec, and D. Lowke, "SCC and UHPC - Effect of mixing technology on fresh concrete properties," in *Advances in Construction Materials*, C. U. Grosse, Ed., ed Heidelberg, Germany: Springer, 2007, pp. 513-522.

[337] B. Cazacliu and N. Roquet, "Concrete mixing kinetics by means of power measurement," *Cement and Concrete Research,* vol. 39, pp. 182-194, 2009.

[338] S. M. Iveson, J. D. Litster, K. Hapgood, and B. J. Ennis, "Nucleation, growth and breakage phenomena in agitated wet granulation processes: a review," *Powder Technology,* vol. 117, pp. 3-39, 2001.

[339] A. Goldszal and J. Bousquet, "Wet agglomeration of powders: from physics towards process optimization," *Powder Technology,* vol. 117, pp. 221-231, 2001.

[340] B. Cazacliu, "In-mixer measurements to describe the mixture kinetics during concrete mixing," presented at the Sixth International Symposium on Mixing in Industrial Process Industries - ISMIP VI, Niagara on the Lake, Ontario, Canada, 2008.

[341] D. Chopin, B. Cazacliu, and F. De Larrard, "Monitoring of concrete homogenisation with the power consumption curve," *Materials and Structures,* vol. 40, pp. 897-907, 2007.

[342] O. Mazanec and P. Schiessl, "Mixing Time Optimisation for UHPC," presented at the Second International Symposium on Ultra High Performance Concrete, Kassel, Germany, 2008.

[343] D. Chopin, F. De Larrard, and B. Cazacliu, "Why do HPC and SCC require a longer mixing time?," *Cement and Concrete Research,* vol. 34, pp. 2237-2243, 2004.

[344] K. Takada and J. C. Walraven, "Influence of mixing efficiency on the properties of flowable cement pastes," presented at the Second International Symposium on Self-Compacting Concrete, Tokyo, Japan, 2001.

[345] J. Dils, G. De Schutter, and V. Boel, "Influence of mixing procedure and mixer type on fresh and hardened properties of concrete: a review," *Materials and Structures,* vol. 45, pp. 1673-1683, 2012.

[346] O. Mazanec, D. Lowke, and P. Schiessl, "Mixing of high performance concrete: effect of concrete composition and mixing intensity on mixing time," *Materials and Structures,* vol. 43, pp. 357-365, 2010.

[347] D. Dollimore and R. J. Mangabhai, "Effect of mixing time on heat evolution pattern of cement pastes," *Thermochimica Acta,* vol. 85, pp. 223-226, 1985.

[348] P. Juilland, A. Kumar, E. Gallucci, R. J. Flatt, and K. L. Scrivener, "Effect of mixing on the early hydration of alite and OPC systems," *Cement and Concrete Research,* vol. 42, pp. 1175-1188, 2012.

[349] K. Takahashi and T. A. Bier, "Mechanisms for the changes in fluidity and hydration kinetics of grouts after mixing," presented at the 7th RILEM International Conference on Self-Compacting Concrete and 1st RILEM International Conference on Rheology and Processing of Construction Materials, Paris, France, 2013.

[350] J. J. Thomas and H. M. Jennings, "Effects of D2O and mixing on the early hydration kinetics of tricalcium silicate," *Chemistry of Materials,* vol. 11, pp. 1907-1914, 1999.

[351] E. Maruya, M. Osaki, and H. Igarashi, "Relationships between rheological constant of cement paste and fluidity of high-fluidity concrete," *Journal of Advanced Concrete Technology,* vol. 4, pp. 251-257, 2006.

[352] D. A. Williams, A. W. Saak, and H. M. Jennings, "The influence of mixing on the rheology of fresh cement paste," *Cement and Concrete Research,* vol. 29, pp. 1491-1496, 1999.

[353] A. Asghari and D. Feys, "Influence of applied maximum shear rate on rheological properties of cement-paste with SCC consistency," presented at the 8th International RILEM Symposium on Self-Compacting Concrete, Washington D.C., USA, 2016.

[354] P.-O. Vandanjon, F. de Larrard, B. Dehousse, G. Villai, R. Maillot, and P. Laplante, "Homogenisation of concrete in a batch plant: the influence of mixing time and method on the introduction of mineral admixtures," *Magazine of Concrete Research,* vol. 55, pp. 105-116, 2003.

[355] K. Yamada, "Basics of analytical methods used for the investigation of interaction mechanism between cement and superplasticizers," *Cement and Concrete Research,* vol. 41, pp. 793-798, 2011.

[356] D. Feys, A. Asghari, E. Ghafari, A. M. Ley Hernandez, F. Van Der Vurst, and G. De Schutter, "Influence of mixing procedure on robustness of self-consolidating concrete," Center for Transportation Infrastructure and Safety2014.

[357] M. Yang and H. M. Jennings, "Influences of mixing methods on the microstructure and rheological behavior of cement pastes," *Advanced Cement Based Materials,* vol. 2, pp. 70-78, 1995.

[358] G. H. Tattersall, *The rheology of fresh concrete*. London, U.K.: Pitman, 1983.

[359] C.-K. Loh, T.-S. Tan, K.-Y. Yong, and T.-H. Wee, "An experimental study on bleeding and channeling of cement paste and mortar," *Advances in Cement Research,* vol. 10, pp. 1-16, 1998.

[360] N. Roussel, "A theoretical frame to study stability of fresh concrete," *Materials and Structures,* vol. 39, pp. 81-91, 2006.

[361] B. Esmaeilkhanian, P. Diederich, K. H. Khayat, A. Yahia, and O. H. Wallevik, "Influence of particle lattice effect on stability of suspensions: applicaion to self-consolidating concrete," *Materials and Structures,* vol. 50, 2017.

[362] H. J. H. Brouwers and H. J. Radix, "Self-compacting concrete: theoretical and experimental study," *Cement and Concrete Research,* vol. 35, pp. 2116-2136, 2005.

[363] F. V. Mueller, O. H. Wallevik, and K. H. Khayat, "Linking solid particle packing of Eco-SCC to material performance," *Cement and Concrete Composites,* vol. 54, pp. 117-125, 2014.

[364] J. E. Funk and D. R. Dinger, *Predictive process control of crowded particulate suspensions: Applied to ceramic manufacturing*. New York, NY, USA: Springer, 1994.

[365] B. Esmaeilkhanian, K. H. Khayat, and O. H. Wallevik, "Mix design procedure for low-powder self-consolidating concrete: Eco-SCC," presented at the 8th International RILEM Symposium on Self-Compacting Concrete, Washington D.C., USA, 2016.

[366] B. M. Aïssoun, S.-D. Hwang, and K. H. Khayat, "Influence of aggregate characteristics on workability of superworkable concrete," *Materials and Structures,* vol. 49, pp. 597-609, 2016.

[367] J. Spangenberg, N. Roussel, J. H. Hattel, E. V. Sarmiento, G. Zirgulis, and M. R. Geiker, "Patterns of gravity induced aggregate migration during casting of fluid concretes," *Cement and Concrete Research,* vol. 42, pp. 1571-1578, 2012.

[368] J. Spangenberg, N. Roussel, J. H. Hattel, H. Stang, J. Skocek, and M. R. Geiker, "Flow induced particle migration in fresh concrete: Theoretical frame, numerical simulations and experimental results on model fluids," *Cement and Concrete Research,* vol. 42, pp. 633-641, 2012.

[369] A. M. Ley Hernandez and D. Feys, "Influence of mix design parameters on dynamic segregation of self-consolidating concrete," presented at the 8th International RILEM Symposium on Self-Compacting Concrete, Washington D.C., USA, 2016.

[370] L. Josserand, O. Coussy, and F. de Larrard, "Bleeding of concrete as an ageing consolidation process," *Cement and Concrete Research,* vol. 36, pp. 1603-1608, 2006.

[371] G. Giaccio and A. Giovambattista, "Bleeding: evaluation of its effects on concrete behaviour," *Materials and Structures,* vol. 19, pp. 265-271, 1986.

[372] C. A. Clear and D. G. Bonner, "Settlement of fresh concrete - an effective stress model," *Magazine of Concrete Research,* vol. 40, pp. 3-12, 1988.

[373] T. C. Powers, "The bleeding of Portland cement paste, mortar, and concrete," *Journal of the American Concrete Institute,* vol. 35, pp. 465-479, 1939.

[374] A. Perrot and D. Rangeard, "Effects of mix design parameters on consolidation behavior of fresh cement-based materials," presented at the 8th International RILEM Symposium on Self-Compacting Concrete, Washington D.C., USA, 2016.

[375] P. H. Morris and P. F. Dux, "Analytical solutions for bleeding of concrete due to consolidation," *Cement and Concrete Research,* vol. 40, pp. 1531-1540, 2010.

[376] J. J. Assaad and J. Harb, "Surface settlement of cementitious-based materials determined by oedometer testing," *Materials and Structures,* vol. 44, pp. 845-856, 2011.

[377] A. Perrot, D. Rangeard, V. Picandet, and Y. Mélinge, "Hydro-mechanical properties of fresh cement pastes containing polycarboxylate superplasticizer," *Cement and Concrete Research,* vol. 53, pp. 221-228, 2013.

[378] J. H. Yim, J. H. Kim, H.-G. Kwak, and J. K. Kim, "Evaluation of internal bleeding in concrete using a self-weight bleeding test," *Cement and Concrete Research,* vol. 53, pp. 18-24, 2013.

[379] T. S. Tan, T. H. Wee, S. A. Tan, C. T. Tam, and S. L. Lee, "A consolidation model for bleeding of cement paste," *Advances in Cement Research,* vol. 1, pp. 18-26, 1987.

[380] T.-S. Tan, C.-K. Loh, K.-Y. Yong, and T.-H. Wee, "Modelling of bleeding of cement paste and mortar," *Advances in Cement Research,* vol. 9, pp. 75-91, 1997.

[381] L. Josserand and F. De Larrard, "A method for concrete bleeding measurement," *Materials and Structures,* vol. 37, pp. 666-670, 2004.

[382] N. Massoussi and N. Roussel, "Bleeding in cement paste: induction, acceleration and consolidation phases," presented at the 8th International RILEM Symposium on Self-Compacting Concrete, Washington D.C., USA, 2016.

[383] N. Mikanovic and C. Jolicoeur, "Influence of superplasticizers on the rheology and stability of limestone and cement pastes," *Cement and Concrete Research,* vol. 38, pp. 907-919, 2008.

[384] N. Mikanovic, C. Jolicoeur, K. H. Khayat, and M. Pagé, "Model systems for investigation of the stability and rheological properties of cement-based materials," presented at the 8th CANMET/ACI International Conference on Recent Advances in Concrete Technology, Montréal, Canada, 2006.

[385] ACI Committee E-701, "E4-03: Chemical Admixtures for Concrete," American Concrete Institute2003.

[386] C. Bigley and P. Greenwood, "Using silica to control bleed and segregation in self-compacting concrete," *Concrete,* vol. 37, pp. 43-45, 2003.

[387] M. Collepardi, J. J. Ogoumah Olagot, U. Skarp, and R. Troli, "Influence of amorphous colloidal silica on the properties of self-compacting concretes," presented at the International Conference in Concrete Constructions - Innovations and Developments in Concrete Materials and Constructions, Dundee, Scotland, 2002.

[388] M. Nehdi, S. Mindess, and P.-C. Aïtcin, "Rheology of high-performance concrete: effect of ultrafine particles," *Cement and Concrete Research,* vol. 28, pp. 687-697, 1998.

[389] K. H. Khayat, M. Saric-Coric, and F. Liotta, "Influence of thixotropy on stability characteristics of cement grout and concrete," *ACI Materials Journal,* vol. 99, pp. 234-241, 2002.

[390] K. H. Khayat and J. Assaad, "Thixotropic-Enhancing Agent - A key component to reduce formwork pressure of SCC," presented at the 1st International Symposium on Design, Performance and Use of Self-Consolidating Concrete, Changsha, China, 2005.

[391] American Society for Testing and Materials, "ASTM C150 / C150M Standard Specification for Portland Cement," ed. West Conshocken, PA: ASTM, 2016.

[392] A. Schwartzentruber and C. Catherine, "La méthode du mortier de béton équivalent (MBE) - Un nouvel outil d'aide à la formulation des bétons adjuvantés, in French (Method of the concrete equivalent mortar (CEM) - A new tool to design concrete containing admixture)," *Materials and Structures,* vol. 33, pp. 475-482, 2000.

[393] D. Feys, "What can go wrong during rheological measurements?," in *NRC Rheology course*, ed. Reykjavik, Iceland, 2014.

[394] L. E. Brower and C. F. Ferraris, "Comparison of concrete rheometers," *Concrete International,* vol. 25, pp. 41-47, 2003.

[395] P. F. G. Banfill, D. Beaupré, F. Chapdelaine, F. De Larrard, P. Domone, L. Nachbaur, T. Sedran, O. Wallevik, and J. E. Wallevik, "Comparison of concrete rheometers: International tests at LCPC (Nantes, France) in October, 2000," National Institute of Standards and Technology (NIST), Gaithersburg, MD, USA2001.

[396] D. Beaupré, F. Chapdelaine, P. Domone, E. Koehler, L. Shen, M. Sonebi, L. Struble, T. David, O. Wallevik, and J. E. Wallevik, "Comparison of concrete rheometers: International tests at MB (Cleveland OH, USA) in May, 2003," National Institute of Standards and Technology2004.

[397] D. Feys, J. E. Wallevik, A. Yahia, K. Khayat, and O. H. Wallevik, "Extension of the Reiner-Riwlin equation to determine modified Bingham parameters measured in coaxial cylinders rheometers," *Materials and Structures,* vol. 46, pp. 289-311, 2013.

[398] G. Heirman, "Modelling and quantification of the effect of mineral additions on the rheology of fresh powder type self-compacting concrete," Doctoral thesis, Department of Civil Engineering, Katholieke Universiteit Leuven, Leuven, 2011.

[399] N. Roussel, "The LCPC BOX: a cheap and simple technique for yield stress measurements of SCC," *Materials and Structures,* vol. 40, pp. 889-896, 2007.

[400] O. H. Wallevik, D. Feys, J. E. Wallevik, and K. H. Khayat, "Avoiding inaccurate interpretations of rheological measurements for cement-based materials," *Cement and Concrete Research,* 2015.

[401] H. Hafid, G. Ovarlez, F. Toussaint, P. H. Jezequel, and N. Roussel, "Assessment of potential concrete and mortar rheometry artifacts using magnetic resonance imaging," *Cement and Concrete Research,* vol. 71, pp. 29-35, 2015.

[402] J. Mewis and N. J. Wagner, "Thixotropy," *Advances in Colloid and Interface Science,* vol. 147-148, pp. 214-227, 2009.

[403] M. A. Schultz and L. J. Struble, "Use of oscillatory shear to study flow behavior of fresh cement paste," *Cement and Concrete Research,* vol. 23, pp. 273-282, 1993.

[404] O. H. Wallevik and J. E. Wallevik, "Rheology as a tool in concrete science: The use of rheographs and workability boxes," *Cement and Concrete Research,* vol. 41, pp. 1279-1288, 2011.

[405] B. Craeye, P. Van Itterbeeck, P. Desnerck, V. Boel, and G. De Schutter, "Modulus of elasticity and tensile strength of self-compacting concrete: Survey of experimental data and structural design codes," *Cement and Concrete Composites,* vol. 54, pp. 53-61, 2014.

[406] K. H. Khayat and J. Assaad, "Use of thixotropy-enhancing agent to reduce formwork pressure axerted by self-consolidating concrete," *ACI Materials Journal,* vol. 105, pp. 88-96, 2008.

[407] H. Vikan and H. Justnes, "Influence of silica fume on rheology of cement paste," presented at the 3rd International RILEM Symposium on Self-Compacting Concrete, Reykjavik, Iceland, 2003.

[408] R. Khatib, D. Feys, K. H. Khayat, and A. Perez-Schell, "Effects of mix design parameters on reducing viscosity of high strength self-consolidating concrete for high-rise construction," presented at the Fifth North American Conference on the Design and Use of Self-Consolidating Concrete, Chicago, IL, USA, 2013.

[409] H. A. Barnes, "Thixotropy - A review," *Journal of Non-Newtonian Fluid Mechanics,* vol. 70, pp. 1-33, 1997.

[410] M. Nehdi and M.-A. Rahman, "Effect of geometry and surface friction of test accessory on oscillatory rheological properties of cement pastes," *ACI Materials Journal,* vol. 101, pp. 416-424, 2004.

[411] A. S. Dukhin and P. J. Goetz, "Acoustic and electroacoustic spectroscopy for characterizing concentrated dispersions and emulsions," *Advances in Colloid and Interface Science,* vol. 92, pp. 73-132, 2001.

[412] V. A. Hackley, L.-S. Lum, and C. F. Ferraris, "NIST Technical note 1492: Acoustic sensing of hydrating cement suspensions: An exploratory study," National Institute of Standards and Technology, Washington D.C., USA2007.

[413] D. J. McClements, "Ultrasonic characterisation of emulsions and suspensions," *Advances in Colloid and Interface Science,* vol. 37, pp. 33-72, 1991.

[414] U. Riebel and F. Löffler, "The fundamentals of particle size analysis by means of ultrasonic spectrometry," *Particle & Particle Systems Characterization,* vol. 6, pp. 135-143, 1989.

[415] A. S. Dukhin and P. J. Goetz, "Acoustic and electroacoustic spectroscopy," *Langmuir,* vol. 12, pp. 4336-4344, 1996.

[416] A. S. Dukhin and P. J. Goetz, *Characterization of liquids, nano- and microparticulates, and porous bodies using ultrasound*. Oxford, UK: Elsevier, 2002.

[417] P. M. Morse and K. Uno Ingard, *Theoretical acoustics*. Princeton, NJ, USA: Princeton University Press, 1968.

[418] R. E. Challis and V. J. Pinfield, "Ultrasonic wave propagation in concentrated slurries - the modelling problem," *Ultrasonics,* vol. 54, pp. 1737-1744, 2014.

[419] A. Shukla, A. Prakash, and S. Rohani, "Particle size monitoring in dense suspension using ultrasound with an improved model accounting for low-angle scattering," *AIChE Journal,* vol. 56, pp. 2825-2837, 2010.

[420] D. G. Aggelis and T. P. Philippidis, "Ultrasonic wave dispersion and attenuation in fresh mortar," *NDT & E International,* vol. 37, pp. 617-631, 2004.

[421] A. Shukla, A. Prakash, and S. Rohani, "Online measurement of particle size distribution during crystallization using ultrasonic spectroscopy," *Chemical Engineering Science,* vol. 65, pp. 3072-3079, 2010.

[422] B. Belzung, F. Lequeux, J. Vermant, and J. Mewis, "Flow-induced anisotropy in mixtures of associative polymers and latex particles," *Journal of Colloid and Interface Science,* vol. 24, pp. 179-187, 2000.

[423] D. Asnaghi, M. Carpineti, M. Giglio, and A. Vailati, "Small angle light scattering studies concerning aggregation processes," *Current Opinion in Colloid & Interface Science,* vol. 2, pp. 246-250, 1997.

[424] C. Moitzi, L. Donato, C. Schmitt, L. Bovetto, G. Gillies, and A. Stradner, "Structure of β-lactoglobulin microgels formed during heating as revealed by small-angle X-ray scattering and light scattering," *Food Hydrocolloids,* vol. 25, pp. 1766-1774, 2011.

[425] A. J. Salem and G. G. Fuller, "Small angle light scattering as a probe of flow-induced particle orientation," *Journal of Colloid and Interface Science,* vol. 108, pp. 149-157, 1985.

[426] F. M. Abuzaina, B. D. Fitz, S. Andjelic, and D. D. Jamiolkowski, "Time resolved study of shear-induced crystallization of poly(p-dioxanone) polymers under low-shear, nucleation-enhancing shear conditions by small angle light scattering and optical microscopy," *Polymer,* vol. 43, pp. 4699-4708, 2002.

[427] J.-P. Fouassier and J. F. Rabek, *Lasers in polymer science and technology: applications*. Boca Raton, FL, USA: CRC Press, 1990.

[428] T. Colman, "Rheological measurements carried out in SALS cell (ppt presentation)," ed: Anton Paar, 2015.

[429] M. I. Mishchenko, L. D. Travis, and D. W. Mackowski, "T-Matrix computations of light scattering by nonspherical particles: a review," *Journal of Quantitative Spectroscopy & Radiative Transfer,* vol. 55, pp. 535-575, 1996.

[430] M. B. Rhodes and R. S. Stein, "Scattering of light from assemblies of oriented rods," *Journal of polymer science: Part A-2,* vol. 7, pp. 1539-1558, 1969.

[431] R. Pasquino, F. Snijkers, N. Grizzuti, and J. Vermant, "The effect of particle size and migration on the formation of flow-induced structures in viscoelastic suspensions," *Rheologica Acta,* vol. 49, pp. 993-1001, 2010.

[432] J. Vermant and M. J. Solomon, "Flow-induced structure in colloidal suspensions," *Journal of Physics: Condensed Matter,* vol. 17, pp. 187-216, 2005.

[433] L. Rayleigh, "On the diffraction of light by spheres of small relative index," *Proceedings of the Royal Society of London. Series A,* vol. 90, pp. 219-225, 1914.

[434] G. Mie, "Contributions to the optics of turbid media, particularly of colloidal metal solutions," *Annalen der Physik,* vol. 25, pp. 377-445, 1908.

[435] D. W. Hahn. (2009). *Light scattering theory*. Available: http://plaza.ufl.edu/dwhahn/Rayleigh%20and%20Mie%20Light%20Scattering.pdf

[436] C. Mätzler, "Research Report No. 2002-08: MATLAB functions for Mie scattering and absorption," Institut für Angewandte Physik, Schweiz2002.

[437] A. J. A. Smith, "The scattering of light by non-spherical particles - Second year report," University of Oxford, Oxford, UK2009.

[438] A. R. Jones, "Light scattering for particle characterization," *Progress in Energy and Combustion Science,* vol. 25, pp. 1-53, 1999.

[439] C. F. Bohren and D. R. Huffman, *Absorption and scattering of light by small particles*: John Wiley & Sons, Inc., 1983.

[440] P. C. Hansen, "Numerical tools for analysing and solution of Fredholm integral equations of the first kind," *Inverse Problems,* vol. 8, pp. 849-872, 1992.

[441] Z. Sun and E. M. Sevick-Muraca, "Inversion algorihms for particle sizing with photon migration measurement," *Fluid Mechanics and Tranport Phenomena,* vol. 47, pp. 1487-1498, 2001.

[442] N. Riefler and T. Wriedt, "Intercomparison of inversion algorithms for particle-sizing using Mie scattering," *Particle and Particle Systems Characterization,* vol. 25, pp. 216-230, 2008.

[443] P. Xu, "Truncated SVD methods for discrete linear ill-posed problems," *Geophysics Journal International,* vol. 135, pp. 505-514, 1998.

[444] J. C. Lagarias, J. A. Reeds, M. H. Wriht, and P. E. Wright, "Convergence properties of the Nelder-Mead simplex method in low dimensions," *SIAM Journal of Optimization,* vol. 9, pp. 112-147, 1998.

[445] P. C. Hansen, "Analysis of discrete ill-posed problems by means of the L-curve," *SIAM Review,* vol. 34, pp. 561-580, 1992.

[446] A. Skarendahl and Ö. Petersson, *First International RILEM Symposium on Self-Compacting Concrete*. Stockholm, Sweden: RILEM Publications, 1999.

[447] F. Vanden Berghen and J. Vermant, *SALS Software v2.01 users guide*. Leuven, Belgium, 2011.